1-1-1996

Viewing the 21 cm sky : a slice of the neutral hydrogen universe.

John G. Spitzak

University of Massachusetts Amherst

VIEWING THE 21 CM SKY: A SLICE OF THE NEUTRAL HYDROGEN UNIVERSE

A Dissertation Presented

by

John G. Spitzak

Submitted to the Graduate School of the
University of Massachusetts Amherst in partial fulfillment
of the requirements for the degree of

Doctor of Philosophy

May 1996

Department of Physics and Astronomy

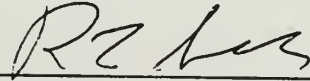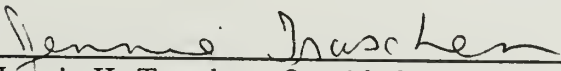# VIEWING THE 21 CM SKY: A SLICE OF THE NEUTRAL HYDROGEN UNIVERSE
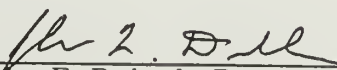
A Dissertation Presented

by

JOHN G. SPITZAK

Approved as to style and content by:

_____
Stephen E. Schneider, Chair

_____
Stephen E. Strom, Member

_____
Ronald L. Snell, Member

_____
Jennie H. Traschen, Outside Member

_____
John F. Dubach, Department Head
Department of Physics and Astronomy

ABSTRACT

VIEWING THE 21 CM SKY: A SLICE OF THE NEUTRAL

HYDROGEN UNIVERSE

MAY 1996

JOHN G. SPITZAK, B.S., UNIVERSITY OF MASSACHUSETTS AMHERST

Ph.D., UNIVERSITY OF MASSACHUSETTS AMHERST

Directed by: Professor Stephen E. Schneider

Among the most fundamental problems in extragalactic astronomy are understanding the processes which led to galaxy formation and establishing the existence and nature of "dark matter" in the Universe. Before any attempt can be made to solve either of these problems, an accurate and thorough knowledge of the true population of galaxies is required. Unfortunately, there is mounting evidence that our knowledge of extragalactic space may be critically incomplete. This deficiency is due primarily to our dependence on galaxy statistics that are largely derived from observations at optical wavelengths. These statistics may include only a sub-population of extragalactic objects which have properties easily detected in that narrow wavelength range, rather than the true population which may have a more diverse range of properties.

To steer ourselves away from this possible optical bias, and thus to obtain a more well-rounded census of galaxy sizes, types, and locations, we have conducted a large-scale, unbiased survey for atomic hydrogen (HI) at 21cm. Because the strength of 21cm emission does not depend on the same forces which drive optical emission, this survey allows us to not only augment the compiled database of galaxies by describing the properties of previously cataloged objects we detect, but more importantly search for new types of objects which have historically remained undetected due to optical biases. Using the NAIC Arecibo Telescope, we have systematically searched a "slice" of extragalactic space known to contain 48

cataloged galaxies. Our survey has re-detected 38 by their 21cm emission, and has failed to detect 10. We have also detected an additional 41 previously unknown objects.

We present atomic hydrogen and optical data for all objects and demonstrate that the newly discovered galaxies represent a population which differs distinctly from the cataloged galaxies in having lower overall luminosities and masses, larger relative HI gas contents, and bluer colors. In addition we show that several extremely low-mass, low luminosity galaxies discovered within 5 Mpc of the Milky Way imply the presence of thousands of similar objects throughout the slice search region. These low-mass objects could, in their great numbers, represent a significant fraction of the total integrated mass of all galaxies in the region. As such, they could have a profound influence on the distribution and evolution processes of all extragalactic objects.

TABLE OF CONTENTS

LIST OF TABLES

CHAPTER 1

INTRODUCTION

Statistical studies form the basis of much of observational astronomy. Studies which examine a single astronomical object outside the Solar System are uncommon. Usually such studies are limited to observations of rare, bizarre, or particularly interesting objects, demonstrating a newly discovered or scarce intermittent phenomenon. In general, they are used to present, rather than solve, physical problems. More common are observations of large numbers of similar objects with the purpose of building a statistical data base of physical properties. These data bases are then used to produce generalized models of classes of objects in an effort to understand the physical processes which lead to their observed properties. Statistical studies of this sort can be very powerful tools, particularly in a non-interactive science such as astronomy, where the objects of study are remote, impossible to influence, and often not thoroughly understood. Yet the Achilles Heel of any such study is its need for a complete statistical sample of objects to be included in its data base. Any bias towards, or "selection," of objects displaying particular physical properties can skew the statistics, and lead to a misunderstanding of the physical processes which lead to those properties. These selection effects plague many aspects of observational astronomy.

The problem of selection effects is particularly acute in extragalactic astronomy, where the objects of study, galaxies, are far from well understood. The available database of galaxies and their properties is extremely sketchy. Only a small minority of observable galaxies have been cataloged, and fewer of these have had their properties examined in any detail. More troublesome, however, is the likelihood that the subset of galaxies which has been cataloged does not represent the full range of physical properties galaxies exhibit, but rather only those which have been historically easy to observe. We might expect that an optical search for galaxies would select only those with the more impressive and extensive surface brightness, missing low surface brightness objects and objects which do not appear to extend across large

1

angles on the sky. Because the vast majority of cataloged galaxies have been located using optical surveys, our knowledge, and our thinking of galaxies and the extragalactic environment is dangerously biased toward high surface brightness objects. Any study which treats the sum of all cataloged galaxies as a statistical cross section of all galaxies may suffer from this bias towards easily observed galaxy types. Before the results of these studies can be trusted, compiling an accurate census of all extragalactic objects is profoundly important.

The usefulness of a complete extragalactic population count becomes clear when considering two of the most profound problems in astronomy; understanding the processes which control galaxy formation and the existence and nature of dark matter. Only with an accurate census can these problems be properly addressed.

Big Questions, Big Problems

Questions of the existence of dark matter and of the process of galaxy formation are among the more profound, and difficult in science. They relate both to the processes which formed the Universe we observe today, and to what fate we can eventually expect for it. They are particularly interesting questions because our inability to answer them easily makes us wonder how well we really understand the workings of the Universe. In addition, they are interesting because they represent pure human curiosity - it is unlikely that answers to them will serve any useful function for us, other than to satisfy a desire to know and understand why things are the way they are, and perhaps also to understand ourselves and how we interpret our surroundings better.

We present a brief description of each of these problems, and an explanation of how we believe they may be influenced by optical selection effects in databases of galaxies, and how improved statistics may help shed some light on them.

Dark Matter

We will do little more than summarize the dark matter, or "missing mass" problem, as a complete description of it is well beyond the scope of this work. However, some of the results which will be discussed in later chapters may relate to the solution to, or may at the very least better define the extent of,

this important and seemingly intractable problem. Short of trying to solve it, a description of the dark matter problem provides justification for this study by demonstrating how fragile and incomplete our knowledge of the content of the Universe is.

Studies of the dynamics of visible objects in the Universe indicate the influence of a mass of matter considerably larger than we have direct evidence for. The larger the scale on which the dynamics are examined, the more profound the discrepancy becomes. In the local solar neighborhood, studies of number densities of stars and their velocities perpendicular to the disk of the Milky Way suggest the presence of up to several times the sum of all known material (stars and gas) in the disk, although the uncertainties in the measurements do just barely allow for no unseen matter (Kuijken, 1991). On the galactic scale, rotation velocities of disk material in galaxies derived both optically and using 21cm observations appear constant, or occasionally increasing, as one looks further from the center of the galaxies, even considerably beyond their optical disks (Kent, 1987). While easiest to measure in spiral galaxies containing strong disk components, non-declining rotation curves can be observed to a greater or lesser degree in all galaxy types (Casertano and van Gorkom, 1991). On average, the accumulated mass of all the directly observable material in galaxies accounts for less than a tenth of that needed to maintain such "flat" rotation curves. Studies of the motion of distant satellites of the Milky Way show that it too has a similar dark matter component, extending in a halo out to ~100 kpc from the Galactic center (Zaritsky, et al., 1989).

The largest structures we observe which are believed to be in virial equilibrium are galaxy clusters. Studies of the motions of individual cluster members, as well as X-ray observations, demonstrate that up to 350 times the mass of the optically observed cluster members is required for them to be in equilibrium (Hughes, 1989, Merritt, 1987). On even larger scales, studies of the distribution and predicted peculiar velocity field of *IRAS* galaxies indicate the need for 500 - 700 times the observed mass (Kaiser, et al., 1991), although previous work has not demonstrated a discrepancy any larger than 300 times the observed mass at the supercluster scale, and it is possible that the velocity fields are being over-interpreted (Praton and Schneider, 1994).

Beyond dynamical measurements, there are theoretical arguments which point to large amounts of missing mass. Big-bang nucleosynthesis models predict the presence of 100-200 times the total of observed matter in baryonic form (Walker, et al., 1991). The size of this discrepancy fits fairly comfortably with that derived from the motions of galaxy clusters, indicating that there is a substantial "missing" baryonic matter problem. In addition, a "flat universe," preferred by some theoretical models of the Universe's origin, requires the presence of 1000-2000 times the integrated matter for which observational evidence exists, much of which must be in the form of "exotic" non-baryonic particles. However, there is as yet no compelling reason to believe that the Universe must be flat, and the exotic particles may not be required at all.

Obviously, an accurate census of the content of extragalactic space is important before the dark matter problem can be properly approached. While much of the missing mass may be in the form of non-baryonic particles, the nucleo-synthesis models predict that at least a significant fraction of it is in the form of baryonic material, which may simply be missing because it escaped detection due to the optical selection effect. A more comprehensive extragalactic survey without the optical bias may go a long way toward locating much of the missing baryonic mass. Moreover, some observations which lead to the dark matter problem depend on a complete knowledge of galaxy types and locations. The measurements of the motions of galaxies in clusters which are used to estimate the total mass of the clusters are fairly sensitive to the definition of where a "cluster" begins, and when and where galaxies become members bound in virialized orbits about a center of mass. Before this can be done accurately, it is vital to know the true content of a cluster - the locations and properties of its individual members.

Galaxy Formation

Galaxies appear to be the basic building blocks of the Universe. To our eye, they have well defined boundaries, and clearly-patterned structures, and seem to fall into a range of types. Much effort has been put into cataloging and describing the types and structures of galaxies, but little is known with certainty about how these features arose. There is even less understood about the process which led from the beginnings of the Universe to individual galaxies. While much work has been done to understand the

internal dynamics of galaxies and plausible models have been presented which describe how they formed from primordial clouds into the objects we observe now, the origins of the necessary primordial clouds is less clear. How was the transition made from a homogeneous matter distribution as observed in the 3K background radiation to the "lumpy" structure of individual galaxies, clusters, filaments, and voids which we observe in the present epoch? Is the galaxy formation process essentially finished, or do evolutionary processes making profound changes continue to occur? Do the large, bright galaxies we see so easily represent all of the massive objects in the Universe or only those which have evolved to be bright?

In what way will a better extragalactic census help answer these questions? First of all, before we can ask how galaxies form, it is important that we understand what a "galaxy" is. Should this definition only include the objects we have observed and think we understand to some degree? Or are there large populations of undiscovered objects which we have failed to detect for one reason or another, and which might represent entirely new types of "galaxies," or at the very least interesting twists on the types we know about? Discovering new populations of objects could entirely change the character of the problem of galaxy formation, since such discoveries will not only introduce new objects whose existence must be explained by any comprehensive model, but also might reveal familiar objects in different or suspended stages in the formation process. For instance, visible "starburst" dwarf galaxies appear to be forming stars at a rate which their small masses would be unable to sustain for long time periods. If, as is suspected, these are short-duration, optically brilliant events which occur periodically in a minority of small galaxies, then a large heretofore undetected population of similar but quiescent objects must exist. The detection, or failure to detect this large population would demonstrate the validity of this premise.

Secondly, the complex large scale structure of the Universe has the majority of known galaxies organized in clusters and superclusters, and seemingly avoiding void regions. Yet it is unclear at present whether these structures contain most of the matter in the Universe, or simply most of the bright galaxies. It is possible that, rather than tracing the "mass" structure (where the bulk of the mass exists), known galaxies describe the "brightness" structure of the Universe (where the mass is somehow consumed by galaxies which are efficient at star formation, thus creating bright objects). An analogous situation is

known to exist in the disks of spiral galaxies, where bright spiral arms are embedded in disks with fairly homogeneous mass distributions. If the known galaxies represent only 1/10 or 1/100 (or even less) of the total mass in extragalactic space as the missing mass arguments indicate, then they can be little more than a brilliant, light-emitting "dusting" on the true mass distribution. It is important that we somehow discover the "mass" large-scale structure before we try to model galaxy formation, and this would require the detection of objects whether they are efficient at star formation or not.

Why Do We Believe the Current Census May Not Be Complete?

Beyond the arguments leading to the dark matter problem, there is some circumstantial, as well as concrete observational evidence that a large undiscovered population of extragalactic objects may exist. Further, the true variety of properties of the real population may be poorly represented by what we now know, a position which would leave us with an inaccurate, and probably misleading view of the Universe

Optical Selection Effects

It is important to carefully examine the methods used to compile much of our knowledge of the contents of the Universe outside our own galaxy. With very few exceptions, initial detections of extragalactic objects have been made at optical wavelengths. Optical plates (usually the *Palomar Observatory Sky Survey,* hereafter referred to as the POSS) are searched in a tedious, but hopefully systematic way for objects which appear extragalactic. This method has produced large lists of galaxies, including some of the best known catalogs such as the *Catalog of Galaxies and Clusters of Galaxies* (CGCG - Zwicky et al. 1961-68), the *Uppsala General Catalog of Galaxies* (UGC - Nilson, 1973) and the *Morphological Catalog of Galaxies* (MCG - Vorontsov-Velyaminov, 1962-68). It is upon these catalogs that many statistical studies are based, and upon which their need for representative cross-sections of galaxy types depends. Unfortunately, a careful investigation of the content of these catalogs indicates they may be seriously biased by selection effects in the optical surveys used to produce them.

The critical property which determines a galaxy's detectability in an optical survey is its surface brightness - its total brightness divided by the solid angle of the sky this brightness is spread over. The dependence on this property makes the detection of galaxies a far more subtle business than the detection

of stars. From our vantage point, stars (other than the Sun) concentrate all of their intrinsic brightness in a single point on the sky. Their detectability is determined by their observed brightness - which scales as the inverse square of the distance to them. Yet because a galaxy's surface brightness is proportional to observed total brightness and inversely proportional to the area it covers on the sky, both of which scale as the inverse square of the distance, its detectability is to first order distance invariant. The properties of a galaxy which determine surface brightness, and thus optical detectability, are primarily *intrinsic*. This is very different from the extrinsic property - distance - which governs a star's detectability. This distinction is important. In compiling a statistical cross-section of stellar types, one can be fairly certain that a volume-limited sample of stars is complete as long as the stars with the lowest intrinsic brightnesses would be detectable everywhere within the volume. If this is not the case, the volume can be reduced until it is true. This solution does not work forever of course - eventually the sample volume will be too small to contain large enough numbers of stars for good statistics, as happens with studies of the least intrinsically bright stellar types. Yet to some degree researchers have control over the detectability of the stars they are searching for. A search for galaxies has no such control. A galaxy may have an intrinsic surface brightness low enough to make it impossible to detect optically at any distance.

The problem in searching for objects by their surface brightness is that we must detect them in the midst of the many sources of "background" surface brightness in the sky. Some of the sources of this background are very familiar to us, such as the glow of the not-entirely transparent night sky, or the Zodiacal light of the Solar System. Yet even if we were able to eliminate the atmospheric and local Solar contributions to the background brightness by observing from an imagined vantage point in interstellar space, we would still be embedded in an object which has a comparatively high surface brightness - the Milky Way Galaxy. For an extragalactic object to be detected it must stand out against this surface brightness, which is roughly 23 V mag/arcsec^2 looking toward the Galactic pole. Inevitably, objects with low surface brightnesses, particularly objects with surface brightnesses lower than 23 V mag/arcsec^2, will be detected only with considerable difficulty. This difficulty may lead to a lower likelihood that they will be detected at all, and hence to an under-representation of such objects in optical catalogs. To illustrate

the dangers of detecting background objects in this environment, Disney (Disney, 1976) suggests imagining an optical search for extragalactic sources from the center of a giant elliptical galaxy, where the mean surface brightness of the sky would be 8 or 9 magnitudes brighter than our own sky. In this situation, only the centers of other giant ellipticals would be visible, and a huge underlying population of comparatively dim objects, which we consider normal galaxies, would be very difficult to detect.

Another illustration of the difficulty can be seen by examining a map of the spatial distribution of all known galaxies. In Figure 1. 1, we have located all galaxies in the RC3 by their galactic longitudes and latitudes. The most notable feature on this map is the "Zone of Avoidance", a 10 degree-wide band which contains the optical disk of the Milky Way, and in which there are very few known galaxies. Even within 30° of the plane (half of the sky) the number density of galaxies are significantly lower. Naturally this region of the sky contains galaxies in numbers similar to any other part of the sky, as some careful searches have indicated (Pantoja, et al., 1994). The point is that this feature is not extragalactic at all, but rather is a region of the sky where detection of galaxies is most difficult because dust in the Milky Way disk reduces their observed surface brightnesses. This shows how dramatically our knowledge of extragalactic space can be influenced by non-extragalactic surface brightness effects.

The 23 V mag/arcsec^2 brightness of the Milky Way does not in any way represent a "hard" limit to the surface brightnesses of objects we can detect. So long as the Milky Way is uniform over size scales larger than the galaxy being observed, the true surface brightness limit of an optical image is also determined by the integration time of the observations used to produce it. On a CCD image, for instance, the surface brightness of a galaxy is added on top of the (often brighter) background surface brightness. When the background level from a blank-sky observation is subtracted, the galaxy's surface brightness will stand out to some degree against the empty sky, particularly if it influences many neighboring pixels. How well it stands out is governed by the statistical error in the measurement of each pixel which remains after the background is subtracted. If the galaxy's surface brightness is high enough compared to the statistical error in many neighboring pixels, then it will be detected. The size of the statistical error scales as the inverse square root of the integration time, so long integration times will aid in the detection of very

low surface brightness objects. The value of the lowest surface brightness which can be detected in a particular survey can be computed based on integration times and sky brightnesses. A subtlety in the process is determining how to include the statistical significance of neighboring pixels. The Palomar Sky Survey plates, from which many optical catalogs are derived, are often quoted as having a surface brightness limit of around 25 mag/arcsec^2.

Yet detectability is only half of the issue. Note that by calling an object "detectable" we mean only that it would appear on the plates as something other than the background surface brightness, not that it would necessarily be recognized as an extragalactic object. To be identified as a galaxy (and thus included in an extragalactic catalog), an object must have angular extent - its detectable surface brightness must extend across enough of the plate (or enough pixels on a CCD) that the image of the object is obviously non-stellar (Disney and Phillips, 1983).

Whether or not an object has a large enough angular extent on the sky to be recognized as a galaxy is strongly distance-dependent. If an object is detectable, it will have some physical size over which it is generating a detectable surface brightness. The angular extent of this physical size on the sky scales as the inverse of the distance to the object. While it is difficult to quantify the angular size over which a galaxy must extend to appear to be a galaxy, it is clear in any case that galaxies with the largest angular sizes would be the easiest to distinguish. Thus we would expect that galaxies with characteristics which maximized their angular size would be preferentially selected in optical surveys. Once again, the important characteristic which determines angular size is surface brightness.

It has been shown by Disney (1976) that we can quantify the surface brightness of maximum angular size. Work by de Vaucouleurs' (1959) have shown that the overall surface brightness characteristics of an individual galaxy is governed by the galaxy's central surface brightness. The surface brightness distribution of normal galaxies as a function of radius and central surface brightness can be approximated by the formula:

$$\log_{10}\left[\frac{\Sigma(r)}{\Sigma(0)}\right] = -\left(\frac{r}{r_s}\right)^{1/\beta} \tag{1.1}$$

where $\beta = 4$ in elliptical galaxies and 1 in disk galaxies. In this equation, r is the radius, r_s is a scale radius, $\Sigma(r)$ is the surface brightness as a function of radius, and $\Sigma(0)$ is the central surface brightness. Integrating this equation over radius, one can eliminate the scale radius r_s and derive a formula for the apparent radius r_{ap} in terms of the total galaxy luminosity L_T, the surface brightness limit $\Sigma(r_{ap})$, and the central surface brightness:

$$r_{ap} = \left[L_T / \Sigma(r_{ap}) \right]^{1/2} \left[\pi(2\beta)! \right]^{-1/2} (0.4 \ln 10)^{\beta} 10^{-0.2\Delta S} (\Delta S)^{\beta} \tag{1.2}$$

where

$$\Delta S = 2.5 \log_{10} \left[\Sigma(0) / \Sigma(r_{ap}) \right]. \tag{1.3}$$

The apparent radius will then be largest where

$$\Delta S = \beta \frac{\log_{10}(e)}{0.2}. \tag{1.4}$$

Work by Freeman (1970) using photometry for spiral and irregular galaxies found that the central surface brightnesses were virtually constant among all members of the sample. Measured in B mag/arcsec^2, Freeman found a mean central surface brightness of $<S_0>_S = 21.65 \pm 0.3$ for the objects in the sample. In an independent study Fish (1964) found a similar trend among a sample of elliptical galaxies, with $<S_0>_E = 14.80 \pm 0.9$. From the above equation, we can predict the central surface brightnesses which would maximize the apparent radii of both types of objects. Using $S_0 = -2.5\log_{10}[\Sigma(0)]$ and $S_{ap} = -2.5\log_{10}[\Sigma(r_{ap})]$, we find that $\Delta S = S_{ap} - S_0 = 2.17$ for spiral and irregular galaxies and $\Delta S = 8.69$ for ellipticals where the apparent radius is maximized. The surface brightness at the apparent radius is simply where the surface brightness drops below the plate limiting surface brightness. If we choose $S_{ap} = 25$, which is within the range of the surface brightness limits usually quoted for the POSS, we obtain $S_0 = 22.83$ for spiral and irregular galaxies and $S_0 = 16.31$ for elliptical galaxies. According to our model,

these are the central surface brightnesses which would maximize the apparent radii, and the chances of detection of these two types of objects. These values are very similar to the surface brightnesses of actual objects found by Freeman and Fish. An even closer match is made with the difference between the central surface brightnesses of the two classes of galaxies, with $(S_0)_S - (S_0)_E = 6.52$ for our model and $<S_0>_S - <S_0>_E = 6.85$ for the Freeman and Fish objects. From a simple model of the surface brightness distribution within normal galaxies, and some knowledge of the photometric sensitivities of optical surveys, we have been able to predict the central surface brightnesses of galaxies most likely to be found by those surveys. This should disturb us, because nowhere in this process did we involve the characteristics of true galaxies. It implies that either optical surveys are selecting only those galaxies with central surface brightnesses which make them easy to detect, or that galaxies have central surface brightness characteristics which carefully match our photometric sensitivity.

Disney and Phillips (1987) point out that our entire knowledge of extragalactic objects is restricted to a narrow range in surface brightness, which closely matches the range of our photometric sensitivity. This is exactly what we would expect when considering the criteria described above. They argue that our picture of the Universe is so influenced by this "single insidious selection effect" that we may only know a small subset of the true population - the tip of a great "iceberg" of objects in extragalactic space.

To illustrate this potential surface brightness selection effect, we have plotted the total photographic absolute magnitude and mean optical diameter of every galaxy in the RC3 for which these data, in addition to redshift velocity, exist (11838 galaxies) in Figure 1. 2. Diagonal lines on the plot are of constant surface brightness, labeled in magnitudes per square arcsecond. All values on this plot are computed using a Hubble Constant of $H_0 = 75$ km/s/Mpc, although it is important to remember that all surface brightness calculations are independent of distance and the Hubble Constant. Note that (as Disney and Phillips point out) virtually the entire range of objects from Seyferts and giant ellipticals down to faint dwarfs have surprisingly similar surface brightnesses. Is it possible that almost every object in the Universe exists in this tiny range of surface brightness?

The tendency of all objects to fall along such a narrow range of surface brightnesses leads us to two possible conclusions, neither of which is particularly attractive. One conclusion is that all extragalactic objects *do* have roughly the same surface brightnesses. Two problems arise from this conclusion - one is that we have no galaxy formation theory which predicts such a result, so it is quite beyond our present understanding, the second is that we must be willing to accept a highly fortuitous coincidence - that our optical sensitivity seems to exactly match the surface brightness range of objects. The alternative conclusion is the one Disney and Phillips arrived at - that our surface brightness sensitivity is selecting only the objects which are easiest to see within its limitations, and that vast numbers of very different objects await our discovery when we divorce ourselves from our optical dependence.

All of the objects plotted in Figure 1. 2 have been picked out as extragalactic due to their optical morphology. Most of these were found on photographic plates using the criteria described above - they had uniformly bright extended emission impressive enough to be spotted. All of the 11838 objects from the RC3 are contained in one or more of the UGC (Nilson, 1973), ESO (Lauberts, 1982), MCG (Vorontsov-Velyaminov et al., 1962-68), CGCG (Zwicky et al., 1961-68), and UGCA (Nilson, 1974) extragalactic catalogs. All of these catalogs used some form of optical technique to locate galaxies on the POSS, subject to the surface brightness selection effects discussed above.

We can qualitatively examine how the surface brightness selection effects would govern the detectability of galaxies located anywhere on Figure 1.2. An object located in the lower right of the diagram would have either low intrinsic luminosity or large size (or both) and would thus have a relatively low surface brightness. Detection of such objects would become increasingly difficult (and thus unlikely) as lower and lower surface brightnesses were sought. Note that almost all of the objects plotted in Figure 1. 2 are located above the 25.0 mag/arcsec^2 constant surface brightness line, which is suspiciously similar to the detection limit normally quoted for the POSS. An object in the upper left of the figure, with high intrinsic luminosity and small size, would be easily detected. However, if it was not obviously extended, it would appear as a bright point source, and could be mistaken for a star. Only objects fairly nearby would not be misinterpreted in this way. If we are only able to discern their extragalactic nature at relatively

short distances, then the volume in which they may exist and still be discovered must be small (determined by the cube of the distance). The total number of objects we are sensitive to will fall off proportionally as the volume shrinks.

Yet not every extragalactic object ever detected was found using conventional optical methods. Figure 1. 3 is a duplicate of Figure 1. 2 with some additional objects plotted (the RC3 galaxies are in gray for clarity). All of these new objects, represented by stars on the plot, are extragalactic sources which were originally located by unconventional means. The 26 unlabeled points are dwarf galaxies in the Virgo cluster, which were located on UK Schmidt plates using a photographic amplification technique by Impey et al. (1988). The limiting surface brightness for their search was roughly 27 mag/arcsec^2, and it is clear from the plot that the locations of the new objects scatter fairly uniformly down to the diagonal line of that surface brightness. There is no indication that the number of objects has any tendency to decline toward 27 mag/arcsec^2- implying that there are more yet to be discovered at lower surface brightnesses. In addition to the Virgo dwarfs, there are four labeled objects of special interest. Malin 1, the prototypical high mass low-surface-brightness (LSB) galaxy, was discovered in the same search as the above 26 objects. However, optical redshifts and HI observations later showed it to be an enormous gas-rich background object (Bothun et al., 1987). Malin 1 is the only one of the 27 LSB galaxies found using the amplification process which yielded a detection in HI. Three other objects plotted on Figure 1. 3 were located originally via their 21cm emission; the M96 intergalactic ring (Schneider, et al., 1989), which has an upper limit in absolute magnitude, since no optical emission has ever been detected from this object; the dwarf galaxy Leo dw A which was accidentally detected during observations of the ring (Schneider, 1989); and the "protogalaxy" discovered by Giovanelli and Haynes (1989b) during 21cm observations of known galaxies.

The surface brightnesses of the HI-detected objects, which are computed using atomic hydrogen diameters, are not easily compared to those of the optically detected objects, which are determined using optical diameters. However, because their detections were obviously not subject to the same surface brightness constraints as those of the optically selected galaxies, they are evidence that it may be correct

13

to conclude that only galaxies with surface brightnesses similar to our optical sensitivity are being detected in optical surveys. It could be that these LSB, atomic hydrogen-rich galaxies represent a glimpse underwater at Disney's "iceberg", and that a thorough search of the sky will reveal large numbers of similar sources.

Quasar Absorption Lines

Further evidence of an undiscovered population exists in the form of absorption features in the spectra of distant quasars. These features fall roughly into three categories (Burbidge, 1981). There are broad line systems and troughs generally thought to be associated with the quasars. There are also large numbers of narrow Lyman-alpha lines (a Lyman-alpha "forest") with no associated metal lines. Finally, there are damped Lyman-alpha lines with associated metal lines. Lynds (1971) first attributed lines of the last two types which he observed in the spectra of QSO 4C 05.34 to foreground collections of material, and predicted that the spectra of all high redshift quasars would exhibit similar characteristics. His prediction has held true in subsequent work (Young, et al., 1979, Chen, et al., 1981, and others).

The origin of the absorption systems has been the topic of some debate, however there are two strong indications that they are due to objects which are not associated with the quasars themselves: higher redshift quasars appear to exhibit more absorbing systems than lower redshift quasars, as would be expected if the absorptions were due to random line-of-sight intersections with a population of bound clumps whose number density decreases as the Universe expands; and there have been detections of galaxies with similar redshift velocities to absorption features in nearby quasars. There is general agreement that these lines represent a population of intervening extragalactic objects. These objects may be extended halos around large galaxies, in which case the number of absorption features indicates that normal galaxies must have halos upwards of 100 kpc in radius (Bahcall, 1975). Or they could be isolated, undetected clouds along the line of sight. In either case, there are far too many absorption features to be accounted for by current counts and sizes of extragalactic sources.

The "forest" lines have implied column densities of $n_{HI} \leq 10^{18}$ cm^2. In practice, this is too low to be detected in emission at 21cm, although they may represent only a small percentage of a much larger

ionized mass of hydrogen. Even the damped systems represent an over-abundance by a factor of ~10 of the number of systems expected based on the cross-section of optically known galaxies. Wolfe (1987) argues that the damped systems represent a population that dominates the baryon content of the Universe at high redshifts. Based on their metal content, linewidths, and column densities, the damped systems resemble disks of modern-day spirals, but there seem to be too many of them. Have the disks shrunk - which is hard to understand from an angular momentum standpoint - or have we overlooked a population of modern-day objects that have high HI column densities and might be detected in emission at 21cm?

How Do We Fix the Surface Brightness Selection Problem?

Both the evidence of the surface brightness selection effects and the quasar absorption spectra indicate the presence of large numbers of extragalactic objects which to date have escaped detection. If such an unknown population exists, we should make whatever efforts are within our abilities to find it. We must tailor observations which will avoid the bias due to optical selection effects, and more accurately assess the true content of extragalactic space.

What wavelengths should be used for these new observations? Certainly optical images can be made "deeper" by performing longer integrations and using more sophisticated instrumentation. This approach essentially lowers what we called the "plate limit" - the lowest surface brightness at which an object is detectable. The success of observations of this type in finding new objects can be seen in the galaxies found by Impey et al. (1988) on Figure 1.3. However, deeper optical images may be effective only at locating the same types of objects we are already familiar with, although in greater numbers and to greater distances. We know that the root cause of our problem is the dependence on optical data to find galaxies, so continued optical observations are probably not the best strategy. A better approach would be to observe at a wavelength which is not sensitive to the same emission that optical instruments are. Our optically generated knowledge is not useless, but to make the most of it, we would be served best by new observations which would complement it, rather than trying to expand it.

What is it that optical instruments are sensitive to? They detect emission which is at optical wavelengths, but what is the source of this emission? Unlike observations of objects in the Milky Way,

measurements of external galaxies are rarely made of individual components of the galaxies. More often they are made of large regions of the galaxies which include a wide range of object types. While emission at a particular wavelength may be produced by many different types of objects within a galaxy, often one of the galaxy's components will produce much more emission than any other, and will dominate the total integrated emission of the galaxy. Virtually all optical emission from a typical garden variety galaxy is produced by stars. Furthermore, the integrated optical emission of a galaxy will tend to be dominated by the emission from young, massive stars, far out of proportion with the fraction of the overall stellar population which they represent. For this reason, galaxies which have large populations of young, massive stars will appear more optically impressive than otherwise similar galaxies with few massive stars. Because massive stars have short lifetimes, it is the galaxies which are undergoing rapid rates of star formation, and are currently producing them, which will be preferentially selected in an optical survey. This preferential selection is strengthened further because most photographic surveys are done in blue light, where the emission from massive stars peaks. The optical bias is really a star formation bias.

The most effective way of searching for objects not found by our present star-formation-sensitive system is to look at wavelengths where emission from young stars and star forming regions does not dominate. Unfortunately, there are not many. Far-infrared (FIR) wavelengths primarily detect the reprocessed emission from protostars and disks around young stars, and dust either heated by massive stars in HII regions (for short infrared wavelengths) or dust warmed by the interstellar radiation field (for longer infrared wavelengths). Most of these sources depend on young, massive stars as the engine driving their emission (Devereux and Young, 1990). Even the dust itself is star formation dependent, since it requires previous generations of stars to create it.

Emission at ultra-violet wavelengths is similarly dependent on stars. Observations at millimeter wavelengths detect CO and other molecules in molecular clouds - once again, regions of star formation. Most radio observations are not directly dependent on star formation, as they detect large high energy radio sources in the centers of some very massive galaxies, and in quasars, although there is a strong FIR-radio correlation (Helou and Bicay, 1993), as galaxies which are strong radio sources are often active star-

forming objects. These observations provide different insights into the same questions of galaxy formation and missing matter that an improved census would, however they detect a similar subset of galaxies as optical studies, and do little to expand the population count.

One observable component of galaxies which does not in some way trace star formation and exists in abundance in most normal galaxies is atomic hydrogen gas. While all other material (save Helium, which is more difficult to detect) must either be processed by stars (in the case of all of the heavy elements), or require conditions which trigger star formation (in the case of molecular hydrogen, which is only produced in abundance in the presence of dust grains and high densities - conditions which also lead to star formation), atomic hydrogen is primordial. It represents the remains of the original gas clouds out of which galaxies are believed to have formed. We might speculate that galaxies could exist along a wide range of different stages in the star formation process, from objects which have never undergone vigorous star formation through those presently forming stars to those which have exhausted the raw materials for star formation. Optical observations would be most effective at detecting galaxies presently forming stars, and somewhat less effective, but still capable of detecting the galaxies which have processed all of their raw material. Other wavelengths are good for detecting subsets of the range optical observations are sensitive to. Infrared and CO observations will most easily detect the galaxies with active star formation, and ultra-violet studies will preferentially find the objects which have processed their raw materials through star formation. On the other hand, atomic hydrogen observations would best detect those objects which had undergone little or no star formation, since these objects would likely have the largest share of their primordial gas remaining, exactly the type of galaxies other wavelength studies are most likely to miss.

Observations of the 21cm line of atomic hydrogen have already demonstrated their utility in locating pools of extragalactic matter which observations at other wavelengths did not indicate. High resolution synthesized images of nearby spiral galaxies at 21cm have shown extensive atomic hydrogen halos well beyond the boundaries of the optical disks (Bosma, 1978). Often these halos contain continuations of the spiral structure of the optical objects. In addition, "accidental" 21cm detections of HI gas clouds with

little or no corresponding optical light or dwarf-like galaxies with substantial HI envelopes indicate there may be a significant unknown population of material which can be detected by its atomic hydrogen emission. The variety, if not the numbers of these objects is impressive. They include the dwarf galaxy Leo dw A which has barely detectable optical emission and the optically invisible, low mass M96 intergalactic ring (Schneider et al., 1989), the nearby "protogalaxy" discovered by Haynes and Giovanelli (1989b), and Malin 1, the prototypical high mass LSB galaxy found in Virgo (Bothun, et al., 1987) as discussed earlier.

Atomic hydrogen observations also lend themselves very nicely to accurate measurements of velocity widths and redshift velocities of galaxies, from which rotation velocities and distances can be derived. Since there are few extragalactic objects which are resolved by even the largest individual radio dishes operating at 21cm, in general, any extragalactic object will be contained within the area of a single telescope beam on the sky, regardless of its orientation. Thus all objects, face-on, edge-on, or in between, with the same 21cm emission, will be measured to have the same HI fluxes by the telescope. Because the 21cm line remains optically thin at almost all plausible column densities, HI masses are easily derived from these HI fluxes. From the rotation velocities and distances, dynamic masses can be calculated.

21cm observations are also more sensitive to face-on disk galaxies than edge on galaxies, exactly the opposite of optical observations. All but the most distant galaxies are resolved by most optical telescopes. As long as they are resolved, their detectability will depend not on their intrinsic brightnesses, but on their surface brightnesses, which is the total brightness of an object divided by the area it covers on the sky, and their observed optical diameters. An object of a given intrinsic brightness will cover a larger area of the sky when oriented face-on than when oriented edge-on. It will thus have a lower average surface brightness, and consequently a lower observed optical diameter (since optical diameters are measured to a limiting surface brightness). This effect is complicated somewhat by the optical depth due to the dust content of the disk. While an optically thin disk will show an increase in both surface brightness and optical diameter when oriented edge-on, an optically thick disk will show little change in surface

brightness, and a *decrease* in optical diameter (Burstein, et al., 1991). Presumably there is a disk orientation which would maximize the chance of detecting an average galaxy by optical observations.

Conversely, because most galaxies are unresolved at 21cm, there is no "atomic hydrogen surface brightness" problem to deal with. However, measurements at 21cm are usually fed into a multi-channel auto-correlator. This is done because the 21cm emission line is so narrow in frequency that any widening of it can be translated into very accurate redshift velocity information. This information is used to extract velocity widths and dispersions of the gas in galaxies (thus optical observations, which have high spatial resolution, and 21cm observations, with high velocity resolution, can be combined to form useful three dimensional pictures of galaxies). The greater the velocity width of an object, the more channels in the correlator its flux will be divided among, and the weaker and more difficult to detect the signal will become (this problem can be alleviated somewhat by summing adjacent channels). Viewing an edge-on galaxy is looking at the gas in the disk along the plane of its rotation around the galaxy center, and seeing the maximum possible difference between the velocities of the material in different parts of its orbit. Thus an edge-on galaxy will have a very high velocity width, will be spread over more correlator channels, and will be more difficult to detect. A face-on galaxy, however, is observed along the axis of rotation, so only the random dispersion velocities of the rotating gas are observed, making its velocity width more narrow, and the object easier to detect. In this way, optical and 21cm observations form a useful complement to each other, as each can be utilized to detect objects the other is less sensitive to.

Atomic hydrogen observations using the 21cm line have some additional advantages which may help them fill in the gaps in our knowledge left by the star formation bias. It is possible that there is a population of undetected "gas rich" galaxies, or galaxies where little of the primordial atomic hydrogen gas has been processed into stars and other types of material. These objects would be expected to have very low rates of star formation, but unusually high HI/total mass ratios. The HI mass is the total mass of atomic hydrogen as measured by the 21cm flux. The total or dynamical mass is inferred from the velocity width of the measured 21cm profile - it is the mass which would require velocities of the magnitude of the velocity width to maintain the object in rotational equilibrium. 21cm observations are particularly

sensitive to high HI/dynamical mass ratio objects. Obviously, higher HI mass will make an object easier to detect. In addition, however, a low dynamic mass will require lower rotational velocities to support the object in equilibrium. Lower rotational velocities lead to lower overall velocity widths for the HI signal from the object. If the same HI flux is packed into a narrower signal, the signal-to-noise ratio of that signal will be higher, and it will be easier to detect.

Outline

We have conducted in many respects the most sensitive systematic HI survey yet attempted in a effort to detect undiscovered extragalactic reservoirs of atomic hydrogen. Our survey has completely sampled a 60 square degree region of the sky out to 8400 km/s redshift, within which we have encountered previously cataloged objects and new, uncataloged sources in roughly equal numbers. The volume of space we searched (which is wedge or "slice" shaped, hence the common use in the following pages of the terms "slice search" and "slice project") contained a variety of extragalactic environments, including clusters, voids, and the transition regions in between. Our 21cm measurements are used to derive HI masses, redshift velocities, velocity widths, and positions of all detected objects. Follow-up optical observations are used to generate magnitudes, colors, morphology of the objects, and dynamic masses (in combination with the HI measurements).

The slice project is described in this dissertation as follows:

Chapter 2 will outline the way our search was conducted, and what reasoning led us to believe it the best approach. We examine the choice of telescope, observing method, and reduction procedures used in the search. It will also describe previous work which either deliberately or inadvertently made progress toward solving the same problems we are working on.

Chapter 3 covers the technical aspects of the original HI observations at Arecibo Observatory, and the reduction procedures used to assure that we were extracting as much as possible out of the 21cm data. In this chapter, we divide our detected HI sources into three categories: "new" extragalactic objects found for the first time by the HI search; "rediscovered" cataloged objects which were found by the search; and "undetected" objects known to be in the search region which were not detected at 21cm. Also discussed

are follow-up observations of detected objects, including higher-sensitivity HI data taken at Arecibo used to determine accurate positions and complete HI fluxes for all detections, and optical CCD observations in using B, R, I, and Hα filters at the Kitt Peak 0.9m telescope.

In Chapter 4 we compile all observed and derived quantities for all objects in the slice search region. These data are presented in a "gallery", showing a fairly complete picture of the slice search's small wedge of the Universe.

Chapter 5 describes the analysis of the results, and the implications of the slice search (and there are many). We combine the data from our many observations and try to identify and explain any trends we see. A particular emphasis is placed on trying to discover the properties which distinguish our "new" objects from our "rediscovered" objects, in the hopes of determining why galaxies end up in one category or the other.

Chapter 6 includes the conclusions we were able to draw from the data, and descriptions of interesting problems the results generate. The data are used to characterize the completeness of current catalogs and optical surveys in general and establish the accuracy of our current extragalactic census. We also describe what follow-up studies we feel should be done to build on our work. In particular, a detailed description of the recently completed "Slice II" Arecibo search, which was inspired by the results of this work will be given.
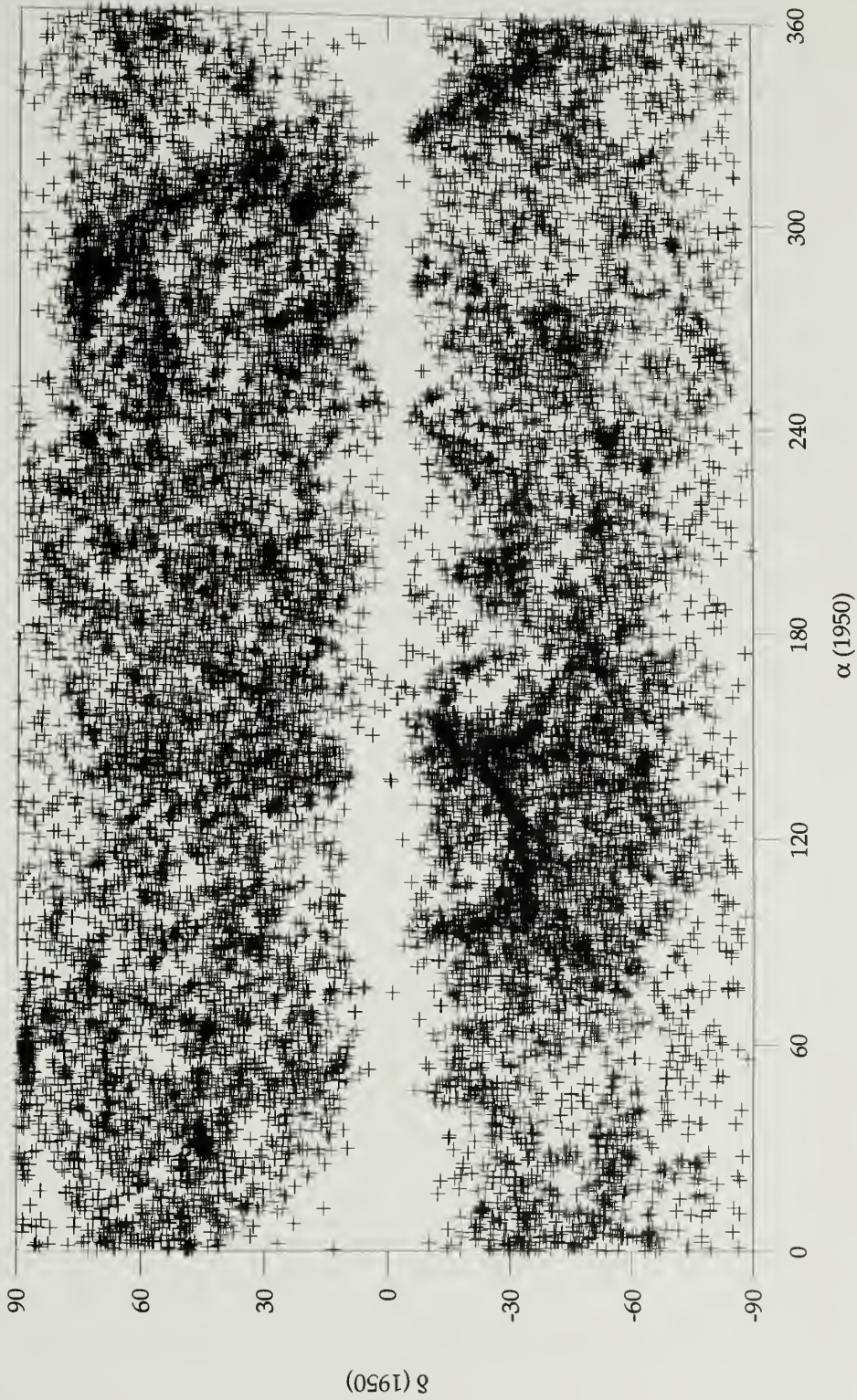
Figure 1.1 Spatial distribution of the galaxies in the RC3 (de Vaucouleurs, 1991). Galactic longitude (α) is plotted on the x-axis, and galactic latitude (δ) is plotted on the y-axis. The white band around δ=90 is the "zone of avoidance".

22
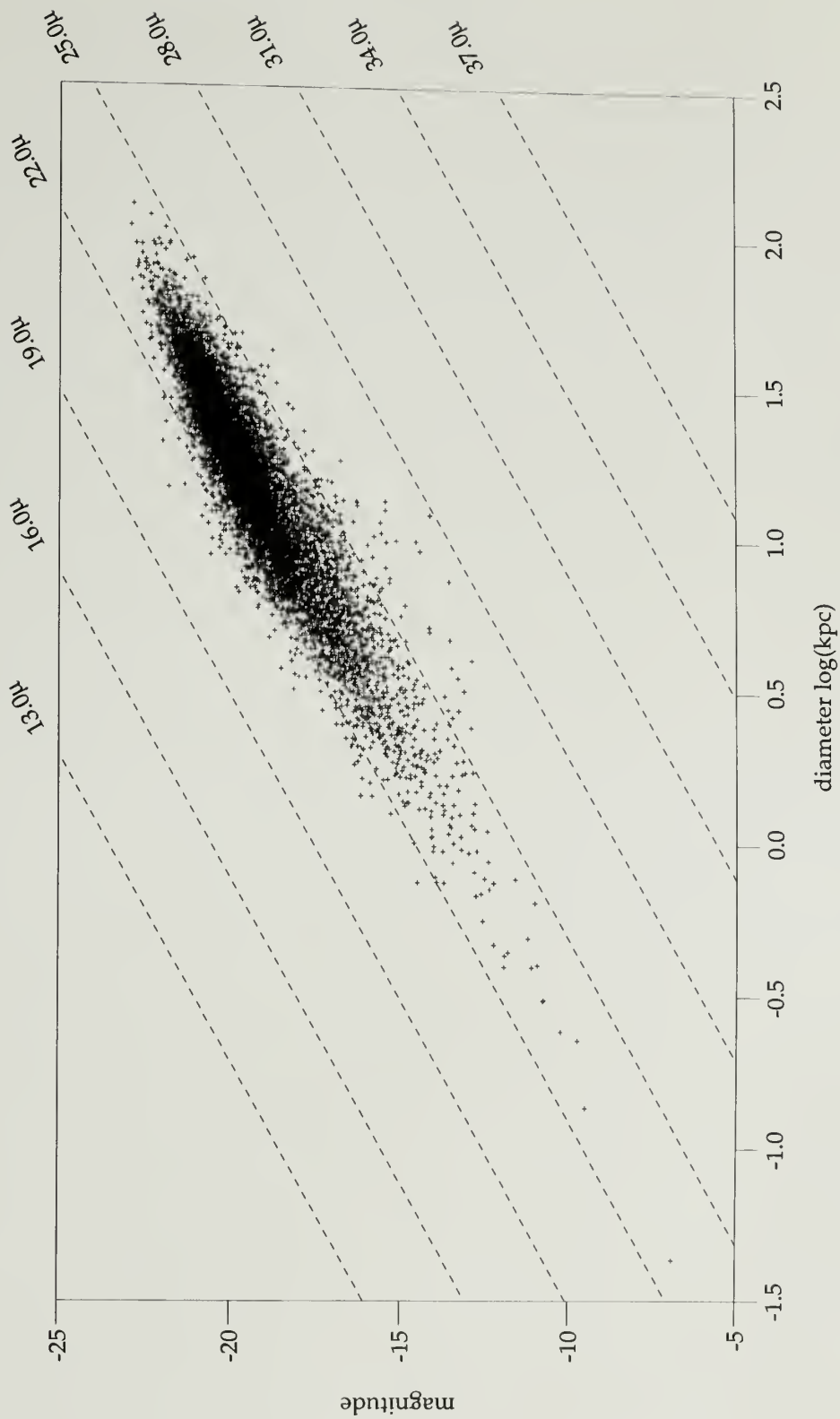
Figure 1.2. The relationship between absolute diameter and absolute magnitude for 11838 Galaxies from the RC3 (de Vaucouleurs, 1991). Diagonal lines are of constant surface brightness. Galaxies which might exist in the lower right of the plot have too little surface brightness to be noticed, those in the upper left are indistinguishable from stars.
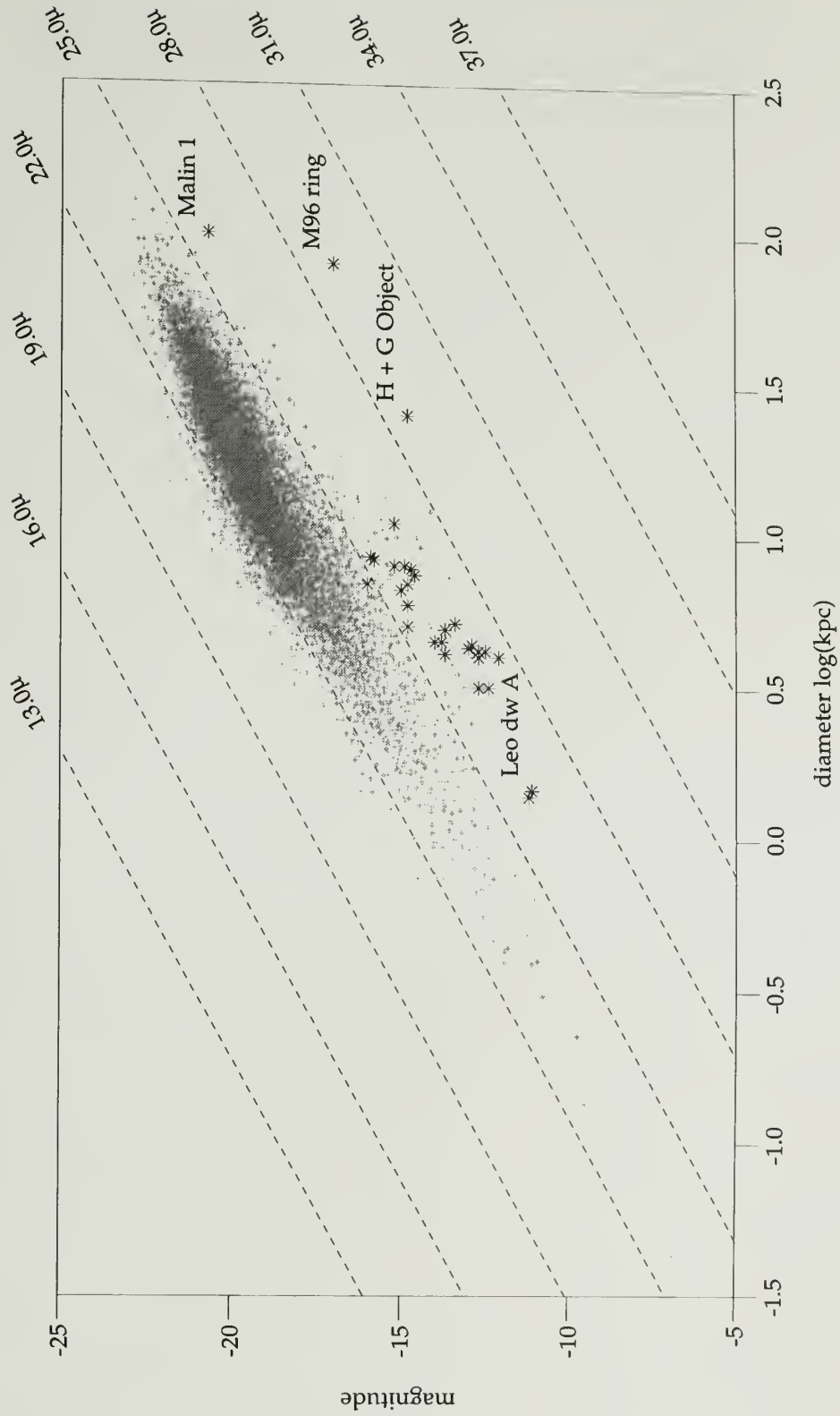
Figure 1.3. Absolute diameters and absolute magnitudes for 11838 Galaxies from the RC3 (de Vaucouleurs, 1991) in gray, with additional objects in black. Diagonal lines are of constant surface brightness.

CHAPTER 2

HOW BEST TO CONDUCT AN HI SEARCH

How would the sky appear if it were viewed at 21cm? The visible extragalactic sky we are familiar with is populated with bright objects - galaxies. These fall into a range of sizes, and have a well-defined variety of morphologies. All, as we have seen in Chapter 1, have similar surface brightness characteristics. They are not scattered randomly throughout the sky, but are arranged in great structures - clusters and superclusters - which imply some sort of order to the Universe which we need to explain. Would the same objects attract our attention at 21 cm? Would their numbers, sizes and morphologies be similar? Would the same large-scale structures still appear important?

Galaxies which are optically bright, particularly spirals and irregulars where star formation is presently active, would stand out at 21cm. Measured in solar units, these galaxies often have comparable HI masses and optical luminosities, suggesting that their atomic hydrogen component is as significant as the light-producing component in the total mass. However, array telescopes have shown us that in many cases HI emission extends well beyond the optical emission of normal spirals, often out to several optical radii (Bosma, 1978). If we were to view the sky at 21 cm, these galaxies would appear larger than they do optically. On the other hand, some very large gas-poor elliptical galaxies which are optically bright would be far less impressive at 21cm than they are at visual wavelengths. Large features which were formerly invisible to us, such as the M96 ring, Malin 1, and the Giovanelli and Haynes proto-galaxy would be seen at 21 cm. It is difficult to say how numerous objects of this type would be, as all have been discovered accidentally, and little is known about their true number density in the Universe. We might also expect to see small clouds of HI, perhaps associated with optical emission characteristic of dwarf galaxies, perhaps not. The encounters with the Impey et al. objects indicate that LSB dwarf galaxies could be very numerous, and Leo dw A and similar findings demonstrate that it might be common for such objects to have measurable atomic hydrogen components.

Observation of atomic hydrogen emission may be a useful tool for finding things which are invisible to us, yet so far it has been used almost exclusively to gather data on objects we already know about. The bulk of extragalactic HI studies have concentrated on optically detected galaxies, and large numbers of them have been detected at 21 cm (these observations are compiled in the HI catalog of Huchtmeier and Richter, 1989). An unbiased 21cm search will help us locate the objects we don't know about, and to view the objects we do know in a new way, increasing our understanding of them. Its purpose is to look at the Universe with "21cm glasses", and see what we see. Yet before starting, it is important to carefully decide on a good search strategy. This decision process has a number of steps - the goals of the search must be carefully defined, the different facilities available for achieving those goals must be assessed, and an approach must be developed which balances what is desired with what is practical to maximum effect.

In this chapter, we discuss the strategy for the HI search. The mission of our atomic hydrogen search is discussed in detail. The merits and drawbacks of different observing instruments, methods, and search regions are used to decide which are the best for our use. The difficulties of balancing instrument time constraints and desires for maximum survey coverage and sensitivity, as well as compromising the twin goals of tailoring a search to find objects with specific interesting characteristics, and avoiding biases in the search which would lessen its chances of finding new objects with unexpected characteristics, are examined. In addition, we discuss previous efforts by other research groups, and how they dealt with the same problems. Finally, we describe the strategy we adopted, and how it approaches the various goals and difficulties we discuss.

Strategies for the Slice Search:

How to Find What We Cannot See

Before we can decide how to perform a search at 21cm, we must clearly define what it is we expect the search to accomplish. In the previous chapter, we discussed the optical bias problem and why we feel that an atomic hydrogen search can help solve it, but what specifically do we wish this search to do? The goals of the slice search can be summarized by two primary purposes:

1. Accurate assessment of the total neutral hydrogen content of extra-galactic space in the present (i.e. local) epoch: This includes a determination of the HI content of known objects as well as unknown objects. What percentage of all galaxies have appreciable atomic hydrogen components? How prevalent are extended halos of atomic hydrogen around galaxies? How much HI is there tied up in non-luminous extragalactic clouds?

2. Examination of the completeness of the present inventory of extra-galactic space: Of the total number of objects out there, how many do we know about, and how many are we missing? How accurate is our picture of the range in sizes, morphologies, and other properties of extragalactic objects? How well do we understand the spatial distribution of galaxies - are voids, clusters, superclusters, etc., really as pronounced as they appear to be?

Designing observing strategies for a search for unknown objects is very different from conventional 21cm extragalactic observations. Normally, the target or targets of observations have known positions. Previous observations at other wavelengths (or at 21cm) may have established some of the properties of the objects and their environments, such as morphology, orientation, approximate angular size, stellar and dust content, redshift velocity, position of near neighbors, etc. Knowing some or all of this information, observations could be tailored to be sensitive to particular properties or locations of interest. Even knowing none of it, the observing strategy could be developed to be optimal for specific objects.

In contrast, to be most effective, a search for unknown objects should rigorously avoid narrowing itself to the detection of particular types of objects, since the properties and locations of the target objects are unknown. Certainly a fair amount is known about the properties of "average" galaxies, and we could observe in such a way so as to maximize the chances of finding them, but this may be a bad idea. Designing our observations to detect the sorts of objects we are familiar with will inevitably lead us to detecting them preferentially, leaving us with the same sorts of biases in our extragalactic samples which the slice search is meant to alleviate. At some level, the "best" search would be a completely "blind" search, designed in complete ignorance of the area it is searching, where the detection of previously cataloged galaxies would be treated in the same way as the detection of new objects.

Of course, the detection of "normal" galaxies in the slice search is desirable, as it will provide a useful basis with which to make statistical comparisons to any new objects we detect. In addition, there are some object types which we would like to make sure we are sensitive to, since accurate assessment of their number densities would be very useful, and past observations have indicated that we may stand a good chance of encountering them. In particular, our search should be sensitive to both of the following types of possible objects:

- Low HI mass sources, presumably small and localized. These objects might be "dwarf" galaxies, with little associated star formation and optical emission, or "HI clouds" with none at all. Being low in mass, they will not require high orbital velocities to maintain their virial equilibrium, so they will likely exhibit narrow linewidths. Prior accidental detections of these objects would include galaxies such as Leo Dw A. While individually of low mass and of little significance, if these objects exist in high enough numbers, they could dominate the integrated mass of all galaxies. Previous studies have indicated both large number densities of objects with low masses (Tyson and Scalo, 1988, Davies, 1990, Staveley-Smith, Davies and Kinman, 1992), and modest and unimportant numbers of them (Hoffman, Lu, and Salpeter, 1992, Briggs, 1990, Weinberg et al., 1991). At present, there simply is not sufficient observational data to establish their true number densities, although this knowledge is critical for understanding the distribution of matter in the Universe.

- Extended HI sources, which could be large envelopes around galaxies, or large, isolated clouds of material. This is a much broader category than the "dwarf/cloud" class of object, and includes items of the M96 ring and Giovanelli and Haynes protogalaxy type, as well as extended envelopes, which have been detected around many galaxies, both optically bright, and virtually non-luminous, such as Malin 1. Where objects in the above category could be expected to be "small but common", objects of this type are likely to be "large but rare". Although detections of them would be much less likely than detections of compact HI clouds would be, discoveries of these objects could potentially be very exciting, as they may represent unknown or suspended stages of the galaxy formation process. Most objects of this type discovered so far have been encountered accidentally. Few successful efforts have

been made to establish how numerous they really are, and such searches have often produced no detections at all (for instance Krumm and Brosch, 1984).

Because galaxies exhibit a wide range of properties, binning them in narrowly defined categories is often deceptive and dangerous. Nevertheless, for the purposes of the following discussion we need to define the "typical" properties of the three types of galaxies we wish our search to be sensitive to. The "dwarf/HI cloud" class objects will typically have atomic hydrogen masses of $M_{HI} = 10^{6-7}M_\odot$, diameters of around $d \cong 3$ kpc, and HI velocity widths (which are measurements of orbital velocities) of $\Delta v \cong 30$ km/s. "Normal" galaxies have $M_{HI} = 10^{9-10}M_\odot$, $d \cong 20$ kpc, and $\Delta v \cong 200$ km/s. The "extended" objects have $M_{HI} \cong 10^{8-9}M_\odot$, $d \cong 50$ kpc, and $\Delta v \cong 100$ km/s. All of these model properties are based on the characteristics of previously discovered galaxies which fall in the individual categories.

In designing a search to be sensitive to the objects described above, we must decide a number of things. We must determine what is the most effective observing instrument to use, what region of extragalactic space we wish to target, and what search method we should use to do the job correctly. These problems are to some degree inter-dependent. Our search method will depend on both our choice of telescope, and on the region we are searching. We have quite a bit of leeway in the choice of our search region, as we don't want to presume where the best location to search is, so we must pick one essentially at random. Before we carefully consider the other two matters, the first thing we must do is choose an appropriate instrument for the slice search.

Choosing a Telescope

Which of the many available telescopes is the best suited for atomic hydrogen searches? The ideal telescope will scan the maximum volume of extragalactic space possible, and be sensitive to the weakest possible signals throughout the volume. The desires for both volume coverage and sensitivity work against one another, as large, sensitive telescopes cover spatial volume slower because of their small beam size than small, less sensitive instruments. At the same time, we must consider the additional question of spatial resolution.

Because 21 cm observations are diffraction limited, their spatial resolution is proportional to their beam size. For single dish instruments, the beam size scales approximately as the inverse of the telescope's diameter. Array telescopes have synthesized beam sizes proportional to the inverse of their telescope spacing, which are much smaller than the "primary" beam sizes which would result if their individual telescopes were used as single-dish instruments. Shostak (1977) has shown the optimal efficiency is attained in a single-dish telescope search when the beam size of the telescope matches the size of the objects being observed - i.e. when the object sizes match or are larger than the resolution of the instrument. The reasons for this are easy to see. The detectability of an object in an HI search is determined by the signal-to-noise ratio (S/N) produced by the measurement used - for an object to be detectable, the S/N should be ~5 or higher. The noise (N), or "system temperature" is a random background level involved in any measurement. Its root-mean-square (r.m.s.) has a fairly stable and predictable value proportional to the inverse square root of the integration time (t), and the value is similar among all single-dish telescopes:

$$S/N \propto t^{\frac{1}{2}}.$$
(2.1)

The signal (S) in a telescope beam is the average of the flux measured over the entire beam. We may define a quantity (x) to be the ratio of the telescope beam area to the area of a target galaxy. In the case where an object does not fill a telescope beam (x>1), the signal to noise ratio will be "diluted" because the signal will be proportional to the galaxy area, while the noise will be proportional to the area of the telescope beam. On the other hand, the S/N will be constant among all single-dish telescopes which have beam sizes smaller than a source (x≤1):

$$\begin{aligned} S/N &\propto x^{-1}\{x > 1\} \\ S/N &\propto const\{x \leq 1\} \end{aligned}.$$
(2.2)

If we are trying to survey an area, the total observing time (T) will be:

$$T = \frac{\text{total area}}{\text{beam area}} \cdot t \propto x^{-1} \cdot t. \tag{2.3}$$

To achieve equal S/N, the observing time (t) will be proportional to x^2. For equal S/N, the total observing time required to survey a given region will be:

$$\begin{aligned} T &\propto x \{x > 1\} \\ T &\propto x^{-1} \{x \leq 1\} \end{aligned} \tag{2.4}$$

This total survey time is minimized when x=1, or when the object size matches that of the telescope beam. Actually, small-beam telescopes can improve S/N by averaging all points where a galaxy is detected, so S/N $\propto x^{-1/2}$ after averaging. Therefore T is constant after some post-processing when x≤1. The situation is slightly more complicated for aperture synthesis instruments. If the synthesized beam of an interferometer is smaller than the source it is observing, some signal from the source is lost (or "resolved out"), and the S/N will be lower.

To increase the chances of detecting extragalactic objects, the S/N of a measurement must be as high as possible. Outside the concerns of resolution discussed above, S/N is proportional to two things - square root of integration time and telescope collecting area. The integration time at any telescope can be increased to increase the S/N, however there are limitations. The Arecibo Telescope in particular has a useful field of view limited to within about 15 degrees of zenith (the useful field has been expanded to 20 degrees away from the zenith with the recent installation of the ground screen). The integration time of a single observation at Arecibo is limited to the time the target of the observation is inside this narrow field of view, although further observations may be made of the same target during later transits. More important than any physical limitation is the problem that telescope time is a valuable commodity, and is in limited supply. Given a fixed amount of telescope time, S/N can be increased by long integrations on individual targets, but at a cost of limiting the number of targets which can be observed. Unfortunately,

the telescopes with the largest collecting areas tend to be the most popular and have the greatest limitations on telescopes time.

Naturally, the larger the volume of space covered in an atomic hydrogen search, the better. How efficiently an instrument can scan volumes of space is determined by the sensitivity of the instrument, and its ability to cover large redshift velocity ranges with adequate resolution. Pointing on a position in the sky, a telescope beam describes a three dimensional, cone-shaped region with the telescope at the apex of the cone (in truth, telescope beams are only roughly circular, so the shape of the cone is very complex, but for the purposes of this discussion this detail is unimportant). The angle of the apex of the cone, which is positioned at the telescope, is the beam size itself. The telescope is sensitive to a bandwidth, translated into a redshift velocity range, and thus a distance range, which describes a frustum of the cone. The limits of this bandwidth, and the volume of the cone surveyed, can usually be determined by the observer, within the confines of the desired redshift velocity resolution and the hardware limitations of the telescope site. Obviously, the larger the bandwidth range, the more volume of space the instrument will scan. However, in addition to the total velocity range we want our instrument to cover, we must consider the velocity resolution we desire within this range. To cover large bandwidths, 21cm telescopes send signals to multi-channel auto-correlation spectrometers. Each channel in the correlator covers a fraction of the total bandwidth - all flux within that bandwidth is integrated within the channel. The velocity resolution of the instrument is the width of each channel, which is normally set at the discretion of the observer. The total velocity coverage is determined by this channel width multiplied by the total number of channels available. It is desirable to have the largest number of channels in the correlator possible, as this will allow us to set the necessary resolution, and cover the maximum velocity range.

What sort of velocity resolution do we want? In a situation analogous to spatial resolution, we have no need for "over-resolving" our sources in velocity. The more the signal from a source is split up into frequency channels, the more likely it will be that it is obscured by the noise levels in each channel. However, extracting some internal velocity information from objects we detect is desirable, as it will help us to compute dynamic masses, and it yields some morphological characteristics. In addition, we don't

wish to under-resolve the narrowest objects we detect, because we will lose S/N if channels are wider than signals. Ideally, we would like a velocity resolution which is slightly smaller than the narrowest, weakest HI source we expect. The dwarf/HI cloud objects, with $\Delta v \cong 30$ km/s are the narrowest signals we are anticipating, so a velocity resolution smaller than that value would be best.

Essentially three classes of instruments are available for 21cm observations. These are: telescope array instruments such as the Very Large Array and Westerbork arrays, where large numbers of telescopes are used to create synthesis images of sources; "small" single dish telescopes such as the (late) Green Bank 300ft (95m), the Green Bank 140 ft, the future Green Bank Telescope (GBT), or the Effelsburg 100m instrument; and "large" single dish telescopes, only one example of which exists - the NAIC 305m telescope at Arecibo, Puerto Rico.

A fair way to decide which of these instruments is best for an atomic hydrogen search is to compare the amount of time a model survey each would take to obtain the same S/N values with our three object types as targets. The survey time and S/N can be computed using the known qualities of each telescope, and those of the objects.

For observations with a single-dish instrument, a simplified model of the signal-to-noise will have two regimes: where the target galaxies are resolved, and where they are unresolved. Which of these regimes each of our three types of objects (dwarf, normal, and extended galaxies, described above) falls into for a particular telescope is determined by the beam size of the telescope, which is inversely proportional to the telescope diameter, and the angular size of the object, which is proportional to the size of the object and inversely to its distance from the Sun. For simplicity, we will use the Green Bank 300 ft telescope as a "typical" small single-dish telescope to compare to the Arecibo 305m, the only large single dish telescope available. Green Bank's beam at 21cm had a diameter of 10', while Arecibo's is 3.3'. From the radius r of an object, we can compute the distance D at which it will make the change from the resolved to the unresolved regime when viewed by a telescope's beam with an angular size α . Maintaining the units we have been using so far:

$$D(Mpc) \cong 7.076 \cdot \frac{r(kpc)}{\alpha(arc\,min)} \qquad (2.5)$$

The distances at which the transition takes place will then be 1.1 Mpc for dwarf objects, 7.1 Mpc for normal galaxies, and 17.7 Mpc for extended objects using the Green Bank telescope. Using Arecibo, the distances will be 3.2, 21.4, and 53.6 Mpc for dwarf, normal, and extended objects respectively. Due to interference from atomic hydrogen in the Milky Way, extragalactic distances of less than 2 Mpc cannot effectively be observed at 21cm, so the Green Bank telescope will not be able to resolve the dwarf objects. The resolution of the VLA in D-array is 45 arc seconds, which will mean that it can resolve the dwarf objects below 13.0 Mpc distance, normal galaxies at 87.0 Mpc distance, and extended objects out to 218 Mpc distance.

We can calculate the relative S/N generated for each type of object observed by each type of telescope in an HI survey in both the resolved and unresolved regimes. For an unresolved source the signal S will be:

$$S \propto d^2 \cdot t \cdot S_{\Delta v} \qquad (2.6)$$

where d is the telescope diameter (or in the case of the VLA, the diameter of a fictitious single-dish telescope with the same collecting area), t is the integration time, and $S_{\Delta v}$ is the flux from the object in a single velocity channel. For comparison purposes, we can assume that our velocity channel widths match the narrowest velocity widths of our target objects - the dwarf objects with Δv = 30 km/s. From the atomic hydrogen mass of each object type, we can then estimate the flux in each channel as:

$$S_{\Delta v} = \frac{1}{2.36 \times 10^5} \cdot \frac{M_{HI}}{D^2} \cdot \frac{30}{\Delta v} \qquad (2.7)$$

Where M_{HI} is the mass of the object in solar masses (M$\odot$), Δv is the object's velocity width in km/s, and D is its distance in Mpc. The noise for an observation will be:

$$N \propto T_{sys} \cdot \sqrt{t} \tag{2.8}$$

Where T_{sys} is the system temperature and t is again the integration time. Using all of the above information, we can then estimate S/N in the unresolved regime:

$$\frac{S}{N}(unresolved) \propto \frac{d^2 \sqrt{t}}{T_{sys}} \cdot \frac{M_{HI}}{D^2 \cdot \Delta v}. \tag{2.9}$$

The key to detecting objects in an HI survey is obtaining a particular S/N level. If we assume we have a desired S/N value, we can solve the above equation for the amount of observing time required to obtain it:

$$t_{S/N}(unresolved) \propto \left(\frac{S}{N}\right)^2 \cdot \left(\frac{T_{sys}^2}{d^4}\right) \cdot \left(\frac{D^4 \cdot \Delta v^2}{M_{HI}^2}\right). \tag{2.10}$$

In the resolved regime, the time required to survey an object (with multiple beams) will also depend on the fraction of an object's area on the sky which the beam is covering:

$$t_{S/N}(resolved) \propto \left(\frac{S}{N}\right)^2 \cdot \left(\frac{T_{sys}^2}{d^2}\right) \cdot \left(\frac{D^2 \cdot \Delta v^2}{M_{HI}^2}\right) \cdot \left(\frac{object\ area}{beam\ area}\right). \tag{2.11}$$

The beam area is inversely proportional to the square of the instrument size d, and the object area is inversely proportional to the square of its distance D. Using these factors in the above equation yields:

$$t_{S/N}(resolved) \propto \left(\frac{S}{N}\right)^2 \cdot \left(\frac{T_{sys}^2}{d^2}\right) \cdot \left(\frac{D^2 \cdot \Delta v^2}{M_{HI}^2}\right). \tag{2.12}$$

In the unresolved regime, the integration time required to obtain a given value of S/N will be proportional to D^4, while in the resolved regime it will be proportional to D^2.

Before we can do a fair comparison of our three telescopes, we must consider the total amount of time each would take to survey a large region of the sky with the same velocity resolution and same total bandpass, with the same S/N values for each of our object types. The amount of time required to survey an area will be inversely proportional to the sky coverage of each telescope (a 3.3' diameter area for Arecibo, and a 10' diameter area for Green Bank). The sky coverage of a single dish instrument is the same as its beam area. However, because it synthesizes a map of a large region (30' in diameter - roughly 83 Arecibo beam areas) of the sky with each integration, the VLA is more efficient at sky coverage. On the other hand, the bandpass coverage of the VLA is only about a fourth of that of Arecibo or Green Bank (which are nearly identical). If we define a quantity A to be the sky coverage of each instrument, and dV to be its bandpass, we can generate an equation for the relative time it would take a telescope in the process of a survey to observe an object in the unresolved regime:

$$t_{Survey}\,(unresolved) \propto \left(\frac{T_{sys}^2}{d^4 \cdot A \cdot dV} \right) \cdot \left(\frac{D^4 \cdot \Delta v^2}{M_{HI}^2} \right) \tag{2.13}$$

and the resolved regime:

$$t_{Survey}\,(resolved) \propto \left(\frac{T_{sys}^2}{d^2 \cdot A \cdot dV} \right) \cdot \left(\frac{D^2 \cdot \Delta v^2}{M_{HI}^2} \right) \tag{2.14}$$

Note that in both of these equations we have dispensed with the dependence on S/N, since we wish to compare the time required for a same-S/N survey.

For the three telescopes, we use values of T_{sys} of 25K, 35K, and 33K for Green Bank, Arecibo, and the VLA respectively. For Green Bank we use a diameter d = 300ft. Arecibo has an effective diameter of d = 700ft. The VLA we give an equivalent diameter of d = 420ft.

In Figure 2.1, we plot t_{survey} for each of the three telescopes observing each of the three model objects to obtain the same S/N. On the x-axis is the $\log_{10}$ of distance to each target galaxy in Mpc, and on the y-axis is the $\log_{10}$ of the survey time. Survey times for the VLA are drawn with dashed lines, those for

Arecibo are solid lines, and those for Green Bank are dotted lines. The nine transition points between the unresolved (high distance) regime where $t_{survey} \alpha D^4$ and the resolved regime where $t_{survey} \alpha D^2$ for each telescope and each object type are labeled as "telescope-object" (i.e. "Arecibo-normal" for Arecibo observing a normal galaxy).

Because we are using a model, the transitions between the "resolved" and "unresolved" regimes for each object type and telescope are very sharp. This would be the case if the column density of atomic hydrogen in a galaxy was uniform over the galaxy's sky coverage. However, because HI is usually centrally concentrated in galaxies, the transition between the resolved and unresolved regimes will be "softened" somewhat in reality. On Figure 2.1, this softening would manifest itself as a curved transition rather than the sharp corners presented.

Our model of t_{survey} has been computed to take into account the sensitivity, spatial and velocity coverage for each telescope in a survey application. Because an HI survey will have a limited amount of telescope time, and the desire is to cover the maximum volume, this is the most efficient way to fairly compare the instruments. It would not be the proper way to assess the efficiency of the individual instruments in observations of a particular object, however.

Figure 2.1 is a little difficult to interpret. One thing which is clear immediately from the plot is that all three telescope types have their strengths and weaknesses. Green Bank clearly requires smaller t_{survey} values for all object types when they are most nearby, while the VLA has the lowest survey times for the most distant objects. Arecibo dominates the medium-distance objects in all categories. Green Bank performs best whenever it can resolve objects, because of its low system temperature. However, it can not resolve objects out to very large distances. In the case of dwarf galaxies, Green Bank is only in the resolved regime at distances where confusion with the emission of the Milky Way would make observations impossible.

In deciding which instrument is best suited for an atomic hydrogen survey, we must consider the redshift velocity ranges we expect to search. Because the mission of the slice search is to find unknown extragalactic objects at 21cm in numbers large enough to allow meaningful statistical interpretation of

them, we wish our search to scan the largest possible volume of space where we are sensitive to each of our categories of objects. This will both guarantee that we find as many things as possible, and maximize our chances of finding anything at all. Unfortunately, being sensitive to our three categories of objects requires the slice search to scan completely different volumes of space. The dwarf/HI cloud class of objects have very low HI masses, and very small sizes. As Figure 2.1 shows, these compact objects will be resolved by all telescope types at only very short distances from the Milky Way. At distances beyond which they are resolved, the time required to detect them goes up sharply. Because the volume of space searched scales as the cube of the distance to which the search is sensitive, the volume coverage of scans which can easily detect these small objects will be small. On the other hand, extended HI sources can be resolved by some telescopes even at very high redshift velocities. Because the detectability of resolved objects is determined by an HI surface brightness, which is independent of distance, the volume coverage of a search for these large objects could be very efficient, since very distant regions could be scanned without losing sensitivity.

Figure 2.1 shows us that all telescopes are at their best when observing normal galaxies, an observation which should perhaps generate a caution in our minds. It is probably no mistake that these telescopes are all tuned to respond to the most "typical" galaxies. But are these galaxies truly the most typical, or are they those which are typically found because they are easy to observe?

The Arecibo telescope was used for the slice search. Because of the importance of detecting dwarf-like objects, our search must cover nearby distances, ideally those just beyond the interference of the Milky Way. At these distances, Arecibo is the most efficient survey instrument for dwarf objects. The VLA is more efficient at scanning for dwarfs beyond distances of roughly 5 Mpc, but at all distances its sensitivity is never as high as that of Arecibo below 5 Mpc, and we would like to be able to detect the smallest possible HI sources. Because it can only resolve dwarf objects at distances where interference from atomic hydrogen in the Milky Way would make detections impossible, Green Bank in all cases is an inferior instrument for dwarf searches. Beyond the short distance sensitivity to dwarfs, we needed a telescope with the highest chance of detecting normal and extended objects over the rest of the search range. Current

VLA bandpass limitations restrict broad band coverage, but Arecibo can cover out to ~100 Mpc in a single spectrum.

Choosing a Search Region

Because a complete search of the whole of extragalactic space is plainly impractical, the slice search must scan a "representative" volume of space. If detections within this volume are numerous enough, then statistical arguments may be made to extrapolate the results to the whole of extragalactic space. Obviously the careful choice of this representative volume is critical for the success of this strategy.

What do we want this "representative" volume to contain? Clearly, since we do not know exactly what we are looking for, nor do we know where we will find it, it would be best to span the whole variety of extra-galactic environments. The better we can do this, the more meaningful our statistical arguments will ultimately be. Locally (i.e. the volume of space within a radius of 100 Mpc of the Milky Way), the variety of extragalactic environments includes dense clusters of galaxies such as Virgo, weaker galaxy concentrations like the Local Group, superclusters containing both, "filaments" and "walls" of connected superclusters, and the void regions in between. It would be best to sample all of these different regions to some degree. A most illustrative way of doing so would be to completely sample a continuous, connected volume which contained all interesting environments, as it would allow us to examine not only the environments themselves, but the space which marked the "transitions" between them. As our definitions of extra-galactic environments are based primarily on detections of galaxies by optical means, we cannot be sure that these same environments will be important, or even detectable, in a study conducted wholly on the basis of HI emission.

An advantage to a continuous, connected search volume is that it would make it easier to recognize the presence and nature of extended HI objects. Some previous HI searches have used a "pencil beam" approach, which involved many scattered single integrations at discontinuous positions on the sky. The nature of objects larger than the beam size would not be appreciated in a pencil beam search. To remain unbiased, the region we scan must be searched "blindly", that is, completely uninfluenced by what is thought to be there. Other previous HI searches have targeted specific environments, such as "clusters" or

39

"voids". While able to tackle particular questions, such as the relative number of unseen dwarfs in cluster and void environments, by restricting themselves to these regions, the researchers are allowing themselves to be influenced by the structure of the Universe as seen through optically prejudiced previous knowledge. An arbitrary grid search pattern based on our terrestrial coordinate systems is superior to one influenced by any perceived knowledge of the area. It is vital that we sample all environments without bias using the same procedure.

The specific location of the slice search was determined in a large part by the choice of Arecibo as a telescope. At we discussed earlier, there is really no problem with this, as any patch of the sky is as good as any other for a blind 21cm search. With Arecibo, we are limited to integrating on positions within $10°$ of zenith if we are to achieve maximum S/N. Higher zenith angles than this can lead to considerable background noise as the illumination pattern begins to pick up ground emission beyond the edge of the dish which causes higher system temperatures and loss of gain (although the recent addition of the "ground screen" around the Arecibo dish has expanded the range of low-noise zenith angles, as we found in some of our follow-up observations). Arecibo's latitude is roughly $18°$, so we are limited to declinations between $8°$ and $28°$. To allow some flexibility in the observations, we may want to observe objects within roughly half an hour of transit, so we are limited more realistically to declinations between $11°$ and $25°$. Objects outside these declination ranges would simply not be within our zenith limitations for long enough to make observing them practical. Further, we want to avoid declinations too close to the telescope's latitude because the telescope cannot slew rapidly enough to keep up with source motion within about $3°$ of zenith. To reduce the number of days over which observing time is spread, our search region needs to stretch over a much greater range in right ascension than in declination. We chose to limit ourselves to a span of a single degree in declination - and for reasons which we will go into in a moment, we picked $23°$ to $24°$.

Within the chosen range in declination, we next had to choose a range in right ascension. Because we expected the slice search to make detections which we would wish to study at other wavelengths (particularly optical wavelengths), we wanted to scan a region well out of the plane of the Milky Way,

where there would be minimal Galactic interference to these wavelengths. Another consideration which could only loosely claim to have astronomical value also led us to pick high Galactic latitudes. At the time of our application for time at Arecibo, the telescope was under considerable proposal pressure by research groups searching for pulsars within the Milky Way. These searches concentrated on the Galactic Plane, as most pulsars were thought to be closely bound to the galactic disk. Furthermore, time for extragalactic studies in the Virgo region (~9-16 hours) was still heavily sought, while the Pisces-Perseus region (~22-4 hours) had been largely "exhausted" by previous studies. To maximize our chances of being awarded observing time, we wished to avoid competing with these other groups. As it turned out, during the normal turn-over time between the submission of our proposal and the actual observing, there was great excitement about the discovery of several pulsars at high Galactic latitudes, so suddenly the time away from the galactic plane was sought by pulsar groups as well. In the end we were awarded time which allowed a search range in RA from roughly 22 00 hours to 04 00 hours.

The specific limits in right ascension and declination of this region were picked because it allowed us to search an area which included parts of the Pisces-Perseus supercluster, the optically bright members of which have been well studied by Haynes, Giovanelli, and others. These studies further provide us with a data base of accurate HI and optical measurements with which we can assess the ability of the slice search to detect objects with known properties. If it is well-designed, the slice search procedure should easily be able to flag these large objects as detections. When it does detect them, the flux measurements it obtains for the known objects can be compared to those of the previous studies to establish our accuracy.

The third dimension of the slice search volume, redshift velocity, was chosen to encompass regions as nearby as possible and volumes known to contain voids and clusters. The velocity resolution of the survey was chosen based on the narrowest velocity-width objects we expected to encounter - roughly 30 km/s. To extract some velocity dispersion information out of objects of this size, we need a velocity resolution of about 15 km/s. While this will over-resolve these narrow objects, causing their total signal strengths to be divided among multiple channels, summations may be done of adjacent velocity channels to simulate larger velocity widths and prevent any loss of signal-to-noise.

Using the Arecibo telescope, we are given 2048 correlator channels to deal with. Since we are collecting both polarizations of the incoming signal, we must use half the channels for each. The polarizations will be combined to increase our signal-to-noise. We are then left with 1024 divisions which can be applied to our chosen velocity range to obtain our velocity resolution. To obtain a velocity resolution of 16 km/s after Hanning smoothing, we use 8 km/s wide channels. This provides us a velocity range of roughly 8000 km/s over our 1024 channels, which is the largest practical bandpass at Arecibo in any case because of limitations of the 21cm feeds.

Where would it best to put this range? We know that we want to span as large a range of extragalactic environments as possible. Although we have continually made the point that our search should be blind to what is known about the space we are scanning, perhaps we should take a look at what the local extragalactic region looks like within the RA and DEC bounds we have chosen. In Figure 2.2, we have plotted the contents of this region as seen by the RC3. All objects between 22 00 and 03 30 hours RA and 18° and 28° DEC have been plotted by their coordinates and redshift velocities. From this plot, some of the structure of this piece of the Universe can be seen easily. Locally, out to about 2000 km/s redshift, there is a collections of objects which can be considered part of the local supercluster. Beyond that, very large structures exist at about 5000 km/s - the Pisces-Perseus supercluster complex. Between these large collections of galaxies are largely empty regions - voids.

In the slice search, we made the decision to anchor the low end of our velocity range at roughly 200 km/s (slightly above 0 km/s to avoid the interference of atomic hydrogen in the Milky Way). While at some level the choice of a low-velocity range is lowering the total volume of our search, we felt it important to be sensitive to the smallest atomic hydrogen masses possible. The high-velocity end of our search will then be at around 8400 km/s, extending well beyond the supercluster structures, sampling what is between us and them, and what is beyond them.

At Arecibo, we are given three 21cm feeds to choose from. The single polarization "flat" feed has the lowest sidelobes of the three, making it the best "mapping" instrument since it will pick up less emission far from the position it is pointing. However, the two "circular" feeds, the 21cm and the 22 cm, are both

dual polarization, and each polarization has a higher gain. Finally, the Arecibo feeds have a declining sensitivity centered around a "tuned" frequency, so that we finally settled on the 22 cm feed focused at a redshift velocity of ~5000 km/s. By tuning to the higher end of our velocity range, we balanced our loss of sensitivity with redshift to some degree.

Observing Method

The nature of a search for unknown HI sources makes it quite different from normal 21 cm observations. A conventional observation of an HI source will involve pointing the telescope "on" the position of the source, that is where the source is known to be, for some integration time, then pointing the telescope "off" the source, that is, where the source is known (or thought!) not to be, for the same integration time. The "off" scan is subtracted from the "on" scan to produce a final spectrum with a good baseline - individually the on and off spectra have very non-flat baselines. However, most of the deviations of the baselines from "flatness" are due to variables within the telescope itself. These can be made the same, or nearly the same, in both the on and off scans by making the conditions under which each is observed as similar as possible. In particular, it is best if both scans are observed with the telescope at the same physical position - the same azimuth and elevation.

In a search for unknown HI sources, conventional on-off procedures are ineffective, simply because a signal is as likely to be found in the off scan as it is in the on scan. A signal in the off scan position would show up as an "absorption" (i.e. negative) feature in the final subtracted spectrum, and could be discovered this way, however such a procedure would be requiring the conditions under which detections were found in the two scans to be different. In any case, a blind search can be conducted in such a way that no time is spent observing "off" scans at all. As we shall see in detail in the next chapter, a blind search can generate low-noise off-scans by summing groups of on-scans which were observed with the telescope at similar azimuth and elevation. This is a very time-efficient way to do observations. In conventional on-off observations, the final signal-to-noise is proportional to the inverse of the square root of the integration time of the two scans (which are generally equal) added in quadrature:

$$S/N \propto \left(\frac{1}{T_{ON}} + \frac{1}{T_{OFF}} \right)^{-\frac{1}{2}} = \frac{\sqrt{T_{ON}}}{\sqrt{2}} \, (\text{for } T_{ON} = T_{OFF}). \qquad (2.15)$$

The total amount of telescope time required for this observation is $T_{ON} + T_{OFF} = 2T_{ON}$. If, on the other hand, we use N on-scans to produce a summary off-scan, the telescope time required to observe each position would be simply T_{ON}, and the signal-to-noise would be:

$$S/N \propto \left(\frac{1}{T_{ON}} + \frac{1}{N \cdot T_{ON}} \right)^{-\frac{1}{2}}. \qquad (2.16)$$

If N is large enough, the noise contributed by the summary off-scan will be negligible, and:

$$S/N \propto \sqrt{T_{ON}}. \qquad (2.17)$$

We can then compare the S/N obtained using the same amount of telescope time using each method:

$$\frac{S/N_{Summary\ OFF}}{S/N_{Conventional\ ON/OFF}} = \frac{\sqrt{2 \cdot T_{SUM}}}{\sqrt{T_{CONV}/\sqrt{2}}} = \sqrt{\frac{4 \cdot T_{SUM}}{T_{CONV}}}. \qquad (2.18)$$

The use of the summary off-scan is four times faster than conventional on/off procedures (two times faster if we count the off scan)..

<u>Previous HI Searches</u>

A number of studies have scanned extragalactic space for unknown atomic hydrogen sources. These have used a variety of techniques, and have met with varying levels of success. These previous searches are of two types:

1. There have been a small number of true "deliberate" 21cm searches performed over the years. These studies have generally been inspired by the same problems and questions which form the motivation for the slice search. They have used a number of different strategies to attack sometimes different

specific goals. In general, they have met with limited success, either in detecting large numbers of new objects, or in establishing very meaningful limits to the numbers of such objects which are possible. Most have been either too low in sensitivity or too small in scope, or both. We will discuss each in detail so that we may learn from them.

2. In addition, there have been a far greater number of "non-deliberate" searches for atomic hydrogen. We can treat the off scans of previous 21cm observations as a very large-scale data base of searches of "unoccupied" extragalactic space. 21cm redshift surveys of galaxies usually scan large ranges in redshift velocity, and stand a good chance of encountering signals beyond those of the targeted objects. While much larger in number and spatial coverage than all of the deliberate HI searches, these non-deliberate searches are difficult both to compile, and to interpret. However, by their sheer numbers, they have probably had better success than the deliberate searches at detecting new objects. The M96 Ring and the Giovanelli and Haynes object are both examples of spurious atomic hydrogen detections in 21cm off scans. We are not able to provide a comprehensive list of all such observations, simply because there are too many (for a reasonably good compilation, the HI catalog of Huchtmeier and Richter contains the most complete list of extragalactic 21cm observations available). However, we will examine some of the larger studies, and the particular results they generated which are of interest to us - detections of unknown extragalactic objects.

Table 2.1 contains a comparison of all of the specific searches we will discuss, both "deliberate" and "non-deliberate". Search numbers and names on Table 2.1 match those which are used in the text. For each search we include the information pertinent to establishing its effectiveness: (2) the telescope used - smaller telescopes generally mean greater volumes of space covered, but with lower sensitivity; (3) the velocity range covered - larger velocities greatly increase the volume of space covered, but at higher velocities the lower limit on the total HI emission of a detectable unresolved source is larger; (4) the number of positions on the sky scanned in the search; (5) the velocity resolution - an "unresolved" source with all its flux in one channel provides little information for mass determinations, and can be diluted by noise if the channel spacing is larger than the source's velocity width; (6) the r.m.s. noise per channel -

basically a measure of the sensitivity of the search, normally a 5 x r.m.s. signal indicates the "sensitivity", although this is an incomplete description of the detection limit as we shall discuss in later chapters; and (7) the total volume of space covered by the search. The total volume of the search V is derived from the beam size β, the limits on the redshift velocity range v_{MAX} and v_{MIN}, the Hubble Constant H_o (we are using a value of $H_o = 75$ Mpc/km/s), and the total number of positions searched N_P, as follows:

$$V = N_P \cdot \frac{\pi}{3} \cdot \left[\tan(\beta) \right]^2 \cdot \left[\frac{v^3_{MAX}}{H_o} - \frac{v^3_{MIN}}{H_o} \right] \qquad (2.19)$$

The computed volumes are in units of $Mpc^3 h_{75}^{-3}$, where h_{75} is the ratio of the true Hubble constant to 75km/s/Mpc. The final column (8) contains the number of "new" objects detected - this number does not include previously cataloged objects which were encountered, or ones in optically obscured regions of the sky. All of the values in Table 2.1 were taken directly from the cited papers, unless otherwise noted in the text below.

In addition to the information in the table, a comparison of the mass sensitivities of the searches is vital to understanding them. In Figure 2.3, we plot the sensitivity of each deliberate search to particular HI masses, and the volume of space over which the search was sensitive to them. All searches are sensitive to a wide range of HI masses, some of them theoretically able to detect some very low-mass objects. However, since any search can detect the smallest masses in only the most nearby regions of its redshift velocity range, and because of the dependence of search volume on the cube of the distance means that relatively tiny volumes will really be searched for these objects, the chance of detecting them is relatively small. There is also a minimum distance of ~2 Mpc imposed by confusion with atomic hydrogen in the Milky Way. In plotting the volume of sensitivity, the figure is showing the relative "odds" that the different searches have of detecting objects of different masses (without factoring in the relative abundances of different mass objects).

In compiling Figure 2.3, we have had to make a number of assumptions about the nature of extragalactic objects, and the searches themselves. On the x-axis is plotted the $\log_{10}$ of the HI mass in

solar masses. On the y-axis is the volume over which each search is sensitive to different HI masses. The quantities on both axes of the plot are functions of the redshift velocity ranges of the specific HI searches. At a particular redshift velocity, there is a minimum HI mass which a search is sensitive to. Within the range of redshift from the low end of the search up to that velocity, the search is sensitive to that HI mass. The minimum HI mass detectable at a particular redshift velocity is computed as follows.

To begin with, we assume that the 21cm signal from an object must be at the 5-sigma level to be detectable. That is, it must be as strong as five times the r.m.s. noise level in an individual velocity channel. This 5-sigma limit would apply to averages of neighboring channels as well. However, when neighboring velocity channels are averaged, their noise level goes down by the square root of the number of channels. If the noise level in individual velocity channels is σ_1, then the noise level in an average of N adjacent channels would be:

$$\sigma_N = N^{-\frac{1}{2}} \cdot \sigma_1 \qquad (2.20)$$

To be detectable, the integrated flux from an object filling N channels with velocity width Δv_1 must be:

$$\int S \cdot dv \; > \; 5 \cdot \sigma_N \cdot N \cdot \Delta v_1 = 5 \cdot \sigma_1 \cdot \Delta v_1 \cdot N^{\frac{1}{2}} \qquad (2.21)$$

The number of velocity channels, N, is simply the velocity width of the object, ΔV, divided by the channel velocity width, Δv_1. The limit on the integrated flux then becomes:

$$\int S \cdot dv \; > \; 5 \cdot \sigma_1 \cdot \Delta v_1^{\frac{1}{2}} \cdot \Delta V^{\frac{1}{2}} \qquad (2.22)$$

We know the HI mass of an object which would produce this minimal signal:

$$M_{HI} = 2.35 \times 10^5 \cdot D^2 \cdot \int S \cdot dv \qquad (2.23)$$

Folding in the value for integrated flux, we can solve for the maximum distance at which an object of a mass M_{HI} would be detectable:

$$D_{MAX} = \left[\frac{M_{HI}}{1.175 \times 10^6 \cdot \sigma_1 \cdot \Delta v_1^{1/2} \cdot \Delta V^{1/2}} \right]^{\frac{1}{2}} \qquad (2.24)$$

The volume within which a search will be sensitive to an object will then be:

$$V = N_P \cdot \frac{\pi}{3} \cdot \left[\tan(\beta) \right]^2 \cdot \left[D^3{}_{MAX} - D^3{}_{MIN} \right] \qquad (2.25)$$

where N_P is the number of search points, β is the telescope beam size, and D_{MIN} is the minimum distance scanned by the search (determined by the low end of its redshift velocity range).

To produce the entries in Figure 2.3, the volume in which each search was sensitive to our three model object types - dwarf, normal, and extended galaxies, was computed. Volumes for objects with intermediate characteristics were extrapolated from these three data points, and cut-offs were applied at the redshift velocity limits of each search and at the 2 Mpc minimum distance limit imposed by the Milky Way. For comparison, a curve representing the slice search is included as a dashed line.

Using Figure 2.3 and Table 2.1, we can now do a point-by-point comparison of the different HI searches.

Deliberate 21 cm Searches

The following is an itemized list of all deliberate HI searches which have been performed. Often, they were targeted toward detecting objects having specific characteristics, or located in particular extragalactic environments. On the whole, they have met with limited success, providing us with a few previously unknown objects to ponder, too small in number to make reasonable statistical extrapolations. More often, they have resulted in no detections at all, generating only upper limits to the number densities of unknown objects of various HI masses (depending on the search sensitivity). There have been surprisingly few true HI searches done, perhaps as a consequence of their continuing failure to generate many detections. Although much can be learned from a study which generates upper limits, they can

certainly be discouraging for the researchers involved, and rarely inspire follow-up work. All of these searches are important for us to look at, as they can tell us to some extent what to do, or what not to do, if we wish to be successful. We present the searches chronologically.

In 1973 and 1974, Shostak, Davis, Roberts, and Condon (Shostak, 1977) used the NRAO 91m telescope in a complex series of 21cm emission and absorption studies to search for unseen galaxies in "blank sky" regions. Two "drift-scan" emission studies were done, generating 5000 spectra. A third emission study comprised the "comparison" fields of another study of bright galaxies. Drift scans involve pointing the receiving instrument at a specific azimuth and elevation, and letting the rotation and orbit of the Earth change the RA and DEC of the observations. While efficient at scanning large areas of the sky, this search method has a low limit to the amount of integration time it can spend on any one object. This integration time can be approximated by the time it would take a particular position to drift through one telescope beam width (in the case of the Green Bank 91m, the 21cm beam width is ~10 arcmin, which passes in $40 \times \cos(\delta)$ seconds). Shostak and Davis performed somewhat unorthodox drift scans, keeping declination fixed in one set, and Galactic latitude fixed in the other. As "off" scans for these drift observations, either fields one degree away, or of a program galaxy, or fields observed ten scans apart were used for subtraction. The fields for the "comparison" observations were simply the locations of off scans from observations of bright galaxies performed for a different study. These are similar to the type of observations which we have discussed in relation to HI surveys (non-deliberate HI searches). Shostak and Roberts searched for objects in these positions by examining the locations of what appeared to be "absorption features" in the subtracted spectra of the original observations. In addition, Shostak and Condon conducted a search for absorption features at the positions of 50 strong quasars. All of this effort generated only one confirmed detection (found in one of the drift scans), although the low redshift velocity (-400 km/s) of this object suggests that it might be a high velocity cloud, and not extragalactic at all. For the most part, this was a good search, and its lack of success can be attributed to both its low sensitivity and its small search volume. Its choice of search regions was good in that most were unaffected by any prior notions of their content. The use of drift scans almost requires an arbitrary choice of observing

region (at least on the small scale), although the use of off-scans (which were 1° away from the on-scans) examines regions which shadow the locations of bright objects, and may have unclear systematic biases. This is a common problem, as we shall see in the section on "non-deliberate" HI searches. Observing the positions of a random set of quasars, since they are distant background objects, should involve no bias towards any particular (foreground) extragalactic environment.

Also in 1973, Mathewson and Cleary (1974) used the 18m telescope at the Parkes Observatory of CSIRO to do drift scan observations in the vicinity of the Magellanic Clouds. They were deliberately searching regions of very local extragalactic space, in redshift velocity ranges between -340 and +380 km/s. In addition to a number of HI clouds, they discovered a structure which arcs through 180° of the sky, which they called "the Magellanic Stream". Work at such low redshift velocities is at the very border of what can be considered "extragalactic", as most of what Mathewson and Cleary found can be considered simply part of the complex outer structure of the gas halo of the Milky Way, and the medium in and around its nearest neighbors. This work inspired a number of other searches for similar objects, which will shortly be mentioned.

Lo and Sargent (1979), using the OVRO 40m and Bonn 100m telescopes, searched regions around three nearby groups of galaxies and found four low surface brightness dwarf galaxies at 21cm, two of which had not been previously cataloged. All detections were made using the Bonn telescope. This search was meant to examine the possibility that HI clouds of the type found by Mathewson and Cleary were commonplace objects in galaxy groups. While the four objects they found had characteristics, such as mass and size, similar to those expected for HI clouds, they also had optical emission, and thus were classified as dwarf galaxies. The sensitivity of the Bonn telescope search was a factor of ten better than that of the OVRO telescope. While unbiased within these regions, their search was clearly restricting itself to scanning extragalactic environments known to be dense with optically bright objects.

Another search for HI clouds in groups of galaxies was performed by Materne, Huchtmeier, and Hulsbosch (1979) using the Dwingeloo 25m telescope. The positions of a few suspicious signals were re-observed using the Bonn 100m for greater sensitivity. This study found no objects of interest, but

generated upper limits to the masses of possible objects of 4.0 and 2.6 x 10^8 M$_\odot$ for the NGC 1023 and CVn II groups respectively.

Once again searching for HI clouds in groups of galaxies, Haynes and Roberts (1979) used the Green Bank 140 ft telescope. They found nothing in all but one of their target galaxy groups. However, within the Sculptor group, they found an impressive total of 30 HI clouds, distributed over a somewhat wider area than the detections by Mathewson and Cleary. Using these data, it was possible to set an upper mass limit of 10^8 M$_\odot$ on HI clouds in all of the observed galaxy groups. All of these searches in galaxy groups were inspired by the success of Mathewson and Cleary, and all may suffer from a bias toward a specific extragalactic environment - galaxy groups. In addition, because of the low redshifts of all of the objects involved, it is unclear whether any of the detections in Sculpter, either by Mathewson and Cleary or Haynes and Roberts, are truly extragalactic objects.

Another search for HI clouds, this time in the Virgo cluster using the Arecibo 1000 ft telescope in a drift-scan mode, was performed by Wetherill, Sullivan, and Heckman (1980). It turned up nothing, and was able to set an upper mass limit of 10^9 M$_\odot$ for unseen HI clouds in and around the Virgo cluster. Only an abstract was published, so the values for the parameters are uncertain. From the listed information, we estimate the values listed in Table 2.1.

As part of an enormous HI survey to find the redshifts of known galaxies (which appears in the list of non-deliberate searches), Fisher and Tully (1981) undertook a search for invisible galaxies in the M81 group. The NRAO 91 m telescope was used for this search, covering a redshift range of -300 to 1300 km/s with 22 km/s velocity resolution. Within this region, masses of $M_{HI} > 3 \times 10^6 D^2$ M$_\odot$, where D is in Mpc, would have been detected. No objects of interest were found.

In 1983, Krumm and Brosch (1984) searched two void regions in Perseus and Hercules for large HI clouds. They suspected that voids might be the most likely locations for non-luminous HI clouds, as tidal forces in more densely populated regions would disrupt such structures. Drift scans through several lines of constant declination were used to search each void, with spectra being produced every twenty seconds. As off scans for each spectrum, an average of four spectra on either side of the "on" (not including

immediate neighbors) was used. Their search covered an enormous volume, but it had fairly poor sensitivity, and no HI sources were detected.

Kerr and Henning (1987) performed a truly "blind" 21cm search of two regions, one in the zone of avoidance, and one in an area of the sky clear of the galactic disk. These were test projects used to determine the effectiveness of 21cm searches in the zone of avoidance. Using the Green Bank 91m telescope, they covered comparatively large volumes, with good sensitivity, in both cases. Beyond the requirement that one be in and one be out of the zone of avoidance, the two search regions were chosen in an essentially arbitrary manner, uninfluenced by their extragalactic content. In the zone-of-avoidance survey, they detected 16 galaxies, only one of which was previously cataloged. The profiles of these objects showed that 9 were typical spirals, and the rest were dwarfs and irregulars. In the positions less affected by foreground dust, they encountered 11 galaxies, 7 of which had been previously cataloged. For our purposes, the remaining four detections are the most interesting, as they demonstrate a fairly high fraction of new detections in a well-studied area. All four objects were visible, but unimpressive, on the POSS plates.

A 1991 search by Weinberg et al. (1991) used the VLA to compare the abundance of unknown HI clouds within "void" and "cluster" regions. Two searches were done, carefully matched in HI mass sensitivity and search volume, one of fields in the Pisces-Perseus supercluster complex, and one in a foreground void. The large collecting area of the VLA achieved the most impressive sensitivity of any search, however its limited number of correlator channels greatly reduced not only its velocity resolution, but the overall volume of space searched. Nevertheless, 10 previously undiscovered dwarf galaxies were detected in the "cluster" volume. There were no detections in the "void" volume. The results of this study not only set limits on the space density of undiscovered objects of different HI masses, but also imply a clear trend of those objects toward cluster locations.

In 1992 Hoffman, Lu, and Salpeter (1992) made a search for HI-rich unseen dwarf galaxies in relatively near-by regions perpendicular to the plane of the local supercluster. They used the Arecibo telescope to point at the positions of a small group of *IRAS* selected galaxies, detecting five previously

cataloged objects and six new objects. All of the new detections appear to be dwarfs, very faint or invisible on the POSS. All are in the vicinity of the bright, previously cataloged galaxies, and upper limits on the space-density of unknown objects in the fore and background voids are set. Like the Weinberg et al. search, this work achieves impressive sensitivity, however the total volume of space it surveys is comparatively small. In addition, the choice of search region is not arbitrary, being targeted at the vicinity of *IRAS* galaxies.

In the most recent search we are aware of, Simpson and Gottesman (1993) scanned a galactic void, a cluster of galaxies, and an "interaction" field (in the vicinity of a field spiral) for HI sources using the VLA. At the time of this publication, not all of the data had been reduced, but one previously uncataloged galaxy had been detected in the interaction field.

Non-deliberate 21 cm Searches

Most single dish HI observations of galaxies require not only integration time on the suspected position of the source, but also equal integration time on "blank sky" - some region, usually nearby, thought to be devoid of HI emission. The blank sky "off" integration is then subtracted from the source "on" to yield a decent baseline. These off scans represent thousands of hours of integration on sky thought to be empty, and together comprise an enormous search for unknown extragalactic HI (there is no such compilation - however the potential is there). Unfortunately, off scans in general are fairly close to the positions of "on" scans, and thus shadow locations, or suspected locations of HI sources. The sum of all such observations could hardly be considered a systematic or unbiased survey. Also, signals in off scans would appear as absorption features in the final spectra, and would tend to be less impressive, both because an emission feature is expected and because such signals are unlikely to be centered in the off scan. In addition, radio interference, which is a major problem at 21cm, has not been carefully monitored so it would be much more difficult (hopeless?) to reject spurious signals in old spectra. In addition to the off scans, large redshift surveys at the positions of optically selected objects have also searched empty regions of extragalactic space, as these surveys usually scan wide velocity ranges. Yet once again, the selection of points is far from random, and chances are good that the observers will automatically

associate emission from any HI source in the velocity range with the visible object. While not a complete list of such observation, Table 2.2 includes a list of some of the largest HI survey studies, including a few which have detected uncataloged objects.

An Ideal Search?

Table 2.1 raises some interesting questions. At first glance, it is not completely obvious why some searches are encountering objects, and others are not. Why have all of the redshift surveys (the non-deliberate category), which have covered immense volumes with impressive sensitivity, encountered almost nothing except the optically detected objects they were looking for? Does this imply that little or nothing remains to be found, and that our HI search will be a waste of time? How can we explain the seeming inconsistencies in the success rates of different searches? For instance, the Krumm and Brosch (1984) survey, which encompassed one of the largest volumes of any search, turn up nothing, when Lo and Sargent (1979) found four objects within a comparatively tiny volume with the Bonn telescope. The answers to these questions may point the way to better search methods.

The low number of unexpected detections in the redshift surveys may indicate the unlikelihood that any objects other than those sought will be found in such studies. The standard procedure in an HI redshift survey is to scan the position of an optically selected object over a wide velocity range (since the redshift velocity of the object is presumably unknown). In this procedure, two positions in space are being searched for HI signals - the "on" position and the "off" position. But we must remember what the purpose of the survey is - to locate a known object in the redshift velocity range. The observers *expect* a detection in the "on" scan, and they *expect* the "off" scan to be empty. Any signal found in the "on" scan will be assumed to be a detection of the object of interest, unless more than one signal appeared in the spectrum. A spurious discovery would thus be misinterpreted. In the "off" scan, a signal would appear as at "absorption" feature in the subtracted spectrum. These negative signals have more of a tendency to be ignored as they are visually less impressive than positive features of the same magnitude (this is a effect easily demonstrated by a few visual tests), and due to the commonness of interference in broad-band HI redshift surveys, which is easy to blame. Despite these drawbacks, the larger redshift surveys have turned

up some interesting new results. Haynes et al. (1988) encountered quite a few multiple signals and unexplained absorption features during a large survey using the Green Bank 91m telescope. The 10 arcmin beam of the 91m can often pick up nearby sources, and many of the signals are probably confused in this way. However, in at least three cases there appears to be the discovery of previously unknown objects. Giovanelli and Haynes (1989a) stumbled across five clearly new objects using the Arecibo 305m telescope, one of which was the "proto-galaxy".

Figure 2.3 can help explain some of the seeming inconsistencies in the success rates of different deliberate searches. The Krumm and Brosch (1984) search had similar sensitivity to that of Lo and Sargent (1979), and encompassed a much larger volume of space. Yet the large volume coverage was achieved by searching a high range of redshift velocities. By scanning distant (high velocity) regions, huge volumes of space can be covered by a single beam. However, emission sources at these large distances must be stronger to be detected, assuming they are unresolved by the beam. By concentrating on high velocities, Krumm and Brosch were restricting themselves to a search for very massive HI sources. In comparison, Lo and Sargent were looking in a very nearby region, and were sensitive to smaller HI masses. All four of the new objects they encountered would have been undetectable if they were at the distances of the Krumm and Brosch search. The difference between the mass sensitivity of these two searches can be clearly seen on Figure 2.3. The HI masses which Krumm and Brosch were capable of detecting are all at the extreme high end of the plot, over 10^{10} M$_\odot$. The detection of an HI mass of this size would have been an impressive find indeed, as very few known galaxies have so much atomic hydrogen. Certainly it is important in any search to cover as large a volume of space as possible, but the trade-off between volume and sensitivity to weak HI sources illustrated by this comparison must be considered.

Two of the most recent deliberate HI searches have achieved much more impressive results. Using the NRAO 91m, Kerr and Henning (1987) covered one of the larger volumes in the table, with impressive sensitivity. Primarily a study of galaxies in the zone of avoidance, this search found 15 previously unknown objects in this region. Of greater interest to us is the "control" experiment which was conducted

in a high-galactic-latitude region. Four new objects were discovered in the area. Weinberg et al. found 10 new dwarf galaxies in galaxy cluster regions in a very high-sensitivity search. Note that the Weinberg et al. search has among the poorest velocity resolutions (column 4) in Table 2.1, and at the same time has very narrow velocity ranges (column 2). These traits, which are shared by the other deliberate search conducted with the VLA by Simpson and Gottesman, are due to the channel limitations of the VLA. As can be seen in the total volumes scanned by each of these searches, these considerably limit the ability of the VLA to scan large volumes of space. Yet both of these searches had detections despite their small volumes because they both were sensitive to very weak signals.

Comparing the slice search, represented by the dashed curves on Figure 2.3, to all other deliberate searches, it is clear that it matches or exceeds all previous efforts in volume scanned for virtually all HI masses. There are a few searches (Hoffman, Lu and Salpeter and Simpson and Gottesman) which scan small volumes for masses below the limit of what the slice search can detect. In addition, the Krumm and Brosch search scanned larger volumes for very HI-massive objects. However, in the ranges between, which include our three "model" galaxy categories, the slice search is covering larger volumes than any search to date.

Another feature of any HI survey, which is not represented on Table 2.1 or Figure 2.3 but is nevertheless important, is the continuity of search locations. Several of the deliberate HI surveys (specifically Shostak, 1977, Krumm and Brosch, 1984, and Weinberg et al., 1991), and all of the redshift surveys, involved pointing the telescope at positions which were not necessarily next to each other. That is, they did not thoroughly scan a continuous region of space. In a blind search, there is statistically nothing wrong with this, if one is comfortable with the implicit assumption that all interesting structure which might be discovered is smaller than the telescope beam. However, we know from our optical catalogs that there appears to be structure on an enormous scale - clusters and voids far larger than the beam of any of the survey instruments. If a survey is to be done, it may be more interesting to completely cover a region of space on the scale of these large structures, and this is best accomplished when search positions are next to each other. Random points in space are useful for bean counting, but they may be

missing the big picture. With this idea in mind, the slice search (as we shall see in the next chapter) is designed to completely cover a region of the sky one degree wide in declination and several tens of degrees wide in right ascension. Being so long in one dimension will allow the slice search to cross many extragalactic environments, and having continuous coverage will allow it to examine not only those different environments but the various stages of the transitions between them.

A problem all of the deliberate searches suffer from is a choice of search region biased by previous optically derived knowledge. Shostak (1977) searched "blank" sky, Lo and Sargent (1979) looked at "groups" of galaxies, Krumm and Brosch (1984) and Kerr and Henning (1987) chose "void" regions, and Weinberg et al. (1991) looked at "void" and "supercluster" regions. In each case, the reasoning for choosing specific environments was sound, as each effort was tackling particular questions. But if we are to achieve a truly unbiased survey which can make statistically significant statements about the global properties of extragalactic space, should we not make every effort to avoid any preconceptions about our search region? The slice search was designed with the belief that it is important not only to search regions which optical studies have determined to be "void" or "cluster" environments, but also the gray areas in between them, all the while being blissfully ignorant of what it "should" run into. The best approach is the most arbitrary, and this was easily achieve by picking a box on the sky based on our terrestrial coordinate system (this also makes observing much simpler, since telescope degrees of freedom are based on the same system). Any structure found in the box can then be considered significant, and a later comparison the optical picture can be made.

In the next chapter we will describe in detail the original slice search HI observations and the reduction procedures we applied to them.

Table 2.1. Deliberate HI Searches

Search	Telescope (21cm beam)	Velocities (km/s)	#Beams	Δv (km/s)	rms (mJy)	Volume Mpc³	Detections
(1)	(2)	(3)	(4)	(5)	(6)	(7)	(8)
Shostak (1977)	NRAO 91m (10')	-400 - 1422	3100	11	32	94	1
		-800 - 2835	2500	11	44	598	0
		1040 - 1890	400	11	12	24	0
		86 - 11000	50	11	18	699	0
Mathewson and Cleary (1975)	Parkes 18m (53')	-70 - 380	3821	14	4100	31	>1
Lo and Sargent (1979)	OVRO 40m (21')	-200 - 800	2563	10.5	96	30	0
	Bonn 100m (9')	-200 - 800	698	5.5	12	1.5	2
Materne, Huchtmeier, and Holsbosch (1979)	Dwingeloo 25m (34')	-456 - 1656	795	16.5	50	219	0
Haynes and Roberts (1979)	NRAO 43m (21')	0 - 2000	2300	21	240	426	30?
Wetherill, Sullivan, and Heckman (1980)	NAIC 305m (3.3')	200 - 2400	7400	35	70	58	0
Fisher and Tulley (1981)	NRAO 91m (10')	-300 - 1300	770	22	13	9	0
Krumm and Brosch (1984)	NRAO 91m (10')	6300 - 9600	3000	45	20	5000	0
		5300 - 8500	3700	45	20	4519	0
Kerr and Henning (1987)	NRAO 91m (10')	300 - 6800	1920	22	18	4061	15
		300 - 6800	860	22	18	1819	4
Weinberg et al. (1991)	VLA-D (.75') (map = 30')	4500 - 5700	12	40	.4	53	10
		2650 - 3850	30	40	1.0	53	0
Hoffman, Lu, and Salpeter (1992)	NAIC 305m (3.3')	-40 - 3600	160	15	1.1	4.3	2
		3600 - 7600	160	15	1.8	36	4
Simpson and Gottesman (1994)	VLA-D (.75') (map = 30')	2788 - 5412	3	41	.45	9.6	1
HI Slice	NAIC 305m (3.3')	188 - 2812					
		100 - 8340	14130	16	2.0	4687	40

Table 2.2. Non-Deliberate HI Searches

Search	Telescope (21cm beam)	Velocities (km/s)	#Beams	Δv (km/s)	rms (mJy)	Volume Mpc³	Detections
(1)	(2)	(3)	(4)	(5)	(6)	(7)	(8)
Fisher and Tully (1981)	NRAO 91m/43m (10'/21') Bonn 100m (9')	0 - 3000	1787	22	18	253	0
Haynes and Giovanelli (1984)	NAIC 305m (3.3')	0 - 12700	324	15	1.5 - 5.0	380	1
Giovanelli and Haynes (1985)	NAIC 305m (3.3')	0 - 12700	415	15	1.5 - 5.0	486	0
Bicay and Giovanelli (1986)	NAIC 305m (3.3')	0 - 12700	260	15	1.5 - 5.0	305	0
Bicay and Giovanelli (1986)	NAIC 305m (3.3')	0 - 12700	318	15	1.5 - 5.0	372	0
Bicay and Giovanelli (1987)	NAIC 305m (3.3')	0 - 12700	162	15	1.5 - 5.0	190	0
Haynes et al. (1988)	NRAO 91m (10')	1500 - 8500	383	22	2.0 - 10.0	1228	3?
Giovanelli and Haynes (1989)	NAIC 305m (3.3')	0 - 20000	1886	15	.7 - 2.5	8628	5
Schneider et al. (1990)	NAIC 305m (3.3')	-400 - 6500	3049	16	2.0 - 10.0	479	0
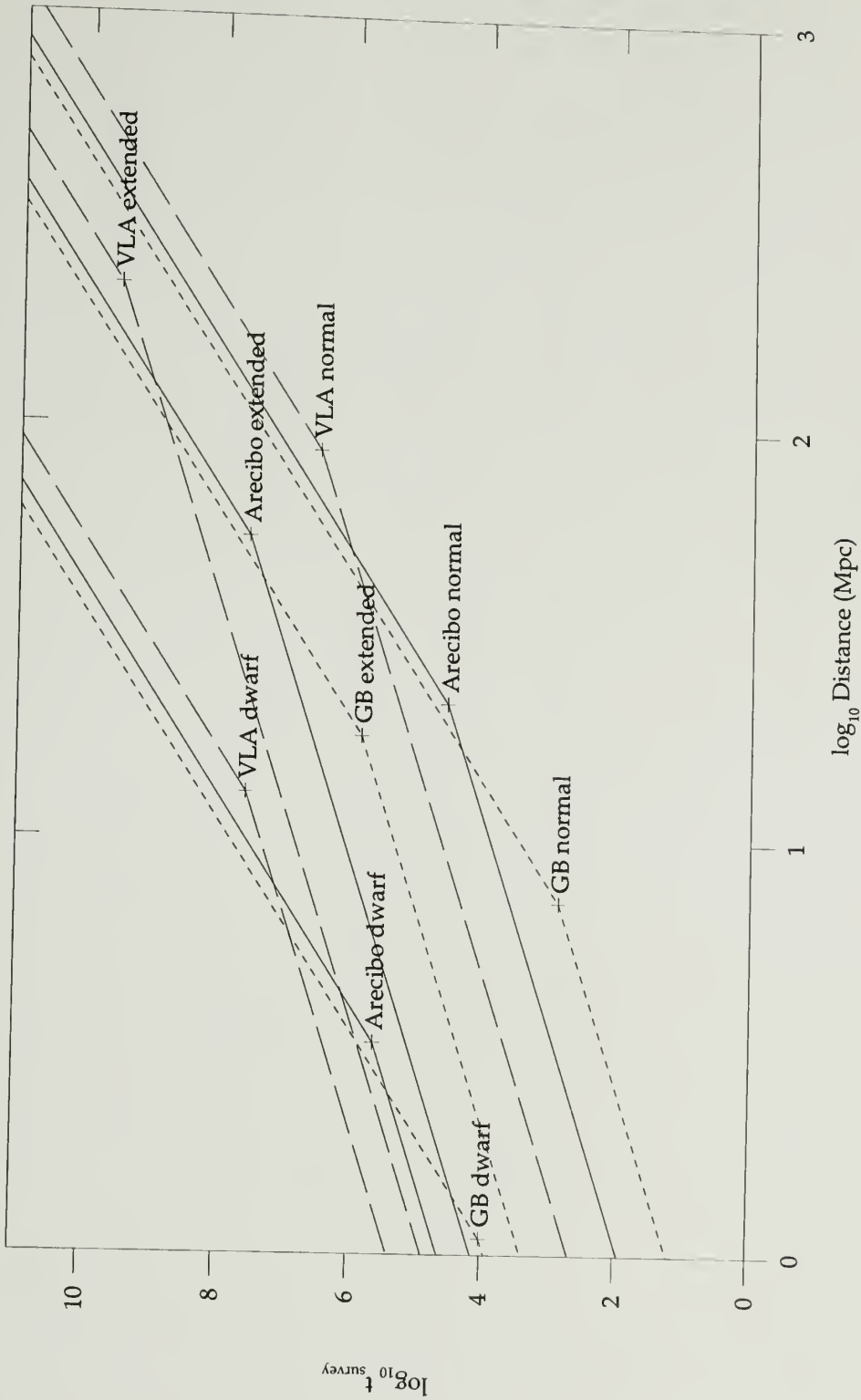
Figure 2.1. The survey time required for Arecibo, GreenBank, and the VLA to detect model galaxies at distances from 0 to 1000 Mpc. Curves for Arecibo are solid lines, those for GreenBank are short dashed lines, and those for the VLA are long dashed lines. The labelled points represent the transitions from the unresolved to the resolved regimes.

60
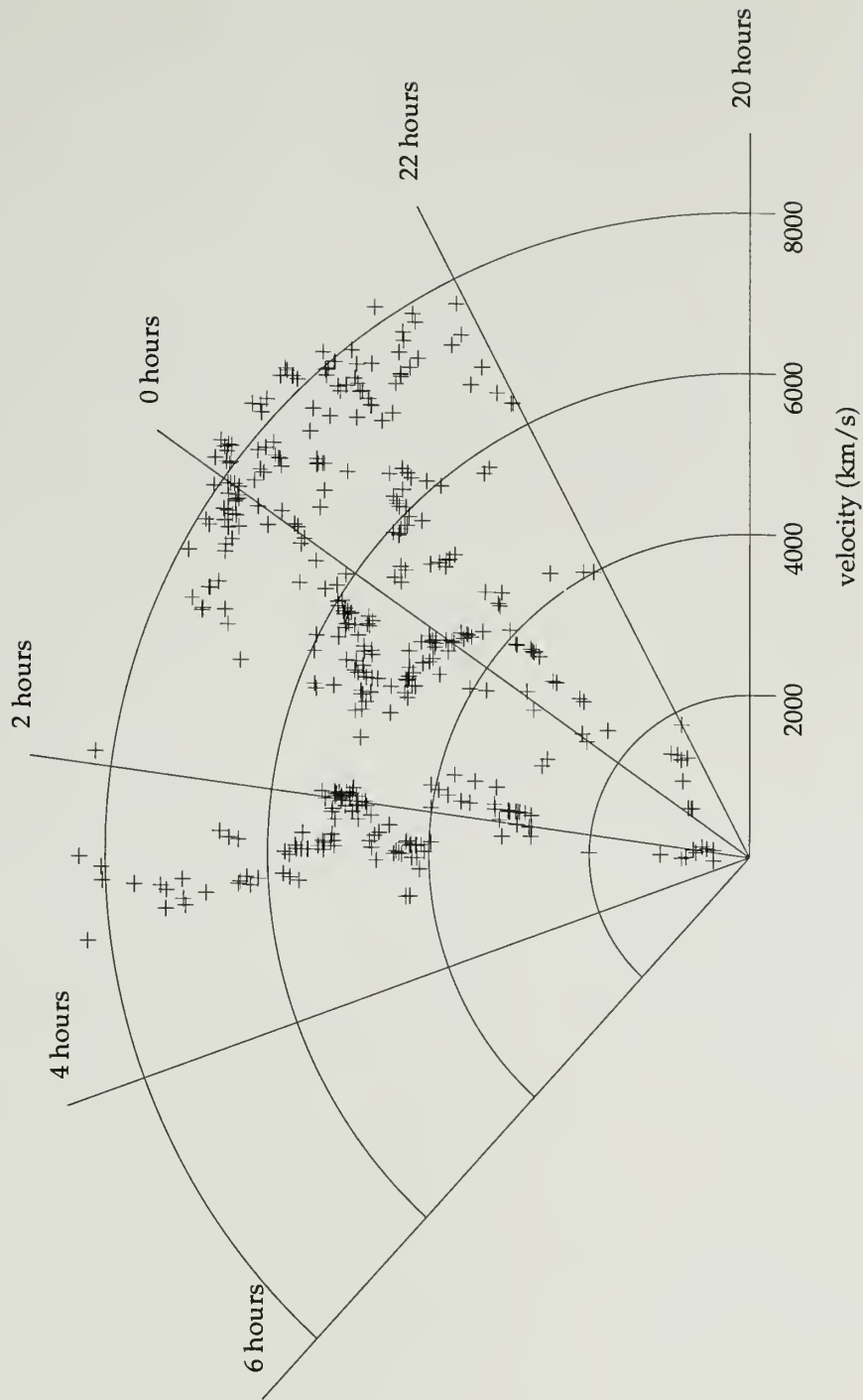
Figure 2.2. RC3 galaxies in the declination range +18 to +28. Radial lines are of constant RA, arcs are of constant redshift velocity.
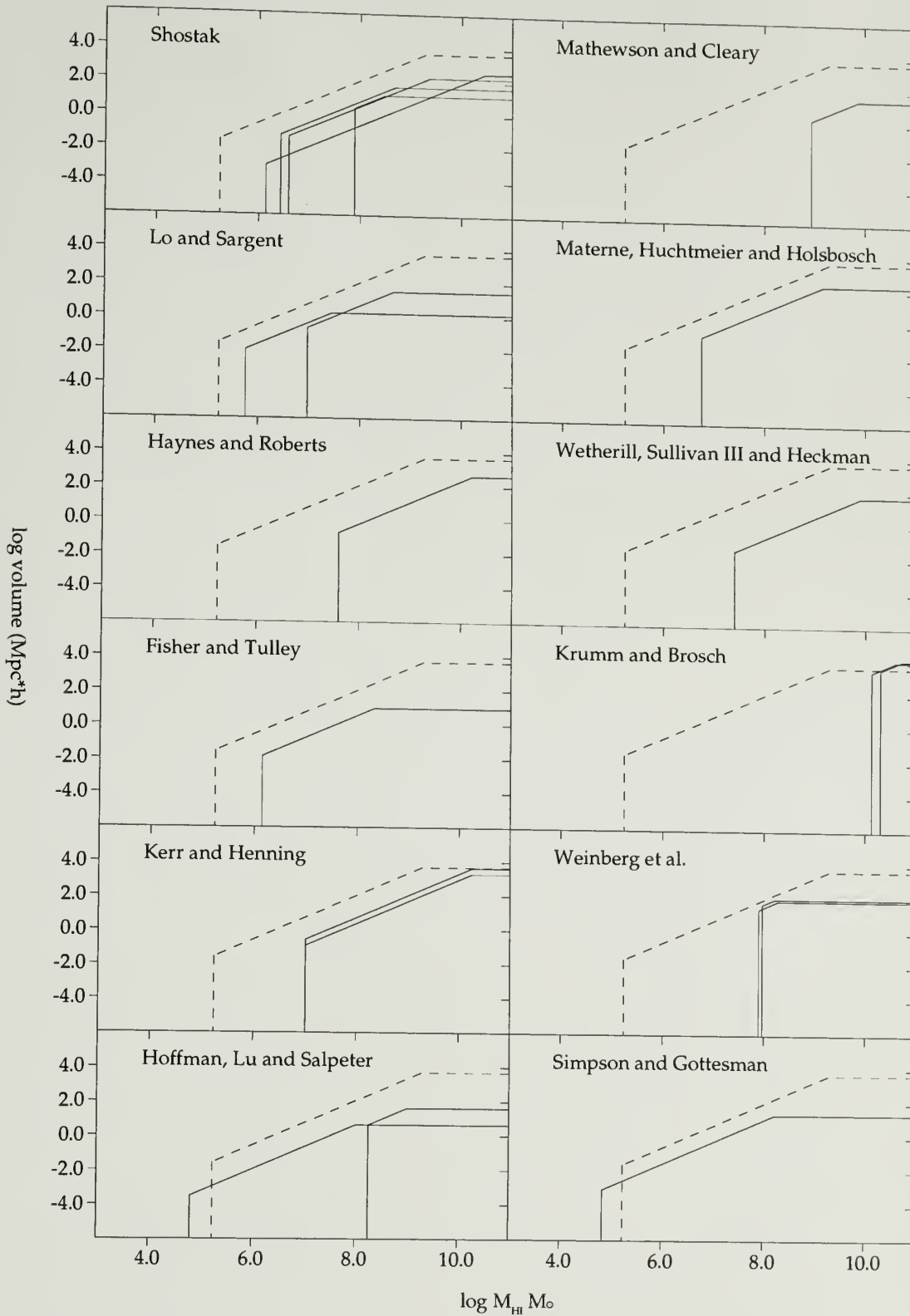
Figure 2.3. HI mass sensitivity vs volume searched (at each sensitivity) for all HI searches. In each plot, the dashed line shows the HI Slice search for comparison.

CHAPTER 3

OBSERVATIONS

The HI survey comprised three groups of observations. The first observations were the original HI search of the slice region which were designed to locate galaxies within the slice search volume. Beyond these, there were follow-up HI observations of objects detected by the first search, and of objects known to be in the slice volume which the slice search failed to detect. These were designed to be more sensitive than the slice observations, and were used to improve the quality of our HI measurements. In addition, optical observations of each object in the slice volume were made to obtain optical magnitudes and sizes of each galaxy.

In this chapter we examine each of the groups of observations in detail, including descriptions of the observations themselves, reduction procedures, and results. We will deal with the original slice search HI observations first, then cover the HI follow-up work, and finally the optical observations. This sequence roughly represents the chronology of the observations themselves, although follow-up observations were begun before the slice search had been completed.

Original HI Slice Observations

The original slice observations were carried out at the NAIC Arecibo telescope in Puerto Rico during November of 1990, February, June, September, and November of 1991, and September of 1992. We describe and explain the strategy used to observe the slice region, the observations themselves, and the reduction procedures used to determine when we were detecting things. Both visual inspections and software schemes were used to detect objects in the slice data.

Observation Strategy

As described in the previous chapter, we chose to search a "slice" of the sky ranging between $22^h 00^m$ and $03^h 24^m$ RA, and from $+23° 0^m$ to $+23° 42^m$ DEC. This area of the sky covers roughly 45 square degrees. A pattern of observing positions was chosen to thoroughly cover this entire region. The slice was divided into 14 rows of constant declination, each containing 1080 observing positions. Observing

positions in alternate rows were offset by half the spacing between each position so that points would be arranged in a close-packed "honeycomb" pattern, with approximately 4 arc minutes between them. Each observation position (except those on the edges of the slice) was surrounded by six others, one each directly to the East and the West, and four more at 60° north and south of East and West (see Figure 3.1). The rows of constant declination were separated by 3.5 arc minutes. Individual points in each row were spaced by 18 seconds in RA, or between 4.19 and 4.11 arc minutes depending on the cosine of the declination. The spacing between each point and those closest to it in neighboring rows ranged from 4.06 to 4.07 arc minutes, depending on the cosine of the declination. Arecibo's 21cm beam pattern has a half-power width of roughly 3.3' at 21cm. Spacing the points in the slice search with 4' distance center-to-center meant that beams in neighboring positions were overlapping at roughly 40% power level, yielding fairly uniform coverage over the search area. A total of 14,130 positions were observed.

To perform a blind search for unknown HI sources, it was necessary to develop unique observing procedures, as those used for normal 21cm observations would not have been effective. One aspect of a search of this kind which makes it very different from most other observations is the difficulty of doing baseline subtraction. Normal radio observation of an astronomical source involves pointing the telescope at two positions - an "ON" position and an "OFF" position. In the "ON" position, the telescope is pointed at the astronomical source itself, and is allowed to integrate for some set amount of time. During this time the telescope is receiving signals from the target source, and from many unwelcome sources such as emission from the ground, imperfect reflectors, losses in cables, etc. These signals are sent through the telescope's "back-end" hardware - receivers and amplifiers designed to detect them. Unfortunately, these receivers and amplifiers respond non-linearly to the total power . This leads to a baseline which can vary tremendously as the total input power changes. In addition, a particular problem at Arecibo is that there are standing waves between the dish and the suspended platform which houses the feeds. The wavelength of these standing waves depends on the precise separation between the dish and the platform. The combination of these effects leads to baseline variations with frequency in the final spectrum which are much larger in magnitude than those caused by signals from the target, and they can easily obscure it.

Fortunately, the effects which cause these variations change fairly slowly with time. Total power levels are usually fairly constant over the time scales of typical astronomical observations (minutes to hours). Standing waves are highly dependent on the geometrical configuration and physical conditions of the telescope - its azimuth and elevation, the temperature of the platform structure and the cables which suspend it, and weather and angle of the sun. Except at times of rapid heating and cooling of the telescope which can happen at sunrise and sunset, or with the passage of severe cloudbursts (an almost daily occurrence at Arecibo during the summer), these conditions are stable over similarly long time scales.

During the length of an "ON" scan integration while the telescope is tracking its source it is also keeping a record of the baseline changes due to the conditions at the time of the observation. A duplicate "record" of the baseline can be made by allowing the telescope to track an empty sky region over the same period of time as the ON-scan, as long as the conditions which led to baseline characteristics are duplicated as carefully as possible. This can be done by performing this second "OFF" scan integration as close to the same time as the ON-scan as possible, and tracking through the same azimuth and elevation range. Because the OFF-scan is integrating on empty sky, it should contain only the baseline information, and nothing else. The OFF-scan can then be subtracted from the ON-scan, leaving the weak signals from the astronomical source as a residual.

This ON-OFF procedure works well when trying to detect the signals for astronomical sources which occupy known positions on the sky. It depends critically on the source being in the ON-scan, and nothing except background being detected in the OFF-scan. Yet in a blind search, the positions of the sources are unknown. A detection is as likely in the OFF-scan as in the ON-scan, since both are identical integrations on positions on the sky which may or may not have astronomical sources in them.

For any position we observe, we need to subtract something analogous to the OFF-scan, since, as described above, astronomical signals in a single scan are obscured by variations in the baseline. One way to approach the problem is to do ON and OFF scans normally, and treat both as searches of positions. Detections may be made in each, and, providing a detection is not made in both at the same velocity,

should appear as positive features in the final subtracted spectra for detections in the ON-scan position, and negative features relative to the baseline for detections in the OFF-scan position. Alternatively, two subtracted spectra could be created for the two positions, with each having the other subtracted from it, and in which one would search for only positive features. In principle, such a procedure would be twice as fast at observing the sky as conventional ON/OFF observations (as both the ON and OFF scans are search positions). Yet there are even more time-efficient methods which may be used for a blind search.

By increasing our integration time on our ON scan, we can decrease the level of the background noise we can theoretically expect in a spectrum. Subtracting an OFF scan adds to the noise somewhat. The theoretical noise of a subtracted spectrum is proportional to the inverse of the ON and OFF integration times added in quadrature:

$$\sigma_{rms} \propto \left(\frac{1}{T_{ON}} + \frac{1}{T_{OFF}} \right)^{1/2} \tag{3.1}$$

In a typical ON/OFF observation the integration time of the ON and OFF scans are matched to minimize the noise for a given total observing time $T_{ON} + T_{OFF}$. The subtraction process increases the background noise level by a factor of $\sqrt{2}$:

$$\sigma_{rms} \propto \left(\frac{1}{T_{ON}} + \frac{1}{T_{ON}} \right)^{1/2} = \frac{\sqrt{2}}{\sqrt{T_{ON}}} \tag{3.2}$$

The total "telescope" time required to make this observation would be twice the ON integration time. Or, in the case of a blind search using both the ON and OFF scans a search positions, the telescope time required to observe a single sky position would be the ON integration time. Yet as it turns out, we are not limited to doing same-duration ON and OFF scans in the slice search. There are a number of different approaches we may use to increase the total integration time used to create OFF scans without increasing our telescope time. These long-integration OFF scans will add less noise to the final subtracted spectra.

The Krumm and Brosch (1983) 21cm search described in the previous chapter gives us a hint as to how we should approach our search strategy. As in the slice search, Krumm and Brosch were scanning positions in rows of constant declination, one after the other. From the scans from each of these positions, they subtracted a composite OFF scan which was the sum of four nearest neighboring scans on either side, not including the two immediately adjacent. This was not an ideal arrangement, as the nearest positions used in the OFF scan were only 10 arcmin away from the ON scan (exactly the width of their telescope beam), and any signal in the ON scan could presumably either extend into, or be detected by sidelobes of the OFF scan positions. Any detection of an object in the OFF scan will weaken its signal in the subtracted spectrum, and must be avoided. In addition, the book-keeping of this strategy will lead to inconsistencies at the ends of the right ascension ranges - are the OFF scans for the last point on either end only taken from one side, or are the end points discarded as ON scans? However, while spending all of their telescope time pointing at ON scan positions, Krumm and Brosch had OFF scans with four times the integration time of their ON scans, yielding improved noise levels:

$$\sigma_{rms} \propto \left(\frac{1}{T_{ON}} + \frac{1}{4 \times T_{ON}} \right)^{\frac{1}{2}} \approx \frac{1.12}{\sqrt{T_{ON}}} \tag{3.3}$$

The total telescope time required for each observation was only the ON integration time (since all four OFF positions were ON observations themselves). Thus these observations took no more time than would have been required for same-duration ON and OFF scans, and at the same time achieved noise levels (and thus signal-to-noise levels) which were roughly 25% better.

The slice search used a similar, but improved approach. We were able to eliminate most of the book-keeping and OFF scan detection problems of the Krumm and Brosch search, and produced an even better final noise level. We performed a one minute integration on each of our slice points. Points spaced 1 minute, 12 seconds apart in RA (16', or every fourth point), but at the same declination, were observed sequentially, meaning we would "leapfrog" over three points (these points would be observed on later

nights). This 16 arcmin spacing is wide enough such that none but the most extended objects will occur in more than one point, and sidelobe overlap between points will not occur. The time required to slew, set-up, and integrate on each point almost exactly matched the time during which the rotation of the Earth would carry the sky through our 1 minute, 12 seconds spacing in RA. Thus each new point would be at almost exactly the same azimuth and elevation as each preceding point, and the telescope would operate in the same zenith angle range for integration after integration. This strategy allowed us to sum groups of 15 sequentially observed points into "super OFF" scans, as baseline deviations depend primarily on telescope zenith angle. The theoretical rms noise level after subtracting the super-OFF from each one minute integration then became:

$$\sigma_{rms} \propto \left(\frac{1}{T_{ON}} + \frac{1}{15 \times T_{ON}} \right)^{\frac{1}{2}} \approx \frac{1.03}{\sqrt{T_{ON}}} \qquad (3.4)$$

The final subtracted spectrum has little more noise than an unsubtracted ON scan. Or, put another way, a similar noise level could be achieved using same-duration ON and OFF scans by increasing the integration time T_{ON} by a factor of 1.87. The slice observations are nearly twice as efficient as a same-duration ON/OFF procedure.

The Observations

Within the slice region, 14,130 sky positions were observed, consuming approximately 300 hours of telescope time. The tunable 22cm "circular" feed was used for all original slice observations (there were two brief periods during our observations when it was unavailable due to equipment problems, during which the fixed 21cm circular feed was used for low-velocity tests - see below). The feed was tuned to its physical limit - 1397 MHz, optimizing our frequency response at about 5000 km/s. This maximum frequency response was roughly twice that at the low-velocity extreme of our bandpass. To some degree, this arrangement helped balance out the sensitivity of the slice search over the velocity search range, as

signal-to-noise levels at the center of the spectra would be higher than at the low-velocity end where weak signals would be easier to detect.

Each signal polarization was fed into two quadrants in the 2048-channel autocorrelator; a 20 MHz wide high frequency quadrant centered at ~1410 MHz, and a 20 MHz wide low frequency quadrant centered at ~1392 MHz, with a roughly 2 MHz overlap. This gave us velocity coverage from 100 km/s to ~8340 km/s with 8.7 km/s resolution. After subtracting the super-off scan, the two polarizations were combined, and the spectrum was Hanning smoothed to yield 17 km/s velocity resolution and a theoretical *rms* noise level of 1.4 mJy at low zenith angles.

Low Velocity Test

Our search was not as sensitive to low velocity, nearby objects (which are potentially very interesting!) as it could have been had we used a feed tuned to a frequency higher than 1397 MHz. In an effort to assess what could have been found by maximizing the sensitivity at low redshift velocities, and to take a look at a sample of negative velocities (and to make use of a block of time in which the 22cm feed was not functioning!), we used the 21cm dual polarization feed to re-observe a small subset of our slice points. The feed was tuned to 1410 MHz, maximizing the gain at about 2000 km/s redshift. A velocity range between -820 and 6900 km/s was scanned for 480 slice points (3% of the slice search). Given our average detection rate (to be discussed later), we would have expected ~3 objects in this area. This small search re-discovered one of the objects detected in the original slice, and found one new object with a redshift of -400 km/s which is probably a high-velocity cloud. However, *no* new objects were found within the velocity range covered by the slice search, and *no* objects detected by the slice search within the new velocity range were missed by the new observations.

Slice Position Naming Scheme

To keep track of observation positions for book-keeping purposes and to identify objects we detected, a naming scheme was developed for the slice points. This scheme, as described here, was applied both to the slice positions themselves, and the objects discovered at those positions. The slice point names may

seem opaque at first, but they are very useful in that they can uniquely identify the position of the center of each observation on the sky.

Each eight character name (the eight character size was chosen to conform to a limit within Arecibo's "*Analyz*" software) begins with a letter code which identifies the declination of the slice point. The slice points were arranged in rows of constant declination, from 23 00 00 to 23 42 30. Row "A" was centered at 23 00 00 declination. Row "B" was 3.5 arc minutes above, centered at 23 03 30. Row "C" was 3.5 arc minutes above that. There were 14 rows, up to "N", which was centered at 23 42 30.

The next five characters identify the "block" of the slice position. All slice positions were observed in groups of 15, spaced 1 min 12 sec apart in right ascension. We call these groups of 15 "blocks". The first four characters of the block identity give the "starting" right ascension of the block (HHMM). The fifth character in the block identity is either A, B, C, or D. The right ascension of the first position in a block is given by the "starting" right ascension (the four digits), plus 18 seconds of time if the fifth character is "B", plus 36 seconds if the fifth character is "C", or plus 54 seconds if the fifth character is "D". The last two digits in the slice position name identify the "member" of the block, ranging from 01 to 15. An additional offset in right ascension of 1 minute 12 seconds times the member number minus one must be added to obtain the right ascension of the center of the slice point.

One more detail remains before the right ascension is accurate. Because the slice positions were arranged in a honeycomb pattern to maximize coverage, every other row of positions is offset by 9 seconds in RA. The true right ascension of a position in rows A,C,E,G,I,K, and M is given by the procedure described in the previous paragraph. The right ascension of positions in rows B,D,F,H,J,L, and N is given by the above procedure plus 9 seconds.

As an example, the slice position named A0154B11 was the position where the first object detected in the slice search was made (thus one of our objects has this name as well). The first letter of the name tells us the position is in row "A", so it is centered on a declination of 23 00 00. The next five characters "0154B" are the block name. They tell us this observation was done in the block which started at right ascension 01 54 00 + 18 seconds = 01 54 18. The last two characters tell us it was the 11th observation in

that block, which means that its right ascension was offset from the beginning of the block by (11 - 1)×(1 min 12 sec) = 720 sec = 12 min 0 sec. So the position of the slice point A0154B11 is 02 06 18.0 +23 00 00. The object found in this slice position which shares its name has a position found from follow-up optical observations which lies within the Arecibo beam centered on the slice position: 02 06 21.6 +23 00 46.

Detection Methods

The purpose of the slice search, above all else, is to locate extragalactic objects, both new and previously cataloged, by their atomic hydrogen emission. The slice observations described in this section are in the end used almost exclusively for this purpose, as the later follow-up observations were developed to examine each of our detections in detail. The analysis of the original slice data concentrates on different methods used to locate objects in the slice search spectra, and little else.

In principle, locating an extragalactic signal in a spectrum is very simple. If the spectrum is the result of a trouble-free integration and has had a similarly trouble free off-scan subtracted from it, it should have a fairly flat baseline with a *rms* noise level which is predictable based on the integration time and the properties of the telescope used. Objects which produce a flux greater than the noise level should stand out as deviations in the spectrum above the background noise level. Objects which produce a lower flux level can not be detected. In the slice search the process turned out to be far more complex than this. The predicted *rms* noise level is an ideal value, which can only be approached by most observations. Any non-optimal condition of the observations such as weather or equipment vagaries produced higher than predicted noise levels. Baselines were sometimes not flat because of rapid temperature changes in the telescope or uncooperative correlators. Galaxies themselves have velocity dispersions which spread their flux over many channels, thus weakening their signal level relative to the background noise. Worst of all, interference signals which come from earth-bound sources produced thousands of features in the spectra which masqueraded as galaxies. Some of these signals were regular and predictable, and a very few of them could be linked to a particular source, but the vast majority would appear and disappear seemingly at

random. Identifying these interference signals proved to be the most time-consuming part of the process of locating objects in the slice search spectra.

Our approach to discovering signals in the 14,130 spectra proceeded along two paths. We subjected each to a careful visual examination, and then a further inspection by software. In both cases, we were locating "suspicious" signals - points in the spectra where one or more channels were many sigma away from the baseline, or where many neighboring channels were a few sigma off the baseline, and where such signals were present in both polarizations. The positions of all suspicious signals were recorded, and were re-observed with a conventional ON/OFF procedure to confirm or eliminate them. Because interference signals in the spectra were very numerous, careful screening processes had to be devised to discard many of them before the confirmation process, otherwise a huge portion of our telescope time would have been consumed doing ON/OFF observations. However, we wanted to be very careful not to eliminate signals which could be real extra-galactic objects.

Visual Search

During the 21cm observations at Arecibo, the individual spectra were examined visually. Each point required one minute of integration, plus 15 seconds or more for slewing and set-up, allowing the observer over a minute in which each could be scrutinized for suspicious signals. As described above, points on the sky were observed in groups of fifteen. After each group of fifteen was completed, the subtracted, combined-polarization spectra were computed and displayed in the control room using the "*Analyz*" spectral line reduction package at Arecibo. Because a group of fifteen spectra had to be completed before any of them could be observed, this process lagged behind the actual observations somewhat.

Any visual search is by nature highly subjective, however we tried to develop a systematic method for our examination. This method evolved over the course of our observations as our knowledge and experience grew.

It was important that our search be consistent throughout the slice observations, so that we could establish limits on the size and strength of signals we were detecting (and failing to detect). In doing so, we had to adjust to a number of quantities which would vary. Each spectrum was presented to us for

visual inspection with an *rms* noise level. Establishing exactly what the limits on detectable signals are within the noise level is not possible, but our experience demonstrated that signals of certain strengths would draw our attention. Specifically, we estimate that signals which had integrated fluxes greater than five times the *rms* noise level in one channel (after Hanning smoothing) would be noticed. We need such a large deviation because there are so many channels in a single spectrum, and the *rms* noise level represents the standard deviation of each measured event - each channel. A deviation three times the noise level, for instance, would statistically be expected approximately 1.5 times in each spectrum, as we have roughly 500 channels in each after Hanning smoothing, and the probability of a three-sigma event in a random distribution is 1 - .997 for each event (each channel). The probability of a five-sigma event in a truly random distribution, on the other had, is 1 - .9999994 for each event, making this something we would only expect in one of every 3200 spectra or so, or roughly five times in the entire slice search of 14,130 spectra. We use this criteria in calculating the HI mass sensitivity curves presented in the previous chapter, and for computations of our detection limits in the analysis chapter.

Unfortunately, the *rms* noise level was not constant throughout the slice observations. The theoretical noise level represented only a low limit to the level we could expect in real observations (although many of our spectra approached the theoretical level). Variations from ideal conditions in the weather, time of day and other factors during observing caused changes (i.e. increases) in the noise level. There were occasionally very poor baselines caused either by inaccurate OFF scans while the Sun was near zenith, or by strong continuum sources in the beam. Signals which would have been visible in a clean, flat spectrum were very difficult to spot in these messy spectra, although some successful efforts were made to remove the bad baselines. Those spectra which were truly useless were re-observed.

Beyond these difficulties, signal strength was not at a consistent level across the entire bandpass. Our feed was tuned to maximize the gain at the center of our bandpass - at about 5000 km/s redshift. However, this meant that the gain at the high and low ends of our spectrum were lower - barely half that at the center. This led to higher effective noise levels on the bandpass edges. There is little we can do to

rid ourselves of these variations. We must simply keep them in mind when trying to establish hard limits to the sizes and signal strengths of the objects we can detect.

A far more insidious problem was one we have already touched on - that of interference signals in the spectra. Dealing with the difficulties outlined above while locating five-sigma events in the spectra is in principle a very easy task (although time-consuming). A simple visual inspection should reveal any five-sigma event, or a fairly straight-forward software filter could be applied to the data. However, the number of interference signals stronger than five-sigma would inundate the list of real signals which would emerge from such a simple screening process. Far more subtle procedures needed to be applied before we could consider any deviation from the background noise an extragalactic signal.

Profiles of some large extragalactic HI sources were easy to spot in the spectra by their shape. They tended to be made up of very strong (more than 5 sigma) signals in many adjacent channels. Some showed two-horned profile structure characteristic of disk galaxies. However, we did not consider any detections certain, regardless of how strong they looked, and all signals were subject to confirmation observations. Narrower signals were often questionable, because their shapes and that of interference signals were very similar. We had a number of ways of screening interference signals from our final list of confirmed detections. When encountering a signal which looked promising in a spectra, we would proceed along the following lines:

1. The signal was examined to see if was polarized, which would mean that it would have very different strengths in the two polarizations. The *Analyz* program allowed us to check both polarizations simultaneously, so the degree of polarization of a signal could be assessed very easily. Interference sources tend to be highly polarized, yet astronomical sources of HI are not, so we were able to dismiss the vast majority of interference signals immediately using this process. However, it should be noted that real signals, while not polarized, may *look* that way due to noise in the different polarization spectra, especially when they are weak. Some care had to be taken when discarding signals using this method.

2. A check was made for a similar signal in previous and following spectra. In this case, we were taking advantage of our observing procedure. The previous and following spectra are not adjacent points, but points spaced 16' apart. Extragalactic sources of this size are very rare. Yet interference signals often have durations longer than the one minute slice integrations, or could be timed to straddle a change in slice positions, and could easily appear in two subsequent slice point observations. Often, we would find an interference spike at a particular frequency throughout a day of observing, or for several days in a row, sometimes constant, sometimes reappearing every few minutes or hours. Signals which exhibited these characteristics were dismissed as interference.

3. Did the signal "look familiar"? Had we seen a very similar signal at the same frequency at previous times in our observing? In examining thousands of spectra, we constructed a library of interference signals we had encountered and dismissed for one reason or another. Often a signal would appear at a frequency for a single spectrum, and then disappear, only to re-occur days later. Others were almost daily features. One particular signal which records suggested had plagued 21 cm observers for over a decade was tracked down during an ambitious evening of observing, and found to be produced by a little used piece of equipment in the control room (which was disconnected). If a signal had the same frequency and strength of an interference signal we had previously encountered, it was called into question. However, we wished to avoid inadvertently eliminating any real features, and the process was applied with considerable care with an eye to erring on the side of believing a signal.

4. Finally, if a feature survived this screening process, it was re-observed with a conventional ON/OFF procedure. The integration time of the ON and OFF scans was determined by the strength of the original signal - weak signals were allotted more time than strong ones. In general, our integration time ranged from two to five minutes. As we have shown, the theoretical signal to noise of a 2^m-ON/2^m-OFF observation is almost identical to that of our slice observations, so in principle it should be enough to duplicate the original signal, if it was real. Some 858 confirmation observations were done throughout the course of the slice observations.

When roughly 70% of our search had been completed, we noticed that our detection rate was seemingly increasing with time - later observing runs were more successful at finding objects in the spectra than earlier ones. We attributed this to a "learning curve" of sorts. As we observed thousands of spectra, we gradually developed an "instinct" for picking out real signals. In light of this finding, we subjected the entire data set to a second visual search, presumably taking advantage of our improved skills. This search generated several hundred new suspicious signals, about half a dozen of which were later confirmed to be real.

Any signals which survived this process were considered true detections of extra-galactic objects. It was only at this point that some effort was made to identify the source of the detection - we were not yet sure whether a detection was due to a cataloged object, or an entirely new galaxy. Further observations, both at 21cm and optical wavelengths, were performed on each confirmed detection as described later in this chapter. The follow-up HI observations allowed us to eliminate any further spurious signals which had managed to slip through this entire screening scheme. A single confirmed detection was eliminated in this way. In all, 99 positions out of the slice total of 14,130 were found by the visual search process. An additional detection of an object was found below the velocity range of the slice search, at -400 km/s, by the "low velocity test" search. The same visual search procedure was applied to the low velocity results. This object is probably a high-velocity HI cloud in our own galaxy. A further detection was made by the software search, as described below, leading to a total of 101 detections of HI features in the slice search. These detections are due to 79 distinct objects.

Software Search

In addition to the search by eye, a software system was developed to scan the slice data. This was used both as a check of the thoroughness of the visual inspection, and as a way of detecting additional signals which it had missed. The visual search is inevitably suspect, as it is certainly subjective, and the improving detection rate mentioned above shows that its effectiveness may not have been constant. Despite efforts to perform the visual search in a consistent manner, there is no doubt that some spectra were searched less carefully, due to observer fatigue with tedious repetition, time pressures, or impending

lunch engagements. It is important to use software, which may not be as robust or thorough as a search by eye, but certainly treats all spectra in a precisely consistent manner, to establish whether significant numbers of measurable signals were missed.

What sorts of signals would the visual search be least sensitive to? What types of object profiles would best be able to escape our detection algorithm? The visual search probably detected all strong, wide signals which appeared in the spectra. However, weak, narrow signals (less than 5 sigma peaks, only one or two channels wide) were often ignored. Our early efforts to confirm some of these signals showed that they were almost always weak, short duration interference. In addition, there were simply too many of them to re-observe - they appeared in perhaps one out of every three or four spectra. However, there are a number of circumstances under which these weak signals should be examined again. A weak signal would certainly become significant if it occurred at the same redshift velocity as another signal in the spectrum of a neighboring search position observed on a different day. It would also be significant if it occurred at a frequency where other signals, presumed to be interference, had rarely or never occurred. It is the nature of the terrestrial sources of interference to repeat themselves at some point, and it is reasonable to expect that during our 300 hours of telescope time spanning almost two years any interference source would make its presence known more than once.

Unfortunately, it is difficult to establish by our visual search algorithm when one of these criteria is met. Because our observing procedure skipped positions to integrate on every fourth point, neighboring points were often examined days, weeks, or even months apart. Thus signals coincident in adjacent points would not have been noticed. Through our experience with interference, we were able to build up a "mental library" of frequencies where it commonly occurred. Yet recognizing when a signal appeared in a position where no interference had ever occurred was probably beyond our abilities in the visual search. It is the duty of the software search to draw attention to these particularly interesting appearances of weak signals.

Another signal which the visual search was probably not very sensitive to would be the type appearing very weakly (perhaps only two or three sigma) in many adjacent channels. Such a profile could easily be

lost in a noisy or not perfectly flat baseline. However software can easily be tuned to spot such occurrences by smoothing over large numbers of channels.

In total, three groups of searches were done, which produced nine different lists of suspicious points. These groups we specifically tailored to spot particular types of suspicious signals. A brief description of the purpose and parameters of each search follows.

Searches 1 and 2: Generate an Interference Table. The purpose of the first software search was to make an original pass at the data and locate all channels in all spectra which had high sigma occurrences in them. A determination was made as to whether each one of these events was an interference source, or a real source. The main idea was to generate a list of known interference positions, which could then be used in other searches.

For all of our software searches, we began with the raw 21cm data. No baselines or offsets were removed, although a "super-off" summary scan was subtracted from each spectrum. The first task of the software reduction was to remove a baseline from each spectrum. While in most cases our baselines were very flat, there were some which were particularly uncooperative. Because the auto-correlator was split into quadrants (two polarizations of high and low frequencies), we began by considering each observation as four individual spectra. We calculated a value to subtract from each channel by moving a "sliding window" through the spectrum. At each channel, we computed the mean values of two blocks of 10 channels spaced 30 channels away on either side. These two mean values, when placed at the centers of the blocks used to create them, defined the baseline which was subtracted from the value of the channel we were considering. Because this method required 35 channels to exist on either side of any channel we wished to baseline-subtract, some data on each edge of our four quadrants could not be processed in this way. On the edges of the quadrants, we used a median filter method to calculate an edge value - the mean of three of the end-most five points. This value was used as one end of the baseline for channels near the edge.

We next Hanning smoothed the data, and calculated a standard deviation for each quadrant of each spectrum. All channels which deviated from the baseline by more than four times the standard deviation

were flagged as potentially "interesting". Next we considered the two polarizations in combination. For each channel flagged as "interesting" by the previous process, there was a matching channel in the corresponding quadrant with the opposite polarization. The mean of the two values in these channels was compared against the standard deviations of all of the channels in the two quadrants - if it was less than five times this standard deviation, then neither of the two channels were considered "interesting" anymore.

At this point, the values in both polarizations of the remaining "interesting" channels were compared to each other. If they were similar in strength, they were considered "signals". If they differed considerably in strength, they were considered "interference". This process was simply a software version of procedure #1 of our visual screening process described above - because interference is often polarized, and extra-galactic HI signals are not, a highly polarized spike is assumed to be interference. Mathematically, the criteria for the decision to call something a signal, as opposed to interference, is as follows:

$$f(R) - f(L) < X \cdot \left[\sigma(R)^2 + \sigma(L)^2 + E^2 \cdot \left(\frac{f(R) + f(L)}{2} \right)^2 \right]^{\frac{1}{2}}$$

(3.5)

where:

$f(R)$ and $f(L)$ are the fluxes in the two polarizations of the channel (left and right).

$\sigma(R)$ and $\sigma(L)$ are the r.m.s. background levels associated with the quadrant containing each polarization.

X is the "deviation" factor - the number of standard deviations the spectra were allowed to deviate by, in this process set to 3.0.

E is the "calibration error", set to .1 for this search.

This equation compares the difference in the fluxes in the two polarizations $f(R)$ and $f(L)$ to a value which measures the noise level combined polarizations (measured by σ (R) and σ (L) combined in quadrature). The deviation factor X determines how many time the noise level this difference must be before a pair of channels are considered interference - in this case we use three times the noise level. However, in the case of a very strong signal the flux in both polarizations may be many times the noise level, and a difference between the polarizations which represents only a tiny fraction of the flux level may easily be greater than three times the noise level. To avoid discarding these strong signals, we include a term in the equation which compares the flux difference to the mean flux in the two polarizations, multiplied by the calibration error E. In this case we are comparing the difference to 10% of the mean flux in the two polarizations. For weak flux levels, the noise terms will dominate this equation, for strong flux levels the mean flux term will dominate.

Our next step was to construct a "hit table". This is a table containing information on each of the 1024 frequency channels for all of the 14,130 points in the search. Using the results of the search so far, we can put each channel in one of three "types": there are "empty" channels, which contain no or low sigma signals, "interference" channels, which were found to have mismatched signals in the two polarizations, and "signal" channels, which have high sigma signals which are well-matched in both polarizations. The hit table we built kept track of which of these three categories every channel of every slice observation spectrum fell into. For the following steps in this software search, the hit table was consulted and changed to match new findings.

Our next step was to screen the remaining "signals" for events which were really due to long time-scale interference. This is analogous to procedures #2 and #3 of the visual search, however with software our scheme is far more systematic. The base assumption of this process is that a signal which occurs in two spectra which were observed chronologically next to each other (meaning they were observed one after the other, as opposed to being next to each other on the sky) is likely to be interference. The reason for this is that points observed chronologically next to each other are separated by 16' on the sky, a distance larger than the extent of all but very few extra-galactic objects. Yet our experience has indicated

that interference signals with duration time-scales of a few minutes were fairly common, and these would show up as signals in the same channels of chronologically adjacent points. Operationally, our software consulted the entire hit table, examining the channels which were observed within ten minutes (before or after in wall-clock time) every "signal" channel. If a signal was found in any of these channels, the status of both it and the original signal were changed to "interference" on the hit table.

Channels neighboring interference may be untrustworthy, as they are likely to be affected by strong interference signals. For this reason, we found every "interference" channel in the hit table and changed the neighboring higher frequency and lower frequency channel to "interference" as well, regardless of what these channels contained. Because of the repetitive nature of interference spikes, we did the same to the matching block of three channels (the channel containing the original interference and its two neighbors) in all points observed within + or - 1440 minutes (one day) of the original spectra. At the end of all of these procedures, we were left with a total of 667 "signals" in the entire data set.

We were then prepared to make a first search of the hit table for the two types of signal profiles which we hope the software search is sensitive to - wide, low sigma signals in many adjacent channels (which this first search, due to the high-sigma parameters in its early stages will probably not be very effective at finding), and weak signals which occur at the same redshift velocities in slice points at adjacent positions in the sky. Two separate processes were applied to the hit table to reveal these types of signals. The first looked for pairs of signals which occurred in neighboring velocity channels in the same spectra. This search (Search #1) revealed 77 points of interest in the data set. Of these, 16 were found to be the locations of objects which had been detected in the visual search. A further 17 were points found by the visual search, re-observed, and found not to be real. 31 were probably due to sources of very long time-scale interference (as they all appeared in the same frequency channels) or difficulties the search algorithms had interpreting the bandpass edges (they appeared in channels on the bandpass edges). The remaining 13 points were considered "suspicious" signals, and were re-observed with ON/OFF observations in a manner similar to the suspicious signals found by the visual search. None were found to be due to extra-galactic sources.

To detect signals at the same redshift velocities in adjacent points of the sky, we searched the six points surrounding the location of each "signal" in the hit table for "signals" at the same channels. This search (Search #2) revealed 23 points of interest. Of these, 10 were due to 4 previously detected objects, 6 were caused by problems at the bandpass edge, and the remaining 6 pointed to 3 possible objects. We re-observed at positions between the positions of each pair of points, and found that each was a strong continuum source. The effect of strong continuum sources was generally to create very bad baselines, which would be difficult to subtract cleanly. The residuals after the baseline subtraction might easily contain what looked to the software search like high-sigma events. Because strong continuum sources might appear in many neighboring channels, it is not surprising that this search procedure would discover them. While not what we were looking for, it was encouraging that the adjacent channels procedure was in fact detecting something *real*.

Searches 3 and 4: Using the Interference Table as a Mask. We next started from the raw data set again, but used the interference detected in the previous search to mask out channels in the spectra. The hope was that without the interference signals, we could search for lower sigma events and not be overwhelmed with spurious signals, and would be considerably more sensitive to weak sources of 21cm emission, and in particular wide, multi-channel signals.

First we applied the interference mask to our entire data set. To do this, we consulted the hit table for every channel in every spectrum. If any of the processes in the first software search labeled the channel as interference, it was eliminated from the search process, and all calculations involved with it (such as the baseline subtraction). Next a "sliding window" was applied to remove a baseline from the data exactly as in the first search. Rather than Hanning smoothing, a boxcar smoothing process with nine channel resolution was applied in an effort to make many-channel signals emerge. Remaining events which were higher than four times the *rms* noise in either polarization and five times the *rms* in the mean of both polarizations were then tabulated.

We then created a second hit table, using a comparison of the signals in each polarization to separate "interference" from "interesting" points, exactly as in the first search. This hit table was searched for

signals which occurred at the same channels in neighboring points on the sky, a process which generated 4 locations around 2 possible objects (Search #3). ON/OFF scans showed that neither of these objects was real. Because of the wide resolution used to do the boxcar smoothing, searches for signals in adjacent channels in the same spectrum would not be illustrative.

This whole process was repeated using a wider boxcar resolution - 17 channels (Search #4). All of the 11 points which emerged had been found by previous searches, and were not re-observed.

Searches 5, 6, 7, 8 and 9: Eliminate Long-Term Interference. From the above three searches, we generated three independent hit tables. In all cases, we made efforts to screen interference sources out of our final data sets, but despite these, we often ended up with obvious long-term interference signals in our final tables. In none of the three searches could we trust high-sigma signals in single channels - there were simply too many (667 in the first search, 1140 in the second, 1329 in the third) to justify ON/OFF observations of them. To limit their numbers, we considered only those which occurred in more than one adjacent channel, or in the same channels in adjacent points. Yet signals narrower than our velocity resolution are certainly possible, and we should make an effort to root them out.

Examining the lists of "interesting" points which remained in the hit tables before looking for neighboring channels or points revealed that many appeared to be repeats of the same signals - interference signals over time-scales large enough to escape our screening processes. In an effort to eliminate these and see what remained we subjected each table to a further search for interference. In this case, any channel which was "interference" in any search point was considered interference-prone at *all* points, and was not considered at any position in the search.

The three hit tables from the previous searches were each subjected to this procedure, producing new hit tables. Five new lists of signals for re-observation were created from these new hit tables. The search for signals in adjacent channels was performed on each of the two boxcar-smoothed data sets (for which the adjacent channel search previously produced too many signals), producing two lists (Search #5 and Search #6) with a combined total of 27 positions of interest. Twenty of these were previously detected objects. Of the rest, all were re-observed, and none were confirmed detections. In addition, we made

three more lists (Search #7, Search #8, and Search #9) containing all of the interesting signals in each hit table - a total of 104 possibilities. Of these points, 36 were points found by other software searches already, and 25 were previously found galaxies. All of the remaining 43 were re-observed, finding a single new detection. This detection was of an extended object which had previously been found in a neighboring slice position by the visual search.

Final Tally of Detections

In the end, through the visual and software searches, the slice observations detected extragalactic atomic hydrogen in 101 of its 14,130 positions. Because some objects extend over several slice points, the 101 detections are due to 79 individual objects. These objects were divided into two categories:

1. Detections which were due to previously known "cataloged" galaxies.

2. Detections which were due to previously unknown "uncataloged" galaxies.

To determine which category each of the objects detected fell into, we consulted a number of catalogs and lists of catalogs. The most useful of these for this work was the NASA Extragalactic Database (NED), a service which could be consulted on-line. We used NED (1993) to look up the names and locations of all objects within a 10 arc minute radius of the position of each of our detections. We then plotted each of these positions on a blown-up patch of the Palomar Sky Survey (POSS) prints, and identified the visual counterpart of each one to see if it could plausibly have been detected by Arecibo's 3.3' beam. If redshift velocities were available for the cataloged objects, these were compared to the redshift velocity of the detection. In addition, HI detections were available for some of the cataloged objects, contained in the HI catalog published by Huchtmeier and Richter (1989). The redshift velocities and relative strengths of these measurements were compared to those of the slice detections.

Deciding whether or not a slice detection was due to a previously cataloged object was rarely difficult with all of this information. The two most common scenarios encountered were either: A cataloged object with the proper redshift was located well within the Arecibo beam radius of the position of the slice detection, or; No cataloged objects were located within 10 arc minutes of the slice detection. In the former case, the detection was considered of a cataloged object, in the latter it was considered an uncataloged

object. Ambiguities remained in situations where a cataloged object was close enough to the Arecibo beam on the sky to cause the detected HI signal, but was accompanied by no redshift velocity information. In these cases we considered the origin of the detection in question. Later HI "hex" at Arecibo and optical observations at Kitt Peak using Hα filters allowed us to determine if the cataloged objects indeed had the correct redshifts (see below). All remaining ambiguities were resolved in this way.

To our two categories of objects (cataloged and uncataloged) we added a third category - undetected. These were cataloged objects known to be in the slice search volume, but which the slice search failed to detect. Our final inventory of objects within the slice search was as follows:

1) Uncataloged objects detected by the slice search: 41

2) Cataloged objects detected by the slice search : 38

3) Cataloged objects the slice search failed to detect: 10

Was the Software Search Worthwhile?

In the end, the software search yielded not a single new object to add to our inventory, although it did detect one known object in a position it had not been noticed before. It is probably important for us to ask ourselves why this aspect of our search was so unsuccessful. One serious disadvantage the software search had was that it was performed *after* the visual search, so it was assigned the task of discovering objects which the visual search had missed. It *was* able to detect large numbers of objects which the visual search had already found. The inability of the software search to find additional objects may indicate that the visual search was highly effective, and that there was little more to be found in the spectra. A second possibility is that the software search was simply not very sensitive. Tuning it to generate a reasonable number of signals was a very touchy business - it was fond of either producing thousands of suspicious signals (which would have overwhelmed our confirmation procedure) or only small numbers of the most obvious signals. We can examine which of these may be the root cause by checking how many of our visually detected objects were found by the software search, and what sorts of HI signals they represented. If the software search found only the strongest HI profiles, perhaps it was tuned poorly. Or if it found most or all of them, perhaps we can feel confident that we are locating everything in the slice region.

Out of the 100 detections in the original slice search data (for the purposes of this discussion, we will not consider the "low velocity" test sample, since it was not subjected to the same detection procedures), 99 were detected by the visual search. A single confirmed detection of a previously-found extended object was the only unique detection made by the software searches. However, an additional 50 of the visually-found positions were detected by one or more of the software searches. While the visual search was very thorough in detecting objects our software algorithms were sensitive to, the reverse was not true. We can trust the computer to find only about half of the objects a human would. A breakdown of the success of each of our nine searches is given in Table 3.1.

In column 1 of Table 3.1, we give the name assigned to each of our software search lists (see the previous discussion for a description of the search associated with each name). Column 2 gives the smoothing technique applied to the data, either Hanning, 9 channel-width boxcar, or 17 channel-width boxcar. Column 3 contains the type of algorithm used to pick suspicious signals out of the hit tables containing channels with possible signals in them. As described in the previous section, the three approaches used were to look for signals in two or more adjacent channels ("adjacent channels"), or look for signals in the same channel in adjacent points on the sky ("adjacent points"), or to screen out all channels which had contained interference at any point in the slice search and use all remaining signals ("screen interference"). Column 4 gives the total number of slice positions which the search indicated as suspicious. All of these points were searched using conventional ON/OFF observations. Column 5 gives the number of these suspicious positions which were the locations of real extra-galactic objects (all but one of which were previously found in the visual search). Column 6 gives the number of positions which were real detections uniquely identified by each search, that is, the number of points which were found by it and no other software search.

This table can aid us in improving the software search technique. From it, it is clear that some types of searches were more effective than others. There are a number of ways to evaluate them. Certainly, at some level we wish to maximize our chances of detecting things, so the searches which found the highest numbers of objects were desirable. Search #1 out-performs all in this category. Yet each "suspicious"

signal which a search finds consumes telescope time to re-observe, whether it is real or not, so at some level we would like a search to have a high ratio of real detections to suspicious points. Search #5 finds only 11 real detections, but these represent 79% of the points it flagged as suspicious, compared with 47% for Search #1. Finally, we should consider the ability of some searches to find objects which no other searches are able to detect. A high sensitivity to particular types of objects which other searches can not find is particularly useful. Search #1 and Search #8 are the most capable in this category.

While the software search was clearly not as successful as the visual search at detecting objects in the slice data, it had some distinct advantages which should be considered. We can be certain the software search was entirely impartial, and equally thorough with all of the data. What effect this might have, and to what extent the visual search may have been more inconsistent is impossible to gauge, however it is arguable that in any statistical study such as this impartiality is a good thing. Another clear advantage of the software search is the time involved in performing it. While software may take a long time to develop, it generally takes very little time to run, and it can be repeatedly run while making small adjustments. While a complex software search might take minutes (or in a few cases hours) to analyze the slice data, the visual search took nearly a week. The visual search was supremely taxing on those unfortunate enough to have to do it, and repeating it was a task which was avoided in all but the most extreme circumstances (in fact, the visual search was repeated only once when it was found to be detecting greater numbers of objects with progressive observations). While there was possibly room for improving the process, there was great resistance to implementing any changes. In contrast, the software search was run many times, which allowed for many adjustments and improvements. Finally, it should be noted that the software search was fairly effective at detecting real objects as a percentage of the number of suspicious signals it produced. Of the 165 positions the software search flagged, 50 turned out to be real objects, a success rate of 37%. The visual search pointed to 858 positions, only 99, or 12% of which were real. Because each indicated point requires additional telescope time to re-observe, this is an important consideration. Perhaps if the software searches were run with lower limiting thresholds, they would not

only have indicated vastly greater numbers of suspicious points, but would also have detected more of the objects found in the visual search.

What sorts of objects is the software search detecting? To further assess the capabilities of software, we would like to know how effective it is at finding the weaker HI signals. Perhaps it is detecting 50% of the objects found in the visual search, but it is of little use to us if it detects only the massive objects easily detected by visual inspection. The one unique detection we can attribute to the software search is encouraging, as it is a very weak signal. In addition, we should look at how effective the software search was at detecting objects which were not previously cataloged, as locating these objects is one of the primary goals of the slice survey.

Of the 43 slice positions which were found by the visual search to be caused by uncataloged objects, 16, or 37% were found by the software search. These signals were due to 14 of the 40 uncataloged objects. Of the 57 slice positions where cataloged objects were detected by the visual search, the software search found 35, or 61%. These signals were caused by 27 of the 39 cataloged objects. Thus the software search is almost twice as effective at locating the cataloged objects as it is at finding the uncataloged ones.

In Figure 3.2 we plot the HI flux against the 20% velocity width for all objects detected by the software search. Also on the plot is the "5σ limit" which we believe approximates the detection limit of the visual search (the derivation of the 5σ limit, as well as the quantities involved in this analysis is included in later chapters). Figure 3.3 is a similar plot showing all of the objects detected by the visual search which were missed by the software search. Predictably, the software search had difficulty detecting those objects which had low integrated HI fluxes (mean HI fluxes of objects in each sample are 3.56±2.49, 1.63±1.08, and 2.63±2.17 for objects found by software, objects missed by software, and objects found by the visual search respectively). In contrast, the software search was about as effective as the visual search at detecting objects with narrow velocity widths (mean 20% velocity widths are 241±142, 191±125, and 216±136 for objects found by software, objects missed by software, and objects found by the visual search respectively).

In Figures 3.4 through 3.11, we examine the effectiveness of each software search individually. While the small numbers of detections in some of the searches make useful interpretation of the plots associated with them difficult, the set as a whole can tell us something. It is pretty clear that all of the searches except Search 1 (Figure 3.4) are sensitive to subsets of the whole range of HI flux and velocity width values. For instance, Search 7, Search 8, and Search 9 (Figures 3.9, 3.10 and 3.11) have effectively eliminated objects with large velocity widths. This might be expected, because these searches were rigorous in eliminating interference, and possibly flagged some of these wider objects as interference. It is also apparent that the wide-boxcar smoothing techniques (Searches 4, 5, 6, 8, and 9) managed to eliminate most of the narrow-width, weak flux objects. This is to be expected, as these searches were meant to be sensitive to wider, low flux objects. However, since these searches show no increased tendency toward detecting these objects either, the wide smoothing techniques can perhaps be considered less than optimally effective. In the end, Figures 3.4 through 3.11 imply that the most effective software technique is also the most obvious - that of Search 1. This was simply to Hanning smooth the data, eliminate obvious interference, and then examine any spot where two or more adjacent channels had signals in them. In future efforts, this may be the avenue to pursue.

Follow-up HI Observations: The Hex Procedure

In the original survey the beam spacing is 4 arcmin. While this spacing is fine enough to detect nearly all sources within the slice area with fairly uniform sensitivity, it does not establish the position or determine the total HI flux as accurately as possible. Therefore we undertook a series of observations at about half of this beam spacing around each of the detected sources.

We developed an observing pattern somewhat like the traditional "on-off" method, but in a single observation the selected position along with six equi-spaced beams around the center. These seven positions formed a hexagonal pattern of one minute "on" observations, and they were followed by a single, shared five minute "off" integration at a position tracking the approximate mean telescope altitude and azimuth during the "on" scans. In the Arecibo telescope-control language we named this pattern "HEX" (for hexagonal), and refer to these as "hex scans" elsewhere in the text.

As discussed earlier, by employing an "off" scan much longer than an "on" scan it is possible to achieve a noise equivalent to a traditional on-off scan (with equal on and off times) of nearly twice the "on" time integration. Thus, each of the hex positions is nearly the equivalent of a two-minute "on", two-minute "off" integration, which would have required 28 minutes (versus 12 minutes) of integration and substantially more overhead in telescope motion. The disadvantage is that by sharing offs, there is some correlation of the noise, although this is usually dominated by the "on" scan contribution.

These observations were carried out mainly with the 22 cm feed tuned to maximize the frequency response at the redshift of the source being examined. For low-redshift sources we either tuned the 22 cm feed to its maximum frequency (corresponding to about 5000 km/s) or used the 21 cm feed. All four segments of the correlator were set to the same central frequency, providing two spectra from each polarization of the feed. This redundancy improves the noise slightly because of the different amplification and correlation pathways used. The spectra were otherwise of the same width and resolution as the original slice spectra.

We re-observed all of the sources with the hex pattern, including several uncertain sources and one (#22--UGC 12663) that had a previously reported detection within our velocity range (Giovanelli & Haynes 1989), but which we were unable to confirm. We were also unable to confirm this detection with standard on-off observations, so it has been dropped
from the list of "slice inhabitants."

For each hex observation we attempted to interpolate a more accurate position by comparing the integrated flux at the three positions with the largest integrated fluxes. We believe these positions are accurate to better than one arcmin. When scheduling permitted we also repeated hex scans around the new positions and further refined our estimates, and this was carried out for most of the sources.

Our final step was to make an improved estimate of the total flux from the source by combining the spectra from the seven hex positions. Based on the beam pattern of the 22 (and 21) cm feed we determined that we could generate a nearly uniform response over an area almost 5 arcmin in diameter with a gain close to forward gain of a single beam by summing the central spectrum with a weight of 0.25

with the six surrounding spectra, each with a weight of 0.5. The integrated flux measured in this combined spectrum reflects the total emission over an area large enough to account for all of the hydrogen in the sources studied here.

It is also of interest to use the ratio of the flux measured in the combined spectrum to that in the central spectrum to estimate the extent of the HI. If the gas is confined to an area approximately smaller than 2 arcmin in diameter, this ratio should be about one since little of the HI extends beyond the high sensitivity portion of the single beam. For extended sources, this ratio grows successively larger as more and more HI is picked up by the surrounding beams. For the most part our sources show ratios near one, although some have ratios significantly larger. Unfortunately, most of the larger ratios are in cases where the source was not well-centered within the hex scan, so the flux ratio is no longer reliable. Nevertheless, this might be an interesting approach in future experiments.

The values (fluxes, velocities, linewidths) we use in our subsequent analyses are those determined from the combined spectra, since these should be the best measure of the overall properties. However, for estimates of the sensitivity of our survey we use the central single-beam flux since this is the maximum response of the telescope to the source.

Optical Observations of the Slice Objects

Optical CCD images of all known objects in the slice region were taken in September of 1991 and November of 1992 using the 0.9 meter NOAO telescope at Kitt Peak. In this section we describe these observations and the reduction procedures applied to them.

The galaxies in our slice can be divided into three groups, which we used to prioritize our optical observing: 1) objects which were detected by the 21cm search but were not known previously (41 total); 2) objects which were detected by the 21cm search and which were previously cataloged (38 total); and 3) objects detected and cataloged previously which were not found by the 21cm search (10 total); .

Optical observations of these objects were intended to accomplish a number of goals. Above all else, we wished to identify, if possible, optical counterparts for all of the detections in the slice search, most importantly those which were new detections (group 1). The identification of optical counterparts, or the

failure to do so, would establish the relative numbers of optically invisible "HI clouds" - objects with little or no stellar emission. Because the slice search is the first to gather a statistically large sample of HI detections in a blind HI survey, it has the first opportunity to assess how common these objects are. Secondly, we wished to examine the stellar populations of our objects, to uncover any commonalty among the stellar characteristics of each group which might explain why they had been previously detected at optical wavelengths or not, or why the slice search was, or was not able to detect them with 21cm observations. Examining the different morphologies of our objects, including the presence of companions and evidence of tidal interaction was also important for identifying the reasons they were detected previously or not. In addition, there is an undeniable desire to know what our detections "look like," particularly in the case of the newly discovered objects, which we are seeing for the first time.

In keeping with these goals, our first priority in our optical observing was to obtain B and R frames for the members of group (1), then the same for groups (2) and (3). After that, we wanted H-α images of group (1), I band images of all objects, and finally H-α images of groups (2) and then (3). Our reasons for this priority structure were as follows. Because they require short integration times and sample generally different bulk stellar populations, B and R frames are ideal for establishing the existence (or non-existence) of optical counterparts to all of our newly-detected objects (group 1), which we considered our first duty. Comparing stellar populations between the three groups was next on the agenda, requiring a complete set of B and R frames for all objects. Next we wished to confirm that any optical counterparts of our new 21cm detections (group 1 again) have the same redshift velocities as our HI profiles do. H-α filter sets have narrow velocity ranges, and can be matched to the 21cm velocities. I filter frames show us very red stellar populations, which would be illustrative if our new objects are dwarfs dominated by old stars. Finally, H-α images show us active regions of massive star formation, and we would like to compare these between all object types.

Telescope time is of course limited, and we did not have the time to observe every object in our list using every filter. However, most of what we wanted to do was completed. B, R, and I filter images required only between 5 and 10 minutes of integration each, and we were able to schedule observations of

all of the objects in our sample at these wavelengths. Most of the new detections (group 1) were observed more than once using the B filter, and occasionally the R filter, to allow higher signal-to-noise combined frame images to be produced. H-α images took considerably longer - between 20 and 30 minutes. All but one of the new 21cm detections (group 1) were completely sampled in H-α. We had time to cover roughly half of the previously cataloged objects detected in the slice search (group 2) as well.

We had roughly 100 objects to observe using 4 different filters. Along with the required calibration frames, we compiled over 600 individual images. As in any enterprise of this size, some mistakes were made, and our data set emerged with some blemishes. Several objects were not properly observed with all of the filters, even when images were taken. Because of the long integration times involved, most of the troubles were with the H-α frames. Since these were being scaled against the R frames, we did not require photometric conditions, and during the 20-30 minutes each of these images required occasionally the appearance of clouds would obscure the sky and/or cause us to lose guide stars and telescope pointing. These problems could occur with the B, R, and I observations as well, but we did not knowingly observe with any of these filters if conditions were not photometric. In addition, the shorter integration times required for these frames allowed them to be re-scheduled easily. Our total allotted telescope time was insufficient for observing all of our objects at H-α, so rescheduling a failed observation of one object was only achieved at the cost of another. Thus unless we were particularly interested in the H-α emission of an object, a "failure" was usually kept as a "partial success", and we moved on to another object. Even good H-α frames proved unsuccessful in many cases because the emission of many of our objects, particularly the new detections (group 1), was extremely faint or invisible.

For both the September, 1991 and the November, 1992 observations, we used the CCD Direct-Imaging Camera of the Kitt Peak National Observatory 0.9 Meter Telescope. For the September, 1991 observations we used the 1024x1024 pixel ST1K CCD chip, a somewhat aged device with many defects. This chip was retired soon after those observations, and in November, 1992 we used the T2KA 2048x2048 chip, which had considerably fewer defects. We made efforts to shift our pointing and position the images of our objects such that they avoided the defects in the ST1K chip, but in some cases this was impossible

due to the size of the objects or the presence of more than one object in the frame, and in some other cases this procedure was done imprecisely, and the defects were not avoided.

Conveniently, the pixel scales of the two chips used are very similar, giving us similar resolution for both sets of observations (the resolution of the ST1K chip was 0.60 arcsec/pixel, while that for the T2KA was 0.68 arcsec/pixel). In addition, the efficiency (DQE) of the two chips are within a few percentage points of each other at all wavelengths. These similarities allow us to cross-compare images from the two observing runs with confidence.

In a few cases bad weather, scheduling difficulties, and low priority conspired to make proper observations of an object impossible even with the short integration B, R, and I filters. These problems were mostly confined to the objects which were not detected at 21cm (group 3). In addition, a couple of objects simply fell through the cracks in our bookkeeping - we had the time to observe them, but failed to schedule them, observed the wrong position, or simply over-looked them.

Reduction

All of our observations at Kitt Peak were performed using the NOAO Image Reduction and Analysis Facility (IRAF) software package IRAF Control Environment (ICE) observing routines. Reducing the images was done following standard techniques, although not necessarily using standard software tools. Most reduction was done in the IRAF image reduction environment. Combined bias (or "zero") frames were produced for each night of observing, and these were subtracted from all image and calibration frames. We were fortunate in that very little flattening was required for most of the images.

Cosmic ray hits were prevalent on all images, particularly the long integration H-α frames. These often caused one or several pixels on the CCD to have very large positive or negative counts which would dramatically alter the final integrated counts. Unfortunately, we found the routines within the IRAF environment ineffective at removing these cosmic ray events from our images. To solve this problem, we wrote a very effective, although computationally intensive routine called *zcosmic* to clean cosmic ray events from our CCD images. Quite simply, the algorithm used was to examine every pixel in an image and decide whether it and the points around it fit a gaussian model with a width matching the seeing for

the image. A *zcosmic* run took a dedicated Sparc IPX approximately 20 minutes to clean a 1024x1024 image of cosmic rays. It was applied to all of our galaxy images.

Once a background was subtracted and images were flattened and cleaned of cosmic rays, multiple images of objects, where they existed, were combined using IRAF procedures. Where stars interfered with images of galaxies, they were removed. Total pixel counts from galaxies were then accumulated, and translated into fluxes using conversions computed from a group of standard stars observed over the course of our telescope time. Final optical flux measurements for each object are presented in the next chapter.
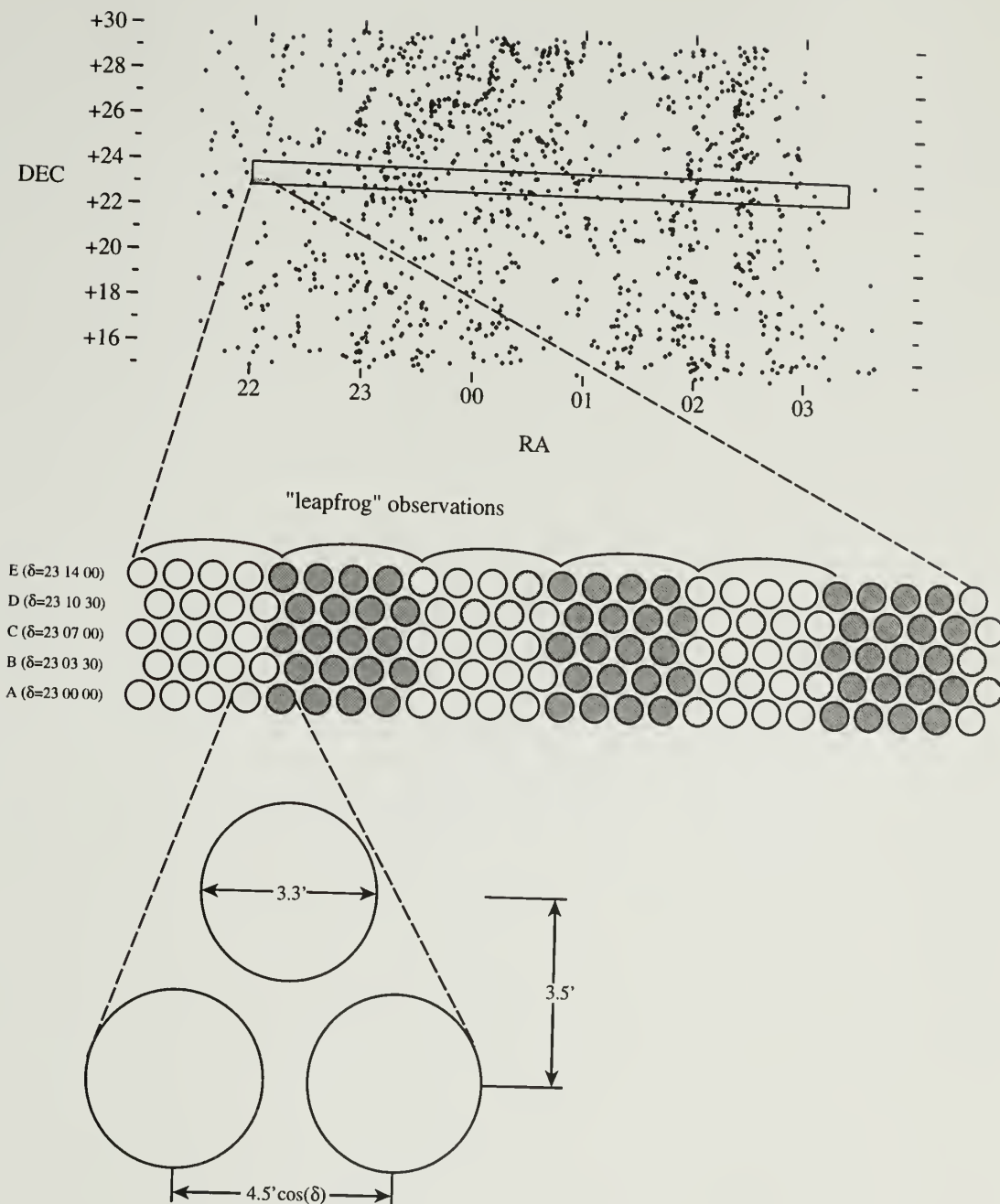
Figure 3.1. Schematic representation of the slice search strategy. The upper plot shows the sky region of the search, with RC3 galaxies represented as dots. The lower plot shows the honeycomb pattern of telescope positions used.
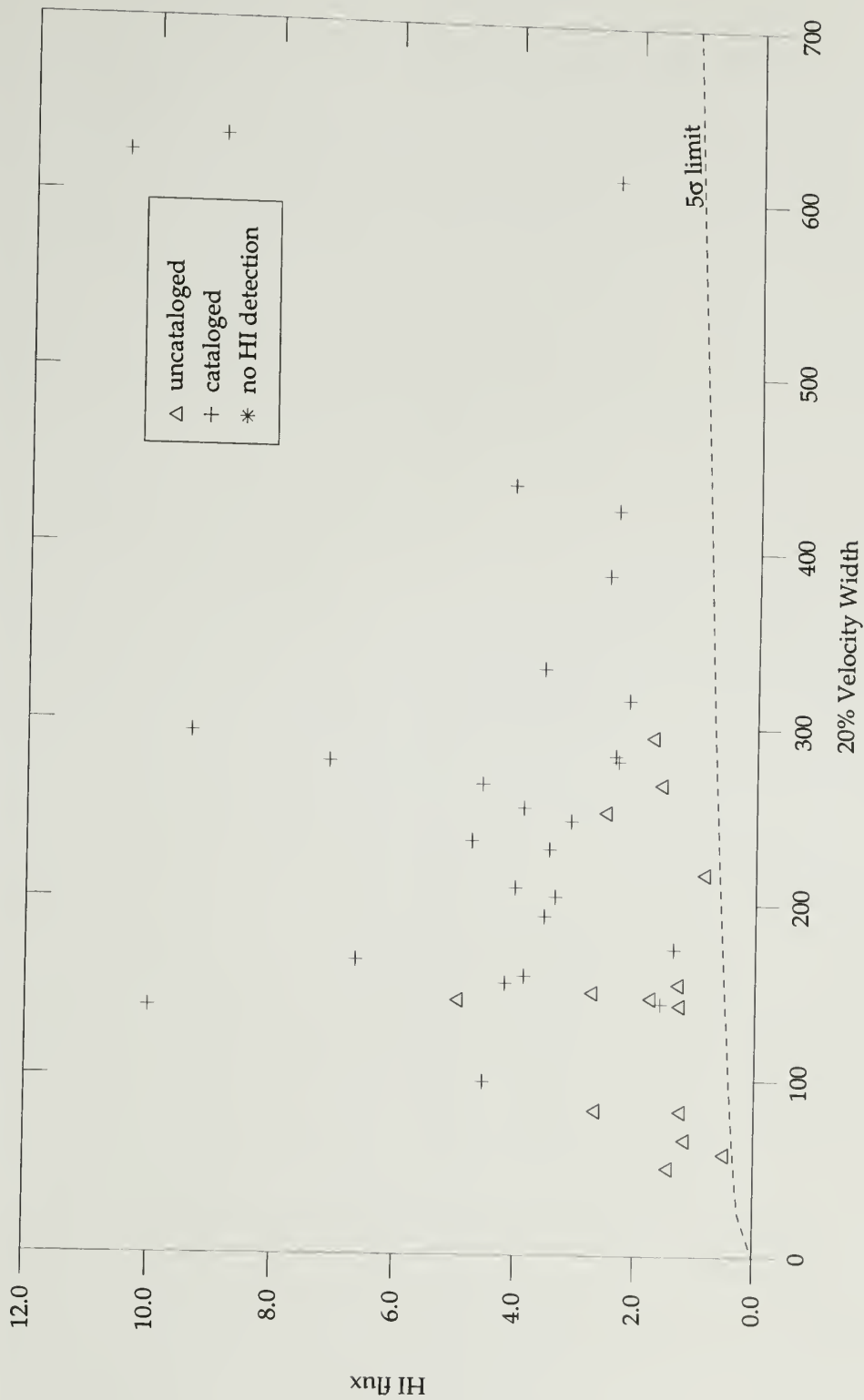
Figure 3.2. HI fluxes and velocity widths of slice objects detected by all software searches. Uncataloged galaxies are represented by triangles, cataloged galaxies by crosses. The dashed line represents the 5σ detection limit.
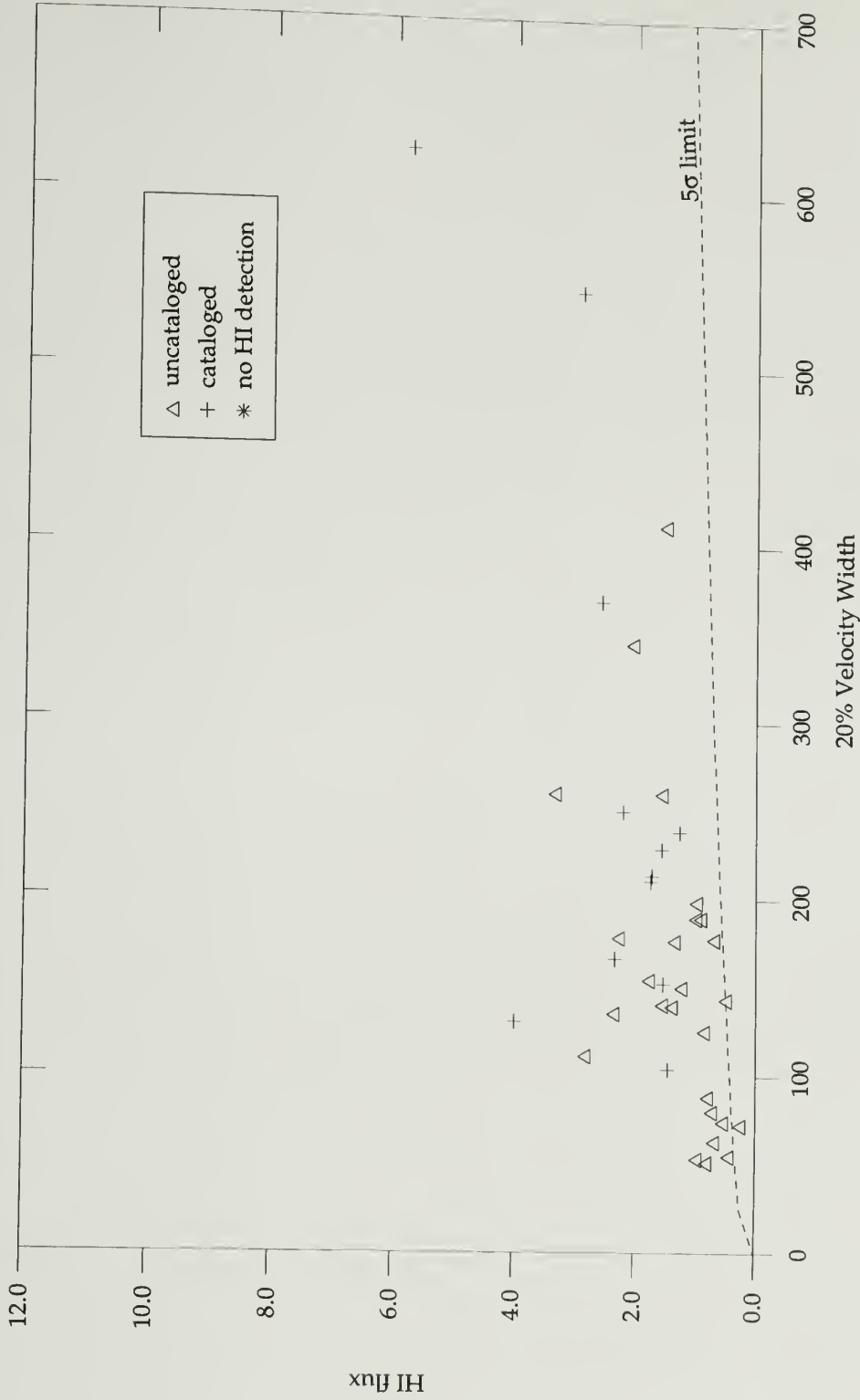
Figure 3.3. HI fluxes and velocity widths of slice objects not detected by the software searches. Uncataloged galaxies are represented by triangles, cataloged galaxies by crosses. The dashed line represents the 5σ detection limit.
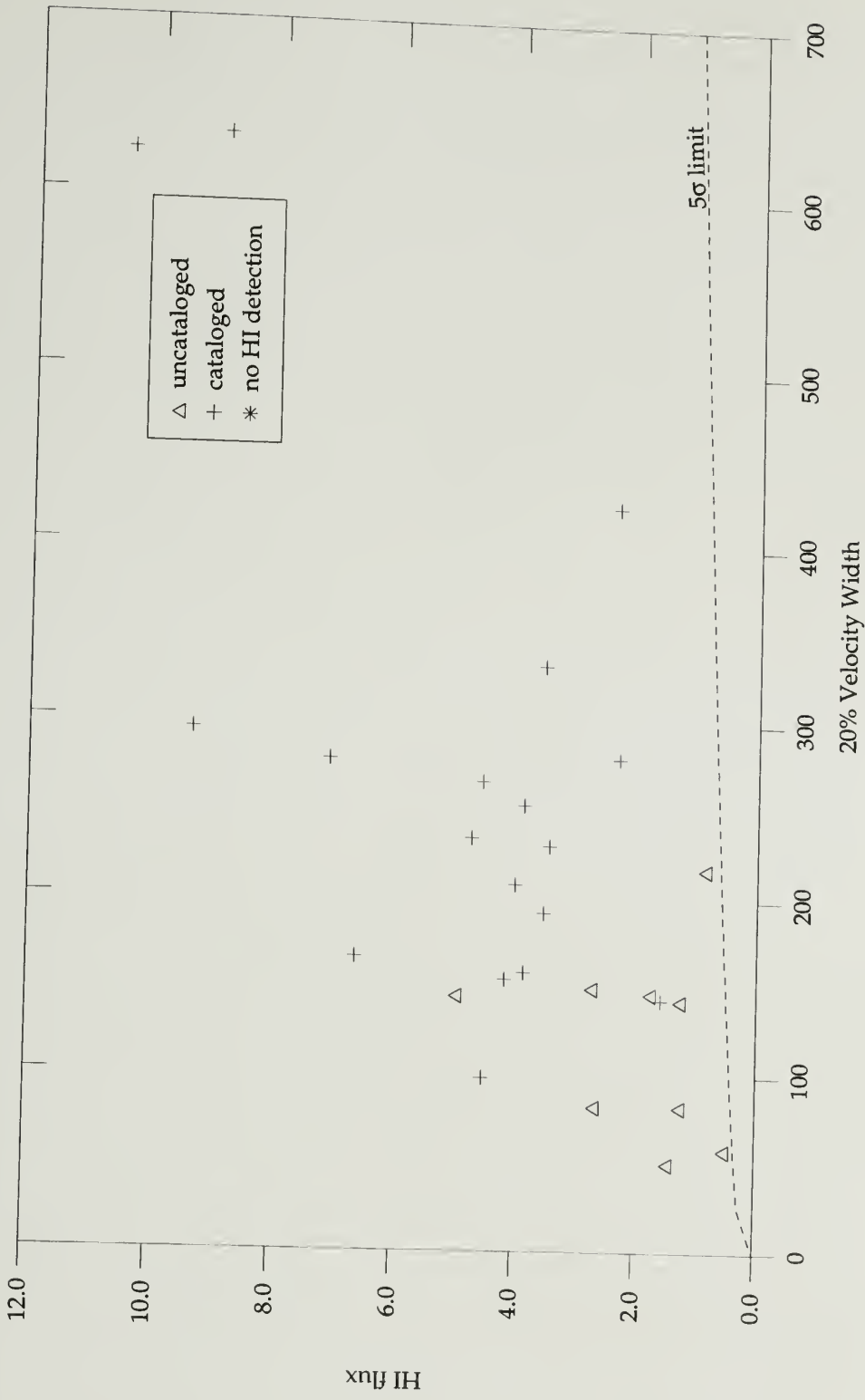
Figure 3.4. HI fluxes and velocity widths of slice objects detected by software Search 1. Uncataloged galaxies are represented by triangles, cataloged galaxies by crosses. The dashed line represents the 5σ detection limit.
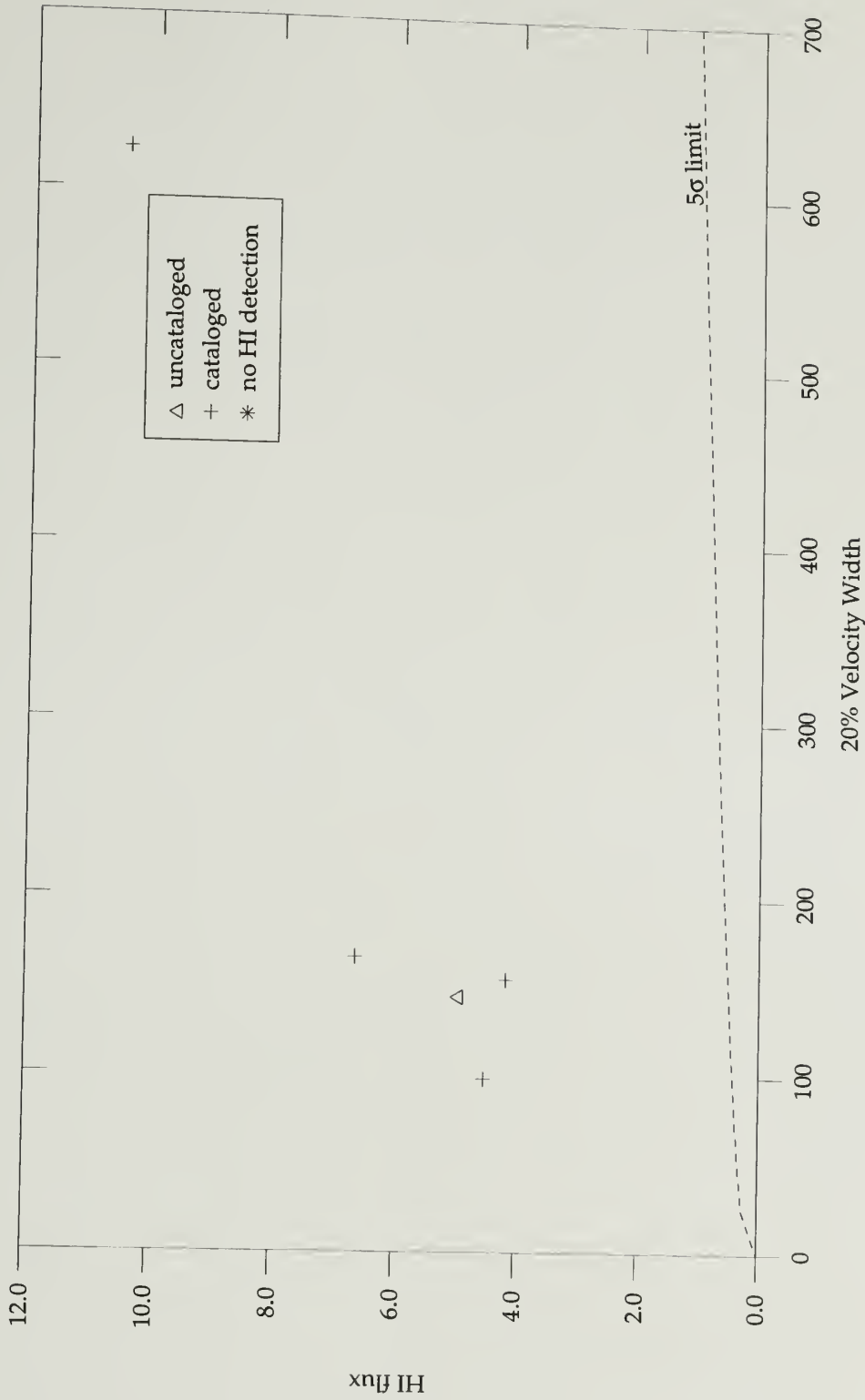
Figure 3.5. HI fluxes and velocity widths of slice objects detected by software Search 2. Uncataloged galaxies are represented by triangles, cataloged galaxies by crosses. The dashed line represents the 5σ detection limit.
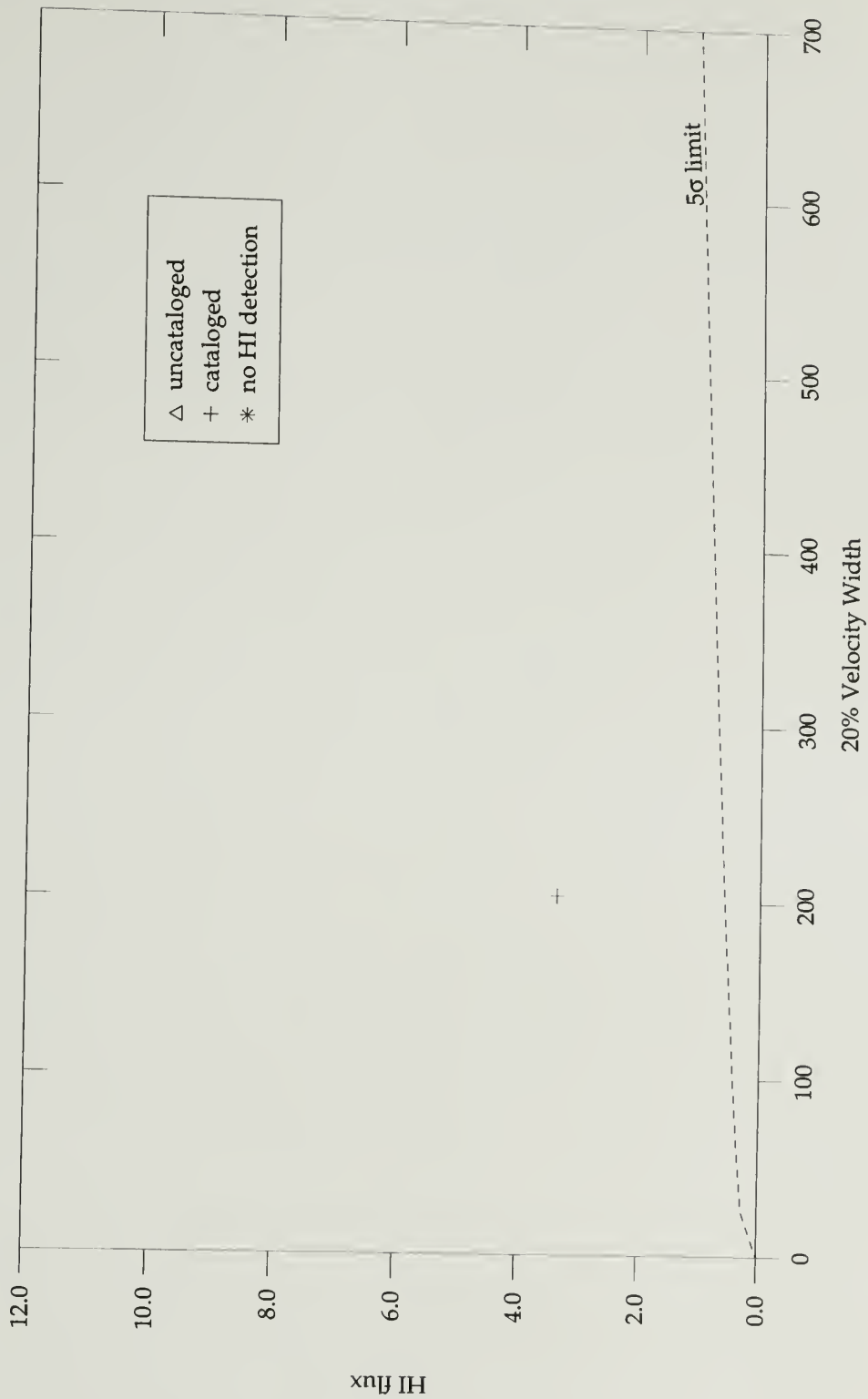
Figure 3.6. HI fluxes and velocity widths of slice objects detected by software Search 4. Uncataloged galaxies are represented by triangles, cataloged galaxies by crosses. The dashed line represents the 5σ detection limit.
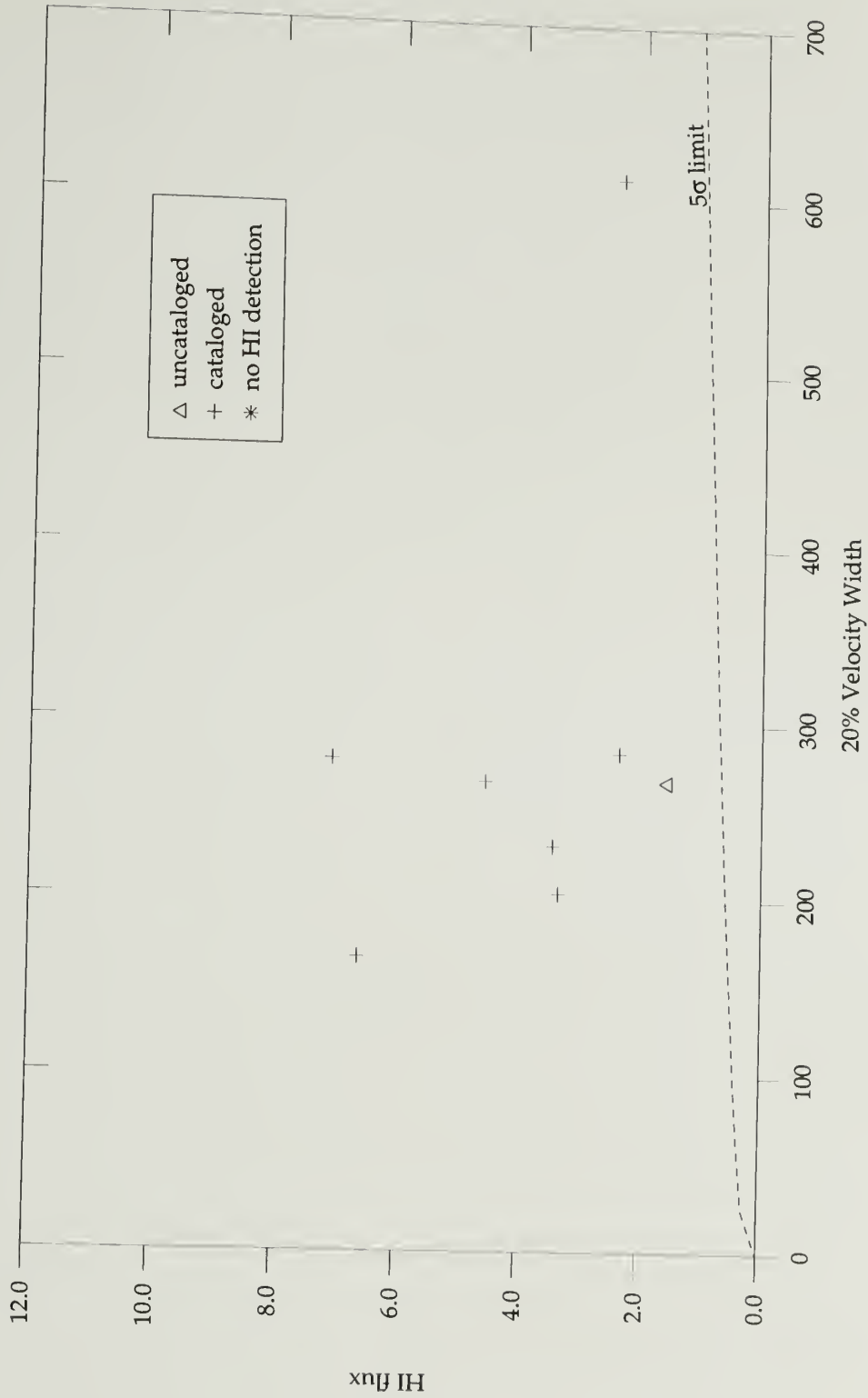
Figure 3.7. HI fluxes and velocity widths of slice objects detected by software Search 5. Uncataloged galaxies are represented by triangles, cataloged galaxies by crosses. The dashed line represents the 5σ detection limit.
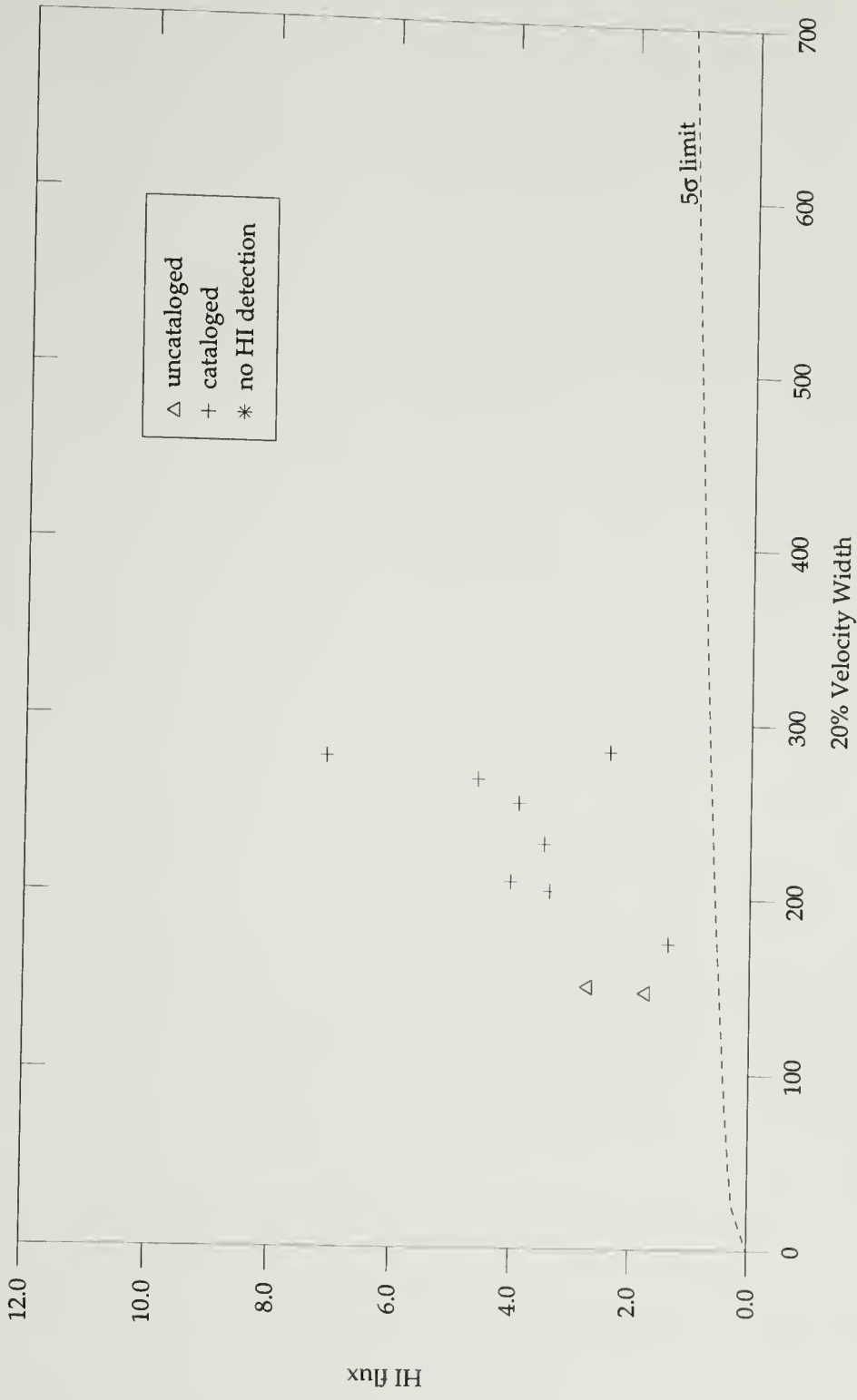
Figure 3.8. HI fluxes and velocity widths of slice objects detected by software Search 6. Uncataloged galaxies are represented by triangles, cataloged galaxies by crosses. The dashed line represents the 5σ detection limit.
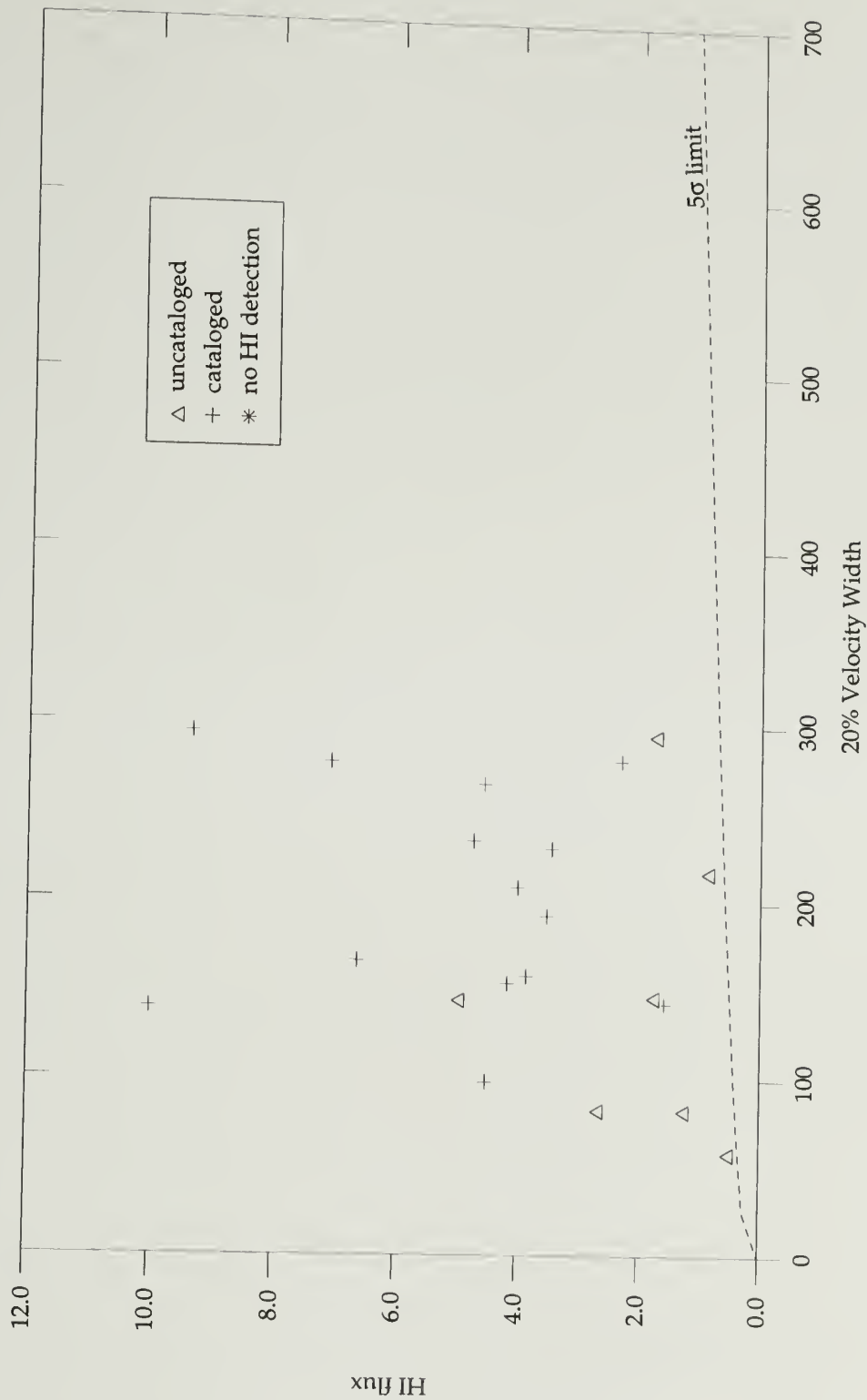
Figure 3.9. HI fluxes and velocity widths of slice objects detected by software Search 7. Uncataloged galaxies are represented by triangles, cataloged galaxies by crosses. The dashed line represents the 5σ detection limit.
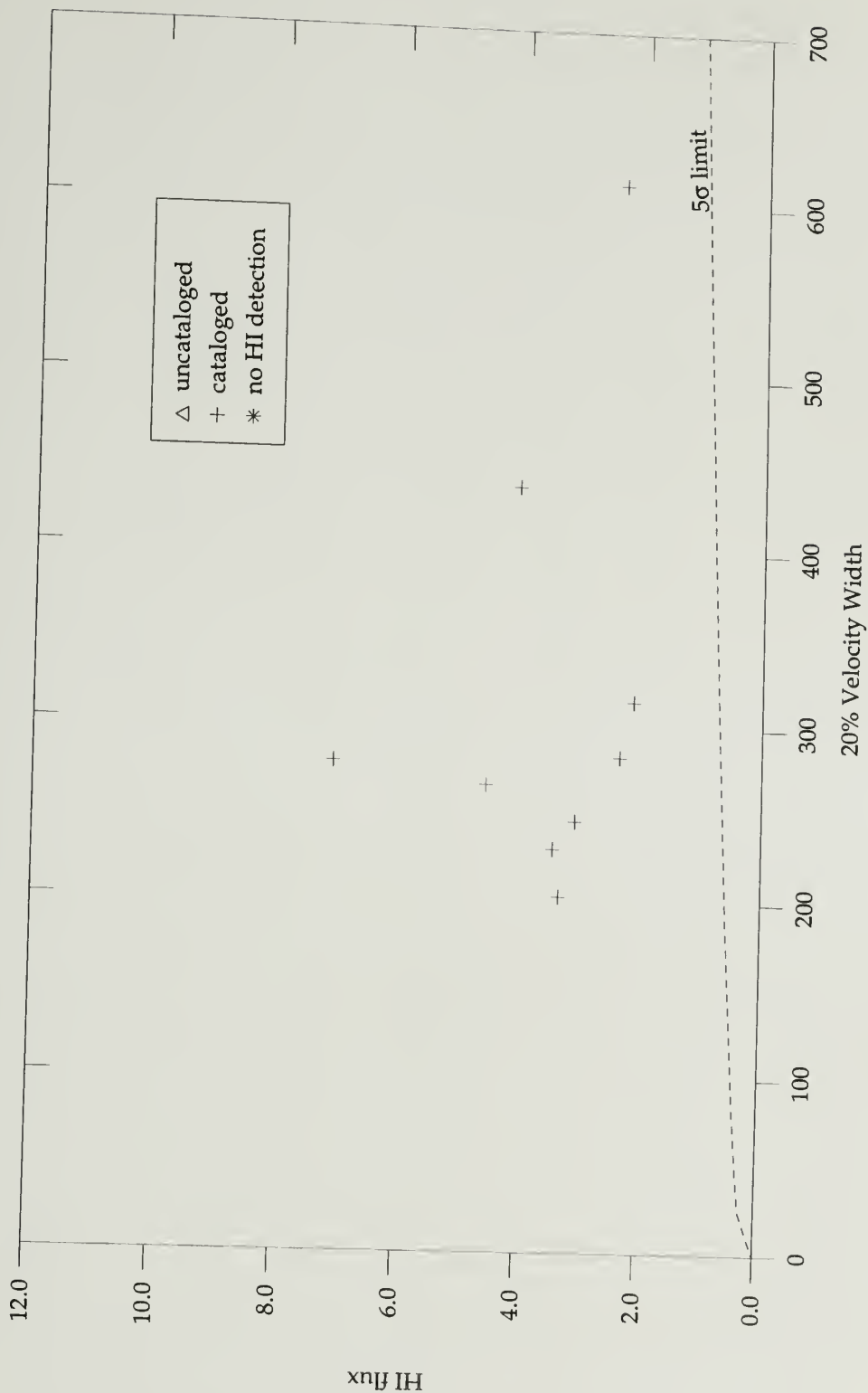
Figure 3.10. HI fluxes and velocity widths of slice objects detected by software Search 8. Uncataloged galaxies are represented by triangles, cataloged galaxies by crosses. The dashed line represents the 5σ detection limit.
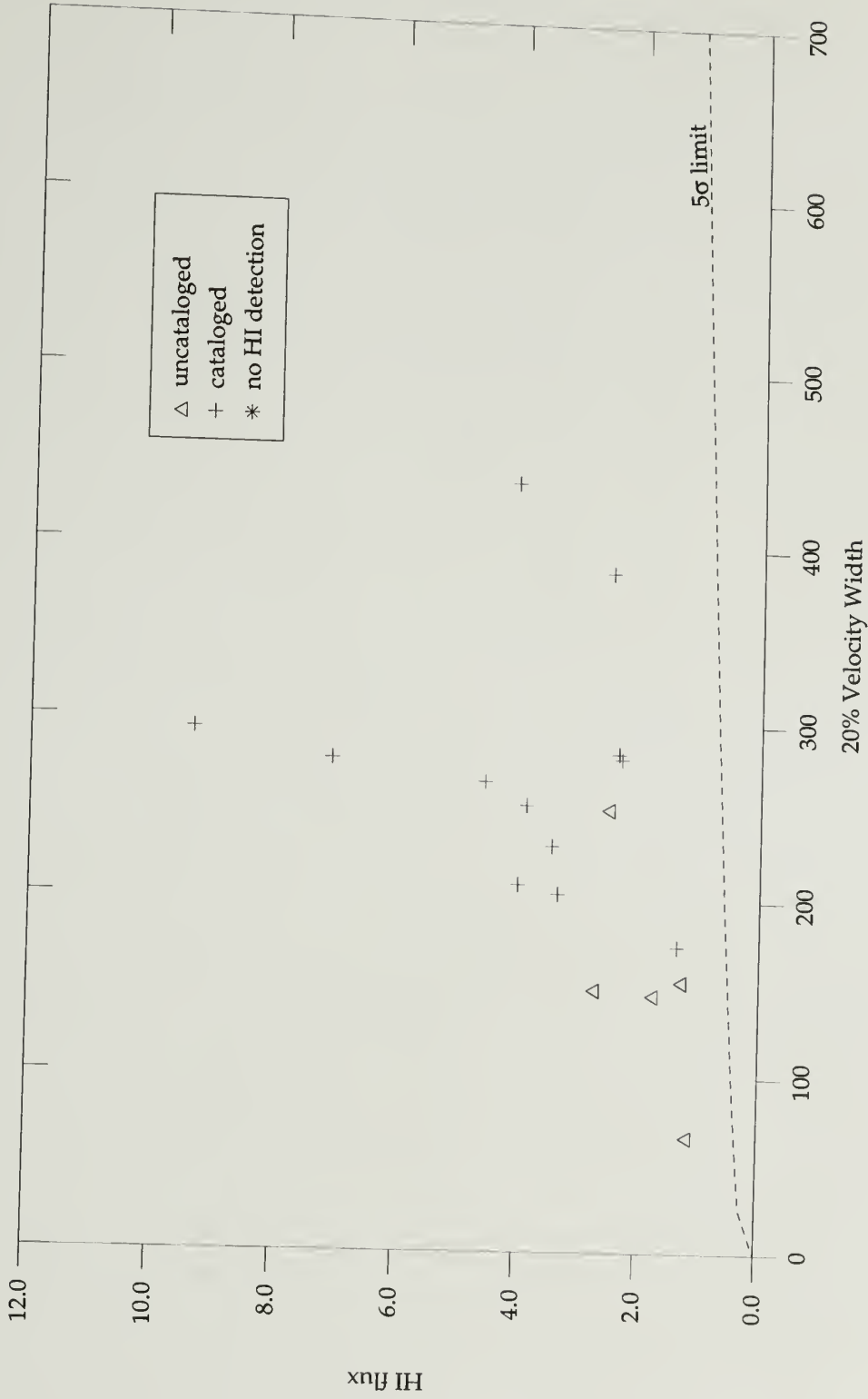
Figure 3.11. HI fluxes and velocity widths of slice objects detected by software Search 9. Uncataloged galaxies are represented by triangles, cataloged galaxies by crosses. The dashed line represents the 5σ detection limit.

**Table 3.1. Software Search Performance**

Search (1)	Smoothing (2)	Search Algorithm (3)	Points (4)	Detections (5)	Unique (6)
1	Hanning	Adjacent Channels	77	36	7
2	Hanning	Adjacent Points	23	11	0
3	9 Channel Boxcar	Adjacent Points	4	0	0
4	17 Channel Boxcar	Adjacent Points	11	2	0
5	9 Channel Boxcar	Adjacent Channels	14	11	0
6	17 Channel Boxcar	Adjacent Channels	13	8	1
7	Hanning	Screen Interference	40	22	1
8	9 Channel Boxcar	Screen Interference	45	18	4
9	17 Channel Boxcar	Screen Interference	29	10	2

CHAPTER 4

THE DATA

In this chapter, we present the physical data, both measured and derived, for all of the objects observed in the HI Slice Search. These data are presented in Tables 4.1, 4.2, and 4.3. Where appropriate, we include descriptions of the processes followed to arrive at individual values. To introduce some order to the large number of quantities we present, the data is divided into three sections: measurements from HI observations (contained in Table 4.1); measurements from optical observations (contained in Table 4.2); and values derived from the measured quantities (contained in Table 4.3). A cross-section of catalog names given to the cataloged objects in the slice region are presented in Table 4.4. We also include a section containing notes describing particularly interesting or unique qualities of many of the objects in the slice search. In the final section in this chapter, we present R-band optical images of all of the slice objects for which we have such data. These objects are scaled such that their relative physical sizes are represented.

HI Data

The measured data associated with the atomic hydrogen observations are listed in Table 4.1. A column-by-column description of each quantity follows:

1.   The first column contains an index number, used to easily associate objects between the tables and the images. The numbers are in order of right ascension except in one instance where a later refinement of position shifted two objects with very similar values.

2.   *Object Name:* For the purposes of listing the slice data, a consistent naming scheme was developed for all objects. The previously cataloged objects in the slice search had names (sometimes several) from the catalogs in which they appeared. Naturally our newly discovered objects had no such names. We present our objects with catalog names where they are available (our preference is to pick UGC names if they exist, and then, in order of preference, NGC, IC, MCG, and finally CGCG names), and with the name of the slice position where they were discovered if they are not

cataloged. Occasionally a newly detected object has detections in several slice positions. In these cases, object names were derived either from the slice position determined to be the closest to the actual position of the object, or in some cases the slice position at which the object was first observed.

3.   *C - Object Category*: Three possible entries in this column tell whether an object is (1) uncataloged, (2) cataloged and detected in the slice search, or (3) cataloged and not detected in the slice search.

4+5. α and δ : Positions for the objects were derived primarily from the optical data, or from the 21cm hex observations if there was considerable disagreement between the two sources. Objects for which positions were derived from the hexes are noted as such below.

6.   *Slice Positions:* These are all of the slice positions where each object was detected in the slice search. The naming scheme for the slice positions, which is based on α and δ, is explained in Chapter 3. A blank entry in this column indicates that the object was not detected in the slice search.

7+8.   *l* and *b:* Positions in galactic coordinates, derived from α and β.

9.   *Sdv*: This column contains the flux integral of the object in Jy km/s. Where objects were detected in the slice search, this is the flux integral of the object in the slice position where it was detected, or in the case of objects detected in multiple slice positions, the flux integral of the *strongest* slice search detection. For objects which were not detected in the slice search, the flux integral was either measured at Arecibo with long integrations, or was taken from the literature if it was available (generally from Huchtmeier and Richter). A negative number indicates an upper limit in the literature or Arecibo observations.

10. Sdv_{hex}: This column contains the combined flux integrals for the hex observations of each object in Jy km/s. The hex observations are described in Chapter 3. Rows without measurements indicate that no hex observations were done for the object.

11. V_{hel}: The heliocentric redshift velocity of each object in km/s. These measurements were taken from the slice observations for objects detected in the slice search. For objects not detected in the slice search, long-integration Arecibo observations were used when detections were made. Velocities from other HI observations in the literature were used in cases where these failed. As a last resort, published optical redshift velocities were used.

12+13. W_{50}, W_{20}. These columns contain the velocity widths of each object at the levels of 50% and 20% of the peak flux in km/s. These values were taken from the slice measurements if they were available, then from long-integration Aricebo measurements, and finally from HI observations in the literature where nothing else was available.

14. rms: This column contains the noise level around the baseline fit on the HI observations used to derive the quoted values of Sdv. These value are in mJy.

15. N_h: This column gives the number of "horns" in the HI profile used for the quoted measurements. Two-horned profiles generally indicate spiral galaxies in other than face-on orientations. Single-horned profiles are indicative of elliptical galaxies.

16. S_{pk}: This column gives the peak flux of the HI profile, in mJy. Negative numbers indicate the HI measurement was an upper limit.

Optical Data

The optical measurements for the objects in the slice search region are listed in Table 4.2. All of these data were measured from the reduced images obtained of the slice objects at Kitt Peak, as described in Chapter 3. The values contained in the individual columns are described below.

1.   Index number.

2.   *Object Name:* See above.

3.   *Object Category:* See above.

4. $p.a._{25}$: This column contains the Position Angle of the major axis of the object as it appears out to a surface brightness limit of 25 mag/arcsec^2, measured in degrees from away from a North-South orientation. All measurements were made using R-band images.

5+6. a_{25} and b_{25}: The semi-major and semi-minor axis of the 25 mag/arcsec^2 isophote. These values are in arc seconds.

7. B_{25}: The integrated B magnitude of the object within the 25 mag/arcsec^2 isophote.

8. R_{25}: The integrated R magnitude of the object within the 25 mag/arcsec^2 isophote.

9. I_{25}: The integrated I magnitude of the object within the 25 mag/arcsec^2 isophote.

10. H_{25}: The integrated H$_\alpha$ magnitude of the object within the 25 mag/arcsec^2 isophote. These measurements are from subtracted H$_\alpha$-R images, which in many cases could not be measured.

11. $p.a._{26}$: This column contains the Position Angle of the major axis of the object as it appears out to a surface brightness limit of 26 mag/arcsec^2, measured in degrees from away from a North-South orientation.

12+13. a_{26} and b_{26}: The semi-major and semi-minor axis of the 26 mag/arcsec^2 isophote, in arcsec.

14. B_{26}: The integrated B magnitude of the object within the 26 mag/arcsec^2 isophote.

15. R_{26}: The integrated R magnitude of the object within the 26 mag/arcsec^2 isophote.

16. I_{26}: The integrated I magnitude of the object within the 26 mag/arcsec^2 isophote.

17. H_{26}: The integrated H$_\alpha$ magnitude of the object within the 26 mag/arcsec^2 isophote.

18. $p.a._{26.6}$: This column contains the Position Angle of the major axis of the object as it appears out to a surface brightness limit of 26.6 mag/arcsec^2, measured in degrees from away from a North-South orientation.

19+20. $a_{26.6}$ and $b_{26.6}$: The semi-major and semi-minor axis of the 26.6 mag/arcsec^2 isophote, in arcsec.

21. $R_{26.6}$: The integrated R magnitude of the object within the 26.6 mag/arcsec^2 isophote.

22. B_0: The central surface brightness of the object in B-band, measured in mag/arcsec^2.

23. R_0: The central surface brightness of the object in R-band, measured in mag/arcsec^2.

24. A_B: The extinction, derived from l and b using the model of Burstein and Heiles (1984) which is based on galaxy counts and local HI column densities.

Derived Quantities

Quantities which were derived from the observed values in the previous tables are listed in Table 4.3. Unless otherwise noted, the formulae used to derived these values are from Schneider, et al. (1986). All values in Table 4.3 which require atomic hydrogen measurements used those taken from the original slice observations, as opposed to the follow-up hex observations. Where optical observables are involved, values measured to the 26 mag/arcsec^2 isophote are used. Calculation of many of these quantities requires a value for the Hubble Constant. As the quantities we derive are used for comparisons among themselves only, we have no need or wish to enter the debate surrounding the value of this constant. For all calculations we choose a "middle of the road" value of $H_0 = 75$ km/s/Mpc, with the sole justification that this value seems to generate the least controversy. Several calculations involve the optical sizes of objects, for which we use optical sizes a_E and b_E which are corrected for extinction:

$$a_E = a_{25} + (a_{26} - a_{25}) \cdot A_B$$

$$b_E = b_{25} + (b_{26} - b_{25}) \cdot A_B. \tag{4.1}$$

The derived quantities by column:

1. Index number.

2. *Object Name:* See above.

3. *Object Category:* See above.

4. *Distance (D):* The distance to the object in Mpc, which is computed using the Galaxy-centered redshift velocity V_0 as follows:

$$D = \frac{V_0}{H_0} \tag{4.2}$$

5. *Radius (r):* The measured radius of the object in kpc. The calculation depends on what is available for each object. For those galaxies for which there are $a_{26.6}$ measurements:

$$r = \frac{1000.0D}{206265} \cdot a_{26.6} .$$
(4.3)

For objects which do not have $a_{26.6}$ measurements:

$$r = \frac{1000.0D}{206265} \cdot a_E .$$
(4.4)

6. *Inclination (i):* The objects presumed inclination, based on the major and minor axis sizes and an intrinsic flattening of 0.15, measured in degrees:

$$\cos^2 i = \frac{(b_E/a_E)^2 - 0.0225}{0.9775}$$
(4.5)

7. *B:* The absolute B magnitude of the object.

8. *R:* The absolute R magnitude of the object.

9. *B-R:* The B-R color of the object.

10. L_B: The total blue luminosity of the galaxy, measured in solar units ($L_\odot$). This value is computed from the absolute B magnitude of the galaxy and the absolute B magnitude of the sun:

$$L_B = 10^{-0.4 \times (B - 5.48)}$$
(4.6)

11. *Surface Brightness (σ):* The surface brightness, measured in mag/arcsec^2, is computed from the b_{25} magnitude of the object (which has been corrected for extinction) and the area of the sky it covers:

$$\sigma = b_{25} + 2.5 \times \log_{10}\left(\frac{\pi \cdot a_E \cdot b_E}{4.0}\right)$$
(4.7)

12. *Atomic Hydrogen Mass (M_{HI}):* The HI mass is computed using the total HI flux and the distance to the object:

$$M_{HI} = 2.35 \times 10^5 \cdot D^2 \cdot Sdv$$
(4.8)

13. *Dynamical (Rotational) Mass (M_d):* The dynamical galaxy mass is computed using the HI velocity width of the object with its radius and inclination as computed above:

$$M_d = 2.3353 \times 10^5 \cdot r \cdot \left(\frac{w_{50}}{2.0 \cdot \sin i}\right)^2$$
(4.9)

In cases where the inclination of a galaxy is zero, we must drop the dependence on i. This approximation is valid in the cases of most elliptical galaxies:

$$M_d(i=0) = 2.3353 \times 10^5 \cdot r \cdot \left(\frac{w_{50}}{2.0}\right)^2 \qquad (4.10)$$

14. M_{HI}/M_d: The ratio of HI to dynamical mass. Because the dynamical mass measures the entire mass of the galaxy while the HI mass measures only one component, this value should in theory never be greater than 1.0. A value for a fairly normal spiral galaxy should be in the neighborhood of 1/10. The tendency toward values near and above 1.0, particularly for our newly discovered objects, is probably a result of visible diameters which are used to compute r being smaller than diameters of the HI extent of these objects.

15. L_B/M_d: The ratio of blue light to dynamical mass. This value measures luminosity produced by the stars contained within a galaxy against its total mass. A typical value for a normal spiral galaxy would be about 1/10.

16. L_B/M_{HI}: The ratio of blue light to hydrogen mass. For a typical spiral galaxy, this value should be about 1.0

Notes on Individual Objects

The following is a list of information of note pertaining to individual objects.

- **1. B2200D-02:** This objects appears to be a small ring on the POSS plate. CCD images show it to be a faint circular blob with an off-center elongated nucleus. Cataloged object MCG +04-52-002 in the field is a blemish on the R-band POSS image. It does not exist. The HI hex profile for this object had some interference at the edge of the feature, but measurements are believed to be OK.

- **2. C2218C-07:** Very optically faint, diffuse object. Combined HI hex measurements indicate the possibility of very weak features at plus and minus 150 km/s relative to the redshift of this object.

- **3+4. UGC 12148/12153:** Visually, this appears to be a closely associated pair of objects. The slice search observations were not able to distinguish them in HI. Follow-up hex observations indicated all of the HI signal was due to UGC 12153. Optical images of these objects were not obtained due to

clerical errors. Without the optical data or HI signal from both objects, it is impossible to be certain if these two objects really are closely to each other.

- **5. N2254A-03:** There are many galaxies visible in the optical image. The hex indicates the object position is slightly west of the position of the slice detection, which would correspond to the largest object in the optical field, as well as the object indicated by the H_α frame.

- **7. H2254D-06:** Optically unimpressive object, but with strong HI signal detected far from the center of the Arecibo beam.

- **8. A2254D-10:** The first detection made by the slice search. An extremely high HI mass to light ratio, and extremely low dynamic to HI mass ratio (although no inclination could be measured for this object, throwing the dynamic mass calculation into question). The hex spectrum has a lot of interference, but measurements look OK.

- **9. G2254A-11:** MSB elliptical with a stellar nucleus. Again, the hex spectrum has a lot of interference, but measurements look OK.

- **10. MRK 317:** HI signal is very weak, but was detected with long-integration HI measurements.

- **11. UGC 12443:** No HI detection, even with long integration (σ=3.9 mJy/channel) HI observations. Enormous bright optical object with box-shaped nucleus and diffuse halo with possible spiral structure.

- **12. UGC 12449:** Very wide HI profile, with peak flux density less than 4.0 mJy/channel. Optically, this appears to be a near edge-on disk-shaped galaxy.

- **13. UGC 12533:** Interference in the hex, but measurements should be OK. Optical images of this object are almost obscured by a very bright star nearby in the field.

- **14. CGCG 476-023:** There is another object in the CCD field, but hex indicates the HI detection is well centered on this position.

- **15. K2312B-09:** MSB irregular blob. Hex indicates object may be slightly SE of this position.

- **16. UGC 12583:** Optical data is missing for this object. Hex positions were not well-centered, and HI data may be unreliable.

- **17+18. UGC 12607/12610:** Five slice positions detected these two bright galaxies. Easternmost galaxy (UGC 12607) appears to have a strong jet (or perhaps superimposed background galaxy) in optical images. An *IRAS* object in the optical field which appears associated was not detected in HI.

- **19. N2312B-15:** Hex indicates this object has quite small extent. A very low surface brightness galaxy, with central surface brightness below 25 mag/arcsec^2. Optical magnitudes are very uncertain. A nearby star is an inconvenience in the optical frames.

- **20. CGCG 476-061:** Interference spike was removed from the hex spectrum. Galaxy may be slightly West of this position. A possible feature at 5000 km/s? There is another object nearby in the CCD image which *looks* like it might be within the slice velocity range.

- **22. UGC 12663:** A long-integration (rms = 1.1 mJy) observation failed to detect this object at 21cm, although Giovanelli and Haynes (ref.) claim a detection at 7964 km/s. It is possible that the true object velocity is outside the slice search's velocity range. Because we have no HI or optical data of our own for this galaxy, it is not included in any of the tables.

- **23. L2330C-03:** Of three visible (and irregular) objects in the CCD field, this is the least optically impressive, and one of two detected in HI (see below - L2330D-02). It is the easternmost - coordinates from the hex observations.

- **24. L2330D-02:** The westernmost of three visible objects on the CCD frame, with L2330C-03 (see above). Strange, tormented structure. These two galaxies have very similar redshift velocities, and together were detected in four slice positions.

- **26+27. E2330A-10A/B:** The larger and brighter of these objects (A) appears to be an edge-on spiral, with a very small companion (B). The HI signals are confused, although (B) appears to have a much narrower profile than (A), allowing parameters for each object to be extracted.

- **28+29. UGC 12914/15:** Optical and HI data are both confused with these closely-interacting galaxies. UGC 12914 is the southwestern object with a narrow HI profile, UGC 12915 is northeastern object with a wide HI profile according to the hexes.

116

- **30. M2348A-13:** The HI signal appears slightly east of the optical position. An MSB galaxy detected in two slice positions.

- **31. J2348A-14:** The HI signal appears slightly east of the optical position.

- **32. UGC 78:** From the CCD field, it can be seen that the cataloged object NGC 8 is really a double star, and not a galaxy at all. Hex indicates HI is slightly southeast of the optical position.

- **33. M0006C-05:** Some interference in the hexes, but measured values should be OK.

- **35. UGC 186:** Optical positions in catalogs are slightly East of our observed position. Our measured flux is slightly smaller than Giovanelli, et al. (ref.).

- **37. L0006B-15:** A very weak HI signal, but a surprisingly wide velocity width. Optical emission is also unimpressive.

- **39. I0024D-01:** There are four equally impressive optical objects in the field, but the hexes and H_α frame indicate that this is the only one we are detecting.

- **41. CGCG 479-040:** Hex indicates this object may be slightly ESE of this position.

- **42+43. UGC 354/356:** Two objects detected in the same slice position. UGC 354 is northeast of UGC 356. Velocity widths from slice observations - the hexes were too noisy.

- **44. NGC 169/169A:** Very close merger pair. NGC 169A is probably not the source of the HI, according to the hexes.

- **45. MRK 344:** Optical redshift (8484 km/s) puts this object on the edge of the slice velocity range. We had a possible detection at 7600 km/s.

- **46. NGC 228:** The coordinates estimated from the hex do not seem to correspond to any of the three optical objects in the CCD field. The H_α frame indicates no emission from any of them. Are we possibly seeing a completely different object in HI?

- **47. J0042A-01:** Very weak HI signal. The hexes indicate the object may be slightly southwest of this position. Optically, this object is almost invisible.

- **48+49. N0042A-05A/B:** Possibly a double detection. Galaxy A is certain. Galaxy B is very weak, both in HI and optically. A third object in the CCD field appears not to be detected at all in HI.

- **50. E0042A-07:** MSB object with a weak HI signal, positioned in the center of a void region.

- **51. N0042C-10:** HI parameters are from the combined HI signals of three positions of an off-center hex observation. Fairly faint object optically.

- **52. UGC 591:** Galaxy detected in two slice positions. Hex indicates the object is slightly south east of the optical coordinates. A peculiar peak shows up in all hex observations - possibly the "irregular envelope" mentioned in the UGC?

- **53. UGC 612:** No optical data for this galaxy, which has a peculiar, triple-horned HI profile.

- **54. CGCG 480-029:** No optical data.

- **55. MCG 04-04-03:** Detected in two slice positions. Averaged across a spike in the HI profile.

- **56. UGC 1084:** Optically, this object is very unimpressive (it is surprising that it was ever cataloged). However, it was detected in four slice positions which describe an extended north-south arc, anchored by the optical image of the galaxy at the north. The hex observations, however, indicated a fairly symmetric object.

- **57. N0118D-12:** Stellar image on the CCD. Detected in three slice positions. Hex indicates the galaxy may be slightly West of the optical position, and the HI signal is extended on a roughly north-south axis.

- **58. K0118B-14:** A very low surface brightness object with a very low redshift velocity. The hex indicates the galaxy is fairly extended in HI.

- **59. J0136B-06:** LSB object with a very narrow HI signal.

- **60. D0136D-10:** HI signal is weak and peculiar. Hex indicates the object may be southeast of this position. Optically it appears to be an uninteresting MSB elliptical galaxy.

- **61. L0136C-13:** M/LSB irregular galaxy. The hex indicates it may be an extended object, possibly slightly south of the optical coordinates.

- **62. UGC 1471:** The largest of three objects in the CCD image, detected in three slice positions. Hexes are not well-centered, but HI is clearly centered on UGC 1471. Other objects in the field are IC 180 and IC 181.

- **64. CGCG 482-046:** Hex indicates the object is slightly southwest of this coordinate. Used standing-wave correction to remove bad noon-time baselines. Possible interference of a narrow feature at 5500 km/s in the HI? Nothing which would correspond is visible on the CCD.

- **65. CGCG 482-050:** No HI detected after a long integration ($rms = 0.48$ mJy).

- **66. IC 190:** No HI detected after a long integration ($rms = 0.48$ mJy). Could this galaxy actually be at the same distance as nearby IC 189 (12347 km/s), and thus outside the slice search limits?

- **67. UGC 1538:** Hex indicates the galaxy is a little southeast of the optical coordinates.

- **68+69. UGC 1551 + N0154D-06:** Two objects detected in the same slice position - one cataloged, the other not. Velocity differences indicate they are unrelated, despite their proximity on the sky. The hex indicates N0154D-06 may be a double source.

- **70. A0154B-11:** Triangle HI profile suggests an irregular galaxy. Optical image appears irregular - galaxy is positioned between two foreground stars.

- **71. K0154B-11:** Hex indicates the object is slightly southwest of the optical position.

- **72. A0154A-15:** Hard to interpret weak HI - combined two hexes with slightly different coordinates. HI object appears centered at about 02 10 50.0 +23 00 30. Optically the object is faint, and has a foreground star obscuring some of it.

- **73+74. CGCG 483-034/036:** There is partial overlap in the HI profiles of these two objects. CGCG 483-036 is the stronger HI signal which looks pretty normal for a spiral. Velocity widths and fluxes are a bit uncertain due to this overlap.

- **75. UGC 1938:** Hex indicates the HI is slightly southeast of this position.

- **76. UGC 1950:** Hex indicates the HI is slightly southeast of this position.

- **77. N0212A-13:** Hex indicates the HI is slightly west of this position.

- **78. H0212C-15:** Hex indicates the HI is slightly southeast of this position. Fairly LSB irregular object with two very bright foreground stars nearby.

- **79. UGC 2020:** Giovanelli and Haynes (ref.) report a position which is quite far East of our optical position. The hex indicates the position may be slightly SSE.

- **80. E0230C-01:** This object was discovered in an off scan of a different object. It's HI signal is fairly strong, but it lands between two slice positions on the sky, and was not detected by the slice search procedure even though its profile appears weakly in both of those scans.

- **81. UGC 2059:** Averaged across interference spike in the middle of the HI profile. A bright spiral galaxy detected in two slice points.

- **82. UGC 2079:** A large, bright spiral detected in two slice points. This galaxy has an uncataloged companion, which was also detected (L0230D-03).

- **83. L0230D-03:** This companion to UGC 2079 has a weaker profile, but horns are shifted in the HI profiles, so parameters are fairly certain.

- **84. UGC 2104:** Bright spiral galaxy with very impressive HII regions. Hex observations indicate the possibility of a small narrow-line source Northeast of UGC 2104.

- **85: B0230A-08:** Very distant LSB object, with patchy appearance.

- **86. UGC 2248:** Several hexes were combined and standing wave corrections were applied to remove bad interference. The galaxy appears to be slightly East of this position in HI.

- **87. UGC 2267:** Hex observations indicate this object may be slightly East of the optical position.

- **88. B0230A-14:** Nearly invisible, lowest redshift (475 km/s) object detected in the slice search. Hex indicates the galaxy may be slightly Southwest of the optical position. Flux ratio is about 1.0.

- **89. D0248A-04:** Hex indicates object may be slightly East of optical coordinates. Flux ratio is about 1.0.

- **90. K0248C-02:** A seemingly invisible object. No optical counterpart could be found, even on combined CCD frames. Optical data are upper limits included for comparison purposes. This object has a very low redshift velocity (411 km/s).

<u>Scaled Images</u>

In the following figures, we plot images of all of our objects to scale - that is, such that they appear to be the correct sizes relative to one another, based on their true physical sizes. All of the objects have apparent sizes on the CCD images, but these sizes are a reflection not only of the true physical sizes of the

objects, but also of their distance away from us. Before we can make a true comparison of the physical sizes, we have to remove the distance dependence, by re-scaling each image based on the object's distance.

The distances to our objects are derived from their redshifts, assuming their redshifts are due entirely to the Hubble flow. This is of course not the case at all - each object has its own individual motions which add to the Hubble flow velocity. As we have no way of knowing these, the measured redshift velocity represents our best guess for the Hubble flow velocity. These velocities are translated into distances by dividing them by the Hubble Constant, a value which is an perennial source of debate, and which historically has remained anything but constant. Since we are interested in the sizes of our objects relative to one another, the choice of Hubble constant is not particularly important as long as the same value is applied to all. However, to provide a scale from which physical sizes (in kpc) can be measured from the images, some value must be chosen. We have adopted the nominal value of 75 km/s/Mpc. With this value for the Hubble constant, the scale of our images translates to 20.0 kpc/inch.

All images are in the R-band. These were chosen for a number of reasons:

- They represent the most complete set of images of the slice objects which we have. Several objects were missed at each band we observed, but we missed the fewest in the R-band, and in no case was an object observed at another band and *not* observed in the R-band.

- Our integrations in the R-band were the longest (when accounting for filter efficiency), so the R-band images were generally of the best quality in terms of signal to noise.

- There are a number of objects which are only visible in the R-band, or are only visible in any detail in the R-band.

- For the most part, the R-band images showed the most diffuse, extensive galaxy structure of all of the bands, giving a better impression of the physical extent of the optical portions of our galaxies.

The figures are divided into three categories for comparison: newly discovered objects (Figure 4.1), cataloged objects detected in the HI search (Figure 4.2), and cataloged objects which were not detected in the HI search (Figure 4.3). Within each figure, objects are arranged roughly in order of right ascension, however some shuffling was done to fit different-sized images on as few pages as possible. In two cases

(in Figure 4.1), objects had such small physical sizes that the scaled images were vanishingly small - in these cases, adjacent "blow-up" images (at ten times the size, or a scale of 2.00 kpc/inch) are provided.

Table 4.1. HI Data for the Slice Objects

(1)	Name (2)	C (3)	α (4)	δ (5)	Slice Pos. (6)	l (7)	b (8)	Sdv (Jy km/s) (9)	Sdv_hex (Jy km/s) (10)	V_hel (km/s) (11)	w_50 (km/s) (12)	w_20 (km/s) (13)	rms (mJy) (14)	N_h (15)	S_pk (mJy) (16)
1	B2200D-02	1	22 02 07.7	23 04 35.0	B2200D-02	80.324	-25.422	1.21	1.64	6206	81	150	3.3	1	18.4
2	C2218C-07	1	22 25 44.8	23 07 12.0	C2218C-07	85.122	-28.779	2.65	3.59	1278	62	82	4.3	1	59.5
3	UGC 12148	2	22 38 51.8	23 08 36.0	C2236C-03	87.979	-30.490	1.54	3.69	7155	84	152	3.1	2	37.6
4	UGC 12153	2	22 38 59.9	23 06 42.0	C2236C-03	87.989	-30.533	4.00	4.77	7154	87	130	3.1	1	51.6
5	N2254A-03	1	22 56 31.0	23 44 10.0	N2254A-03	92.378	-32.109	0.83	0.96	7189	39	125	3.4	1	15.9
6	CGCG 475-028	3	23 00 39.6	23 29 21.0	--	93.217	-32.788	0.47	--	7775	156	161	0.5	2	2.6
7	H2254D-06	1	23 01 12.8	23 24 58.0	H2254D-06	93.308	-32.913	2.80	2.87	1155	96	111	4.2	2	34.2
8	A2254D-10	1	23 05 38.6	22 59 15.0	A2254D-10	94.139	-33.771	1.43	1.61	6336	31	50	3.5	1	46.6
9	G2254A-11	1	23 06 05.7	23 21 31.0	G2254A-11 / G2254B-11	94.456	-33.491	2.71	3.49	4270	130	149	3.6	2	30.2
10	MRK 317	3	23 11 17.3	23 32 53.0	--	95.836	-33.860	0.17	--	6122	108	128	0.4	1	2.1
11	UGC 12443	3	23 11 59.7	23 24 43.0	--	95.939	-34.054	-0.10	--	6048	--	--	0.4	-	-0.8
12	UGC 12449	3	23 12 23.3	23 00 38.0	J2312B-06	95.823	-34.454	0.69	--	7935	438	458	0.6	2	3.3
13	UGC 12533	2	23 18 22.8	23 31 54.0	C2312D-07	97.603	-34.572	2.38	3.24	5961	578	612	3.2	2	12.5
14	CGCG 476-023	2	23 20 08.8	23 05 52.0	C2312A-08	97.835	-35.135	1.37	2.26	5042	118	174	2.6	2	18.7
15	K2312B-09	1	23 21 45.5	23 34 04.0	K2312B-09	98.481	-34.855	1.75	2.07	5895	122	154	3.3	2	18.5
16	UGC 12583	2	23 22 04.9	23 42 41.0	M2312C-09	98.634	-34.754	2.37	4.84	5063	264	283	2.8	2	23.0
17	UGC 12607	2	23 25 11.0	23 18 45.0	F2312D-11 / G2312D-12 / F2312A-12	99.239	-35.401	6.65	8.93	3403	95	166	3.5	1	82.9
18	UGC 12610	2	23 25 35.2	23 15 20.0	E2312B-12 / F2312B-12	99.317	-35.489	9.36	13.71	3556	269	294	3.5	2	67.0
19	N2312B-15	1	23 29 08.4	23 45 29.0	N2312B-15	100.476	-35.334	0.77	0.88	4009	59	88	3.5	1	17.3
20	CGCG 476-061	2	23 29 33.5	23 16 48.0	F2312C-15	100.367	-35.813	2.21	2.84	6989	239	249	3.2	2	19.6
21	UGC 12655	2	23 29 58.8	23 39 14.0	L2312D-15 / L2330A-01	100.648	-35.502	2.36	3.13	5095	408	423	3.4	2	13.3
23	L2330C-03	1	23 31 57.0	23 38 30.0	L2330C-03 / M2330D-02	101.159	-35.678	0.97	1.95	5603	164	189	3.6	2	14.4
24	L2330D-02	1	23 32 13.2	23 41 33.0	L2330D-02 / M2330A-03	101.252	-35.652	2.33	--	5558	111	135	2.0	1	21.7
25	UGC 12694	2	23 33 20.3	23 20 27.0	G2330D-03 / F2330D-03	101.393	-36.073	4.02	5.47	3054	188	208	3.9	2	36.7

Table 4.1 (cont.)

(1)	Name (2)	C (3)	α (4)	δ (5)	Slice Pos. (6)	l (7)	b (8)	Sdv (Jy km/s) (9)	Sdv_hex (Jy km/s) (10)	V_hel (km/s) (11)	w50 (km/s) (12)	w20 (km/s) (13)	rms (mJy) (14)	N_h (15)	S_pk (mJy) (16)
26	E2330A-10A	1	23 40 42.8	23 13 58.0	E2330A-10	103.325	-36.751	2.03	2.73	5355	331	344	3.5	2	14.6
27	E2330A-10B	1	23 40 45.4	23 13 14.0	E2330A-10	103.332	-36.766	0.66	--	5271	43	63	3.6	1	15.6
28	UGC 12914	2	23 59 05.8	23 12 40.0	E2348B-10	108.412	-37.975	4.18	--	4546	126	154	4.0	2	35.2
29	UGC 12915	2	23 59 08.6	23 12 59.0	D2348B-10	108.427	-37.972	10.49	12.63	4389	558	623	3.7	2	23.0
30	M2348A-13	1	00 02 30.9	23 41 27.0	M2348A-13 M2348B-13	109.519	-37.692	2.25	2.67	6573	133	178	3.6	2	22.5
31	J2348A-14	1	00 03 46.4	23 30 55.0	J2348A-14	109.825	-37.928	3.31	4.21	4574	197	259	3.6	2	21.2
32	UGC 78	2	00 06 18.3	23 32 16.0	J0006A-01 J0006B-01	110.551	-38.031	3.54	3.94	4528	152	192	4.2	1	29.7
33	M0006C-05	1	00 11 22.9	23 41 27.0	M0006C-05	112.037	-38.109	1.27	1.19	6201	138	154	2.7	2	10.6
34	UGC 179	2	00 16 25.2	23 12 00.0	D0006C-09 E0006D-09	113.382	-38.792	4.75	5.59	4459	221	234	3.6	2	37.8
35	UGC 186	3	00 17 14.3	23 29 44.0	--	113.680	-38.530	0.65	--	5829	389	405	0.6	2	2.9
36	UGC 210	2	00 19 29.4	23 27 37.0	I0006B-12	114.326	-38.643	3.89	4.78	4479	237	253	3.9	2	28.0
37	L0006B-15	1	00 23 19.0	23 38 41.0	L0006B-15	115.470	-38.580	0.96	1.06	5679	190	198	3.9	2	9.3
38	UGC 186-OFF	2	00 23 21.6	23 29 44.0	U186-OFF	115.458	-38.730	1.57	2.32	7389	206	228	2.8	2	13.3
39	I0024D-01	1	00 24 50.3	23 26 40.0	I0024D-01	115.882	-38.822	1.54	1.75	5884	188	259	3.5	2	6.8
40	UGC 321	2	00 29 54.2	23 07 00.0	C0024A-06	117.325	-39.273	3.46	4.52	4658	213	230	3.5	2	27.9
41	CGCG 479-040	2	00 30 58.6	23 07 22.0	C0024D-06	117.644	-39.290	2.32	2.42	5190	268	280	3.5	2	15.9
42	UGC 354	2	00 33 16.3	23 45 57.0	N0024D-08	118.388	-38.694	1.27	1.52	5614	222	238	2.8	2	7.2
43	UGC 356	2	00 33 26.7	23 40 57.0	N0024D-08	118.430	-38.780	2.91	3.49	5252	524	544	4.1	2	16.0
44	NGC 169/169A	2	00 34 13.2	23 42 50.0	M0024C-09 N0024C-09	118.660	-38.762	5.76	8.05	4618	549	625	5.0	2	23.0
45	MRK 344	3	00 35 53.5	23 20 13.0	--	119.118	-39.164	0.14	--	7566	134	171	0.5	2	1.5
46	NGC 228	2	00 40 17.0	23 13 00.0	E0024C-14 D0024C-14	120.410	-39.340	2.34	3.16	7423	114	166	3.6	1	25.8
47	J0042A-01	1	00 42 12.4	23 31 58.0	J0042A-01	120.995	-39.041	0.52	0.49	6650	61	74	3.3	1	10.9
48	N0042A-05A	1	00 46 48.5	23 45 12.0	N0042A-05	122.356	-38.844	0.67	1.19	7157	138	177	2.9	2	10.6
49	N0042A-05B	1	00 46 54.3	23 45 40.0	N0042A-05	122.385	-38.836	0.47	--	7159	128	143	1.3	2	4.7
50	E0042A-07	1	00 49 13.6	23 12 28.0	E0042A-07	123.067	-39.392	0.70	0.77	2622	66	80	3.8	2	13.0
51	N0042C-10	1	00 53 35.7	23 46 58.0	N0042C-10	124.349	-38.805	0.42	0.27	4962	47	55	2.5	2	11.2
52	UGC 591	2	00 54 38.2	23 37 06.0	L0042C-11 K0042C-11	124.661	-38.964	3.36	4.32	4834	171	203	3.8	1	32.8

Table 4.1 (cont.)

(1)	Name (2)	C (3)	α (4)	δ (5)	Slice Pos. (6)	l (7)	b (8)	Sdv (Jy km/s) (9)	Sdv_hex (Jy km/s) (10)	V_{hel} (km/s) (11)	w_{50} (km/s) (12)	w_{20} (km/s) (13)	rms (mJy) (14)	N_h (15)	S_{pk} (mJy) (16)
53	UGC 612	3	00 56 20.1	23 34 58.0	--	125.162	-38.987	0.52	--	5086	283	300	0.5	2	2.3
54	CGCG 480-029	3	00 56 42.0	23 42 53.0	--	125.263	-38.852	0.38	--	5043	136	173	0.4	2	3.0
55	MCG 04-04-03	2	01 17 14.9	23 42 02.0	M0100B-15 M0100C-15	131.264	-38.447	3.10	3.94	6777	224	246	3.2	2	22.4
56	UGC 1084	2	01 28 35.0	23 41 40.0	K0118D-09 M0118D-09 L0118D-09 M0118A-10	134.523	-38.020	4.53	6.70	3415	63	98	4.2	1	104.3
57	N0118D-12	1	01 32 25.6	23 45 00.0	N0118D-12 M0118A-13 N0118A-13	135.600	-37.788	4.95	7.52	3316	115	144	3.9	2	64.4
58	K0118B-14	1	01 33 52.4	23 33 34.0	K0118B-14	136.062	-37.903	1.15	1.75	563	51	66	6.6	1	31.7
59	J0136B-06	1	01 42 21.2	23 30 59.0	J0136B-06	138.460	-37.481	0.49	0.66	3874	44	58	3.3	1	17.6
60	D0136D-10	1	01 47 52.7	23 09 02.0	D0136D-10	140.124	-37.489	1.49	2.14	5614	332	411	2.3	2	11.2
61	L0136C-13	1	01 51 05.9	23 39 55.0	L0136C-13	140.823	-36.782	1.74	1.87	2914	118	146	3.6	2	20.7
62	UGC 1471	2	01 57 06.5	23 24 07.0	H0154B-03 H0154C-03 G0154C-10	142.558	-36.605	3.87	5.34	4919	124	158	3.9	2	41.3
63	J0154B-04	1	01 57 57.0	23 30 46.0	J0154B-04	142.740	-36.437	1.37	1.84	5029	121	139	3.7	2	17.1
64	CGCG 482-046	2	01 58 18.5	23 10 30.0	D0154C-04	142.975	-36.729	1.75	2.42	5041	171	210	3.1	2	13.8
65	CGCG 482-050	3	01 58 59.5	23 26 52.0	--	143.047	-36.420	-0.12	--	4727	--	--	0.5	-	-0.7
66	IC 190	3	01 59 17.3	23 18 30.0	--	143.185	-36.528	-0.13	--	4769	--	--	0.5	-	-0.8
67	UGC 1538	2	02 00 30.3	23 31 20.0	J0154C-06	143.422	-36.233	1.59	2.19	2832	122	143	3.8	2	21.2
68	UGC 1551	2	02 00 48.4	23 50 03.0	N0154D-06	143.372	-35.916	10.02	16.28	2671	122	139	3.6	2	147.0
69	N0154D-06	1	02 00 57.2	23 47 08.0	N0154D-06	143.431	-35.951	1.72	2.33	4812	252	294	2.9	2	12.4
70	A0154B-11	1	02 06 21.6	23 00 46.0	A0154B-11	145.205	-36.238	2.50	3.06	8162	169	251	2.8	1	22.3
71	K0154B-11	1	02 06 17.6	23 36 18.0	K0154B-11	144.922	-35.692	1.23	1.55	5105	64	82	3.2	1	21.7
72	A0154A-15	1	02 10 47.0	23 01 26.0	A0154A-15	146.367	-35.847	0.23	0.34	2452	54	72	2.5	2	7.4
73	CGCG 483-034	2	02 22 20.5	23 37 29.0	L0212C-09	149.035	-34.225	1.46	1.66	6574	69	104	3.6	1	21.7
74	CGCG 483-036	2	02 22 30.5	23 36 10.0	K0212D-09	149.088	-34.229	1.73	2.31	6631	180	213	2.9	2	15.3
75	UGC 1938	2	02 25 32.5	22 59 27.0	A0212B-12	150.170	-34.479	4.09	5.80	6399	398	436	3.4	2	24.0
76	UGC 1950	2	02 25 48.8	23 44 25.0	K0212C-12	149.928	-33.928	2.15	2.79	6287	296	315	3.5	2	14.1
77	N0212A-13	1	02 26 32.6	23 44 45.0	N0212A-13	150.017	-33.700	1.57	1.82	5484	247	267	3.0	2	11.2

Table 4.1 (cont.)

(1)	Name (2)	C (3)	α (4)	δ (5)	Slice Pos. (6)	l (7)	b (8)	Sdv (Jy km/s) (9)	Sdv_hex (Jy km/s) (10)	V_hel (km/s) (11)	w_50 (km/s) (12)	w_20 (km/s) (13)	rms (mJy) (14)	N_h (15)	S_pk (mJy) (16)
78	H0212C-15	1	02 29 32.0	23 25 50.0	H0212C-15	150.923	-33.676	1.25	1.29	4159	120	142	2.5	2	12.4
79	UGC 2020	2	02 30 01.7	23 06 25.0	C0230A-01	151.222	-33.912	4.58	5.77	5563	250	266	3.8	2	27.2
80	E0230C-01	1	02 30 41.6	23 15 42.0	E0230C-01 F0230D-01	151.301	-33.705	1.33	1.82	4414	160	176	3.3	2	15.1
81	UGC 2059	2	02 31 51.0	23 11 31.0	D0230B-02 D0230C-02	151.623	-33.644	8.92	12.84	4360	606	633	3.1	2	33.4
82	UGC 2079	2	02 33 16.6	23 40 56.0	L0230C-03 M0230D-03	151.697	-33.058	7.10	9.17	5649	246	278	2.9	2	42.7
83	L0230D-03	1	02 33 12.7	23 36 50.0	L0230D-03	151.719	-33.125	0.84	--	5734	177	217	1.9	2	6.8
84	UGC 2104	2	02 34 34.8	23 04 55.0	C0230D-04	152.350	-33.448	2.58	2.70	8239	319	368	2.3	2	12.3
85	B0230A-08	1	02 38 25.5	23 03 05.0	B0230A-08	153.295	-33.050	0.89	1.23	7661	174	189	3.0	2	11.9
86	UGC 2248	2	02 44 01.5	23 23 27.0	H0230C-12	154.422	-32.118	2.50	3.66	6196	345	386	2.2	2	14.8
87	UGC 2267	2	02 44 59.0	23 11 40.0	D0230B-13 D0230C-13	154.763	-32.176	3.56	4.07	6054	319	332	3.4	2	20.6
88	B0230A-14	1	02 45 48.4	23 03 50.0	B0230A-14	155.034	-32.191	0.95	1.01	469	30	53	4.8	1	32.0
89	D0248A-04	1	02 51 47.3	23 10 19.0	D0248A-04	156.349	-31.382	1.53	1.55	6071	116	140	3.4	2	16.1
90	K0248C-02	1	02 54 41.0	23 34 10.0	K0248C-02	156.756	-30.691	0.79	0.99	411	31	51	5.2	1	30.9

Table 4.2. Optical Data for the Slice Objects

	Name	C	$p.a._{25}$	a_{25}	b_{25}	B_{25}	R_{25}	I_{25}	H_{25}	$p.a._{26}$	a_{26}	b_{26}	B_{26}	R_{26}	I_{26}	H_{26}	$p.a._{26.6}$	$a_{26.6}$	$b_{26.6}$	$R_{26.6}$	B_0	R_0	A_B
(1)	(2)	(3)	(4)	(5)	(6)	(7)	(8)	(9)	(10)	(11)	(12)	(13)	(14)	(15)	(16)	(17)	(18)	(19)	(20)	(21)	(22)	(23)	(24)
1	B2200D-02	1	-	14.4	14.4	16.7	15.8	15.4	17.0	-	16.8	16.8	16.7	15.7	15.3	17.1	-	25.4	21.6	15.5	23.5	22.4	0.40
2	C2218C-07	1	90	14.4	9.6	17.9	17.1	16.7	20.2	90	24.0	19.3	17.3	16.5	16.0	22.6	90	28.8	19.2	16.5	24.1	23.3	0.15
3	UGC 12148	2	-	-	-	-	-	-	-	-	-	-	-	-	-	-	-	-	-	-	-	-	0.19
4	UGC 12153	2	-	-	-	-	-	-	-	-	-	-	-	-	-	-	-	-	-	-	-	-	0.19
5	N2254A-03	1	300	19.0	5.4	17.2	15.8	15.5	16.8	300	21.8	8.2	17.1	15.7	15.3	16.7	300	54.4	10.9	15.6	22.5	21.1	0.19
6	CGCG 475-028	3	210	10.9	8.2	18.2	16.0	14.1	-	210	13.6	10.9	18.1	15.8	14.0	-	210	46.2	21.8	15.4	23.0	20.7	0.22
7	H2254D-06	1	150	16.8	9.6	17.5	16.5	15.4	18.2	150	19.2	12.0	17.4	16.4	15.1	18.1	150	31.2	19.2	16.2	23.0	22.0	0.23
8	A2254D-10	1	-	4.8	4.8	19.7	18.2	18.1	19.5	-	9.6	9.6	19.0	17.3	17.4	18.9	-	19.2	19.2	17.9	24.0	22.6	0.23
9	G2254A-11	1	180	14.4	9.6	17.4	16.1	15.5	20.1	180	19.2	16.8	17.1	15.8	15.3	20.1	180	24.0	19.2	15.8	23.2	21.7	0.25
10	MRK 317	3	155	13.6	8.2	17.5	15.3	14.1	-	155	13.6	10.9	17.4	15.2	14.0	-	155	27.2	38.1	14.3	21.1	19.1	0.26
11	UGC 12443	3	120	38.4	28.8	14.3	12.7	12.0	-	140	55.2	36.0	14.1	12.5	11.9	-	120	86.4	60.0	12.5	19.0	17.4	0.23
12	UGC 12449	3	125	26.4	28.8	16.8	15.1	-	16.7	125	28.8	7.2	16.7	15.0	-	-	125	33.6	9.6	15.2	21.5	19.7	0.21
13	UGC 12533	3	245	32.6	5.4	16.3	14.4	-	-	245	32.6	5.4	16.3	14.4	-	16.5	245	62.6	13.6	14.1	21.4	19.4	0.20
14	CGCG 476-023	2	45	14.4	12.0	16.2	15.4	15.0	19.4	45	19.2	14.4	16.2	15.3	14.9	-	45	21.6	21.6	15.2	21.5	20.6	0.16
15	K2312B-09	1	122	13.6	5.4	18.3	17.5	17.2	18.7	95	24.5	16.3	17.5	17.1	17.0	19.3	122	16.3	13.6	17.2	23.2	22.3	0.15
16	UGC 12583	2	-	-	-	-	-	-	-	-	-	-	-	-	-	18.0	-	-	-	-	-	-	0.14
17	UGC 12607	2	345	43.2	33.6	13.4	12.6	12.2	12.6	225	52.8	38.4	13.3	12.6	12.2	-	225	69.6	62.4	12.5	20.0	19.2	0.16
18	UGC 12610	2	45	43.2	24.0	14.5	13.3	12.8	14.9	60	64.8	36.0	14.3	13.1	12.6	12.6	60	67.2	43.2	13.2	20.3	18.9	0.17
19	N2312B-15	1	-	0.0	0.0	21.1	20.3	-	-	-	10.9	10.9	19.1	18.3	-	14.8	-	13.6	13.6	18.0	25.4	24.4	0.15
20	CGCG 476-061	2	175	16.8	12.0	15.9	14.7	14.1	-	175	24.0	16.8	15.8	14.6	14.0	-	210	36.0	24.0	14.5	20.8	19.5	0.14
21	UGC 12655	2	320	38.1	24.5	14.3	12.8	12.1	-	320	51.7	32.6	14.3	12.7	12.0	-	320	89.8	51.7	12.5	19.6	17.8	0.16
23	L2330C-03	1	220	13.6	5.4	17.5	16.6	16.2	17.6	220	16.3	8.2	17.4	16.6	16.1	17.4	220	32.6	13.6	16.5	21.9	21.0	0.14
24	L2330D-02	1	-	8.2	8.2	18.5	17.7	17.0	-	-	10.9	10.9	18.6	17.6	16.8	-	-	16.3	16.3	17.7	23.0	22.3	0.14
25	UGC 12694	2	330	28.8	26.4	14.3	13.1	12.6	-	330	43.2	28.8	14.2	13.1	12.5	-	345	48.0	40.8	13.0	20.5	19.0	0.10
26	E2330A-10A	1	316	28.8	4.8	17.1	15.7	15.1	-	316	31.2	9.6	16.9	15.6	15.0	-	316	33.6	14.4	15.6	22.6	21.0	0.10
27	E2330A-10B	1	15	7.2	4.8	18.8	18.1	17.8	-	15	9.6	7.2	18.6	18.0	17.7	-	15	16.8	7.2	17.9	22.9	22.2	0.11
28	UGC 12914	2	265	55.2	38.4	13.8	12.3	11.6	13.3	265	67.2	55.2	13.7	12.1	11.4	13.1	265	93.6	57.6	12.0	20.7	18.6	0.16
29	UGC 12915	2	130	45.6	12.0	14.7	13.3	12.6	14.3	130	48.0	16.8	14.6	13.2	12.5	14.1	130	64.8	31.2	13.1	21.8	19.8	0.16
30	M2348A-13	1	-	10.9	10.9	17.7	16.6	16.0	16.8	-	19.0	19.0	17.3	16.2	15.6	16.4	190	29.9	24.5	16.1	23.2	21.7	0.19
31	J2348A-14	1	40	21.8	10.9	16.5	15.4	15.0	15.6	40	24.5	10.9	16.5	15.4	15.0	15.6	40	29.9	16.3	15.3	22.3	21.1	0.20
32	UGC 78	2	110	38.1	13.6	15.1	14.0	13.7	-	110	43.5	16.3	15.0	14.0	13.6	-	110	51.7	29.9	13.9	21.2	20.2	0.18
33	M0006C-05	1	130	27.2	10.9	16.0	15.0	14.6	-	130	29.9	10.9	16.0	15.0	14.6	-	130	38.1	16.3	14.9	22.1	21.0	0.13
34	UGC 179	2	90	31.2	14.4	15.5	14.6	14.1	-	90	36.0	19.2	15.4	14.5	14.1	-	90	38.4	21.6	14.5	21.5	20.2	0.09
35	UGC 186	3	60	28.8	14.4	15.2	13.7	13.1	-	60	36.0	14.4	15.2	13.7	13.1	-	60	38.4	19.2	13.7	20.7	18.5	0.10
36	UGC 210	2	60	31.2	14.4	15.4	14.5	14.0	-	60	33.6	14.4	15.4	14.5	14.0	-	255	38.4	24.0	14.4	21.3	20.0	0.08

Continued, next page.

127

Table 4.2 (cont.)

(1)	Name (2)	C (3)	$p.a._{25}$ (4)	a_{25} (5)	b_{25} (6)	B_{25} (7)	R_{25} (8)	I_{25} (9)	H_{25} (10)	$p.a._{26}$ (11)	a_{26} (12)	b_{26} (13)	B_{26} (14)	R_{26} (15)	I_{26} (16)	H_{26} (17)	$p.a._{26.6}$ (18)	$a_{26.6}$ (19)	$b_{26.6}$ (20)	$R_{26.6}$ (21)	B_0 (22)	R_0 (23)	A_B (24)
37	L0006B-15	1	16	16.3	13.6	17.7	16.7	16.2	17.7	16	21.8	19.0	17.5	16.4	15.9	17.2	65	29.9	24.5	16.4	23.6	22.5	0.09
38	UGC 186-OFF	2	-	-	-	-	-	-	-	-	-	-	-	-	-	-	-	-	-	-	-	-	0.08
39	I0024D-01	2	120	14.4	12.0	16.9	16.0	15.6	17.1	120	16.8	14.4	16.8	15.9	15.6	16.9	135	24.0	19.0	15.9	22.0	21.0	0.07
40	UGC 321	2	300	31.2	9.6	15.7	14.7	14.3	-	300	38.4	14.4	15.6	14.7	14.2	-	300	40.8	14.4	14.7	21.9	20.7	0.04
41	CGCG 479-040	2	135	24.0	12.0	15.7	14.6	14.1	-	135	26.4	14.4	15.7	14.6	14.1	-	135	31.2	13.6	14.6	21.8	20.4	0.05
42	UGC 354	2	140	21.8	8.2	16.5	15.4	14.8	15.8	140	27.2	8.2	16.5	15.4	14.7	15.8	320	49.0	13.6	15.1	22.1	20.8	0.06
43	UGC 356	2	35	65.3	32.6	13.7	12.2	11.6	13.7	35	76.2	40.8	13.6	12.2	11.5	13.7	35	133.3	59.8	11.7	19.5	17.8	0.05
44	NGC 169/169A	2	0	51.7	27.2	13.9	12.2	11.5	-	0	68.0	32.6	13.7	12.1	11.4	-	0	95.2	56.2	11.9	20.8	18.9	0.05
45	MRK 344	3	5	13.6	8.2	17.2	15.7	14.7	-	50	24.5	16.3	16.9	15.4	14.4	-	200	32.6	21.8	15.3	21.2	19.6	0.04
46	NGC 228	2	330	26.4	19.2	15.2	13.7	13.1	-	330	40.8	38.4	14.9	13.5	12.8	-	330	50.4	40.8	13.6	19.9	18.3	0.08
47	J0042A-01	1	285	8.2	5.4	18.9	18.1	17.8	18.2	285	10.9	8.2	18.6	17.8	17.5	17.8	330	13.6	10.9	17.7	23.1	22.3	0.08
48	N0042A-05A	1	195	13.6	8.2	16.9	15.3	14.5	-	195	13.6	8.2	16.9	15.3	14.5	-	195	27.2	19.0	15.2	20.8	19.2	0.09
49	N0042A-05B	1	195	8.2	5.4	18.2	17.1	16.4	-	195	8.2	5.4	18.2	17.1	16.4	-	195	13.6	10.9	16.3	23.7	22.8	0.09
50	E0042A-07	1	330	14.4	9.6	16.6	15.8	15.4	16.3	330	16.8	14.4	16.5	15.7	15.3	16.2	330	21.6	16.8	15.7	20.8	20.1	0.08
51	N0042C-10	1	125	13.6	8.2	18.0	16.8	16.5	-	125	16.3	10.9	17.8	16.6	16.2	-	35	19.0	16.3	16.4	23.5	22.5	0.12
52	UGC 591	2	119	24.5	13.6	15.5	14.7	14.2	-	250	32.6	24.5	15.4	14.5	14.0	-	120	43.5	35.4	14.4	21.1	20.3	0.10
53	UGC 612	3	-	-	-	-	-	-	-	-	-	-	-	-	-	-	-	-	-	-	-	-	0.10
54	CGCG 480-029	3	-	-	-	-	-	-	-	-	-	-	-	-	-	-	-	-	-	-	-	-	0.11
55	MCG 04-04-03	2	90	16.3	13.6	16.9	15.9	15.4	-	295	27.2	19.0	16.6	15.7	15.2	-	305	32.6	24.5	15.6	22.6	21.4	0.22
56	UGC 1084	2	245	16.3	8.2	17.9	16.8	16.8	-	245	27.2	13.6	17.3	16.2	-	-	35	46.2	21.8	15.8	23.8	22.6	0.27
57	N0118D-12	1	-	10.9	10.9	17.3	16.0	15.6	17.6	119	16.3	13.6	17.2	15.9	15.5	17.4	30	54.4	46.2	15.0	22.3	21.0	0.34
58	K0118B-14	1	50	13.6	5.4	18.7	18.1	17.7	18.6	235	13.6	8.2	18.6	17.9	17.6	18.5	50	19.0	13.6	17.6	24.2	23.6	0.36
59	J0136B-06	1	271	10.9	8.2	18.6	17.6	17.1	18.8	271	16.3	10.9	18.4	17.4	16.8	18.5	-	21.8	21.8	17.1	23.8	22.9	0.33
60	D0136D-10	1	75	12.0	7.2	17.4	16.2	15.6	17.9	75	16.8	9.6	17.3	16.1	15.5	17.8	75	21.6	12.0	16.0	21.0	19.9	0.29
61	L0136C-13	1	290	19.0	10.9	17.2	16.2	15.7	19.5	95	27.2	10.9	17.1	16.1	15.6	19.5	265	51.7	16.3	15.9	23.1	21.8	0.37
62	UGC 1471	2	195	43.2	38.4	14.0	12.6	11.9	-	195	52.8	43.2	13.9	12.5	11.9	-	195	74.4	50.4	12.4	19.8	18.2	0.33
63	J0154B-04	1	0	16.3	10.9	17.7	16.9	16.6	17.5	0	19.0	13.6	17.6	16.8	16.4	17.1	0	29.9	27.2	16.5	23.4	22.6	0.31
64	CGCG 482-046	2	80	16.8	12.0	15.8	14.8	14.2	-	80	19.2	12.0	15.8	14.7	14.2	-	80	24.0	14.4	14.7	21.0	19.9	0.31
65	CGCG 482-050	3	60	16.8	12.0	16.2	14.7	14.1	-	60	19.2	14.4	16.2	14.7	14.1	-	60	24.0	24.0	14.7	20.8	19.3	0.30
66	IC 190	3	160	21.6	14.4	15.7	14.2	13.5	-	140	31.2	21.6	15.6	14.1	13.4	-	160	45.6	31.2	14.0	20.8	18.3	0.30
67	UGC 1538	2	196	21.8	16.3	17.0	15.9	15.4	-	185	27.2	16.3	16.6	15.6	15.0	-	184	32.6	16.3	15.6	23.1	22.0	0.30
68	UGC 1551	2	135	62.6	54.4	13.9	12.8	12.3	-	135	70.7	59.6	13.8	12.7	12.3	-	135	81.6	73.4	12.7	22.3	20.9	0.30
69	N0154D-06	1	0	19.0	10.9	16.9	15.8	15.4	16.6	0	24.5	16.3	16.8	15.6	15.3	16.0	0	27.2	21.8	15.6	22.8	21.5	0.30
70	A0154B-11	1	120	24.0	7.2	16.3	15.4	14.9	16.3	120	26.4	7.2	16.2	15.3	14.8	16.2	120	31.2	12.0	14.9	20.7	20.2	0.30
71	K0154B-11	1	225	10.9	5.4	18.2	17.3	16.8	19.0	225	16.3	10.9	17.9	16.8	16.4	17.9	270	27.2	19.0	16.5	23.2	22.3	0.28

128

Table 4.2 (cont.)

(1)	Name (2)	C (3)	$p.a._{25}$ (4)	a_{25} (5)	b_{25} (6)	B_{25} (7)	R_{25} (8)	I_{25} (9)	H_{25} (10)	$p.a._{26}$ (11)	a_{26} (12)	b_{26} (13)	B_{26} (14)	R_{26} (15)	I_{26} (16)	H_{26} (17)	$p.a._{26.6}$ (18)	$a_{26.6}$ (19)	$b_{26.6}$ (20)	$R_{26.6}$ (21)	B_0 (22)	R_0 (23)	A_B (24)
72	A0154A-15	1	65	13.6	5.4	17.9	16.8	16.1	--	65	16.3	8.2	16.4	15.0	14.6	--	65	32.6	16.3	14.1	23.6	22.6	0.28
73	CGCG 483-034	2	30	24.5	13.6	16.2	15.2	14.7	--	30	24.5	16.3	16.2	15.2	14.6	--	30	27.2	16.3	15.1	22.3	21.4	0.26
74	CGCG 483-036	2	285	19.0	13.6	15.9	14.8	14.2	--	285	21.8	19.0	15.8	14.7	14.2	--	285	27.2	24.5	14.5	21.1	19.9	0.27
75	UGC 1938	2	105	26.4	9.6	15.7	14.3	13.6	--	105	31.2	12.0	15.6	14.2	13.6	--	105	33.6	26.4	14.2	21.2	19.5	0.30
76	UGC 1950	2	121	29.9	13.6	15.8	14.4	13.8	--	106	46.2	21.8	15.6	14.3	13.6	--	106	46.2	24.5	14.3	21.3	19.6	0.33
77	N0212A-13	1	151	27.2	8.2	16.3	15.1	14.7	15.5	151	27.2	8.2	16.3	15.1	14.7	15.5	151	54.4	16.3	15.0	22.0	20.7	0.34
78	H0212C-15	1	180	12.0	7.2	17.8	16.7	16.0	17.3	180	21.6	12.0	17.4	16.3	15.2	16.6	180	28.8	36.0	15.5	23.2	22.1	0.39
79	UGC 2020	2	160	33.6	9.6	16.1	15.0	14.5	--	160	43.2	12.0	16.0	15.0	14.5	--	160	50.4	24.0	14.9	21.9	20.5	0.41
80	E0230C-01	1	150	19.0	5.4	17.7	16.2	15.6	16.8	150	24.5	8.2	17.6	16.0	15.4	16.8	150	29.9	16.3	15.9	23.0	21.5	0.40
81	UGC 2059	2	135	38.4	33.6	14.3	12.6	11.8	--	135	55.2	50.4	14.1	12.4	11.6	--	105	105.6	96.0	12.2	19.7	17.6	0.39
82	UGC 2079	2	106	49.0	24.5	14.8	13.6	13.1	--	100	51.7	29.9	14.7	13.5	13.0	--	100	62.6	59.8	13.4	22.1	20.6	0.36
83	L0230D-03	1	166	21.8	8.2	17.0	15.9	15.2	--	166	21.8	8.2	17.0	15.9	15.2	--	166	24.5	10.9	15.8	21.9	20.8	0.36
84	UGC 2104	2	35	26.4	16.8	15.7	14.4	13.8	--	35	33.6	19.2	15.7	14.4	13.7	--	35	40.8	28.8	14.3	21.9	20.1	0.42
85	B0230A-08	1	65	9.6	4.8	18.7	17.9	17.5	--	65	16.8	7.2	18.3	17.6	17.2	--	90	16.8	12.0	17.5	23.5	22.7	0.40
86	UGC 2248	2	125	24.0	14.4	15.9	14.2	13.4	--	125	36.0	21.6	15.7	14.1	13.1	--	120	45.6	38.4	13.9	20.9	18.9	0.51
87	UGC 2267	2	110	28.8	19.2	15.5	13.8	13.0	--	110	40.8	24.0	15.4	13.7	12.9	--	160	67.2	50.4	13.5	21.4	19.4	0.52
88	B0230A-14	1	330	10.9	8.2	19.0	18.2	18.0	19.4	-	13.6	13.6	18.7	17.9	18.0	19.4	330	16.3	13.6	17.9	24.1	23.4	0.54
89	D0248A-04	1	100	7.2	4.8	19.4	18.2	17.7	21.6	100	14.4	7.2	18.7	17.6	17.0	19.4	100	16.8	14.4	17.2	23.8	22.6	0.56
90	K0248C-02	1	-	2.7	2.7	20.8	19.8	18.3	--	-	5.4	5.4	19.8	19.5	18.3	--	-	5.4	5.4	19.1	24.4	22.7	0.60

Table 4.3. Derived Quantities for the Slice Objects

(1)	Name (2)	C (3)	D (Mpc) (4)	r (kpc) (5)	i (deg) (6)	B (7)	R (8)	B-R (9)	L_B ($10^9 L_\odot$) (10)	σ (mag/arcsec²) (11)	M_{HI} ($10^9 M_\odot$) (12)	M_d ($10^9 M_\odot$) (13)	M_{HI}/M_d (14)	L_B/M_d (15)	L_B/M_{HI} (16)
1	B2200D-02	1	82.5	10.2	0	-18.3	-19.0	0.7	3.20	23.5	2.62	3.331	0.787	0.96	1.22
2	C2218C-07	1	16.9	2.4	46	-13.5	-14.2	0.7	0.04	24.5	0.24	0.864	0.278	0.04	0.16
3	UGC 12148	2	95.3	--	--	--	--	--	--	--	7.88	--	--	--	--
4	UGC 12153	2	95.3	--	--	--	--	--	--	--	10.18	--	--	--	--
5	N2254A-03	1	95.9	25.3	75	-17.9	-19.2	1.3	2.29	23.4	2.08	2.072	1.002	1.10	1.10
6	CGCG 475-028	3	103.8	23.2	41	-17.1	-19.2	2.1	1.10	24.2	1.19	66.714	0.018	0.02	0.93
7	H2254D-06	1	15.5	2.3	55	-13.7	-14.6	0.9	0.05	24.1	0.16	1.607	0.101	0.03	0.29
8	A2254D-10	1	84.6	7.9	0	-15.4	-16.8	1.4	0.22	24.4	2.71	0.379	7.160	0.57	0.08
9	G2254A-11	1	57.1	6.6	44	-16.7	-17.9	1.2	0.76	23.9	2.67	11.831	0.226	0.06	0.28
10	MRK 317	3	81.9	10.8	50	-17.3	-19.4	2.1	1.32	23.7	0.27	10.627	0.025	0.12	4.92
11	UGC 12443	3	80.9	33.9	44	-20.5	-22.0	1.5	24.35	23.1	-0.15	--	--	--	--
12	UGC 12449	3	106.0	17.3	83	-18.5	-20.1	1.6	4.07	23.2	1.82	168.438	0.011	0.02	2.23
13	UGC 12533	2	79.8	24.2	86	-18.4	-20.2	1.8	3.46	23.0	4.85	406.509	0.012	0.01	0.71
14	CGCG 476-023	2	67.5	7.1	36	-18.1	-18.8	0.7	2.69	23.0	2.42	14.530	0.167	0.19	1.11
15	K2312B-09	1	78.9	6.2	64	-16.4	-17.1	0.7	0.58	24.3	3.03	5.736	0.528	0.10	0.19
16	UGC 12583	2	67.8	--	--	--	--	--	--	--	5.24	--	--	--	--
17	UGC 12607	2	45.7	15.4	40	-20.1	-20.8	0.7	16.73	22.4	4.39	16.611	0.264	1.01	3.81
18	UGC 12610	2	47.8	15.6	57	-19.1	-20.2	1.1	6.77	23.3	7.36	79.646	0.092	0.09	0.92
19	N2312B-15	1	53.9	3.6	--	-13.0	-13.7	0.7	0.02	--	0.60	--	--	--	0.04
20	CGCG 476-061	2	93.6	16.3	45	-19.1	-20.2	1.1	6.84	22.9	5.85	92.412	0.063	0.07	1.17
21	UGC 12655	2	68.4	29.8	51	-20.0	-21.5	1.4	16.12	22.9	3.44	410.512	0.008	0.04	4.69
23	L2330C-03	1	75.2	11.9	67	-17.0	-17.8	0.8	1.01	23.4	2.59	18.850	0.137	0.05	0.39
24	L2330D-02	2	74.6	5.9	0	-16.0	-16.7	0.8	0.39	24.3	3.04	3.630	0.839	0.11	0.13
25	UGC 12694	2	41.2	9.6	29	-18.9	-20.0	1.1	5.56	22.7	2.18	74.135	0.029	0.07	2.55
26	E2330A-10A	1	72.0	11.7	84	-17.3	-18.6	1.3	1.31	23.7	3.32	64.926	0.051	0.02	0.39
27	E2330A-10B	1	70.8	5.8	48	-15.6	-16.2	0.6	0.27	23.9	0.78	0.965	0.806	0.27	0.34
28	UGC 12914	2	61.4	27.9	45	-20.3	-21.7	1.4	20.85	23.3	3.70	44.813	0.083	0.47	5.63
29	UGC 12915	2	59.3	18.6	76	-19.3	-20.7	1.3	8.50	22.7	10.44	307.210	0.034	0.03	0.81
30	M2348A-13	1	88.5	12.8	0	-17.3	-18.3	1.0	1.29	24.2	4.91	11.341	0.433	0.11	0.26
31	J2348A-14	1	61.8	9.0	62	-17.7	-18.7	1.0	1.80	23.5	3.78	22.300	0.170	0.08	0.48
32	UGC 78	2	61.2	15.3	71	-19.0	-20.0	1.0	6.42	23.0	3.47	19.923	0.174	0.32	1.85
33	M0006C-05	1	83.6	15.4	68	-18.7	-19.7	0.9	4.88	23.3	2.09	17.042	0.122	0.29	2.34
34	UGC 179	2	60.4	11.3	63	-18.5	-19.4	0.9	3.94	23.3	4.80	34.441	0.139	0.11	0.82
35	UGC 186	3	78.7	14.7	62	-19.4	-20.8	1.4	8.76	22.9	0.95	142.320	0.007	0.06	9.26

Continued, next page.

130

Table 4.3 (cont.)

(1)	Name (2)	C (3)	D (Mpc) (4)	r (kpc) (5)	i (deg) (6)	B (7)	R (8)	B-R (9)	L_B ($10^9 L_\odot$) (10)	σ (mag/asec²) (11)	M_{HI} ($10^9 M_\odot$) (12)	M_d ($10^9 M_\odot$) (13)	M_{HI}/M_d (14)	L_B/M_d (15)	L_B/M_{HI} (16)
36	UGC 210	2	60.7	11.3	64	-18.6	-19.5	0.9	4.29	23.2	4.15	39.315	0.105	0.11	1.04
37	L0006B-15	1	76.8	11.1	33	-16.8	-17.8	1.0	0.84	24.8	1.47	66.242	0.022	0.01	0.57
38	UGC 186-OFF	2	99.6	--	--	--	--	--	--	--	5.41	--	--	--	--
39	I0024D-01	1	79.5	9.3	34	-17.7	-18.5	0.9	1.83	23.7	2.60	52.874	0.049	0.03	0.71
40	UGC 321	2	63.3	12.5	74	-18.4	-19.3	1.0	3.42	23.1	4.25	30.730	0.138	0.11	0.80
41	CGCG 479-040	2	70.4	10.6	61	-18.6	-19.7	1.1	4.22	23.1	2.82	49.981	0.056	0.08	1.50
42	UGC 354	2	76.0	18.1	70	-18.0	-19.0	1.1	2.38	23.3	2.07	50.462	0.041	0.05	1.15
43	UGC 356	2	71.2	46.0	61	-20.6	-22.1	1.5	27.38	23.2	4.16	824.832	0.005	0.03	6.58
44	NGC 169/169A	2	62.8	29.0	60	-20.1	-21.8	1.7	17.81	23.0	7.45	587.675	0.013	0.03	2.39
45	MRK 344	3	102.1	16.1	53	-17.9	-19.4	1.5	2.25	23.6	0.34	22.448	0.015	0.10	6.56
46	NGC 228	2	100.3	24.5	42	-19.9	-21.4	1.4	14.32	23.2	7.46	35.888	0.208	0.40	1.92
47	J0042A-01	1	90.0	5.9	49	-16.0	-16.7	0.8	0.38	24.2	0.99	1.950	0.507	0.20	0.39
48	N0042A-05A	1	96.8	12.8	54	-18.1	-19.7	1.6	2.74	23.2	2.62	18.662	0.140	0.15	1.05
49	N0042A-05B	1	96.8	6.4	50	-16.8	-17.9	1.1	0.83	23.5	1.03	9.024	0.115	0.09	0.80
50	E0042A-07	1	36.3	3.8	48	-16.3	-17.0	0.8	0.51	23.2	0.24	1.521	0.157	0.33	2.13
51	N0042C-10	1	67.6	6.2	53	-16.3	-17.4	1.1	0.51	24.3	0.45	1.075	0.419	0.48	1.14
52	UGC 591	2	65.9	13.9	55	-18.7	-19.5	0.8	4.72	23.1	4.41	29.945	0.147	0.16	1.07
53	UGC 612	3	69.3	--	--	--	--	--	--	--	0.59	--	--	--	--
54	CGCG 480-029	3	68.7	--	--	--	--	--	--	--	0.42	--	--	--	--
55	MCG 04-04-03	2	92.0	14.5	38	-18.2	-19.1	0.9	2.99	24.0	7.84	94.942	0.083	0.03	0.38
56	UGC 1084	2	47.3	10.6	61	-15.9	-16.9	1.0	0.36	24.4	3.52	2.745	1.281	0.13	0.10
57	N0118D-12	1	46.0	12.1	22	-16.4	-17.5	1.1	0.56	23.6	3.73	56.251	0.066	0.01	0.15
58	K0118B-14	1	9.3	0.9	63	-11.5	-12.0	0.4	0.01	24.4	0.04	0.140	0.253	0.05	0.18
59	J0136B-06	1	53.5	5.7	45	-15.4	-16.3	0.8	0.23	24.6	0.44	1.099	0.404	0.21	0.53
60	D0136D-10	1	76.7	8.0	55	-17.3	-18.4	1.0	1.35	23.4	2.96	66.327	0.045	0.02	0.46
61	L0136C-13	1	40.7	10.2	62	-16.3	-17.1	0.8	0.50	24.0	0.73	9.187	0.079	0.05	0.68
62	UGC 1471	2	67.5	24.3	31	-20.5	-21.7	1.2	24.89	23.0	5.71	71.303	0.080	0.35	4.36
63	J0154B-04	1	68.9	10.0	47	-16.8	-17.5	0.6	0.84	24.4	2.06	13.475	0.153	0.06	0.41
64	CGCG 482-046	2	69.1	8.0	48	-18.7	-19.6	0.9	4.75	22.5	2.72	21.579	0.126	0.22	1.75
65	CGCG 482-050	3	64.9	7.6	44	-18.2	-19.5	1.3	2.87	23.0	-0.12	--	--	--	--
66	IC 190	3	65.5	14.5	48	-18.7	-20.1	1.3	4.77	23.1	-0.13	--	--	--	--
67	UGC 1538	2	39.7	6.3	47	-16.4	-17.3	0.9	0.57	24.3	0.81	8.832	0.092	0.06	0.71
68	UGC 1551	2	37.5	14.8	31	-19.3	-20.2	0.9	8.18	23.7	5.38	41.569	0.129	0.20	1.52
69	N0154D-06	1	66.0	8.7	54	-17.5	-18.5	1.0	1.60	23.8	2.39	42.737	0.056	0.04	0.67

Table 4.3 (cont.)

(1)	Name (2)	C (3)	D (Mpc) (4)	r (kpc) (5)	i (deg) (6)	B (7)	R (8)	$B-R$ (9)	L_B ($10^9 L_\odot$) (10)	σ (mag/asec²) (11)	M_{HI} ($10^9 M_\odot$) (12)	M_d ($10^9 M_\odot$) (13)	M_{HI}/M_d (14)	L_B/M_d (15)	L_B/M_{HI} (16)
70	A0154B-11	1	110.8	16.8	75	-19.3	-20.0	0.7	7.85	22.8	8.82	25.554	0.345	0.31	0.89
71	K0154B-11	1	70.0	9.2	57	-16.4	-17.2	0.8	0.56	23.9	1.78	2.688	0.663	0.21	0.31
72	A0154A-15	1	34.6	5.5	66	-15.5	-16.5	1.0	0.25	23.3	0.10	0.958	0.100	0.26	2.56
73	CGCG 483-034	2	89.6	11.8	55	-18.8	-19.7	0.9	5.27	23.5	3.13	4.173	0.750	1.26	1.68
74	CGCG 483-036	2	90.3	11.9	41	-19.2	-20.1	1.0	7.27	23.0	4.43	44.966	0.099	0.16	1.64
75	UGC 1938	2	87.3	14.2	70	-19.3	-20.6	1.2	8.44	22.8	10.38	127.617	0.081	0.07	0.81
76	UGC 1950	2	85.8	19.2	64	-19.3	-20.5	1.2	7.88	23.5	4.82	104.599	0.046	0.08	1.63
77	N0212A-13	1	75.0	19.8	75	-18.4	-19.4	1.0	3.61	23.1	2.41	64.914	0.037	0.06	1.50
78	H0212C-15	1	57.4	8.0	56	-16.5	-17.4	0.9	0.64	23.9	1.00	8.444	0.118	0.08	0.64
79	UGC 2020	2	76.1	18.6	76	-18.8	-19.6	0.8	4.96	23.4	7.86	61.731	0.127	0.08	0.63
80	E0230C-01	1	60.8	8.8	74	-16.7	-18.0	1.3	0.72	23.9	1.58	12.181	0.130	0.06	0.46
81	UGC 2059	2	60.1	30.8	27	-20.1	-21.6	1.5	16.53	23.2	10.89	2733.942	0.004	0.01	1.52
82	UGC 2079	2	77.2	23.4	59	-20.0	-21.0	1.0	16.11	23.4	12.86	96.325	0.133	0.17	1.25
83	L0230D-03	1	78.4	9.3	70	-17.8	-18.7	0.9	2.12	23.5	1.21	16.604	0.073	0.13	1.75
84	UGC 2104	2	111.8	22.1	54	-20.0	-21.0	1.1	14.99	23.3	7.93	173.638	0.046	0.09	1.89
85	B0230A-08	1	104.1	8.5	64	-17.0	-17.5	0.5	0.94	24.0	3.13	15.936	0.197	0.06	0.30
86	UGC 2248	2	84.5	18.7	54	-19.3	-20.7	1.4	8.51	23.4	6.15	169.865	0.036	0.05	1.38
87	UGC 2267	2	82.6	26.9	53	-19.7	-21.1	1.4	11.33	23.4	6.53	217.246	0.030	0.05	1.73
88	B0230A-14	1	8.2	0.6	26	-11.3	-11.8	0.5	0.00	24.9	0.02	0.147	0.108	0.03	0.31
89	D0248A-04	1	82.9	6.7	58	-16.1	-17.0	0.8	0.45	24.3	2.50	6.332	0.395	0.07	0.18
90	K0248C-02	1	7.4	0.2	0	-9.7	-10.0	0.3	0.00	24.0	0.01	0.009	1.360	0.13	0.10

Table 4.4. Cataloged Object Names Cross-Reference

	NGC/IC	UGC	MCG	CGCG	MRK	IRAS	OTHER
3	IC 5242	UGC 12148	MCG 04-53-10	CGCG 474-020			
4	IC 5243	UGC 12153	MCG 04-53-11	CGCG 474-021			
6				CGCG 475-028			
10					MRK 317		ANON 2311+23
							KUG 2311+235
11	NGC 7539	UGC 12443	MCG 04-54-35	CGCG 475-048			
12		UGC 12449					
13		UGC 12533		CGCG 476-013			
14				CGCG 476-023		IRAS 23183+2332	
16		UGC 12583		CGCG 476-031			
17	NGC 7673	UGC 12607	MCG 04-55-14	CGCG 476-061	MRK 325		
18	NGC 7677	UGC 12610	MCG 04-55-15	CGCG 476-064	MRK 326		
20				CGCG 476-073			KUG 2329+232
21		UGC 12655	MCG 04-55-25	CGCG 478-012			
25	NGC 7712	UGC 12694	MCG 04-55-30	CGCG 477-040			
28		UGC 12914	MCG 04-01-10	CGCG 477-041			
29		UGC 12915	MCG 04-01-11	CGCG 478-013			
32	NGC 9	UGC 78	MCG 04-01-30	CGCG 477-059			
34		UGC 179	MCG 04-01-49	CGCG 478-053			
35	IC 1540	UGC 186	MCG 04-01-50	CGCG 478-054			
36		UGC 210	MCG 04-02-13	CGCG 479-016			
40		UGC 321	MCG 04-02-27	CGCG 479-037			
41			MCG 04-02-30	CGCG 479-040			
42		UGC 354	MCG 04-02-32	CGCG 479-043			
43	NGC 160	UGC 356	MCG 04-02-33	CGCG 479-044			
44	NGC 169	UGC 365	MCG 04-02-35	CGCG 479-049			
45				CGCG 479-049			
46	NGC 228	UGC 458	MCG 04-02-48	CGCG 479-062	MRK 344		
52		UGC 591	MCG 04-03-23	CGCG 480-025			
53		UGC 612	MCG 04-03-29	CGCG 480-028	MRK 350		
54				CGCG 480-029		IRAS 563+2334	
55			MCG 04-04-03				
56		UGC 1084					
62	NGC 776	UGC 1471	MCG 04-05-28	CGCG 482-037			
64				CGCG 482-046			

Table 4.4 (cont.)

	NGC/IC	UGC	MCG	CGCG	MRK	IRAS	OTHER
65				CGCG 482-050			
66	IC 190			CGCG 482-052			
67		UGC 1538	MCG 04-05-40				
68		UGC 1551	MCG 04-05-45	CGCG 482-061		IRAS 2008+2350	
73			MCG 04-06-28	CGCG 483-034			
74				CGCG 483-036			
75		UGC 1938	MCG 04-06-54	CGCG 483-063			
76		UGC 1950	MCG 04-06-56	CGCG 483-065		IRAS 2258+2334	
79		UGC 2020	MCG 04-07-07	CGCG 484-005			
81	NGC 984	UGC 2059	MCG 04-07-12	CGCG 484-010			
82		UGC 2079	MCG 04-07-14	CGCG 484-012			ANON 233+23
84		UGC 2104	MCG 04-07-18	CGCG 484-016		IRAS 2345+2304	
86		UGC 2248	MCG 04-07-21	CGCG 484-018		IRAS 2440+2323	
87		UGC 2267	MCG 04-07-23	CGCG 484-019			

1: B2200D-02
6206 km/s

2: C2218C-07
1278 km/s

5: N2254A-03
7189 km/s

7: H2254D-06
1155 km/s

8: A2254D-10
6336 km/s

9: G2254A-11
4270 km/s

15: K2312B-09
5895 km/s

19: N2312B-15
4009 km/s

23: L2330C-03
5603 km/s

24: L2330D-02
5558 km/s
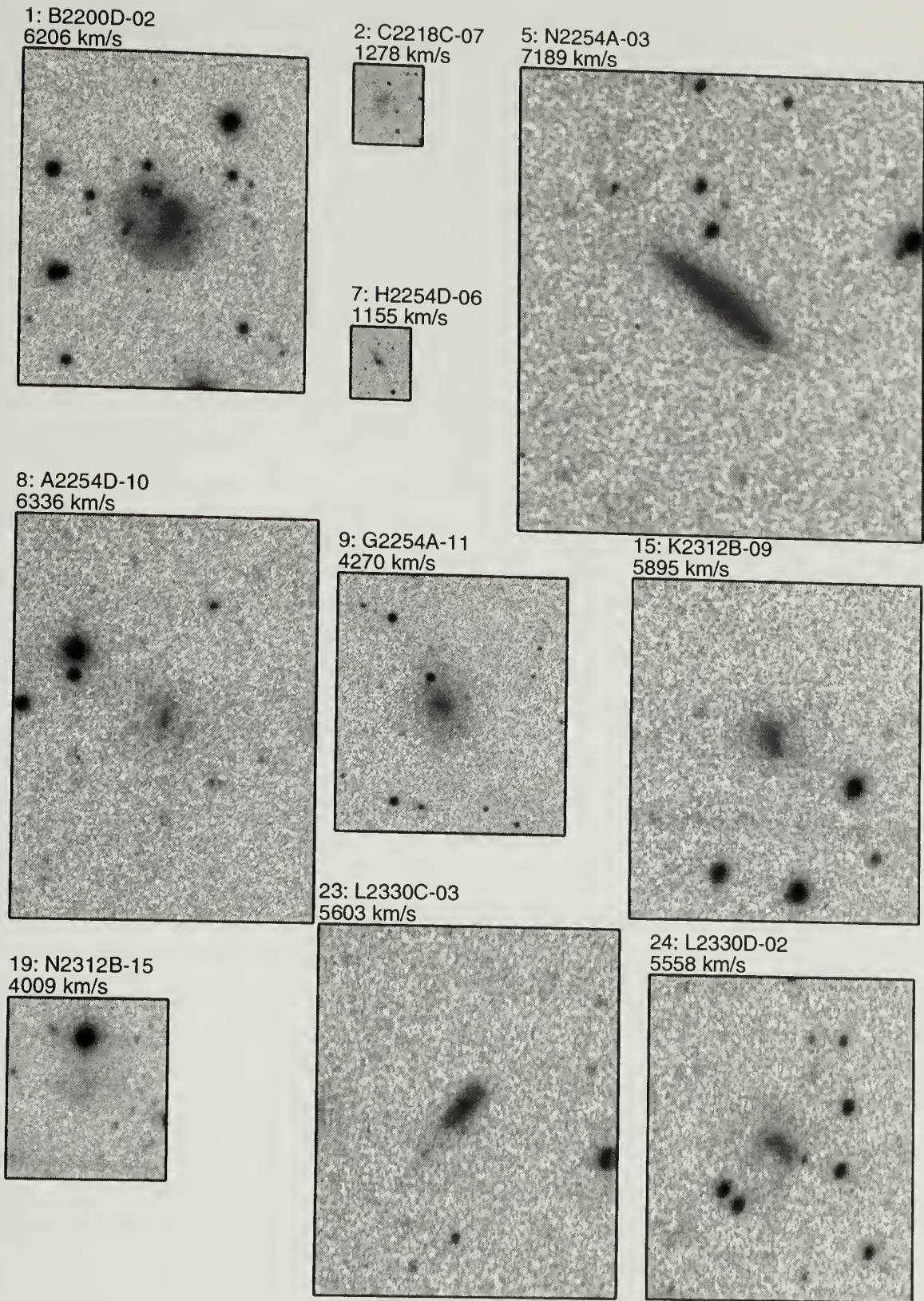
Figure 4.1. R-band images of the uncataloged objects detected in the HI slice search. Images are scaled at 20,000 kpc/inch. Continued, next page.

Figure 4.1. (cont.)

136
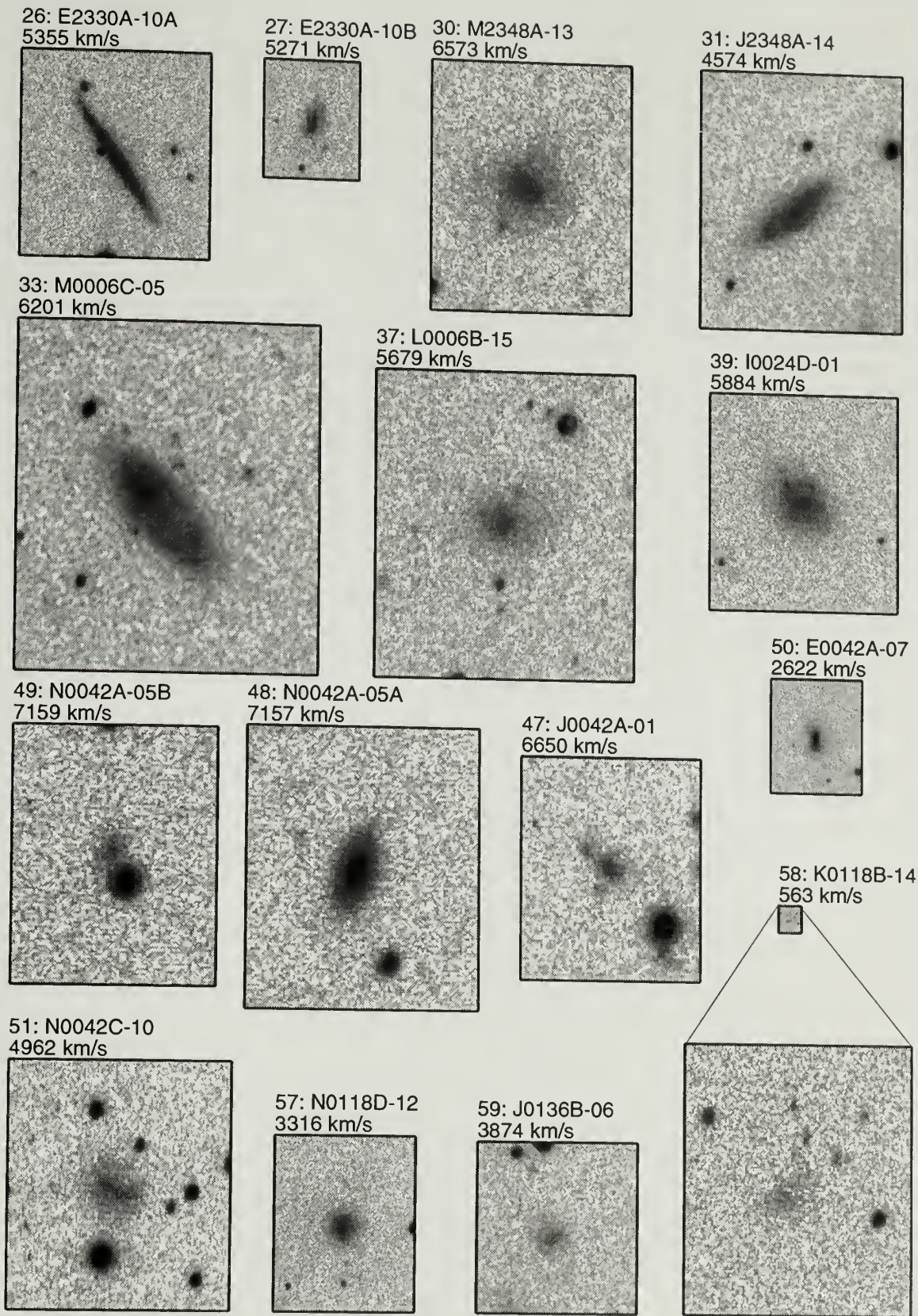
60: D0136D-10
5614 km/s
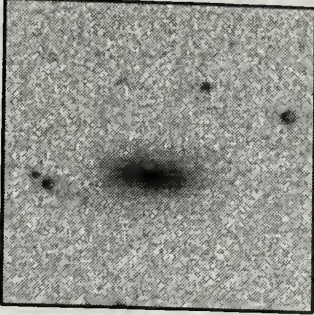
63: J0154B-04
5029 km/s
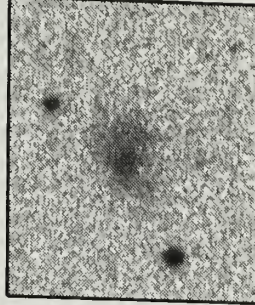
69: N0154D-06
4812 km/s
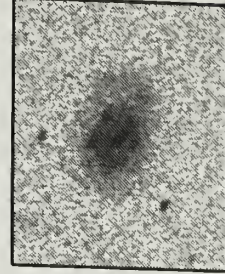
70: A0154B-11
8162 km/s
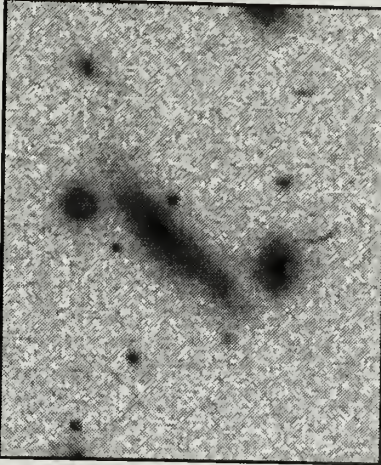
61: L0136C-13
2914 km/s
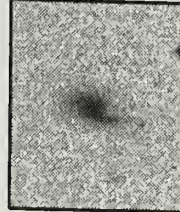
77: N0212A-13
5484 km/s

71: K0154B-11
5105 km/s
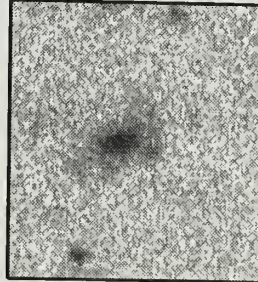
72: A0154A-15
2452 km/s
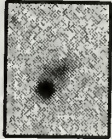
80: E0230C-01
4414 km/s
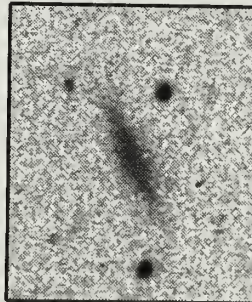
83: L0230D-03
5734 km/s

78: H0212C-15
4159 km/s
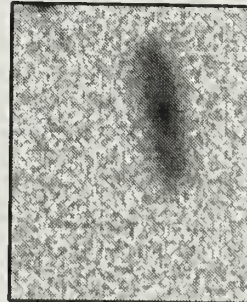
Figure 4.1. (cont.)

85: B0230A-08
7661 km/s
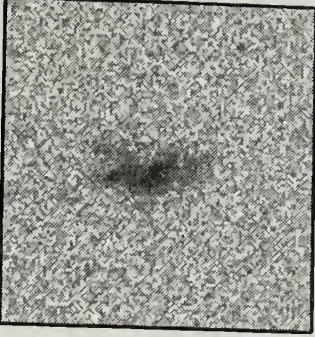
89: D0248A-04
6071 km/s
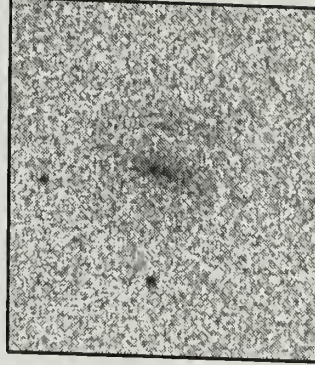
88: B0230A-14
469 km/s

Figure 4.1. (cont.)
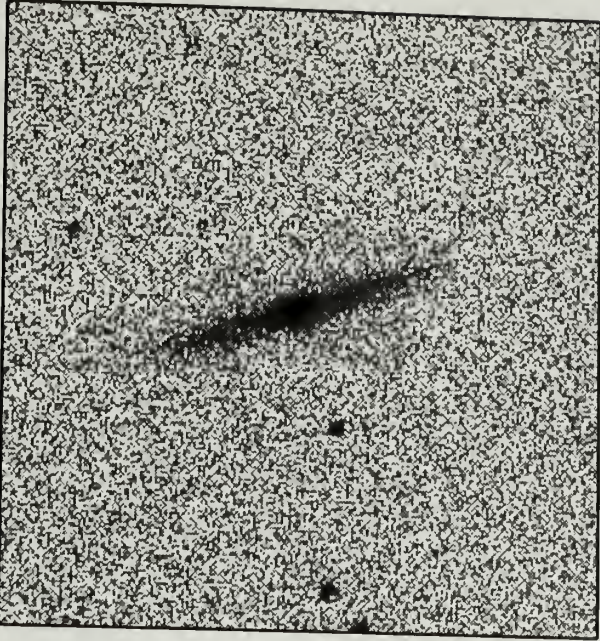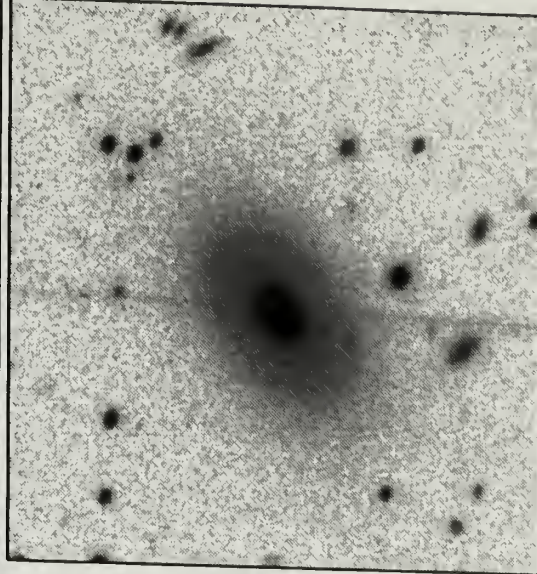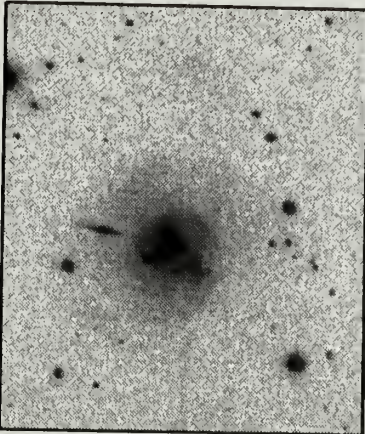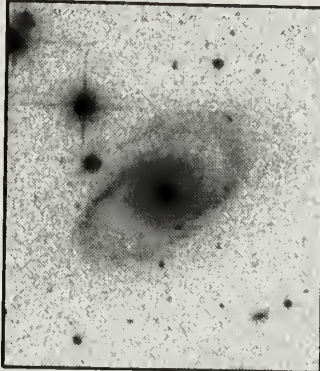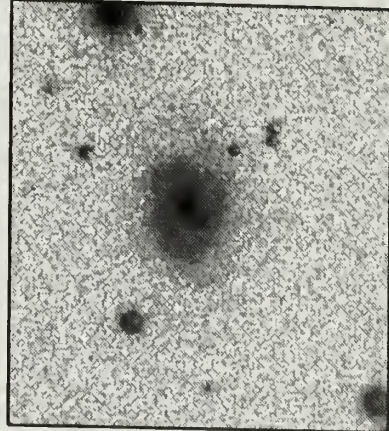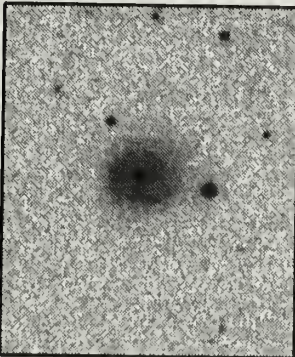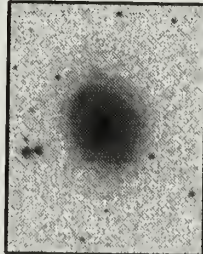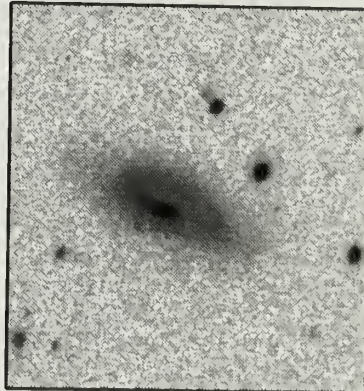
Figure 4.2. R-band images of the cataloged objects detected in the HI slice search. Images are scaled at 20,000 kpc/inch. Continued, next page.

28/29: UGC 12914/12915
4546 km/s
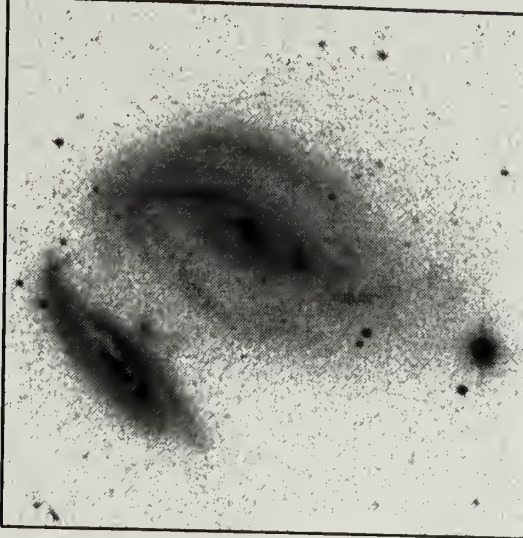
43: UGC 356
5252 km/s
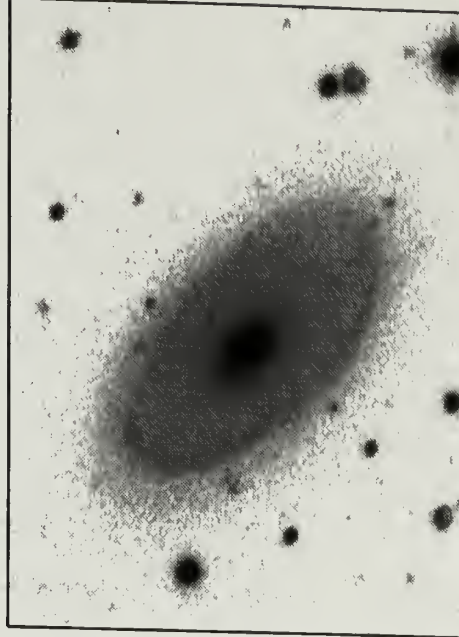
42: UGC 354
5614 km/s

34: UGC 179
4459 km/s
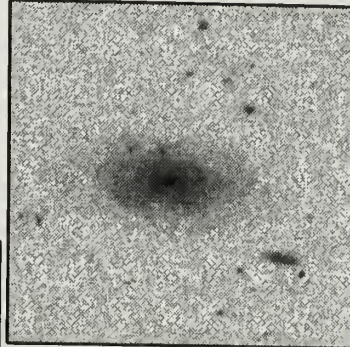
36: UGC 210
4479 km/s
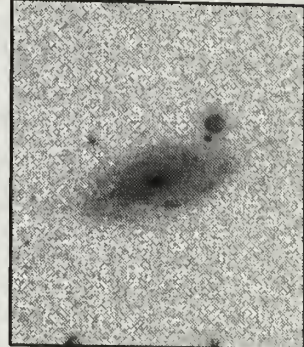
46: NGC 228
7423 km/s
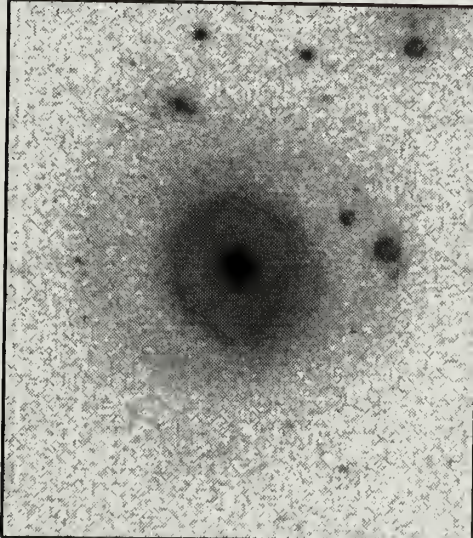
40: UGC 321
4658 km/s
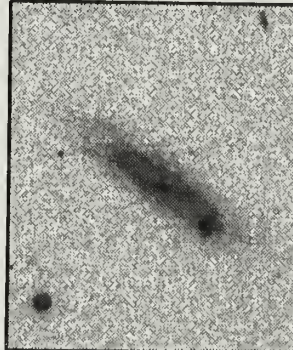
41: CGCG 479-040
5190 km/s

Figure 4.2. (cont.)

140
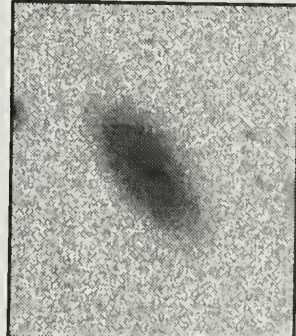
44: NGC 169
4618 km/s
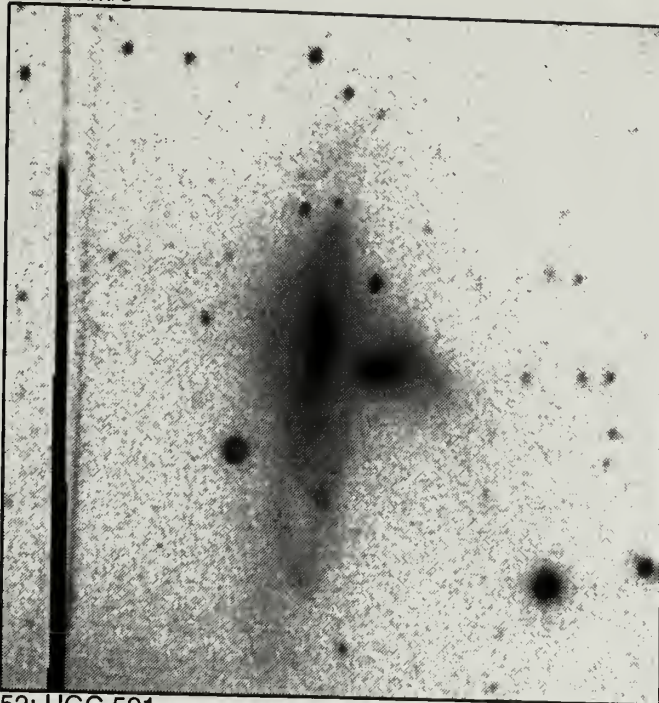
62: UGC 01471
4919 km/s
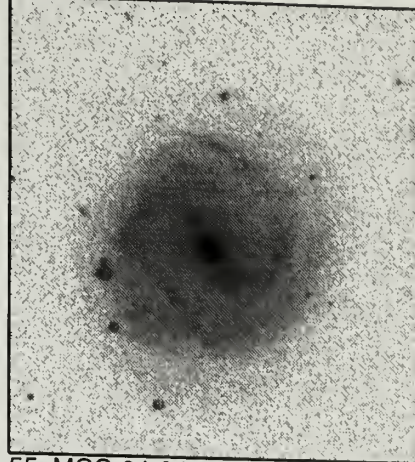
55: MCG 04-04-03
6777 km/s
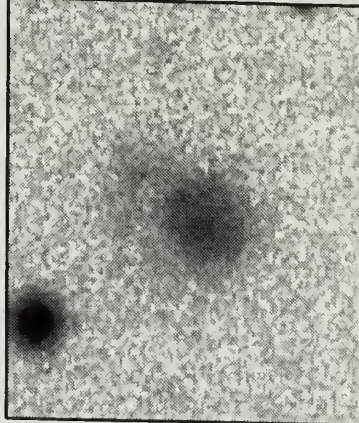
52: UGC 591
4834 km/s
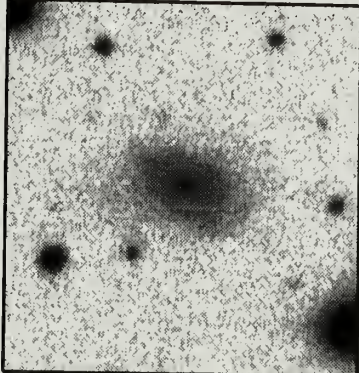
68: UGC 1551
2671 km/s
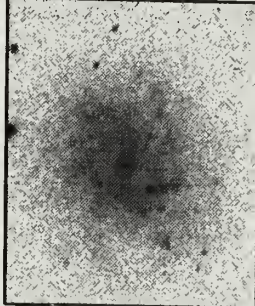
67: UGC 1538
2832 km/s

56: UGC 1084
3415 km/s
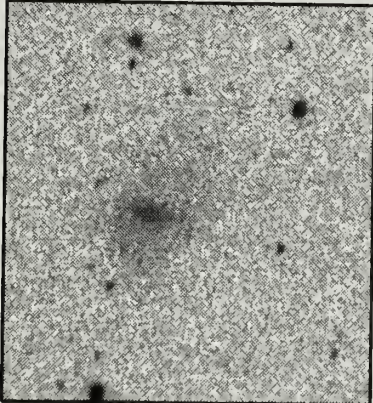
73: CGCG 483-034
6574 km/s
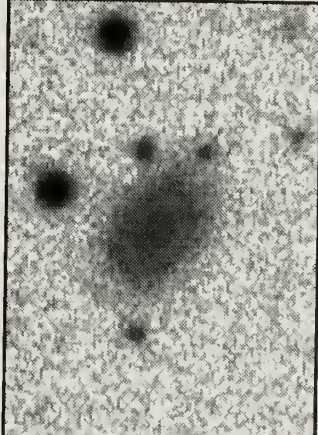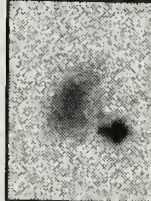
64: CGCG 482-046
5041 km/s

Figure 4.2. (cont.)

141
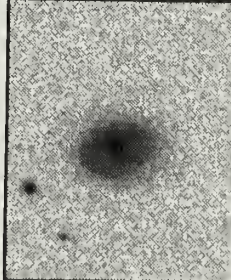
75: UGC 1938
6399 km/s
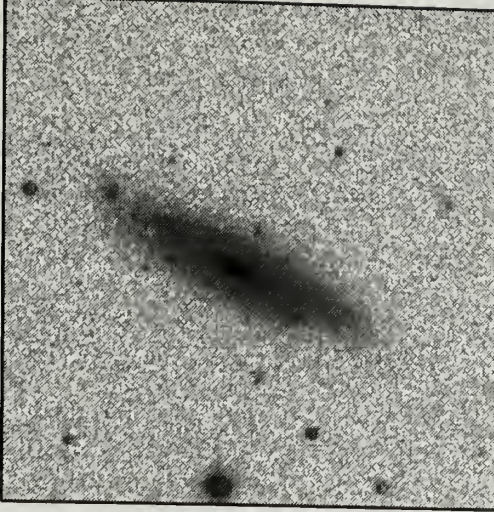
81: UGC 2059
4360 km/s
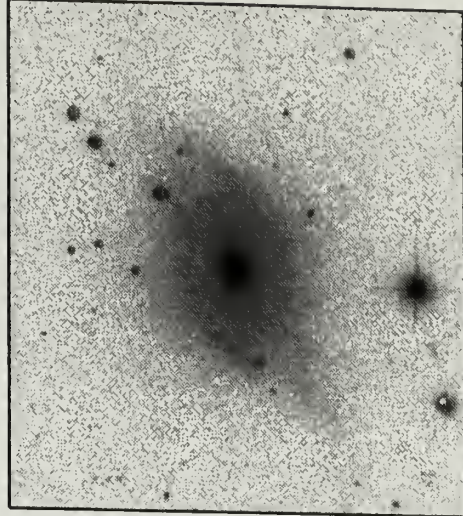
74: CGCG 483-036
6631 km/s
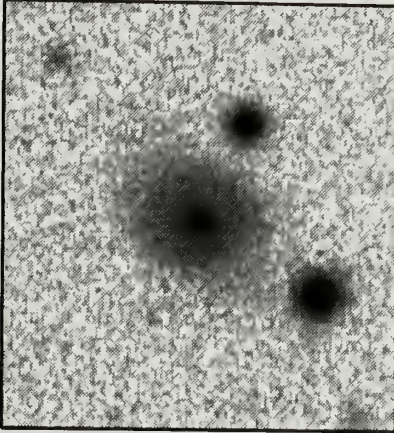
79: UGC 2020
5563 km/s
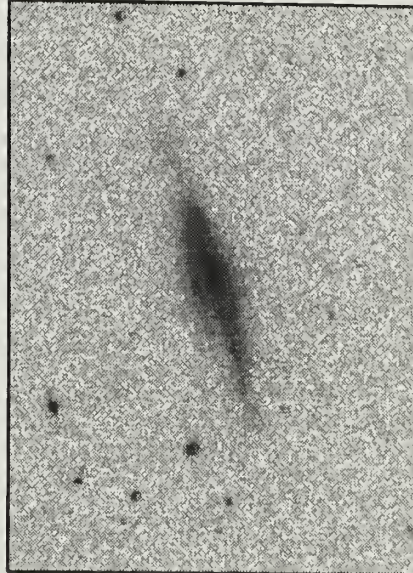
76: UGC 1950
6287 km/s
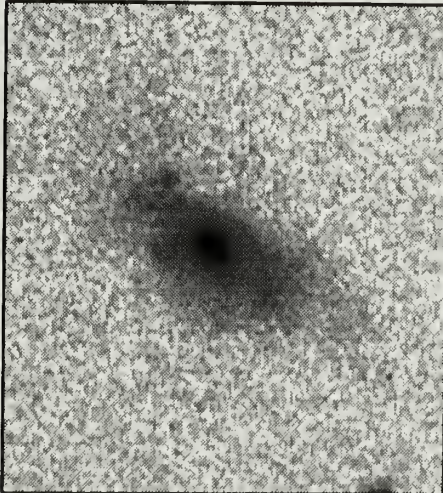
Figure 4.2. (cont.)

82: UGC 2079
5649 km/s
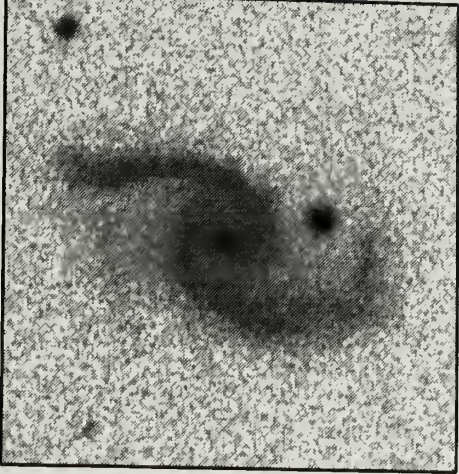
84: UGC 2104
8239 km/s
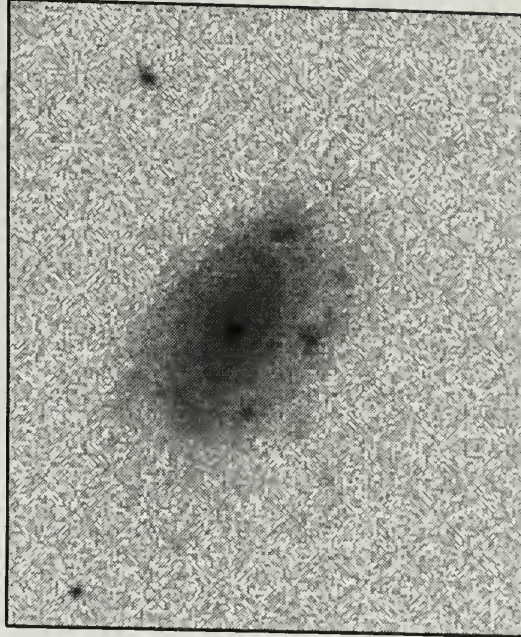
86: UGC 2248
6196 km/s
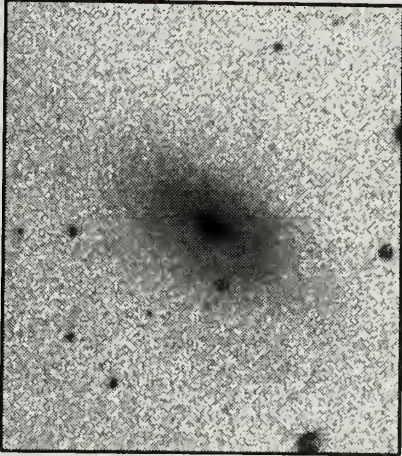
87: UGC 2267
6054 km/s

Figure 4.2. (cont.)

143
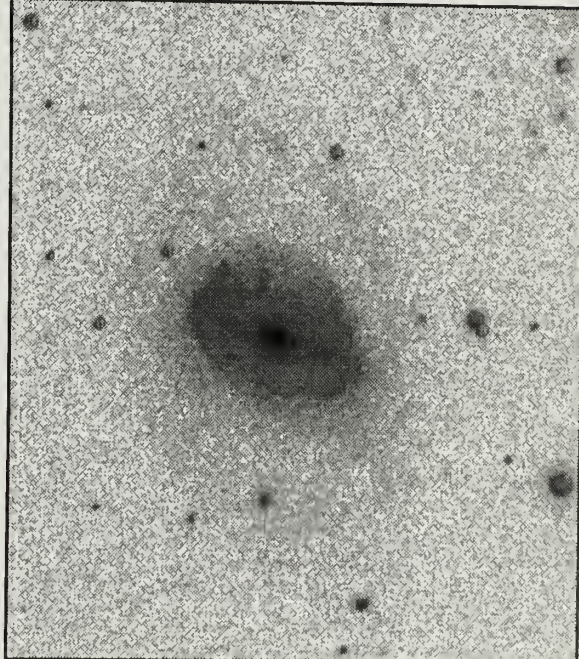
6: CGCG 475-028
7775 km/s
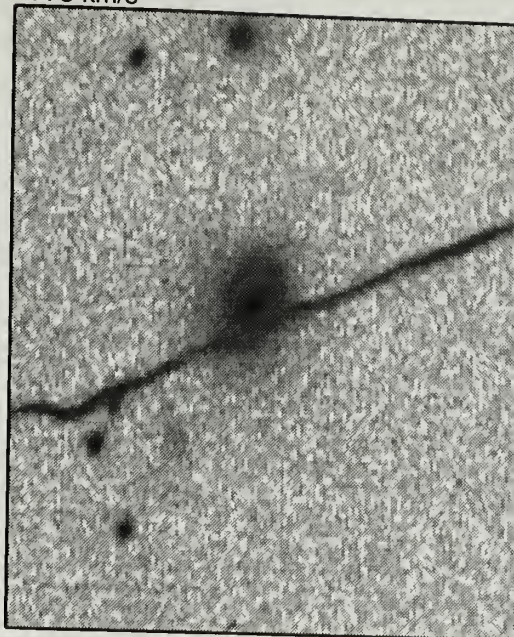
10: MRK 317
6122 km/s
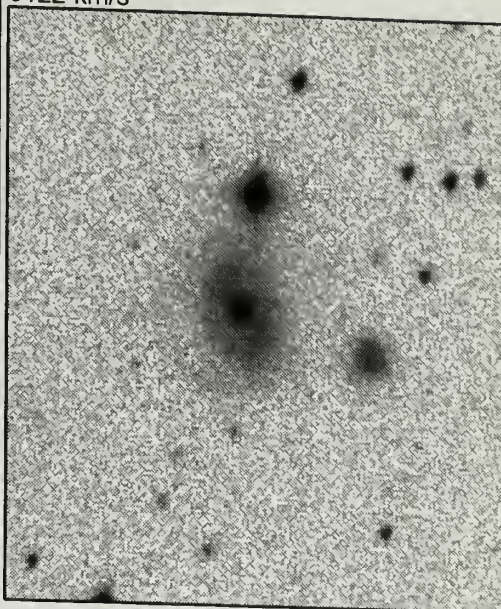
11: UGC 12443
6048 km/s
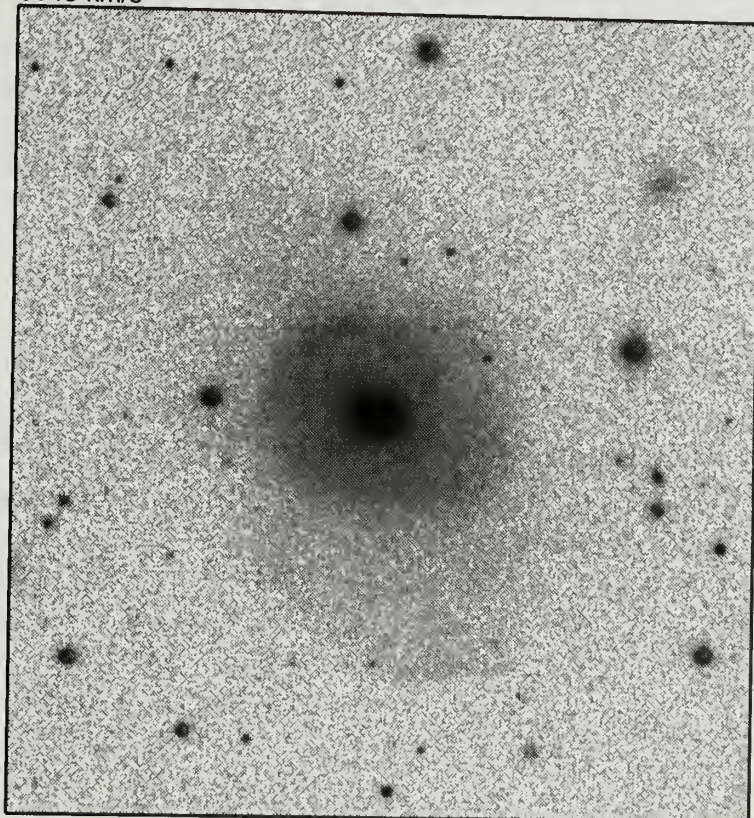
Figure 4.3. R-band images of the slice objects not detected in the
HI search. Images are scaled at 20,000 kpc/inch. Continued, next page.

144

12: UGC 12449
7935 km/s
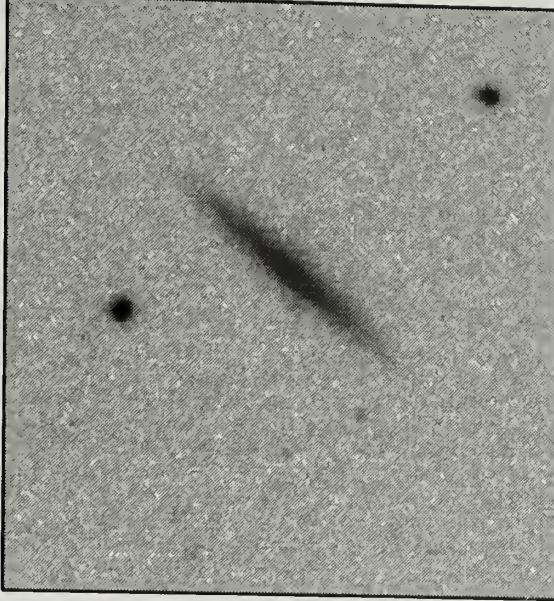
35: UGC 186
5829 km/s
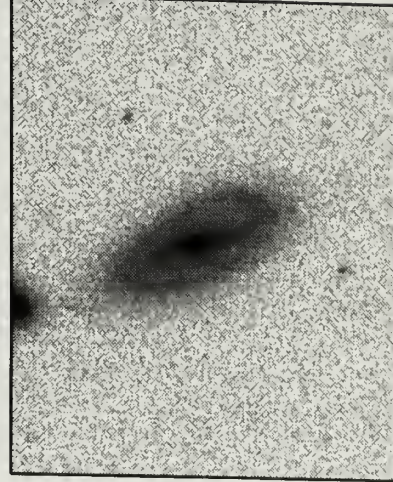
45: MRK 344
7566 km/s
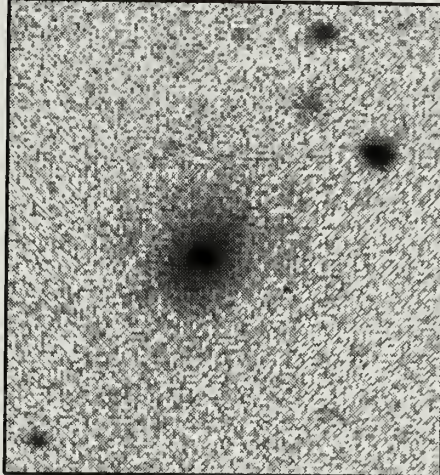
65: CGCG 482-050
4727 km/s
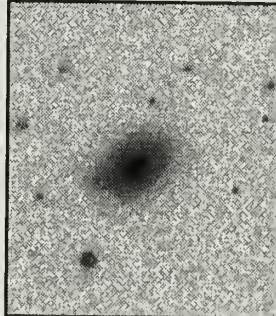
66: IC 190
4769 km/s
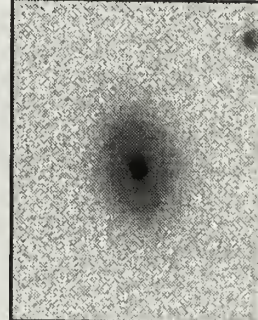
Figure 4.3. (cont.)

CHAPTER 5

RESULTS AND ANALYSIS

In this chapter, we present our analysis of the findings of the slice search. There are many ways in which the slice search data can be examined, and we by no means exhaust the possibilities. However, we make an effort to cover what we found to be the more intriguing topics.

One of the most interesting results of the slice search is the sheer number of new objects discovered by their atomic hydrogen emission. While we had high hopes of finding new galaxies when we undertook the search, our success rate was as high as what we most optimistically expected. Although the numbers have appeared several times in the text already, we once again present the final scoreboard:

1) Uncataloged objects detected by the slice search: 41

2) Cataloged objects detected by the slice search : 38

3) Cataloged objects the slice search failed to detect: 10

What do these numbers tell us? In all of our analysis, we treat the population of galaxies within slice search region as a statistical sample of the population of the Universe. This is the most scientifically useful way to look at the data. Interpreted "literally", the slice search is only a very thorough census of a fairly unremarkable wedge of space which reveals the existence of some interesting new objects, but little more. But as a model of the Universe, the slice becomes far more illustrative. The numbers and properties of the galaxies within it can be used to represent galaxies everywhere. Trends indicated in the slice data may be indicative of trends in the entire population of galaxies, and may be used to challenge or possibly change the way we think about overall galaxy properties. This approach is valid both because the slice search was designed to carefully and thoroughly search a region of space without bias toward particular galaxy types or properties, and because the detection rate was high enough to allow meaningful statistical arguments.

If the slice region can be treated as a statistical cross section of the Universe, then the search results - 40 new objects in a region previously known to contain 50 - imply that the list of cataloged galaxies under

counts the extragalactic population by at least half. On the surface this is not surprising, as any deep optical survey would find more objects in a region than those cataloged, and one would not have to go much deeper than the POSS plates to double the number. What we will see, however, is that we are finding objects that would probably not be detected optically except by a very much deeper optical survey. The slice data will show us that there exists a large population of galaxies in the Universe of which we have had no knowledge. That catalogs do not list all galaxies is certainly not a surprise, but the magnitude of their shortfall is considerable.

One of the primary missions of our analysis is to discover what properties these new objects exhibit that make them different from the objects we already know. This information is interesting for two reasons:

1. It will help us understand why these objects were not cataloged before, and why the atomic hydrogen search was so successful at detecting them.

2. It may alter our understanding of what a "normal" galaxy is, and subsequently our understanding of the structure and content of the Universe.

The chapter is organized into sections, each devoted to a particular analysis approach. These different sections are inter-dependent, as we note in them. The following analysis topics are included in the chapter:

- The positions of objects in space: We examine the locations of the objects detected in the slice search relative to each other and relative to the previously mapped large-scale structure in the region, with the purpose of answering two questions: Are the positions of the new and the cataloged objects correlated, anti-correlated, or entirely unrelated? Do the objects in the slice search describe the same large-scale structure as was previously thought to exist in the region?

- The shapes of the HI and dynamic mass functions: The slice observations produce a reasonably complete sample of the variety of galaxies contained within a specific region of space. This sample is used to examine the relative numbers of galaxies of different masses, and how they compare to findings of previous research.

- The dynamic mass as a function of distance: A small number of the slice objects are found to have very large dynamic masses. These objects also appear at very similar redshift velocities. The possible causes and meanings of this finding are investigated.

- The dynamic mass to HI mass ratio: The slice objects are examined in terms of the ratio of their dynamic mass (which is expected to represent total mass) and their atomic hydrogen mass. If this ratio is significantly different between the cataloged and uncataloged samples, then it may indicate why some objects were easy to detect optically, which others required 21cm observations to find them.

- The blue luminosity as a function of distance: The differences in intrinsic luminosities of the cataloged and uncataloged samples of objects are shown to be markedly different. This difference is a likely factor in determining whether objects are optically detectable or not.

- Mass to light ratios: We look at the ratios of both dynamic and atomic hydrogen masses to intrinsic blue luminosity for the slice objects. Differences in these ratios between uncataloged and cataloged object samples are examined.

- Slice object colors: The colors of the slice objects are used to determine their stellar populations, and what sorts of galaxies they may represent. Specifically, the uncataloged objects may be part of the "missing" population of blue dwarfs proposed by (Tyson).

- Surface brightness selection effects: We return to one of our original motivations in performing the slice search - the surface brightness selection plots presented in Chapter 1. Our new objects are plotted on these same figures to see if we are uncovering the new populations we expect.

The bulk of the analysis contained in this chapter is based on the observed and derived quantities of the slice objects as presented in the tables in the previous chapter.

Positions of the Slice Detections

In this section, we examine the physical positions of the objects within the slice search region. The analysis in this section has two primary aims. First of all, we wish to discover where the newly-detected slice objects are in relation to the cataloged objects. There are three possibilities - new objects could share the same approximate locations and structures as cataloged objects, new objects could be located where

cataloged objects weren't, or new objects could be located in a pattern seemingly unrelated to that of the cataloged objects. Each of these possibilities has potential implications. The second purpose is to compare the locations of all objects in the slice region to the structure of the surrounding region to see if they followed that structure, and to what degree.

The physical position of an object is defined by its RA, DEC, and distance. The redshift velocity can be converted to approximate distance using the Hubble Constant, although in our analysis we simply plot "distance" in terms of the redshift velocity. In this analysis, it is important to keep in mind that the conversion to distance from redshift is only perfectly accurate for galaxies which have no local velocities of their own relative to the systematic velocity of the Hubble Flow. We know that the local velocities of galaxies, which are randomly oriented relative to the Milky Way, can have magnitudes of up to several hundred km/s. Because we have no way of measuring these velocities, they introduce errors in the physical locations we arrive at. The size of these is not related to the magnitudes or redshift velocities. For very distant, high-redshift objects the errors are minor, but for nearby low-redshift objects the errors in the computed distances may be comparable to the distances themselves.

In Figure 5.1, we examine the positions of the slice objects. Uncataloged, newly-detected objects are plotted as triangles, cataloged HI-detected galaxies are drawn as crosses, and cataloged objects with no HI-detection are represented by stars. It is clear from the plot that a certain amount of structure in the positions of the objects exists. Galaxies appear to populate a number of linear regions, and are non-existent in a few fairly large areas. It is also clear from the plot that, with a few exceptions, the uncataloged objects closely follow the same structure as the cataloged objects. The most glaring exception is the gathering of uncataloged objects which exists at very low redshift velocities. As we shall see in a later section of this chapter, these objects are all very small and low-luminosity, difficult to detect at any great distance in HI, and even more difficult to detect optically at all. We will show that it is likely that objects similar to these exist in great numbers throughout the slice region, however they can only be detected nearby.

Figure 5.2 shows the same slice objects, but super-imposed on the distribution of RC3 objects in a slice 10 degrees thick in declination located between plus and minus five degrees of the slice search region (these objects, which are represented in gray, are the same plotted in Figure 2.2). We can see from Figure 5.2 that the previously cataloged RC3 objects have a fairly well-defined structure to their locations - they are not randomly distributed in space. It is also clear that the slice objects follow the same structure. In particular the regions between redshifts of 2000 and 6000 km/s appear to have very well organized structures in both the RC3 and the slice objects. In addition, the number of cataloged objects in the slice region (49) is basically consistent with the number of RC3 objects in the 10 degree-thick region (457 with redshifts between 100 and 8340 km/s), which represents roughly thirteen times the volume (the slice search covered a declination range from +22 58 30 to +23 43 00). Overall, the slice search is detecting new, uncataloged objects at a rate of roughly one for every one object the 10 degree-thick RC3 slice would predict in a similar volume (40 vs 34).

Below redshift velocities of 2000 km/s, the story is somewhat different. The slice region contains no cataloged galaxies at these low redshifts, but from Figure 5.2 the uncataloged objects detected there appear to have a distribution similar to the nearby RC3 objects. The RC3 contains 31 objects in the redshift range between 100 and 2000 km/s within the 10 degree-thick slice, representing roughly 7% of the total between 100 and 8340 km/s. It is interesting to note that while overall the slice search detects new objects at a rate of one for every cataloged object predicted by the thick RC3 slice, below 2000 km/s it finds 5 new objects compared to the 2 or 3 (31/13) the RC3 slice predicts. Naturally, such small numbers cannot be trusted too far, but the indication is that the slice search is detecting nearby objects at an even higher rate than it detects objects over the entire redshift range.

From the two figures, it would seem that we can conclude that the newly detected slice objects are located in the same places the cataloged objects were. The same structures, and the same voids between them appear in all of the object samples. It would also appear that low redshift velocity objects exist in higher numbers than we would be led to expect by the numbers of similarly-located galaxies in the catalogs. This point will become more important later on.

The Shapes of the HI-Mass and Dynamic Mass Functions

We have established that the slice search achieved reasonably complete and unbiased coverage of fairly typical volume of nearby extragalactic space. The sample of objects detected in the search can be trusted, to a greater accuracy than perhaps any other published sample, to be a good representation of a convolution of the number density of all extragalactic objects, and the sensitivity of the Arecibo telescope and our observing program to them. Thus, it is reasonable to believe that if we can de-convolve these two functions - remove the sensitivity of our system - a statistical representation of the true population of extragalactic objects should emerge.

What might this tell us? One severe deficiency in our knowledge of the extragalactic environment is the uncertainty in the number density of low mass, low luminosity extragalactic objects. For high mass, high luminosity galaxies, it is clear from observational evidence that the number density of such objects declines very sharply as a function of mass and luminosity. There are greater and greater numbers of objects detected as more modest masses and luminosities are studied. This trend continues down to the point where the techniques used to detect galaxies historically (large-scale plate surveys) are unable to find objects easily. It is not clear whether the number density continues to increase (and at what rate), decreases, or remains roughly the same for smaller and smaller objects. Because small galaxies are inherently under-luminous (and, as the slice results indicate, occasionally invisible), they are unquestionably under-represented in the optically-selected catalogs. Yet it is virtually impossible to accurately de-convolve the true number density of low mass objects from the high-mass/high-luminosity skewed sensitivity of the searches used to find the cataloged objects (although some have taken a stab at it -see for instance Tyson and Scalo, 1988, and Briggs and Rao, 1993), leading to huge uncertainties in the number counts of these objects.

The slice search, on the other hand, is not necessarily sensitive to the same types of objects as optical searches. Because it works within a well-defined volume of space and uses consistent and well understood methods of detection, its sensitivity to different types of objects is comparatively easy to quantify. In addition, compared to previous surveys at 21cm (Weinberg, et al., 1990, and others), it has generated

fairly high number statistics in a fairly large and hopefully representative volume. Perhaps it can make a contribution to this problem.

The distribution of the numbers of extragalactic objects is most commonly represented as a "luminosity function" - the number density as a function of total object luminosity. This tendency is a reflection of the optical bias inherent in almost all extragalactic studies. As objects were discovered by studying optical plates, their most obvious measurable quantity was their luminosity, so this became the most convenient way to bin them. While not incorrect in any way, interpreting the meaning of the shape of the luminosity function in the light of the complex optical sensitivity is difficult (Tyson and Scalo, 1988). Generating an accurate luminosity function of galaxies from HI data as we would have to do with the slice results has some additional difficulties. If 21cm information is all which is available, then general (and possibly catalog-biased) rules must be applied to translate HI fluxes to luminosities. Also, in the case of a 21cm search which is meant to be blind to optical emission, considering the luminosity function of galaxies seems a bit out of place. For this reason, rather than studying a luminosity function, we examine first the "HI mass function" - the distribution of extragalactic objects as a function of HI mass. While the HI mass does not represent the entire mass of galaxies (often it amounts to less than 10% of the total), it has an importance similar to luminosity (blue luminosity is also about 10% of dynamical mass when both quantities are measured in solar units), and is the most accurately measured mass quantity which we can derive from the slice data.

Previous studies have looked at the HI mass function. Shostak (1977), using emission and absorption observations (see Chapter 2) to search for unseen HI dwarfs derived upper limits to the space density of unseen objects, and compared these to known optical sources. Shostak's upper limits allow for great numbers of invisible galaxies, with space densities of objects rising by roughly an order of magnitude for each drop of an order of magnitude in object mass, but his survey did not actually find any of these objects. Briggs (1990) proposed a flatter HI mass function, where the space density of low-mass objects was little higher than that of high-mass objects. This same paper contained a translation to HI mass of the model luminosity function derived by Tyson and Scalo (1988) to account for optical selection effects. This

was accomplished by using an intermediate value for the HI surface density of galaxies. Interestingly, this Tyson and Scalo-inspired HI mass function increased rapidly for galaxies with masses less than $10^{6.5}$ M$_\odot$, enough such that these objects would constitute a larger fraction of all of the HI mass than all of the more massive galaxies. Weinberg, et al. (1991) also derived an HI mass function based on the detections in their HI search which showed fairly modest rises in the space density of low-mass galaxies.

In Figure 5.3, we present a histogram showing the HI mass function of all of the objects known in the slice search volume. The objects are divided into three categories: previously cataloged galaxies detected in the slice search (gray histogram bars); galaxies newly discovered by the slice search (unshaded bars); and galaxies which were not detected in the slice search in HI (black bars). HI flux measurements for the objects which were not detected have been obtained either from long integration observations by the authors or from the literature (see previous chapter). The HI mass is given in units of M$_\odot$, and is plotted on a $\log_{10}$ scale to accommodate the extremely wide range of values (3.5 orders of magnitude). The HI mass function in Figure 5.3 peaks between 10^9 and 10^{10} M$_\odot$, and shows a sharp decline in the number of objects with masses above 10^{10} M$_\odot$. HI masses decline less rapidly below 10^9 M$_\odot$, and may level off to some degree at very low masses. Each of the three categories of objects shows a peaked distribution which declines at low and high masses, although these distributions have narrower ranges and different peaks. The previously cataloged objects represent the bulk of the most HI massive galaxies, with an average log of the HI mass of 9.69, and only one of them has an HI mass less than 10^9 M$_\odot$. The cataloged galaxies which were not detected have lower HI masses, averaging 8.81 in the log. The newly discovered galaxies have an average HI mass of 9.03 in the log, higher than the non-detected objects. Yet some of the newly discovered galaxies are extremely non-massive, with two objects (B0230A-14 and K0248C-02) having HI masses near 10^7 M$_\odot$.

Figure 5.4 shows a similar histogram of the distribution of the log of dynamic mass among the same three categories of objects (the "dynamic mass function"). The computation of dynamic mass is based on optical sizes, HI velocity widths, and inclination measurements, all of which are less accurately known than the HI flux and redshift velocity values used to compute the HI masses of objects (the previous

chapter details how both of the quantities are derived). Thus the dynamic mass is a less well-known quantity than the HI mass, yet it represents a more complete measurement of the "true" mass of a galaxy. Two of the uncataloged slice objects - B0230A-14 and K0248C-02 - have no optical because they were not detected optically. The dynamical masses computed for these two objects are based on estimates of their sizes and upper limits on their optical properties. Comparing Figures 5.3 and 5.4 reveals some important distinctions:

- We notice that the mean values for all objects are higher for dynamic mass than HI mass. For cataloged objects, this difference is about an order of magnitude (1.14 in the log), for the undetected cataloged objects it is slightly higher (1.91 in the log) and for the newly discovered objects is somewhat smaller (.70 in the log). The ratio of dynamic mass to HI mass of 10 to 1 for the cataloged galaxies agrees well with the accepted value for the ratio for normal spiral galaxies (*reference*). For the undetected galaxies this ratio ranges between 10 to 1 and 100 to 1, a result not unexpected for these HI-deficient objects.

- The overall dispersion in dynamic masses is higher than that for HI masses by an order of magnitude (in fact, it may be higher still, as the two "invisible" slice detections which could not be included on the dynamic mass plot because they lacked optical data are the same objects, B0230A-14 and K0248C-02, which have the lowest HI masses). This higher dispersion is to be expected with the greater uncertainties in the dynamic mass calculations.

- The cataloged objects detected in the slice have dynamic masses very similar to the cataloged objects not detected in the slice (mean values of 10.83 and 10.72 in the log respectively), while they have very different HI masses (9.69 and 8.81 respectively).

- It is apparent that the newly discovered objects have on average much lower dynamic masses, differing in the mean from the cataloged objects by over an order of magnitude. Yet these numbers must be called into question, because the optical sizes and inclinations of the newly discovered objects are more uncertain, and may under-estimate the dynamic mass.

Analysis of the HI and dynamic mass functions may now proceed along a number of different paths.

Detection Rates for Optical and HI Surveys

We can use the histograms to begin to understand what sorts of objects our HI search is detecting. When these objects differ from those detected in optical surveys, we want to know how they are different, what new populations they represent, and what their relative importance is in the grand scheme of the Universe. Any search for extragalactic objects is going to be sensitive to a subset of the total population of objects in its search volume, objects which exhibit particular emission characteristics, some intrinsic, some due to position, orientation, or distance. Different types of searches will have different, and sometimes overlapping subsets of objects which they are sensitive to. Searches will not be sensitive to the same types of objects over the entire volume of space - small objects with weak emission characteristics, for instance, may only be detected if they are nearby, in a fraction of the overall search volume.

We can use Figures 5.3 and 5.4 to begin to understand what qualities in a galaxy allow it to be found or to escape detection in a particular type of survey (HI or optical). If we assume that the optical luminosity of a galaxy is what determines its detectability in optical surveys, and its likelihood of inclusion in optical catalogs (which seems a very reasonable thing to assume), we can conclude from the histogram in Figures 5.4 that the optical luminosity of galaxies is linked to its dynamic (or "true") mass. The cataloged (optically detected) objects dominate the high-mass end of the histogram, implying that high dynamic mass leads to a high probability of optical detection. The low-mass objects in the histogram were all detected by the HI search, but escaped detection in optical surveys. This is not an unexpected result - we would anticipate that the most massive galaxies are the ones which form the most stars, and are the brightest, leading to a higher likelihood of detection in optical surveys. It is interesting to note that the cataloged galaxies detected in the slice search have effectively the same mean dynamic mass as the undetected galaxies, re-enforcing the idea that it is dynamic mass that leads to high luminosity and optical detection.

The situation gets a little more interesting when we examine the HI mass of the three samples. The cataloged objects are not only massive overall, they also have a fair amount of HI mass. In Figure 5.3, it can be seen that the cataloged objects once again dominate the high-mass end of the histogram. This is

even true for the cataloged objects not detected in the slice search. While the undetected objects have distinctly lower HI masses than the detected objects (which is to be expected, since they weren't detected in the HI survey!), they are not by any means the least massive objects in HI. Both histograms show clearly that the least massive objects both in HI and dynamic mass are those detected first with the slice search. The implication of this analysis is that optical catalogs only contain the most massive objects, and greatly under-represent small galaxies If optical luminosity is indeed well-correlated with dynamic mass, then we would expect just this result.

The discovery of large numbers of low-mass objects could greatly alter our understanding of the content of the Universe, particularly if, as we have found, optical catalogs tend not to include them. Figures 5.3 and 5.4 do not show the slice search detecting these small objects in great numbers - in both cases the number of detections declines rather rapidly for low-mass objects. Yet the histograms as presented do not tell the whole story. Because low-mass objects are harder to detect, the slice search is sensitive to them in only the small portion of its search volume which is nearby. We can see clear evidence that the slice search is detecting some very low mass objects at only nearby distances by looking at figures 5.5 and 5.6, which plot the $\log_{10}$ of HI and dynamic mass of each object against distance. In both plots, there is a definite trend toward detecting smaller galaxies at shorter distances. There is also a clear lack of detections of larger objects at these same shorter distances. This is simply because their number densities are small enough that they are statistically unlikely to be found in the tiny search volume being scanned by the slice search at these distances. The detection of the smaller objects in these volumes demonstrates that, contrary to what the histograms in Figures 5.3 and 5.4 imply, the number densities of these small objects is high in comparison to that of massive galaxies.

To examine the true relative number densities of different-sized objects, we must de-convolve the HI mass and dynamic mass functions from the "sensitivity function", which describes the ability of the slice search to detect galaxies as a function of their HI mass. If one considers the entire volume of a search, the sensitivity function tells us the fraction of that volume in which objects having different characteristics could be detected. De-convolving the sensitivity function from detection rates is accomplished by

"adjusting" counts of objects by the inverse of the fraction of the total search volume in which they could be detected. For instance, if a search detects a single galaxy which has very strong emission characteristics, and the sensitivity function of the search shows that it would have detected the object at any point within its search volume, then the measured "true" number density of similar objects would be (1 object)/(entire search volume). On the other hand, if the search detects one weakly emitting object, and the sensitivity function shows that the search can only detect such objects over a tenth of its volume, then the measured "true" number density of those objects would be (1 object)/(entire search volume/10). Without including the sensitivity function of a search, raw measured number density counts will under-represent the small, weakly-emitting objects which cannot be detected over the entire search volume.

For an optical survey, determining the sensitivity function would be extremely difficult. Trying to determine one which could be applied to the collected library of optically detected galaxies is virtually impossible. The primary difficulty in doing so is that optical searches do not have a well-defined search volume. An optical search is sensitive to a particular range of surface brightnesses and angular sizes (see chapter 1), which to some extent can be quantified. Yet an optical search, either of a plate or a CCD image, of necessity must discard distance information - all objects appear on a two dimensional projection of three dimensional space. Distances to detected objects must either be measured by other means (time consuming) or inferred (dangerous). Unless the distances are found, it is impossible to decide what volume of space a search is scanning for each type of object. In addition, objects of radically different sizes may be assumed to have very similar characteristics if their mutual distances conspire so as to make them appear similar on a plate, leading to number density counting errors. All of these problems are compounded when considering all previous optical searches, and added to them are the difficulties of combining different sensitivities for different searches, and determining sensitivities for old and poorly documented searches.

In contrast, the sensitivity function of a 21cm search like the slice project is very easy to determine. Because 21cm observations scan well defined redshift velocity ranges, we can easily determine the maximum distance searched (assuming the translation of redshift velocity to distance can be trusted, an

assumption we *must* make). From this, it is a minor exercise to find the total volume of space searched. The next step in determining a sensitivity function is finding the fraction of this total volume within which the search is sensitive to objects possessing different values of the quantity being measured - in this case, HI mass.

Computing an HI Sensitivity Function

Detecting an HI signal in a spectrum, either by eye or using software, is in the simplest interpretation just a matter of recognizing it as not belonging to the background noise in the spectrum. In reality, the job is made more complex by the presence of interference spikes masquerading as extragalactic sources and untidy baselines (see Chapter 3), but because we have re-observed all potential sources, we can ignore the complications. In general, for the signal profile of an object to be recognized reliably, it must be higher than five times the background noise level (σ), where σ is a measure of the rms noise for a feature of comparable width to the signal. The height of a galaxy profile in a spectrum is determined by two things, the total integrated flux of the object ($\int S dv$, measured in Jy km/s), and its velocity width (Δv, measured in km/s). To define this "5σ detection limit" for the slice search, we use the single channel *rms* noise level obtained after Hanning smoothing to velocity channel widths of 16 km/s (see Chapter 3):

$$\sigma_{16 km/s} = 2 mJy \tag{5.1}$$

The total profile width in channels (W) can be estimated using the velocity width at the 20% peak flux level for each object:

$$W = \left[\left(\Delta v_{20\%}/16 km \cdot s^{-1}\right) + 1\right]. \tag{5.2}$$

After smoothing the spectrum to the profile width, the noise is reduced by a factor of $\sqrt{W}$. The 5σ uncertainty in the integrated flux is then:

$$
\begin{aligned}
5\sigma \text{ limit } &= 5 \times \frac{\sigma_{16 km/s}}{\sqrt{W}}\left(W \times 16 km \cdot s^{-1}\right) \\
&= 0.16 \text{ Jy} \cdot km \cdot s^{-1} \times \sqrt{W}
\end{aligned}
\tag{5.3}
$$

From the width $\Delta v_{20\%}$ of an object, we can compute W, and then compare its flux (in Jy km s^{-1}) to that of the 5σ limit. If it has a higher flux than this limit, it should be detectable in the slice search. If it has a lower limit, it should not be detectable.

We can examine the accuracy of the 5σ limit by plotting the measured values for flux ($\int$Sdv) and velocity width ($\Delta v_{20\%}$) of all of the objects involved in the slice search. In Figure 5.7 we plot these values, along with a line representing the 5σ limit defined by the above equation. The crosses in Figure 5.7 represent cataloged objects detected in the slice search, the triangles are objects newly discovered by the slice search, and the stars represent the objects the search failed to detect. Note that all of the undetected objects fall below the 5σ limit line, while all but two of the detected objects fall above it. A clearer picture of the quality of this dividing line can be seen in Figure 5.8, where we plot a histogram of the fluxes of each object divided by the flux required to meet the 5σ limit based on each object's velocity width. In this figure it is obvious that the 5σ limit does a good job of dividing the objects in the slice volume into those which were detected and those which were not.

The two HI-detected objects which do fall below the 5σ limit line are worth looking at. One of them, N0042A-05, is actually a double object. It is likely that it was only discovered in the HI search because of a second, stronger-emitting companion in the same Arecibo beam. In any case, it is very close to the cutoff, and may have been detectable on its own. The second object is A0154A-15, which is a weak HI detection. The flux values from the original slice observations did not agree well with the follow-up hex fluxes for this object, and it is possible that this very marginal detection was a fortuitous coincidence of noise adding in the right spot. It is also possible that we may be able to detect signals lower than 5σ if their signals are narrow.

We know that the flux received from a source is proportional to the inverse square of its distance from us. If we know its distance from us, then we can compute a "distance limit" (D_L) for the object - the distance at which it would have the 5σ limiting flux (which I will now call F_L). This would be the maximum distance at which we could detect this object. The distance limit for an object with measured flux F and distance D would be:

$$D_L = D \cdot \sqrt{\frac{F}{F_L}} \qquad\qquad (5.4)$$

We can compute F_L for a source if we know its velocity width Δv. For the objects in the slice search, we have all of this information.

From the distance limit we can find the volume V_L in which the slice search was sensitive to a particular object. This volume can be expressed as a fraction of the total slice search volume (V_{MAX}). It is proportional to the cube of the distance limit D_L, unless the distance limit is higher than the maximum distance D_{MAX} of the slice search, in which case it will be the entire volume of the slice search :

$$\text{If } D_L > D_{MAX} : \quad V_L = V_{MAX}$$

$$\text{If } D_L < D_{MAX} : \quad V_L = \left(\frac{D_L}{D_{MAX}}\right)^3 \cdot V_{MAX} \qquad\qquad (5.5)$$

These "sensitivity volumes" can then be used to adjust the counts of each object to account for the volume in which each could have been detected by the slice search. For instance, if an object was detected by the slice search, and we found through the above process that $V_L = V_{MAX}/2$, we could say that the one detection in half the search volume implied approximately two objects within the entire search volume. Only by adjusting the counts of each object in this way can reasonable comparisons be made between the number densities of different objects.

Adjusting the HI and Dynamic Mass Functions

We can adjust our HI and dynamic mass functions using the sensitivity function to produce new histograms showing the "true" numbers of different-sized objects contained within the slice search. To begin this process, we produce new versions of Figures 5.3 and 5.4 in Figures 5.9 and 5.10. In these histograms, we have dispensed distinguishing between "cataloged", "cataloged undetected", and "newly discovered" objects, and have lumped the entire slice contents together. We have also plotted the histograms on a logarithmic scale, and have added error bars. The error bars extend to plus or minus $\sqrt{n}$, where n is the number of objects in each histogram bar. This has produced an odd result in the case

of the histogram bars which contained only one object. These bars have non-sensible lower limits to the error bars (as $1 - \sqrt{1} = 0$, and $\log(0)$ cannot be plotted). In these cases, we have dispensed with the lower limits to the error bars, with the understanding that they do extend to zero.

It is clear from the error bars in both Figures 5.9 and 5.10 that anything we can say about the low-mass ends of the mass functions is going to be very uncertain. This is inevitable, as we are dealing with very few detections (one or two detections in each histogram bar), and thus very poor statistics. Unfortunately, this is one of the regions of the mass function which we are most interested in.

In Figures 5.11 and 5.12, we have plotted new histograms of the HI and dynamic mass functions (once again on a log scale) where we have adjusted the count of each object using the process described above. The shaded histograms represent the unadjusted mass functions (the same as those plotted in Figures 5.9 and 5.10), and the unshaded histograms represent the adjusted mass functions. To produce the adjusted histograms, we have used the known HI flux, velocity width, and distance to each object found in the slice search to compute the fraction of the total search volume in which the object could have been detected. We have then assumed that the detection of the object "implied" the existence of a number of similar objects in the slice volume equal to the inverse of this fraction. The adjusted histograms plot the distribution of objects whose existence is implied in this way. In the case of high-mass objects (typically > $10^9 M_\odot$) which were detectable throughout all of the slice search volume, no adjustment is necessary. However, in the case of the low-mass objects, the adjustment is very large, with single detections implying the existence of thousands or tens of thousands of similar objects.

The histogram of the adjusted HI mass function in Figure 5.11 shows a dramatic increase in the number of objects at the low-mass end of the function. This increase at the extreme low end is of more than a factor of ten over the lowest order of magnitude in mass. This result implies that the increase in the number density of these small objects may be greater than the decrease in their mass, which would mean that their integrated mass was larger than that of higher mass objects. Figure 5.13 shows the log of the integrated mass of each histogram bar in Figure 5.11. In the figure, shaded histogram bars represent the integrated mass of the observed objects. The unshaded bars represent the integrated mass of implied

and observed objects, which are found using the same arguments used to produce Figure 5.11. In Figure 5.13, there is a peak in the contribution of different-mass objects to the total mass integral at HI masses in the range of 10^9 to $10^{9.5}$ M$_\odot$. Collectively, the mass contribution of galaxies declines as their HI mass declines, down to mass in the range of 10^8 to $10^{8.5}$ M$_\odot$. However, at this point there is a turn-around, and an increase in the contribution from HI masses of $10^{8.0}$ down to $10^{7.0}$ M$_\odot$.

However, we know that HI mass makes up only a fraction of the total mass in most galaxies. The dynamic mass may be a more accurate measure of the "true" mass of galaxies. The histogram of the dynamic mass function in Figure 5.12 shows a sharp increase in the number of low-mass objects. In looking at this figure, it is important to remember that we are dealing with an HI-selected sample. Many of the low-mass objects have very low optical luminosities, and the measurements of their optical sizes are probably under-estimates. The dynamic mass calculated for an object is proportional to the optical diameter (see Chapter 4), so we can expect that the dynamic masses we have computed for these low-mass, low-luminosity objects are too low.

Figure 5.14 shows the integrated mass of each histogram bar in Figure 5.12 to show the contribution of galaxies of different masses to the total mass integral. As in Figure 5.13, we see a peak in the contribution of galaxies with dynamic masses near 10^{11} to 10^{12} M$_\odot$. The contribution declines for lower and lower mass objects, until at the extreme low-mass end we observe a turn-around, similar to that seen in Figure 5.13.

These results could indicate something very important. Recent observational evidence has implied that the curve of the number density of small galaxies flattens, or even declines, at lower masses. Because the galaxies at the lower end of the mass function are so small, if their numbers are not significantly higher than those of the high-mass galaxies, they will not contribute significantly to the total mass integral. Thus the mass in the Universe would be dominated by the large, bright galaxies we can see (and in a few odd cases by very massive objects we cannot see), and the low-mass objects are comparatively unimportant. Yet the our result implies that the low-mass galaxies may yet amount to something. We recall from Figures 5.3 and 5.4 that the low mass end of both the HI and dynamic mass functions are

occupied by objects first detected in the slice search. Objects which are smaller still are not detectable by the slice search, but if the trend seen in Figures 5.13 and 5.14 extended to these smaller masses, then their numbers would be sufficient to contribute an even greater fraction of the mass integral. If this were the case, then it would be possible for the mass integral of all of the objects in the slice search volume to be dominated by small galaxies which have never been detected optically. The new objects detected by the slice search are insufficient to make any such claim, however.

It is important to remember through the whole of this analysis that our statistics are, in a word, weak. The interpretation that low-mass galaxies might be numerous enough to contribute significantly to the integrated mass of all galaxies is based on only a handful of objects. The error bars on our histograms at the low-mass end are large, and can accommodate both this interpretation, and a totally insignificant number of small galaxies. We present the interpretation only as an intriguing possibility. The slice search findings do not provide us with a large enough sample of objects to say much more than this.

Complications in the Interpretation of the HI Mass Function

The above discussion depends heavily on the accurate calculation of the masses of the smallest objects detected in the slice search. In the low-mass extremes of our adjusted HI and dynamic mass functions, we are using the detections of only a handful of tiny objects as evidence for the existence of tens of thousands of objects in the slice volume with a collective mass comparable to that of all of the largest galaxies. Yet it is possible that the masses calculated for these objects are the most uncertain. There are a number of reasons why these calculations are not good. The dynamic mass calculations depend on the measurements of optical sizes, and these are highly uncertain for the least massive objects which all are barely discernible optically. Much more important is the problem that both HI and dynamic mass calculations depend on measurements of the distances to these objects, and distances are found using the redshift of the HI signal.

What about the redshift is specifically inaccurate for low-mass objects? All of the low-mass objects we have found are at low redshifts - around 1000 km/s or less. We know that the random motions of galaxies in the neighborhood of the Milky Way can be of the order of hundreds of km/s. These random

velocities represent an uncertainty in the redshift. For high-redshift objects, uncertainties of a few hundred km/s are small compared with the redshifts of the objects due to the Hubble flow. However, for the small, nearby objects, the uncertainty begins to become a large percentage of the Hubble redshift.

The problem could be worse than this though. We consider a population of objects with very low redshift velocities - around 500 km/s. Objects whose own velocities were oriented away from the Milky Way would have measured redshifts higher than their true redshift. Objects with random velocities oriented toward the Milky Way would have measured redshifts lower than their true redshifts. In both cases, the distances to these objects would be inaccurate - the object with higher redshift would be assumed to be farther away than it was, leading to an over-estimate of its mass, and the object with the lower redshift would be assumed to be closer than it actually was, leading to an under-estimate of its mass. However, it is far more likely that the object with the lower velocity would either be lost in the confusion due to the HI signal of the Milky Way and not detected, or would perhaps be dismissed as a high-velocity cloud if it were. This would cause the slice search to preferentially sample objects with measured redshifts higher than their true redshifts, at least in the realm of low-mass, nearby objects. This would lead to an over-estimate of the masses of these objects as a group. It is not clear how serious this problem might be.

On the other hand, the same difficulty would lead to an under-count of the numbers of these objects. Consider once again a sample of low-mass objects with randomly oriented velocities relative to the Hubble flow. We would fail to detect some of the objects with non-Hubble flow velocities toward the Milky Way if these velocities were high enough such that their measured velocities would be negative or low enough to cause confusion with the HI in the Galaxy.

In a final thought on the subject, we should consider the possibility that we are over-counting nearby low mass objects because we are observing from inside the Local Supercluster, a region which might be expected to contain a high density of such objects. All of these difficulties must be taken into account when interpreting the histograms in Figures 5.13 and 5.14, where very small numbers of objects imply large results.

Counting More Massive Galaxies

We can use a different approach to estimate the number of high-mass galaxies which have not yet been observed in the slice region We can consider the slice as having been scanned by two independent searches - the atomic hydrogen slice search, and an optical search which is the summation of all optical galaxy surveys. The objects detected in the slice region represent a subset of the total slice population which is the convolution of the sensitivity functions of the search techniques used and the properties of the objects themselves. We know that neither search, optical or atomic hydrogen, is detecting all of the objects in the region, as they each are sensitive to objects that the other is not. We can surmise that there are objects in the region which neither search is detecting, and which remain to be found by some other technique. But do we have any idea how many there might be?

To make a first guess at the number of unseen objects, we must make what is probably a very bad assumption. That is that the properties which determine the detectability of a galaxy in an optical survey (surface brightness, angular size, whatever) are not related to the properties which determine its detectability in an atomic hydrogen search. In truth, we know this is not the case. Clearly to some degree these properties are correlated - we know for instance that very big, optically bright spiral galaxies which are easily seen optically are also easily detected in atomic hydrogen.

Secondly, we must eliminate any flux-limited basis to the numbers of objects we are detecting with either search. This eliminates all consideration of low-mass objects, which are only detectable to short distances. Objects with dynamical masses above $10^{10} M_\odot$ were detected by both searches out to their survey limits. Therefore we can assume that objects with masses greater than or equal to this to be detectable throughout the slice region by both searches.

We define three constants:

N_H - the number of objects with $Md > 10^{10} M_\odot$ detected in the atomic hydrogen search (51).

N_O - the number of objects with $Md > 10^{10} M_\odot$ detected in the optical search (37).

N_B - the number of objects with $Md > 10^{10} M_\odot$ detected in both searches (33).

And three unknowns:

N_T - the total number of objects with Md>10^{10}M⊙ in the region searched.

f_H - the fraction of this total which can be detected by an atomic hydrogen search.

f_O - the fraction of the total which can be detected by an optical search.

We know:

$$N_H = f_H \cdot N_T$$
$$N_O = f_O \cdot N_T \tag{5.6}$$

If we can make the assumption that the detectabilities of galaxies with Md>10^{10}M⊙ by the two search methods are uncorrelated:

$$N_B = f_H \cdot f_O \cdot N_T \tag{5.7}$$

We can then solve for the unknown N_T:

$$N_T = \frac{N_H \cdot N_O}{N_B} = \frac{(51) \cdot (37)}{(33)} \cong 60 \tag{5.8}$$

We can briefly examine what effect our "bad" assumption has on this analysis. If the properties which determine the two fractions f_H and f_O are correlated to some degree, this would lead to an over-count of the value of N_B. From the above equation, it can be seen that a larger-than-correct value for N_B would lead to a lower-than-correct value for N_T. The value for N_T, 60, can be considered an lower limit to the number of objects within the slice search region.

Another Look at Dynamic Mass - Where are the Biggest Galaxies?

We can see from Figure 5.4 that the most massive galaxies in the slice search region are the previously cataloged objects. We may also examine *where* these massive objects are located. In Figure 5.6, we plot the log of the dynamic mass of each of the slice objects against its redshift velocity. From the figure, it is clear that the objects with the lowest masses in the slice sample are located at nearby low redshift velocities. As we discussed in the previous section, this is not representative of the true distribution of these low-mass objects. In reality what it shows us where they can be detected. Galaxies with such low masses not only cannot generate enough luminosity to be detected optically, but also do not have enough atomic hydrogen mass to be detected by the HI search except at very short distances.

Figure 5.6 also shows us the clear difference between the typical dynamic masses of the cataloged and the uncataloged objects. While there is some mixing in the neighborhood of $M_d=10^{10\text{-}11}M_\odot$, there are no uncataloged objects with masses greater than $M_d=10^{11}M_\odot$, but 13 cataloged objects, and below $M_d=10^{10}M_\odot$, there are 20 uncataloged objects and only three cataloged objects. Quite clearly, large dynamic masses in galaxies is in some way related to optical detectability. This could be only a matter of bulk - larger objects have more of everything, including mass and luminosity. Massive galaxies would almost certainly generate more stars, and thus more optical luminosity, than small ones. Not only do they have a greater pool of material from which to draw to fuel for stars, but the more vigorous dynamic processes required to support them would lead to more of the waves and shock fronts which are thought to trigger star formation.

The dynamic masses in Figure 5.6 are plotted on a log scale because they range over four orders of magnitude. An interesting result becomes clear, however, when we plot the dynamic masses on a linear scale, as we have done in Figure 5.15. As we might expect, the bulk of the galaxies in the slice sample cluster at the bottom of the plot, and little information can be gleaned from their distribution. However, there are six unusually massive objects (all cataloged), which stand out above the crowd. What is more, these objects are all in a narrow range of redshifts - all within 750 km/s of a redshift of 5250 km/s.

We must ask ourselves what it is about these redshifts which leads to the formation of such massive galaxies. If we return to Figure 5.2, we see that the velocity range in which these massive galaxies exist, 4500 - 6000 km/s, is also the velocity range where the structure of the galaxies in the slice is most clearly organized. Galaxies in the region are tightly clustered around several "threads" in which all six of the most massive objects are located (the objects are, 13: UGC 12533, 21: UGC 12655, 29: UGC 12915, 43: UGC 356, 44: UGC 169/169A, and 81: UGC 2059). We know that this velocity range in the slice region contains part of the Pisces-Perseus supercluster complex, the largest structures in the vicinity of the slice search. The centers of large galaxy clusters are thought to be sites of galaxy mergers. These super-massive galaxies may be the results of such "cannibalism". In fact, examination of the optical images of these objects shows two of them (29 and 44) to actually be pairs of closely-interacting galaxies. However,

a clear interaction with another object brings up a different explanation for the high dynamic mass measurements. The HI measurements which produced the velocity widths of these objects were unable to distinguish between the two members of the interacting pairs. The velocity width measurement would then be artificially high if the two members had different systemic velocities (which is very likely). An artificially high velocity width or an underestimated inclination angle would lead to an over-estimate in the dynamic mass of the system.

The images of UGC 12533 (13) are of very poor quality, due to a bright foreground star in the CCD field, so little can be learned from visual examination of this object. It appears to be a fairly normal edge-on spiral galaxy with no obvious companions. The other three galaxies (21, 43, and 81) are quite similar optically. Despite their enormous dynamic masses, none appear particularly large (remember the optical images are scaled so galaxies have the correct physical size relative to each other) compared with galaxies with much more modest masses. All have large, bright nuclei, and fairly amorphous, undeveloped halos lacking much obvious spiral structure (to a fan of interesting galaxy structure, they are "spectacular in their dullness"). The most massive object detected in the slice search - UGC 2059 (object 81) has no spiral arms, but does exhibit an odd, tortured structure to its halo, possibly as a result of a recent encounter.

HI Mass vs Dynamic Mass

Another way we can examine the slice objects is by comparing their dynamic and hydrogen masses. In a typical spiral galaxy, we would expect the hydrogen mass to represent about 1/10th of the total mass of the galaxy. In Figure 5.16, we plot the dynamic and hydrogen masses of all of the objects in the slice search. The objects on the plot are divided by type - triangles for uncataloged objects, crosses for cataloged objects, and stars for objects with no HI detection (HI measurements for these galaxies are from long-integration follow-up atomic hydrogen observations). Included on the plots are dashed lines representing ratios of hydrogen mass to dynamical mass. In addition, Figure 5.17 shows a histogram of the dynamic to hydrogen mass ratios with uncataloged objects in white, cataloged objects in gray, and objects with no HI detection in black.

As expected, the bulk of cataloged galaxies cluster around an HI to dynamic mass ratio of 1/10, with a mean value of -1.15 in the log. There are a few outliers on both the high and the low ratio side. These out-lying values could represent the true mass ratios in these galaxies, or they could be the result of other factors, mostly due to uncertainties in the dynamic mass measurements. For instance, a spiral galaxy could yield a low dynamic mass measurement and thus an anomalously high ratio if it were oriented near to face-on, because then we would not measure the true orbital velocity of the material in the disk, but rather the lower magnitude random velocities perpendicular to the disk. Our dynamic mass calculations are inclination corrected, so this would only be a problem in galaxies which are oriented face-on (or so close that our measurements of major and minor axis were identical), where no inclination correction could be done. Out of 39 cataloged objects we would expect 1 or 2 to be oriented within 15 degrees of face-on, where measurement of differences between the major and minor axis would be difficult. Figure 5.17 shows two cataloged objects with ratios greater than -.5 in the log. Certainly, not all of the cataloged objects are spirals, but it likely that at least some of these extremely high ratios are due to orientation.

On the other hand, an anomalously low ratio could be produced by a galaxy which had a close interacting companion which would tend to exaggerate the velocity width. Interestingly, the four cataloged (and detected in the HI slice) objects with the lowest ratios are the four of the five objects with extremely high dynamic masses mentioned in the previous section. This might lead us to believe that they are not massive due to mergers as we discussed above, as mergers would presumable maintain atomic hydrogen gas and the same dynamic to hydrogen mass ratios (although there is evidence that galaxies in clusters can be "stripped" of their HI mass), but possibly due to artificially high velocity width measurements.

Compared to the cataloged objects, the galaxies which were not detected in the HI survey have extremely low HI to dynamic ratios, with a mean value of -1.86 in the log. There is nothing at all surprising about this. By being difficult to detect at 21cm, these objects have clearly demonstrated that they have a deficiency in their atomic hydrogen content, so if they have perfectly normal dynamic masses (and Figure 5.4 shows that they are all pretty average), their mass ratio would inevitably be low.

In contrast to both the cataloged objects and the undetected objects, the uncataloged galaxies have very high HI to dynamic mass ratios, with a mean value of -0.69 in the log. From Figure 5.16, it is clear that there is no correlation of this trend with the overall sizes of the galaxies - from the smallest to the largest uncataloged objects, the mass ratio appears fairly constant. While we might expect galaxies found by their 21cm emission to have proportionally larger atomic hydrogen components, there are a number of other possible reasons for the high ratio which we must consider. From the figures, we can count three uncataloged objects (and one cataloged object) with ratios of HI to dynamic mass of greater than 1.0. These ratios are clearly not correct, as the atomic hydrogen component is only a portion of the total mass of any galaxy, and the dynamic mass is expected to represent the total mass of an object. We can be pretty sure that the dynamic mass is being under-estimated in these objects. How is this happening? One possibility is that the sizes measured for the uncataloged objects are too small. As mentioned in previous sections, we must constantly be suspicious of dynamic mass calculations for the HI-selected uncataloged objects. We can see from Figures 4.1 and 4.2 that the uncataloged objects are generally much less luminous than the cataloged objects. Many of them are barely detectable (we know, in fact, that two of them are invisible), and measurement of their optical sizes is difficult. We can expect that there would be inaccuracies in the measurements of their optical sizes, specifically leaning toward under-estimates due to the difficulty of detecting extremely faint optical emission at their extreme edges. The dynamic mass we calculate (see Chapter 4) may be low because it is proportional to the optically measured size of the object.

There is little doubt, however, that much of the trend toward low dynamic to hydrogen mass ratios in the uncataloged objects is real. This ratio provides us with a perfectly straight-forward explanation for the inability of optical surveys to detect these objects previously. As a group, these objects have a higher proportion of their mass in atomic hydrogen than "normal" (i.e. optically cataloged) galaxies do. Very simply, this trait would leave less mass doing other things, such as forming molecules and molecular clouds, and from them star forming regions, stars, HII regions, and all the things which are associated with optical luminosity.

Where are the Brightest Galaxies?

If the uncataloged galaxies indeed do have much of their mass in the form of atomic hydrogen, and as a result less in luminosity-generating forms, we would expect that as a group these galaxies would be under-luminous. In Figure 5.18, we have plotted the blue luminosities (in $M_\odot$) of the slice objects. It is plain from the figure that there is a clear division between the cataloged and uncataloged objects in the sample. Not only are the mean values for these two groups very different (8.68 in the log for the uncataloged galaxies and 9.82 in the log for the cataloged galaxies), but there is virtually no overlap in their dispersions. Unsurprisingly, intrinsic optical luminosity is a critical feature in determining the detectability of an object in optical surveys.

In Figure 5.19, we plot the logs of the blue luminosities of the slice objects against their redshift velocities. In the figure, it can be seen that the cataloged and uncataloged objects are separated into two groups, except in two places. One is at the high redshift, high distance end of the plot, where the highest luminosity uncataloged objects are also. Compared to the cataloged objects, the luminosities of these objects are still low, but it is certainly their great distance which caused them to be missed in optical searches which detected similar-luminosity objects nearby. The second location is that of the two lowest-luminosity cataloged objects, which both have fairly low redshift velocities. Most probably, it was their small distances which allowed these under-luminous objects to join the optical catalogs. It is interesting to note, however, that all of these "overlap" objects are literally surrounded on the plot by objects belonging to the other category. Clearly blue luminosity is not the only factor which determines an object's detectability in optical surveys - there must be other properties which allow these objects, which according to the figure have very similar properties, to end up in different categories.

In Figure 5.20, the blue luminosities of the slice objects are plotted on a linear scale against their distance. As with the dynamic masses, we can see a tendency for the brightest objects to appear around redshift velocities of 5000 km/s, where the most organized cluster structures are. As with dynamic mass measurements, galaxies should fare very well in dense cluster environments in terms of intrinsic luminosity. Mergers and tidal interactions, activities which are thought to be common in dense cluster

environments, are thought to trigger bursts of star formation, both through the production of shock fronts, and by the introduction of fresh pools of gas and dust to a galaxy. These are the same forces which would lead to high dynamic mass measurements, and indeed most of the objects which have unusually high dynamic masses also stand out by their blue luminosity.

<u>Mass-to-Light Ratios of the Slice Galaxies</u>

In the sections above, we have investigated the dynamic and atomic hydrogen masses of the slice objects, and their intrinsic luminosities. We may now compare the different mass estimates to the luminosities to examine differences in the importance of each component between the cataloged and uncataloged galaxies. In a typical spiral galaxy such as the Milky Way, we would expect blue luminosity to be about 10% of the dynamic mass when both quantities are measured in solar units. Because the HI to dynamic mass is similarly expected to be about 10%, the ratio of blue luminosity to HI mass would be near 1.0 (0.0 in the log) for a normal galaxy.

In Figures 5.21 and 5.22 we present the logs of the intrinsic blue luminosity (L_B) to dynamic mass ratios and blue luminosity to atomic hydrogen mass ratios for the objects in the slice search region. All quantities are measured in solar units. Beyond the expected difference in the mean values for these two ratios, a clear difference in the distribution of measurements can be seen between the two plots.

The blue luminosity to dynamic mass ratios shown in Figure 5.21 are very close to what we would expect for normal galaxies. Galaxies of all types - uncataloged, cataloged, and those not detected in HI, all have virtually identical mean values for the ratio (-1.02, -1.01 and -1.30 in the log respectively). Within the limits of their small total numbers, each category shows a fairly neat gaussian distribution about a peak value very near 10%. A skewed high value tail to the distribution can be explained by anomalously low dynamic mass measurements due to the inclination and size-related difficulties involved in making these measurements as we discussed in previous sections. Despite all of the differences in the mean blue luminosities and mean dynamic masses measured for the different categories of objects in the slice search, a constant ratio of these two quantities appears to be maintained across all types.

In contrast, Figure 5.22 shows that the blue luminosity to atomic hydrogen mass ratios divide the slice objects in to two categories. As expected, the cataloged objects have ratios which peak fairly near 0.0 in the log (mean of 0.14) with a long tail toward values of 1.0. At the extreme high end are clustered the objects which were not detected in HI (mean value of 0.56 in the log), which is hardly surprising as these objects have already demonstrated themselves to be deficient in atomic hydrogen. The uncataloged objects, on the other hand, have a much lower peak to their distribution (mean value of -0.35 in the log). These objects have a far larger component of their mass in the form of atomic hydrogen than the cataloged objects.

The implication of these two plots is that dynamic mass and blue luminosity are directly related across a wide range in both values. To first order, this is telling us only that larger objects tend to be brighter as well, but with the large differences in the fraction of atomic hydrogen mass between the different objects, this good correlation is a little surprising. We might expect that with a large fraction of the total mass in atomic hydrogen, a galaxy's star formation and optical luminosity have to be depressed, simply because there would be less mass in the form of stars. This would lead to a lower value of the blue luminosity to dynamic mass ratio for the uncataloged objects which we know have more of their mass in the form of atomic hydrogen. Yet there is no evidence for such a difference.

The two plots also indicate that there are real physical differences between the galaxies which were previously cataloged and those found originally by the slice search by their 21cm emission. The uncataloged objects aren't just slightly fainter and smaller versions of their cataloged counterparts. As a group, they appear to be comprised of a different mix of components, with more atomic hydrogen and fewer stars as a fraction of their total mass.

The Slice Galaxy Colors

In Figure 5.23, we examine the colors of the slice galaxies. The colors are obtained by subtracting the absolute red magnitudes from the absolute blue magnitudes. Higher-numbered results indicate a "redder" colored object. The colors of galaxies tell us something about their stellar populations. In general, a redder color indicates a galaxy has an "evolved" stellar population - that its optical emission is dominated

by low-mass stars, and that little current star formation is going on, while a blue color indicates that a galaxy's emission is dominated by bright, young stars, and that active star formation is taking place on a fairly wide scale.

From the figure, we can see that the three categories of slice objects have distinctly different colors, with mean values of 0.90 for the uncataloged objects, 1.12 for the cataloged objects, and 1.61 for the objects which were not detected in HI. These differences are even more extreme when we examine the central colors of the objects, as is done in Figure 5.24. The central colors of the uncataloged objects have a mean value of 1.08, compared to 1.46 for the cataloged objects and 1.94 for the objects which were not detected in HI. The extreme redness of the objects which were not detected in HI indicates these objects as a group are not actively forming stars. We also know that they are deficient in atomic hydrogen, implying that they have consumed their reservoirs of gas long ago in older generations of stars. The uncataloged objects, however, are blue, implying that these objects are actively engaged in large scale star formation, although a blue color can also imply low metallicity and less reddening.

The blueness of the uncataloged objects is intriguing in that Tyson(*Ap.J.* **335**, 552) found large numbers of faint blue galaxies in deep CCD images, leaving them to wonder why similar objects could not be observed at nearby redshift velocities. Could it be that the nearby uncataloged slice objects, with their low masses, large (implied) numbers, and extremely blue colors represent this population?
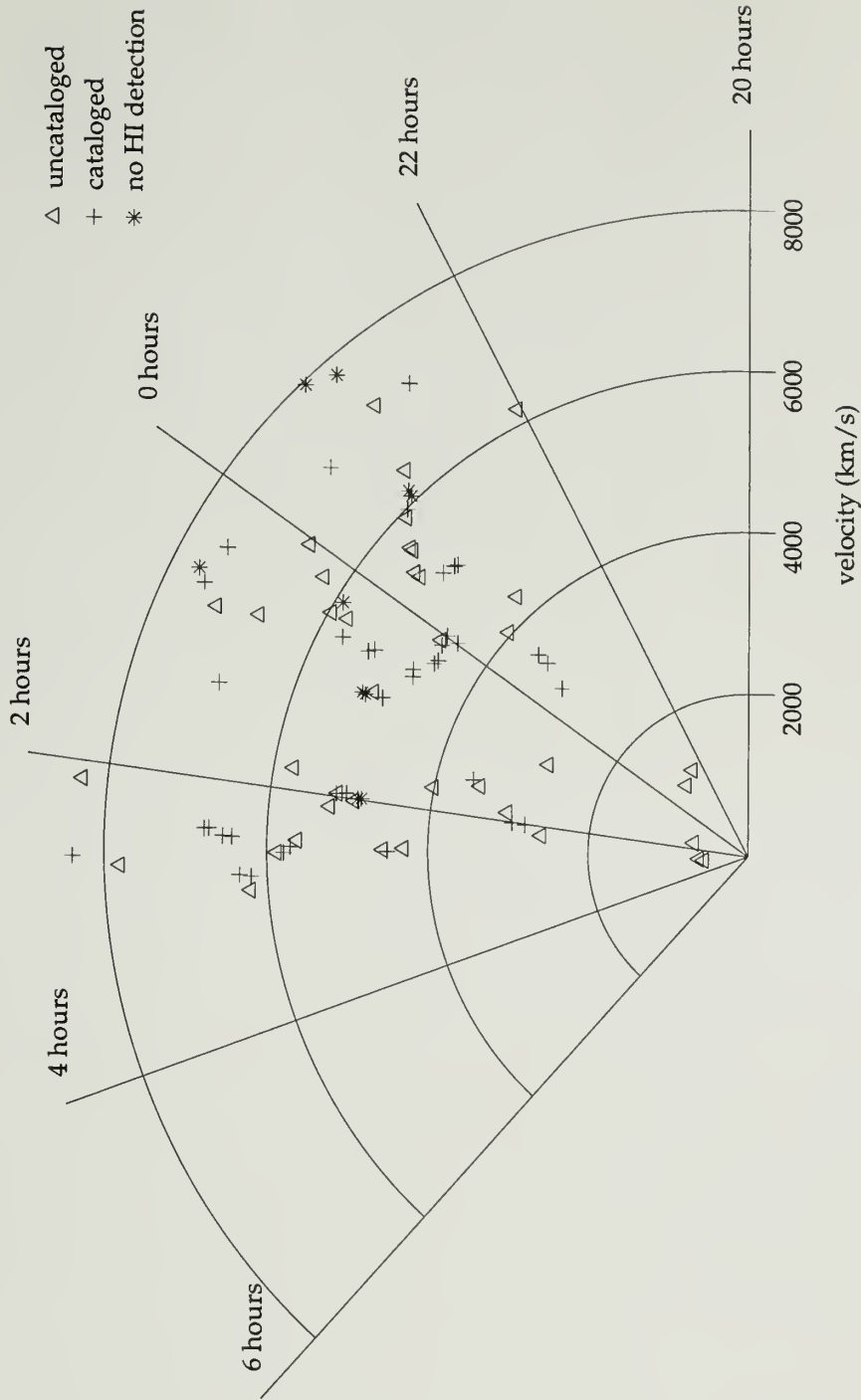
Figure 5.1. Positions of the objects detected in the slice search. Uncataloged
HI-detected galaxies are marked by triangles, cataloged galaxies with HI detections
are marked by crosses, and galaxies not detected in the HI search are marked
by stars. Radial lines are of constant RA.
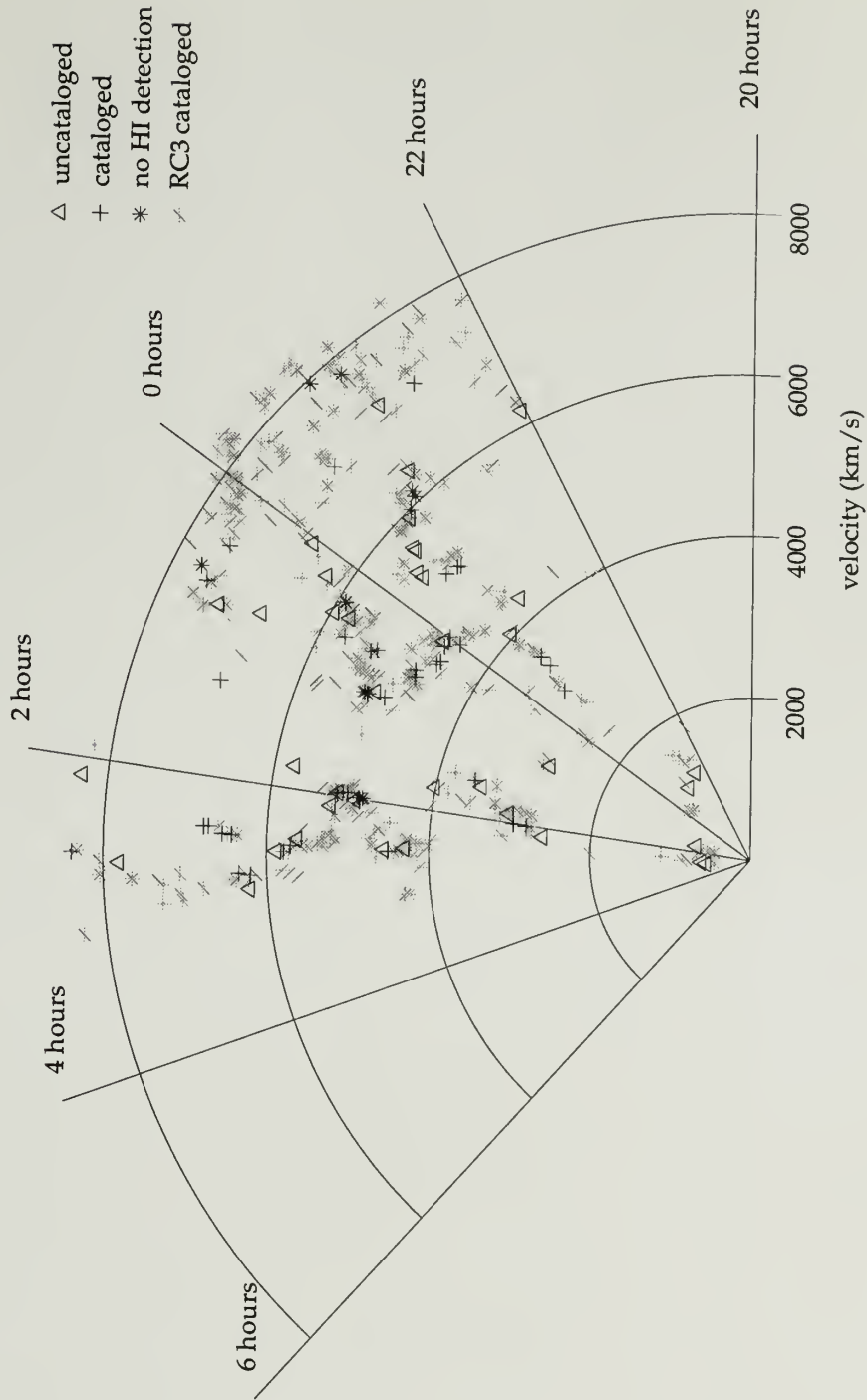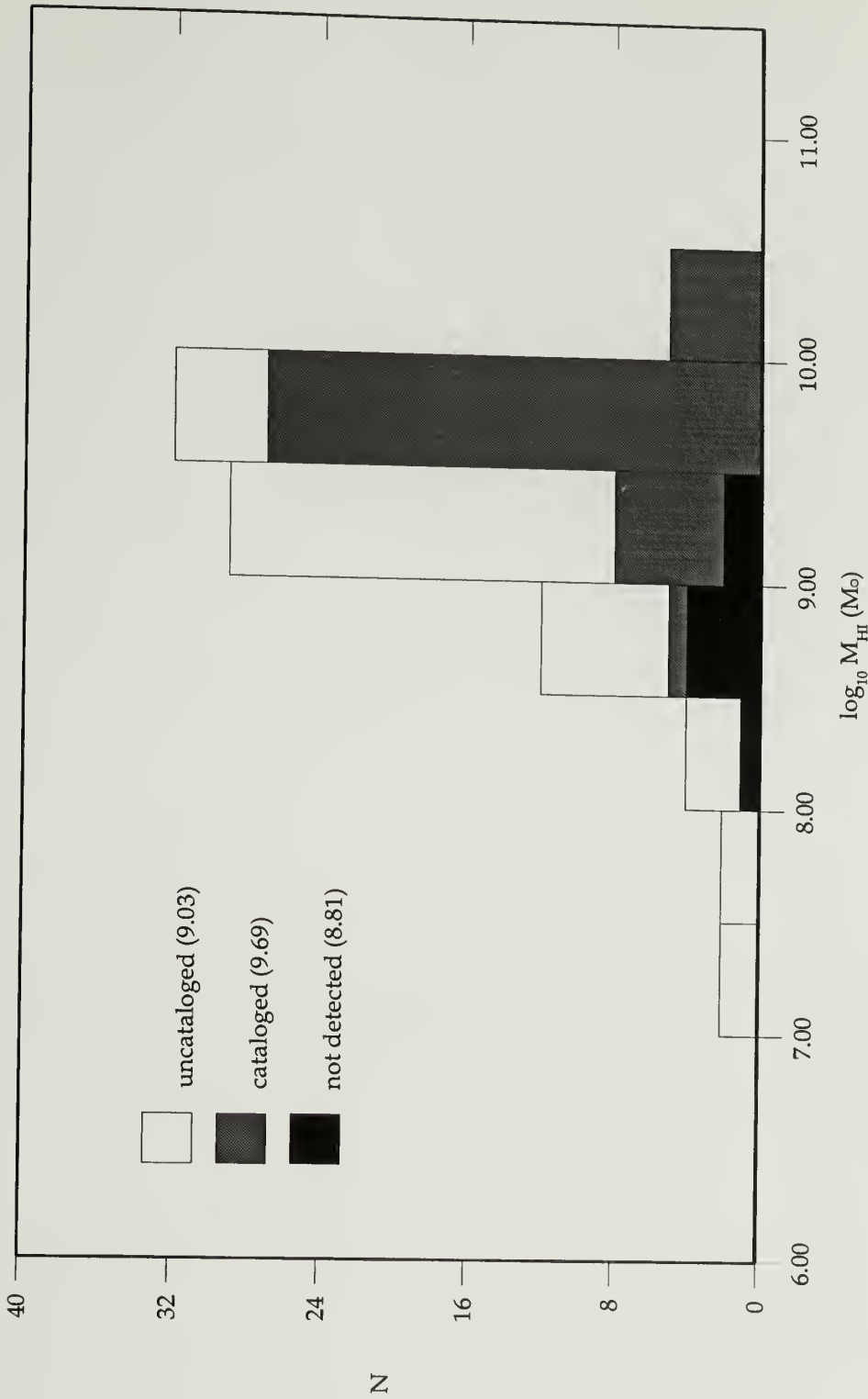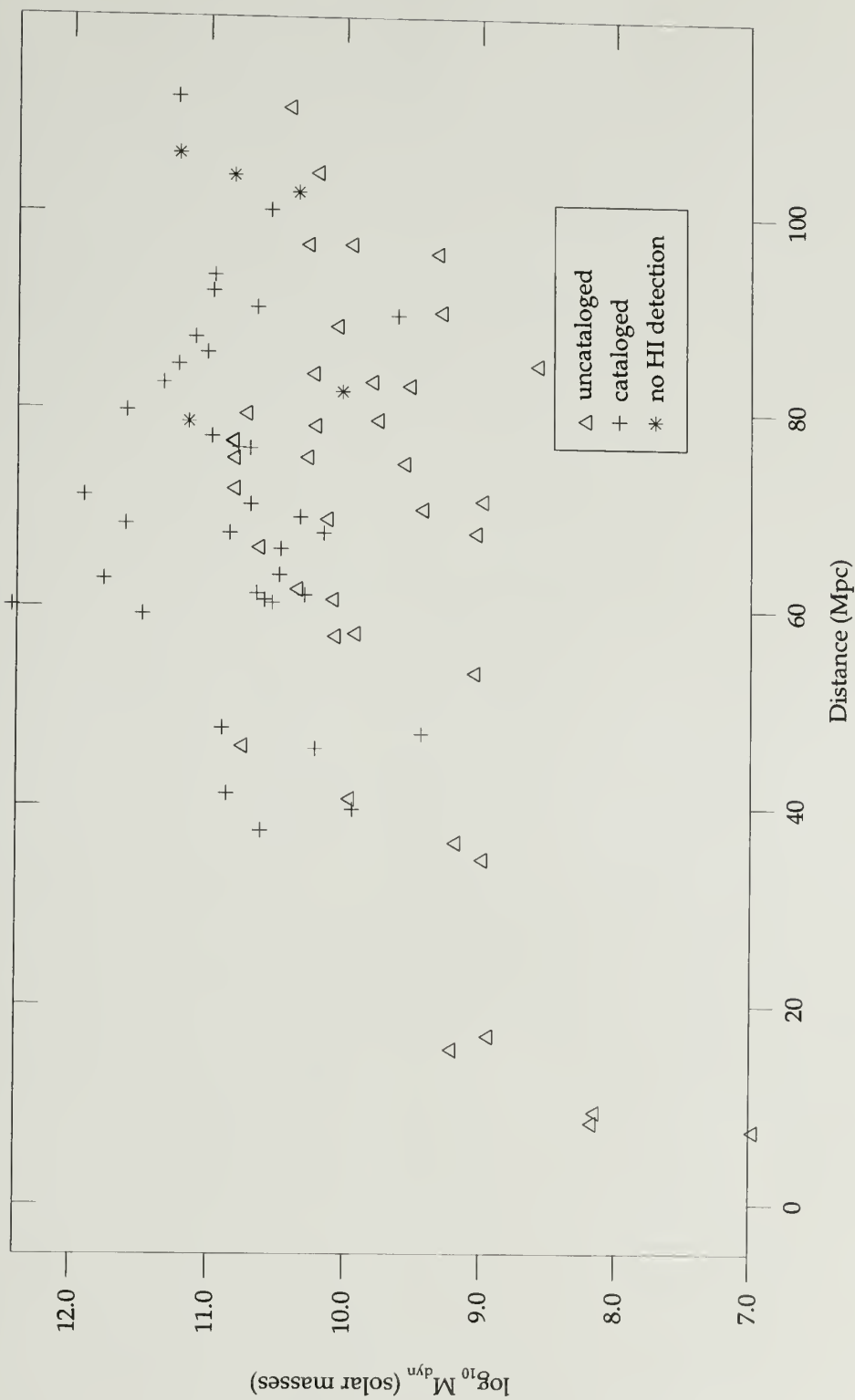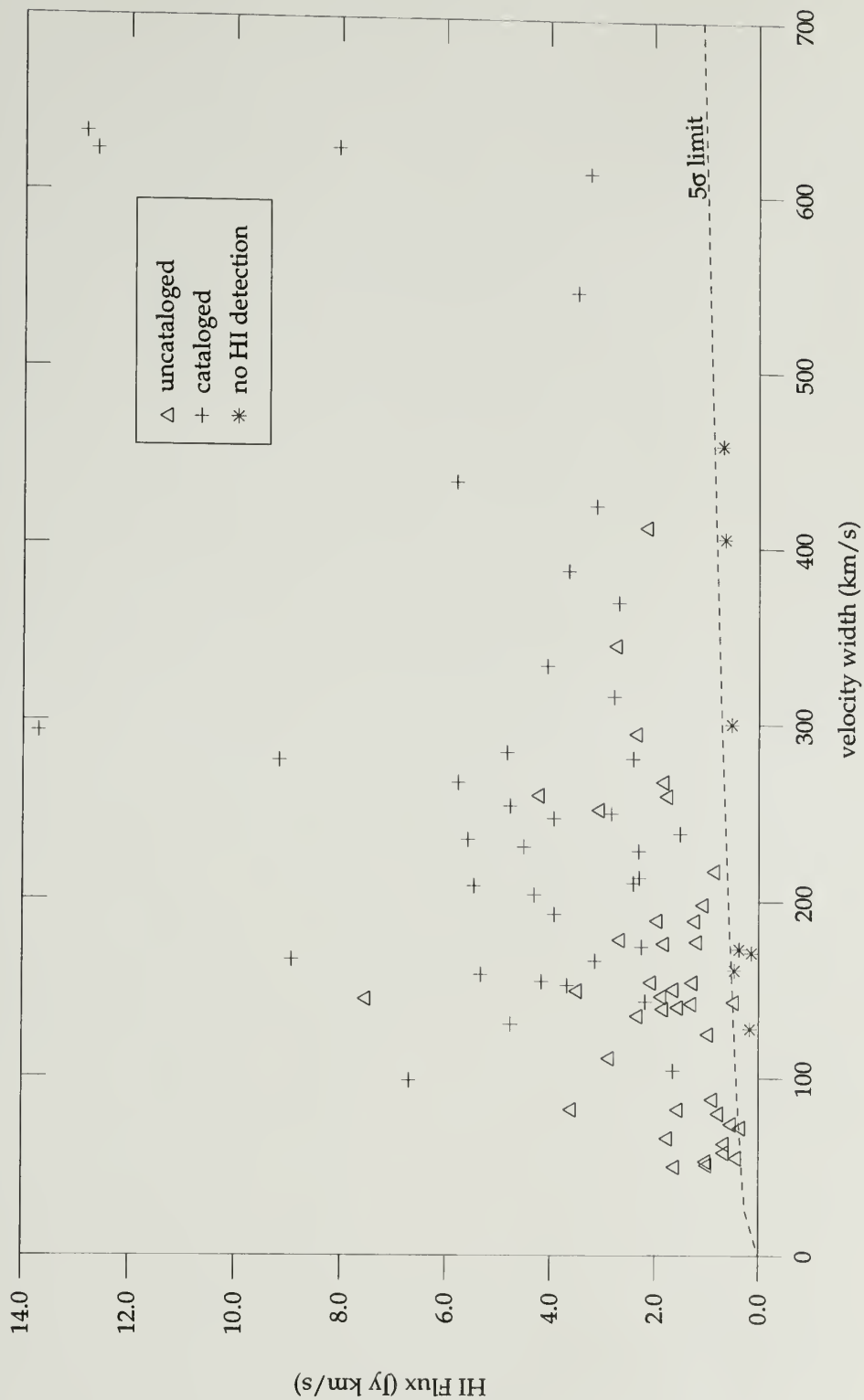
Figure 5.2. Slice object positions vs RC3 objects in the declination range +18 to +28. Uncataloged HI-detected galaxies are marked by triangles, cataloged galaxies with HI detections are marked by crosses, and galaxies not detected in the HI search are marked by stars. RC3 galaxies are gray stars.

Figure 5.3. Hydrogen masses of the slice objects. White bars are the uncataloged HI-detected galaxies, gray bars are the cataloged galaxies with HI detections, and black bars are the galaxies not detected in the HI search.
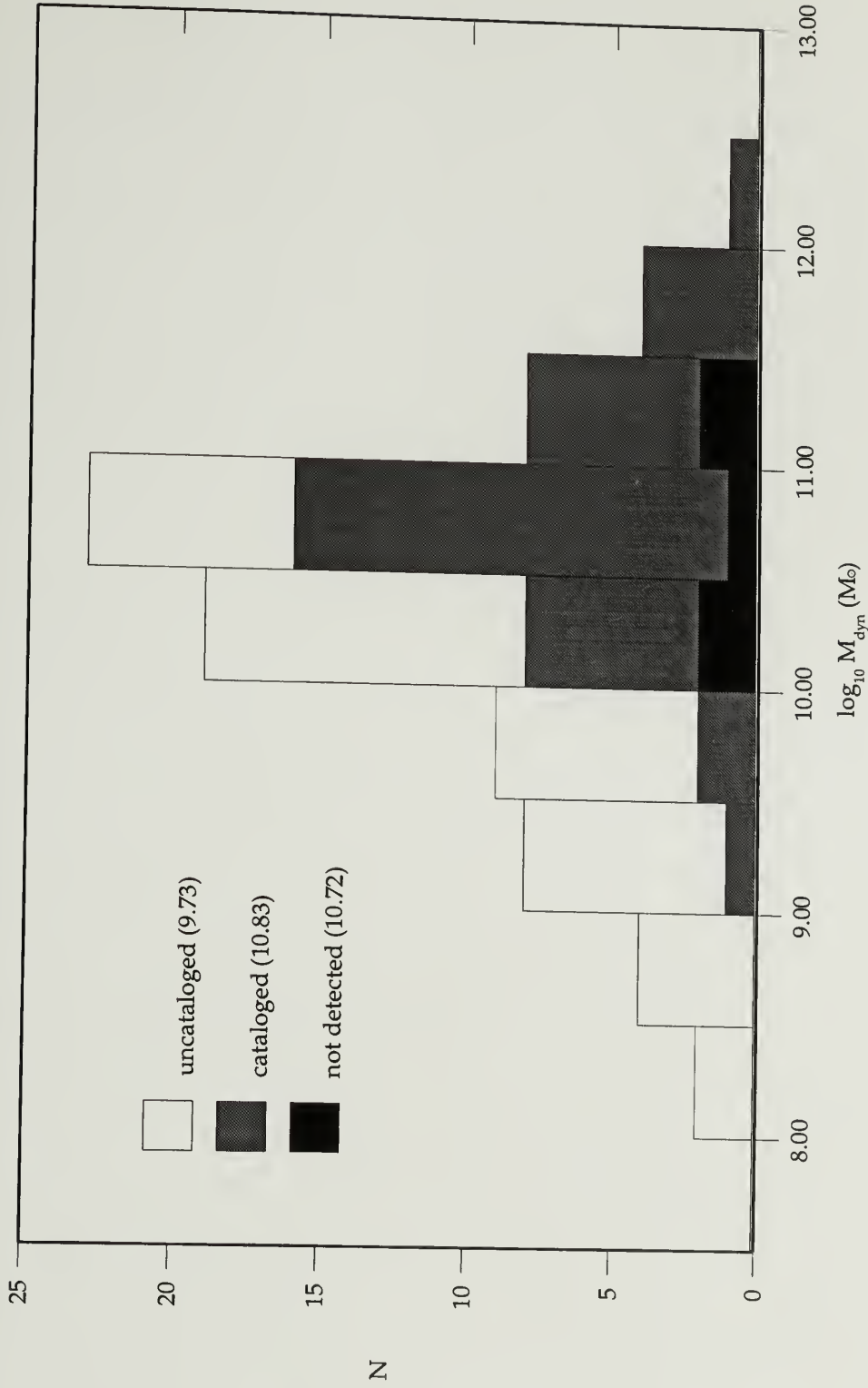
Figure 5.4. Dynamical masses of the slice objects. White bars are the uncataloged HI-detected galaxies, gray bars are the cataloged galaxies with HI detections, and black bars are the galaxies not detected in the HI search.
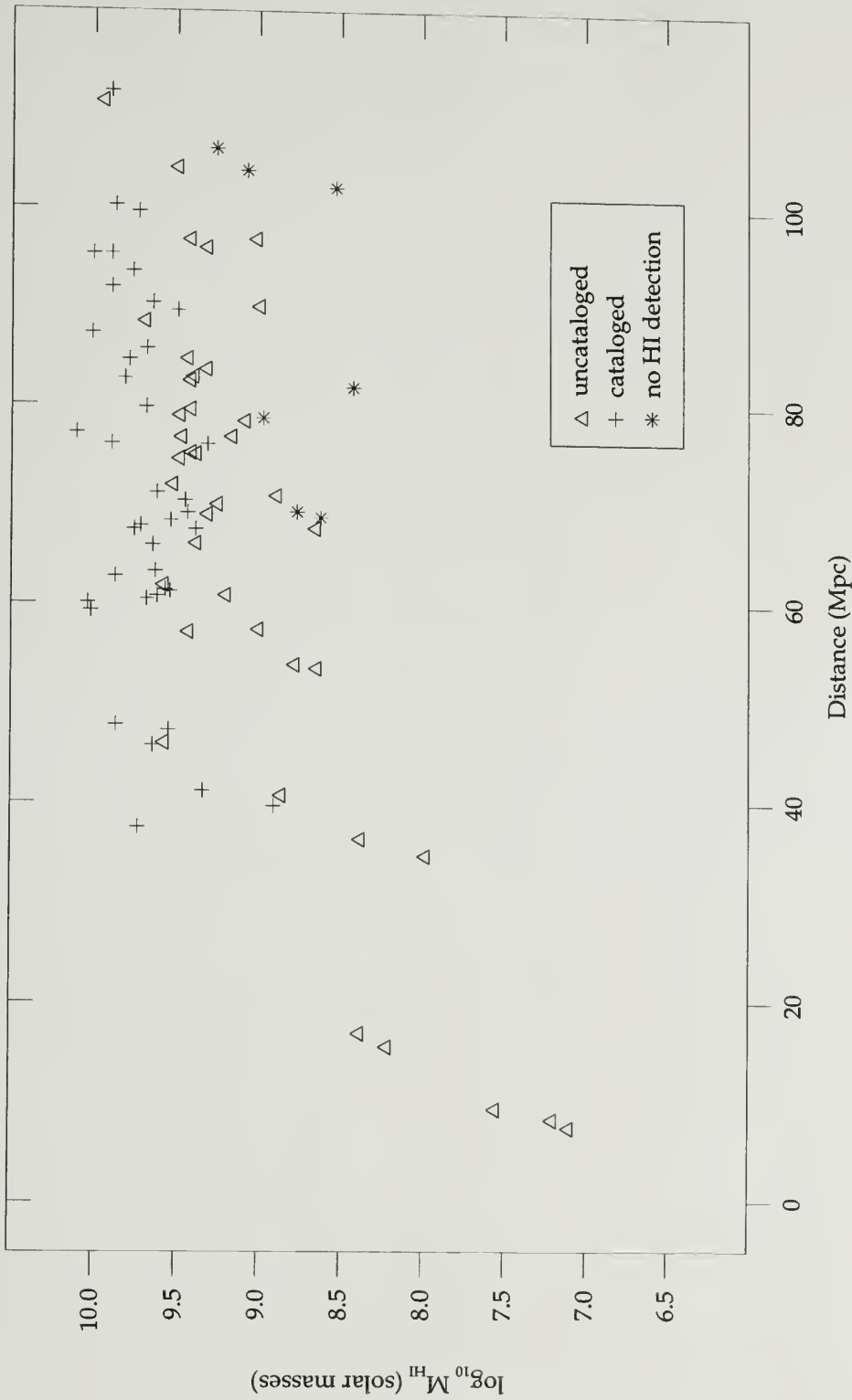
Figure 5.5. Hydrogen masses of the slice galaxies plotted against their distances. Uncataloged HI-detected galaxies are marked by triangles, cataloged galaxies with HI detections are marked by crosses, and galaxies not detected in the HI search are marked by stars.

Figure 5.6. Dynamical masses of the slice galaxies plotted against their distances. Uncataloged HI-detected galaxies are marked by triangles, cataloged galaxies with HI detections are marked by crosses, and galaxies not detected in the HI search are marked by stars.

Figure 5-7: Detection Limit

Figure 5.7. HI fluxes of the slice galaxies plotted against their velocity widths.
Uncataloged HI-detected galaxies are marked by triangles, cataloged galaxies with
HI detections are marked by crosses, and galaxies not detected in the HI search
are marked by stars. The dashed line represents the 5σ detection limit.
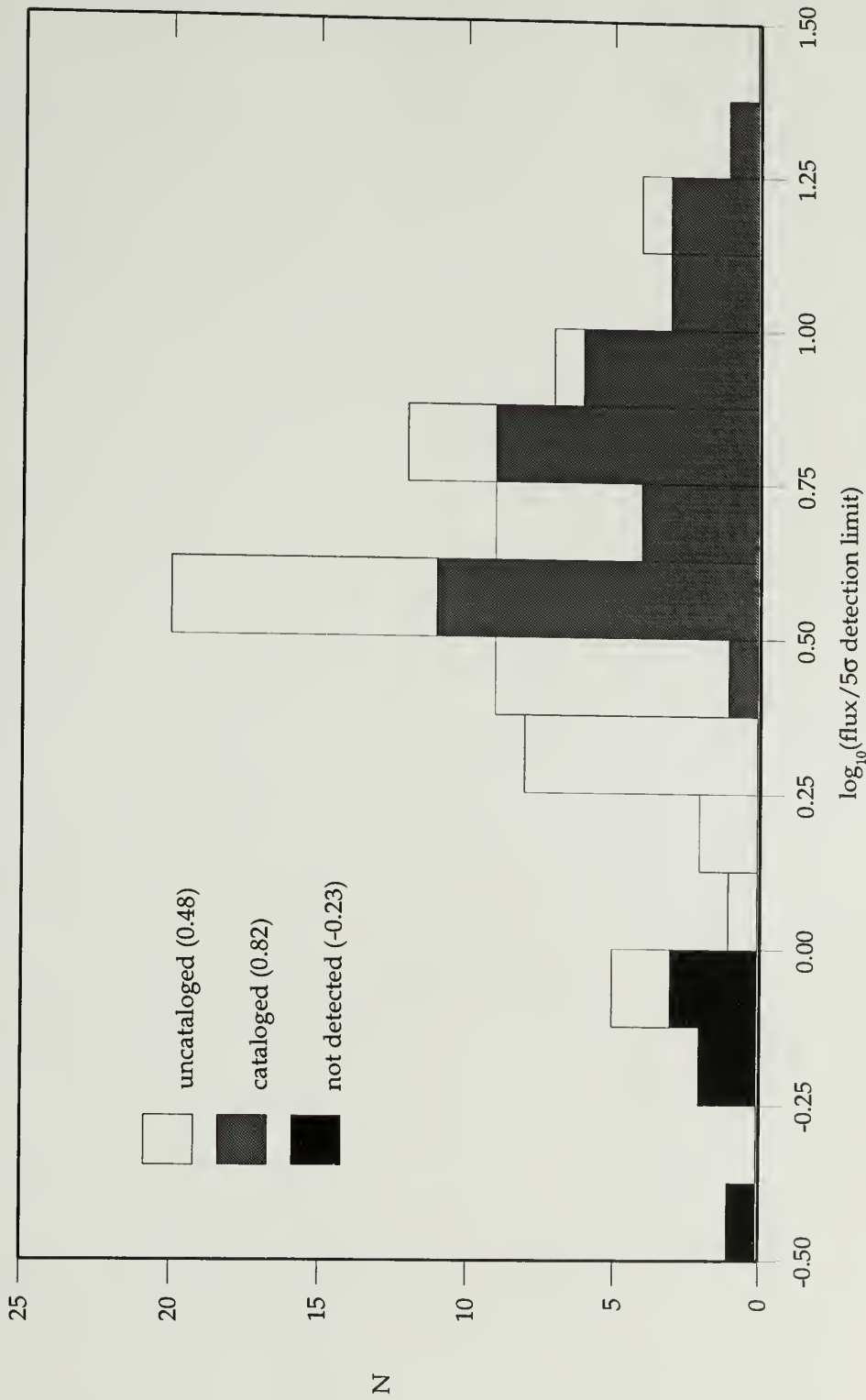
Figure 5.8. Ratios of the measured fluxes of the slice objects to the 5σ flux level. White bars are the uncataloged HI-detected galaxies, gray bars are the cataloged galaxies with HI detections, and black bars are the galaxies not detected in the HI search. Galaxies with values below zero are theoretically "undetectable."
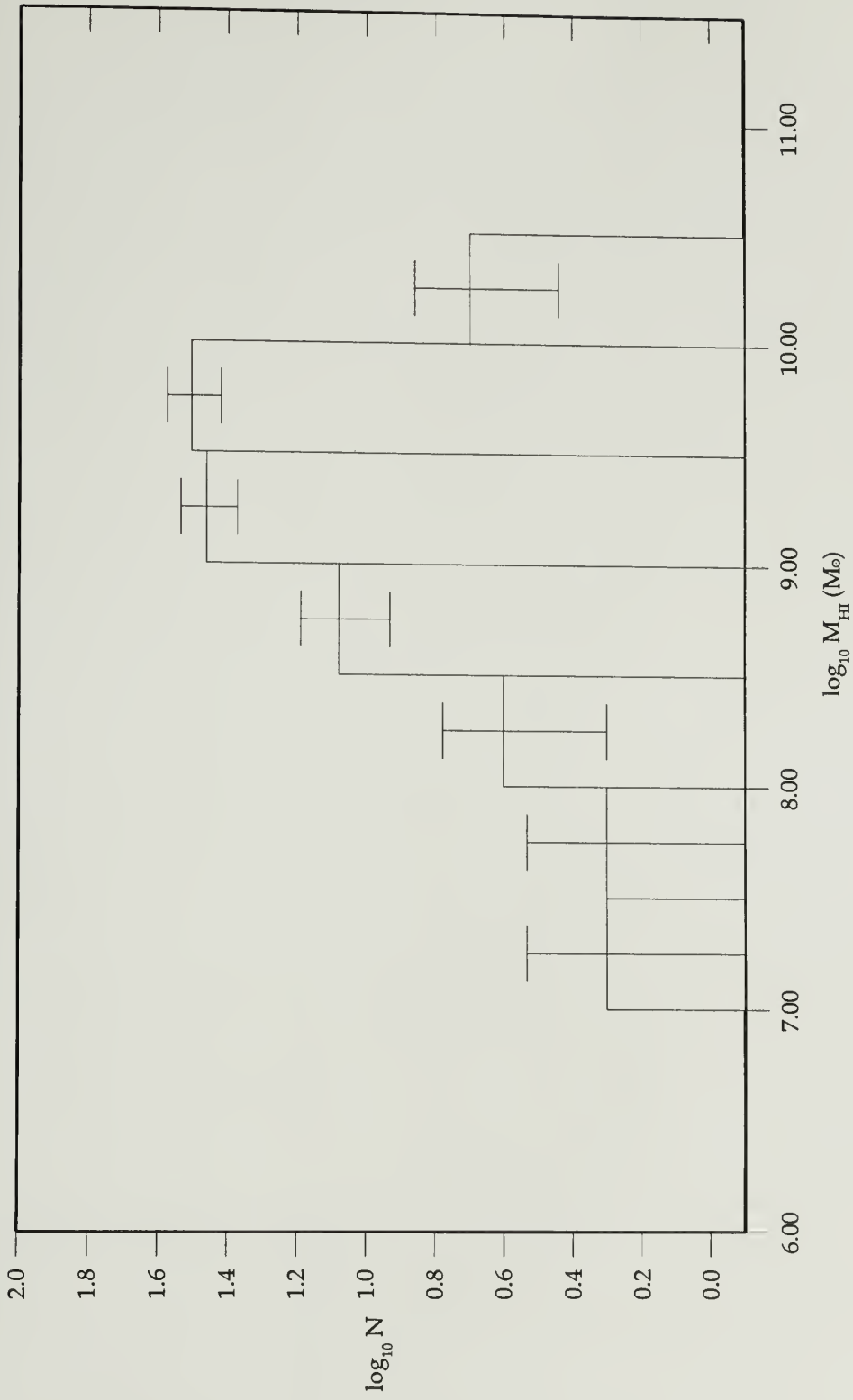
Figure 5.9. Hydrogen masses of all slice objects on a $\log_{10}$ scale. Errors in the histogram bars are indicated by brackets.
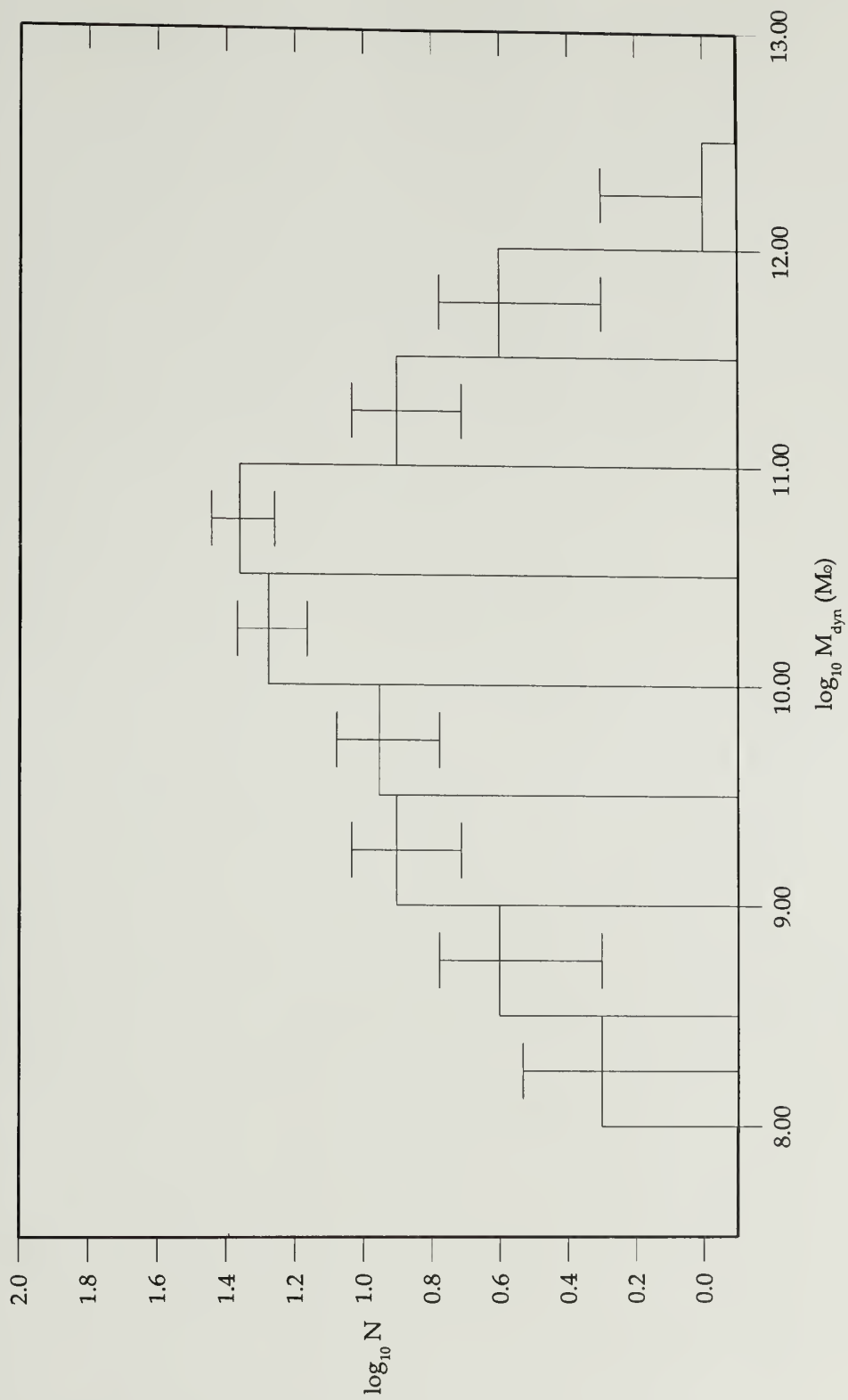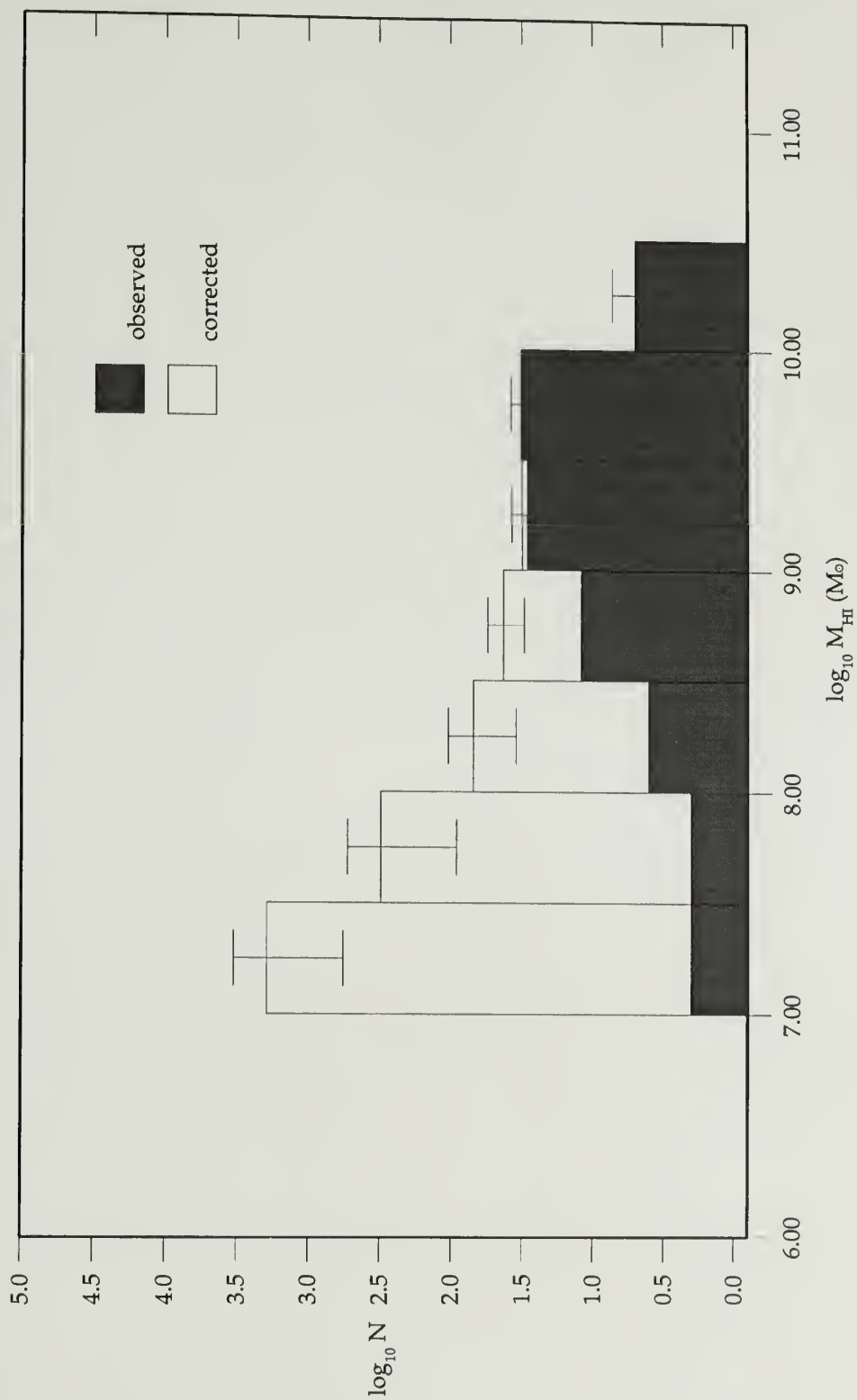
Figure 5.10. Dynamical masses of all slice objects on a $\log_{10}$ scale. Errors in the histogram bars are indicated by brackets.
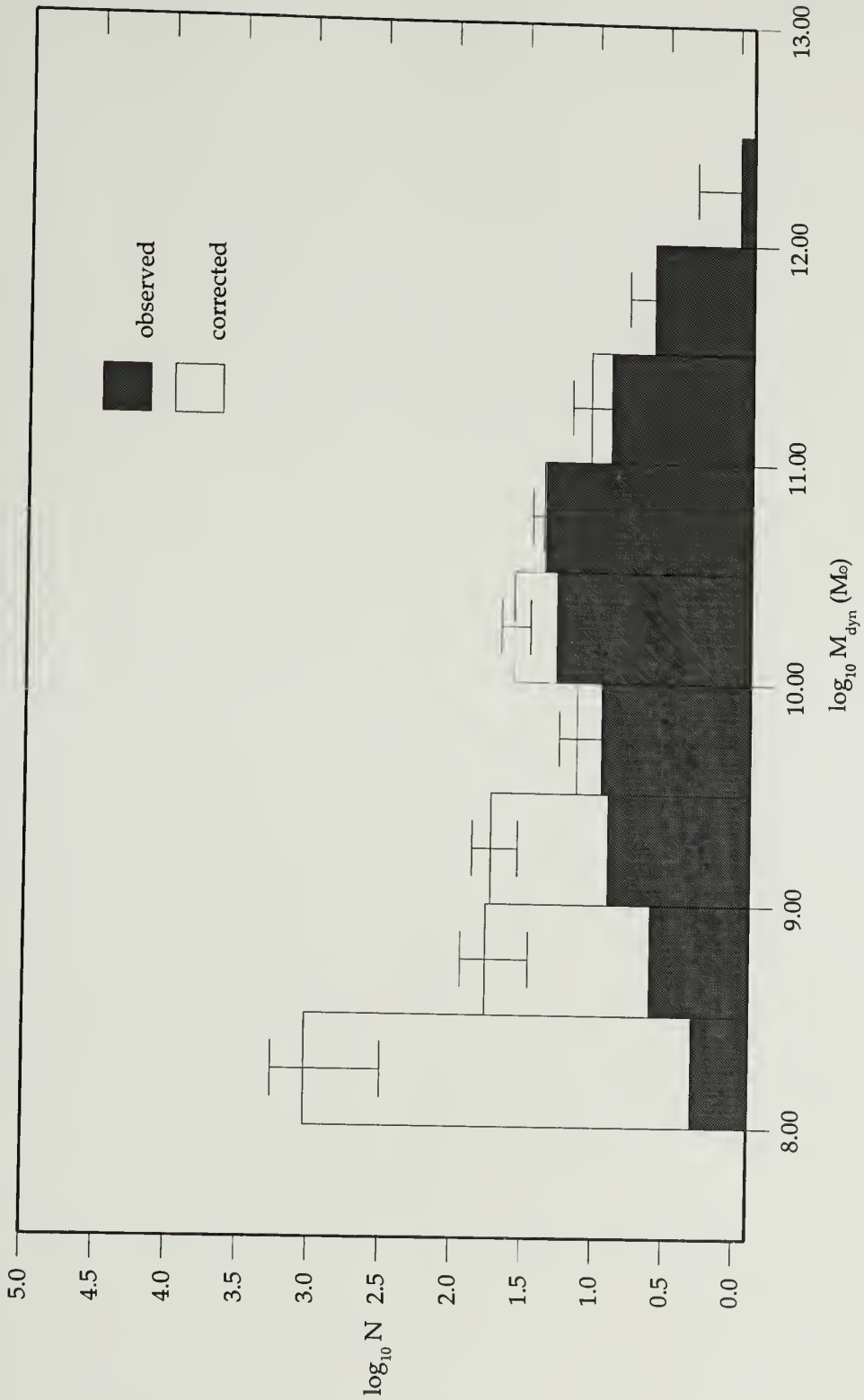
184

Figure 5.11. Observed and "corrected" hydrogen masses of all slice objects on a $\log_{10}$ scale. Shaded bars represent the observed numbers of objects (as presented in Figure 5.9). Unshaded bars are object counts which have been adjusted to the volume of sensitivity.
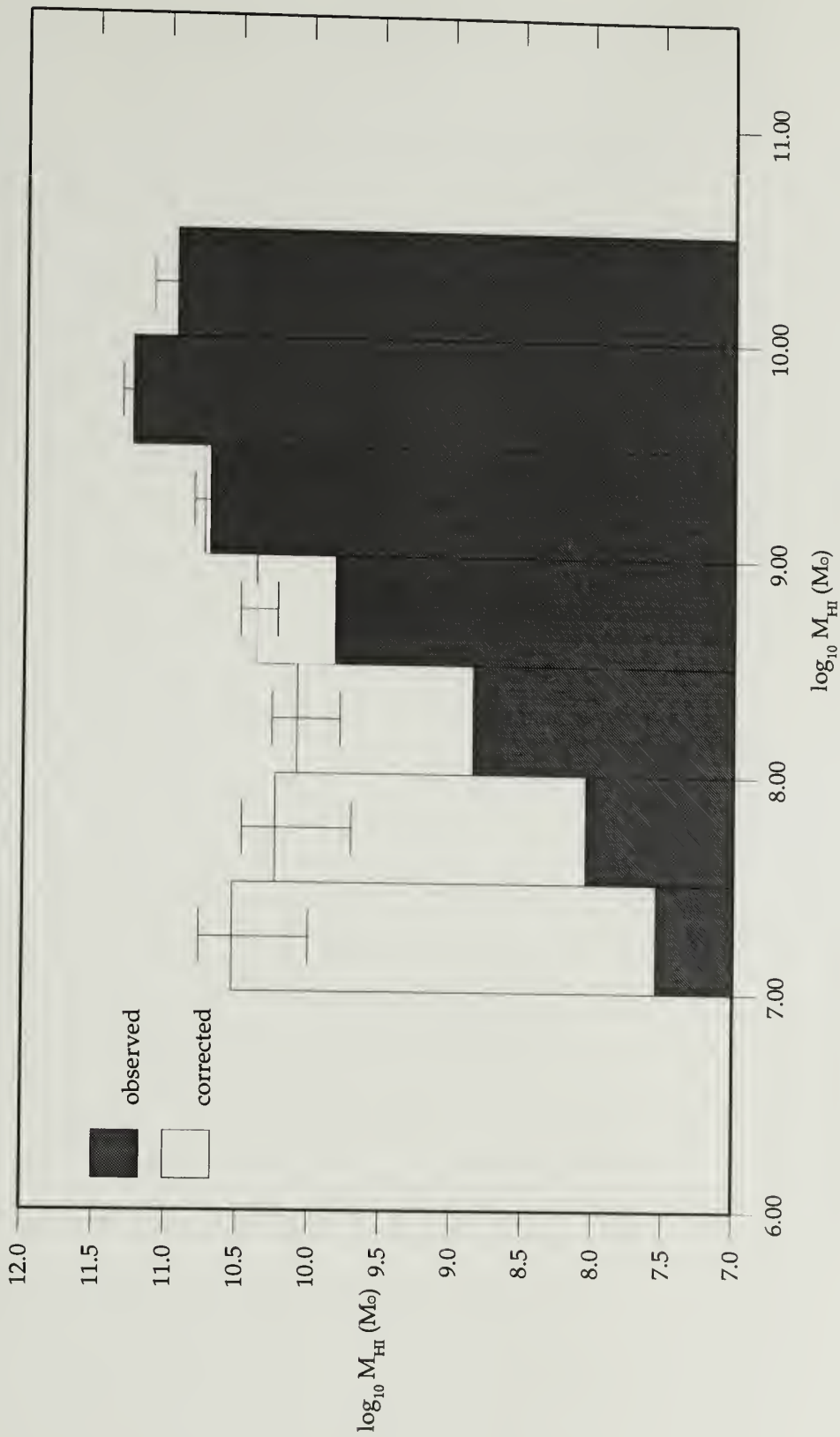
Figure 5.12. Observed and "corrected" dynamical masses of all slice objects on a $\log_{10}$ scale. Shaded bars represent the observed numbers of objects (as presented in Figure 5.10). Unshaded bars are object counts which have been adjusted to the volume of sensitivity.

Figure 5.13. Observed and "corrected" integrated atomic hydrogen mass per decade of all slice objects. Shaded bars represent the integrated HI mass of observed objects. Unshaded bars are integrated mass which has been adjusted to the volume of sensitivity.
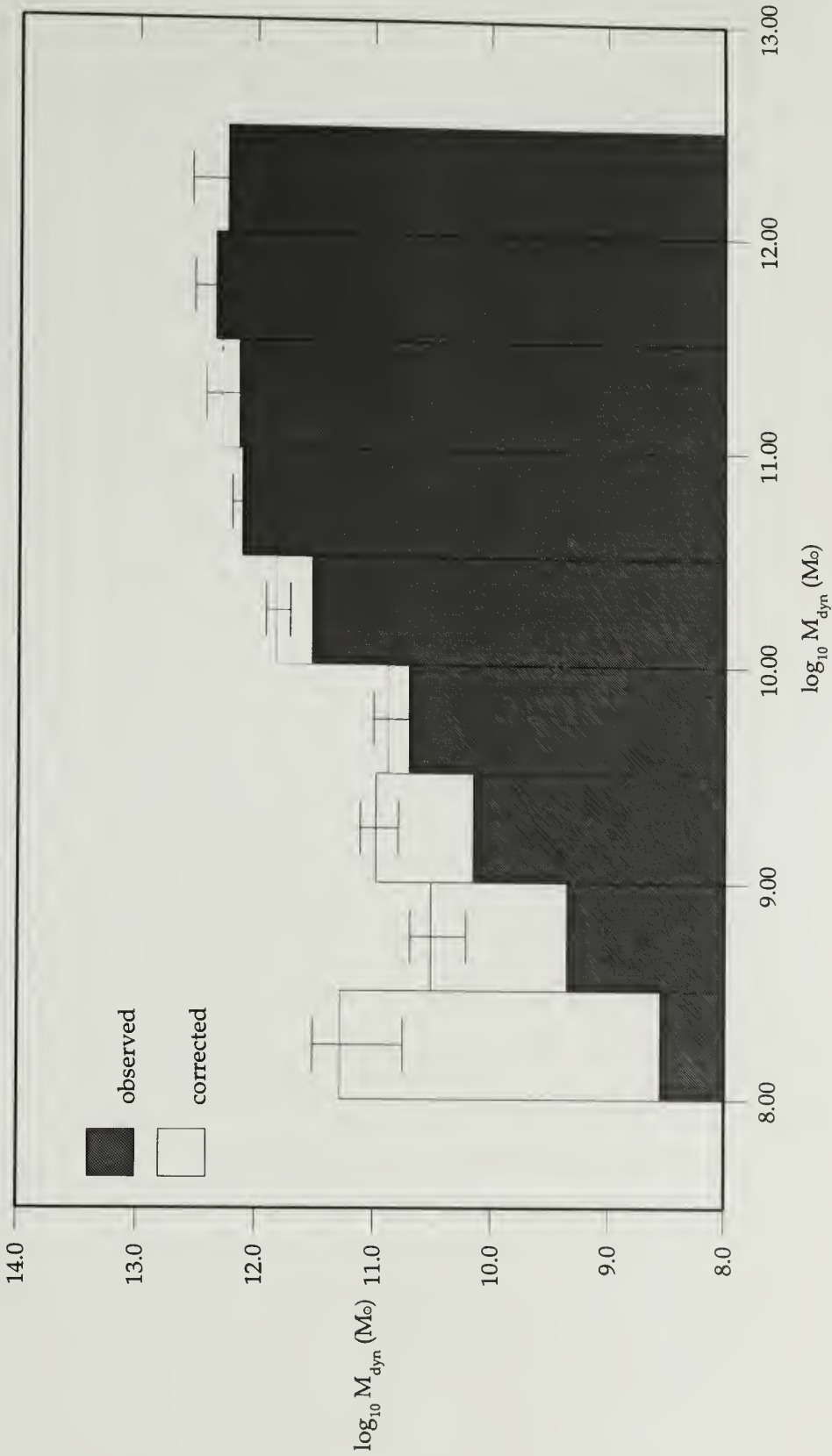
Figure 5.14. Observed and "corrected" integrated dynamical mass per decade of all slice objects. Shaded bars represent the integrated dynamical mass of observed objects. Unshaded bars are integrated mass which has been adjusted to the volume of sensitivity.
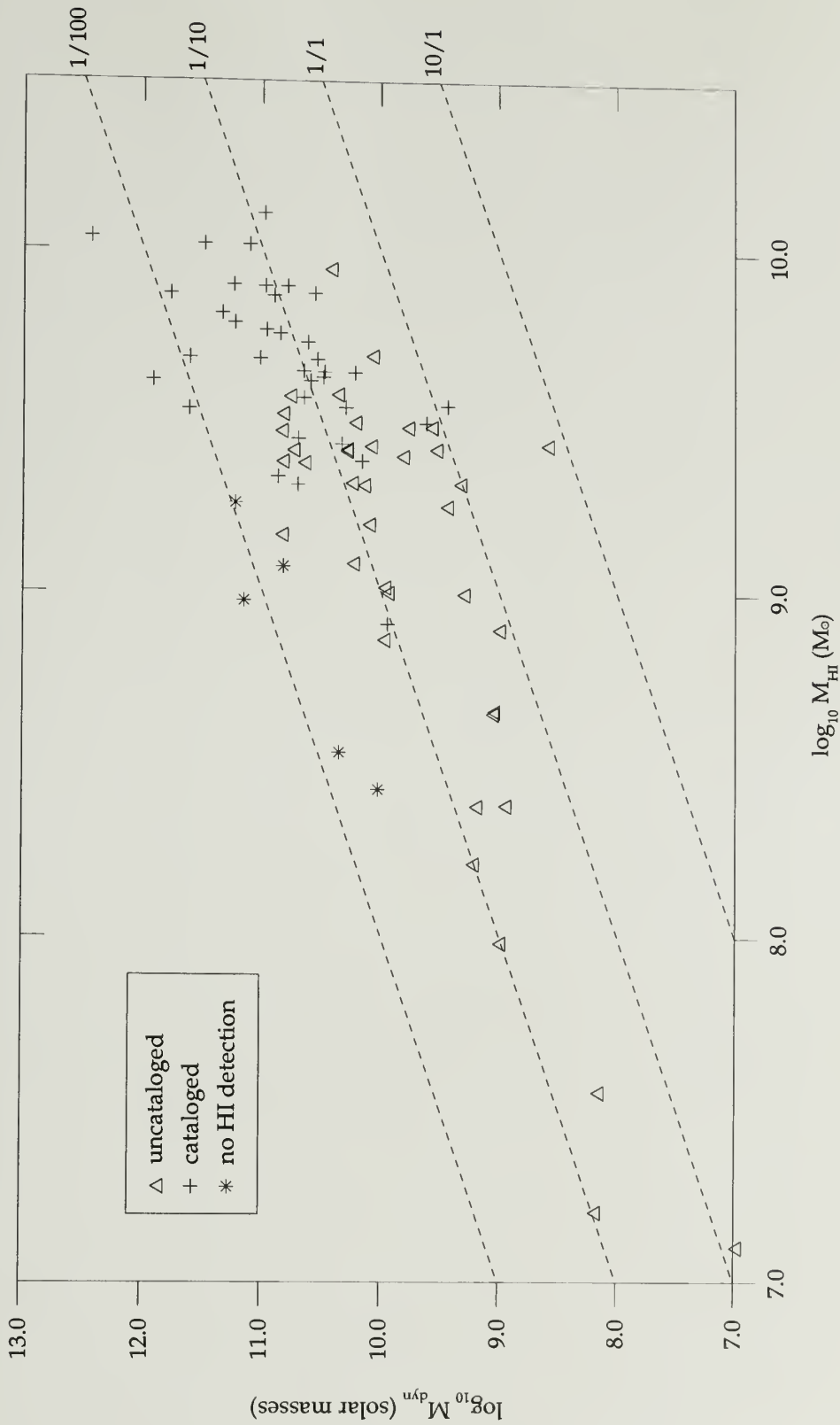
Figure 5.15. The dynamical masses of slice galaxies plotted against their distances. Uncataloged HI-detected galaxies are marked by triangles, cataloged galaxies with HI detections are marked by crosses, and galaxies not detected in the HI search are marked by stars. Six galaxies stand out with unusually high dynamical masses.

Figure 5.16. Dynamical masses of the slice objects plotted against their HI masses. Uncataloged HI-detected galaxies are marked by triangles, cataloged galaxies with HI detections are marked by crosses, and galaxies not detected in the HI search are marked by stars. Dashed lines show ratios of HI to dynamical mass.
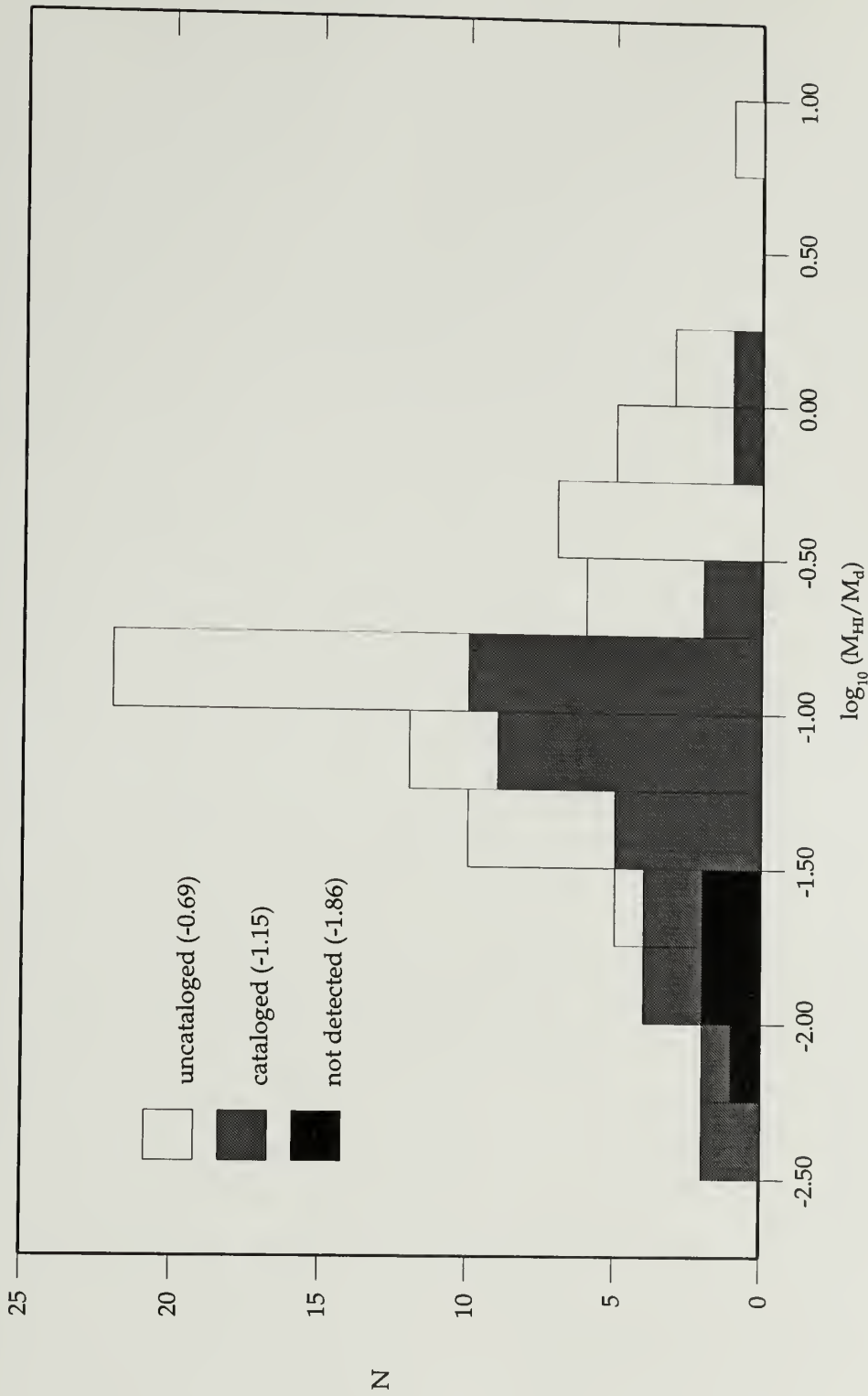
Figure 5.17. Ratios of atomic hydrogen to dynamical mass for all slice objects. White bars are the uncataloged HI-detected galaxies, gray bars are the cataloged galaxies with HI detections, and black bars are the galaxies not detected in the HI search. Values higher than 0.0 are physically impossible, and indicate measurement errors.
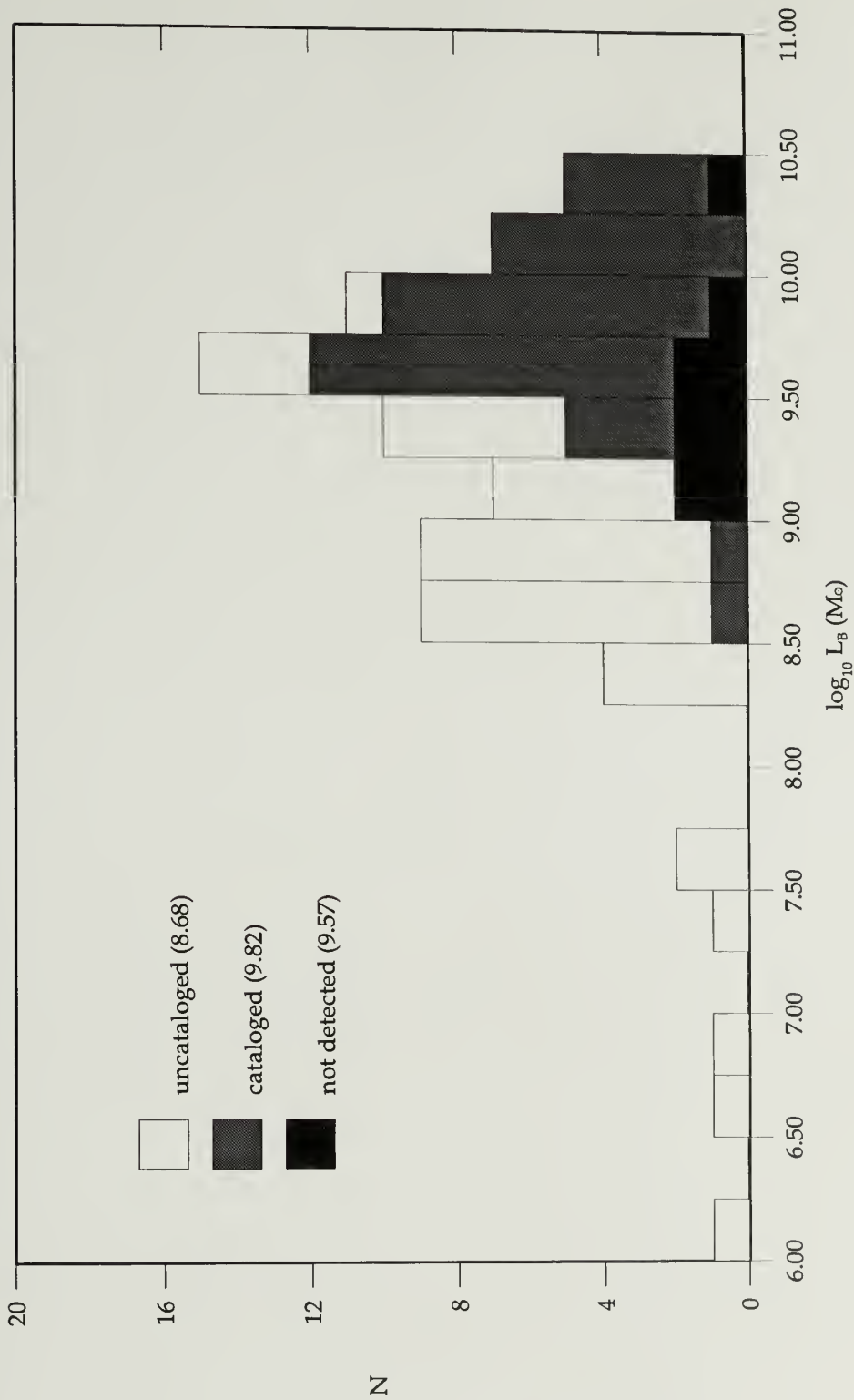
Figure 5.18. Integrated blue luminosities of the slice objects. White bars are the uncataloged HI-detected galaxies, gray bars are the cataloged galaxies with HI detections, and black bars are the galaxies not detected in the HI search.
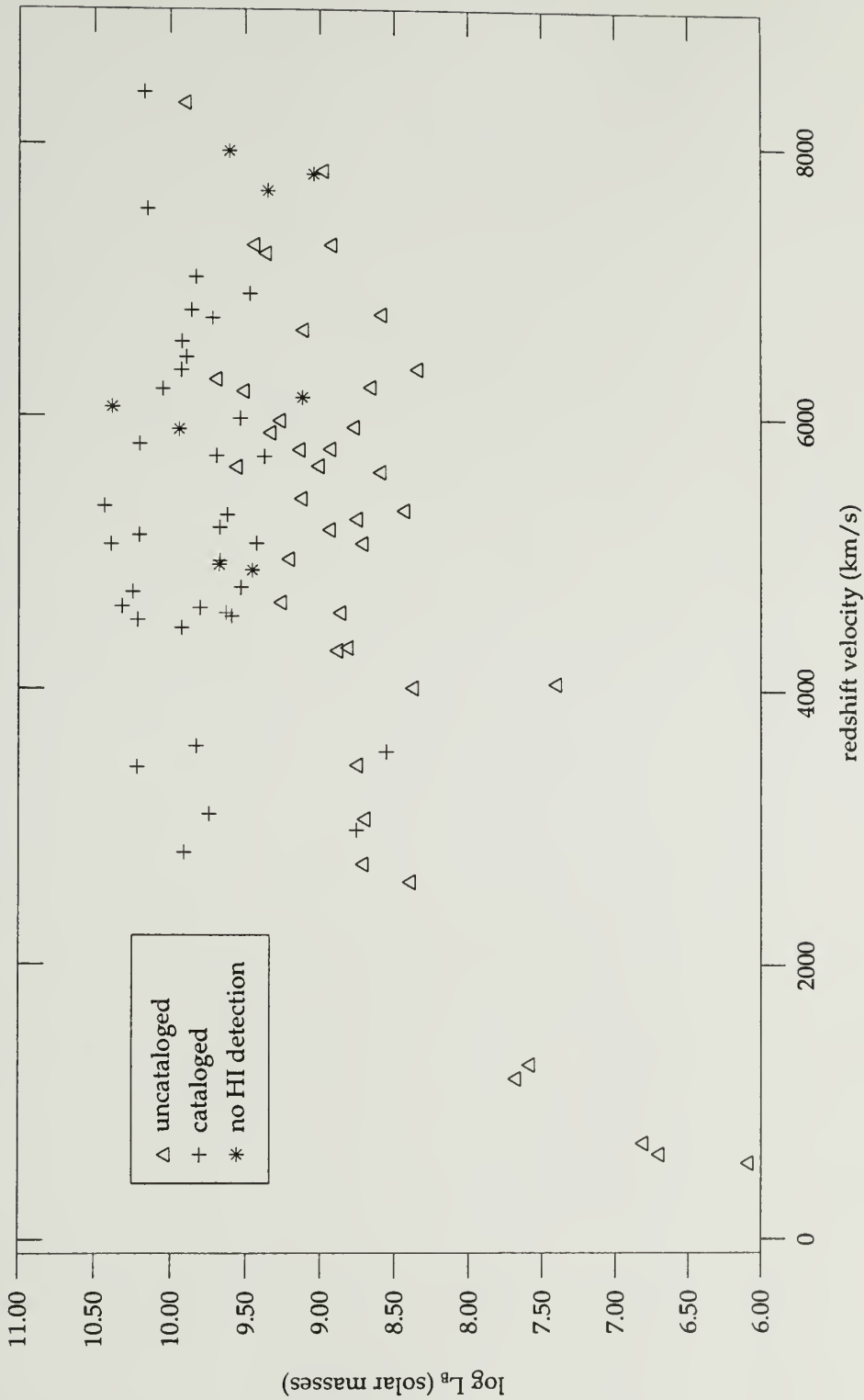
Figure 5.19. The blue luminosites of the slice objects as a function of distance (log scale). Uncataloged HI-detected galaxies are marked by triangles, cataloged galaxies with HI detections are marked by crosses, and galaxies not detected in the HI search are marked by stars.

Figure 5.20. The blue lumniosities of the slice galaxies as a function of distance (linear scale). Uncataloged HI-detected galaxies are marked by triangles, cataloged galaxies with HI detections are marked by crosses, and galaxies not detected in the HI search are marked by stars.
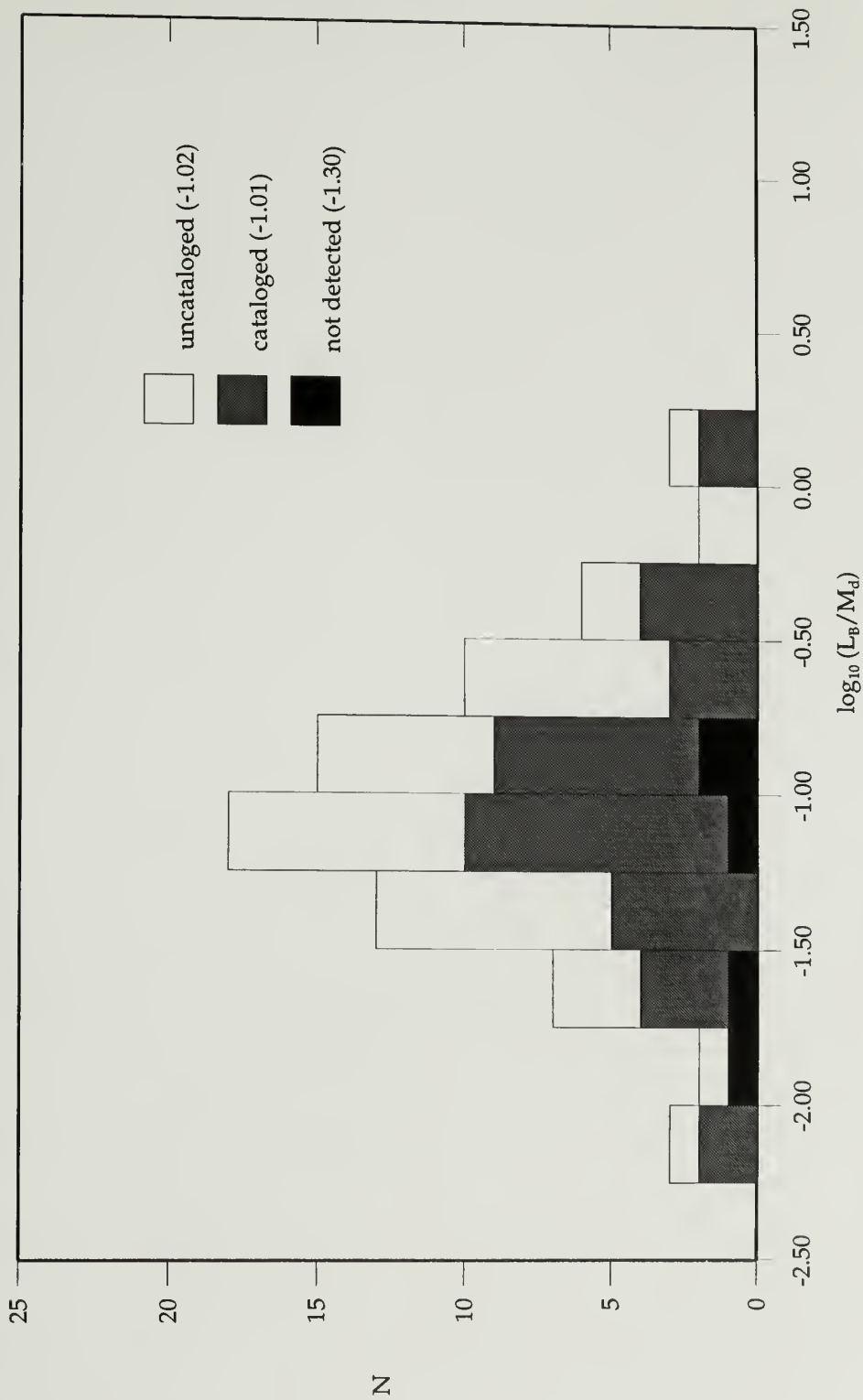
194

Figure 5.21. Ratios of blue luminosity to dynamical mass for all slice objects. White bars are the uncataloged HI-detected galaxies, gray bars are the cataloged galaxies with HI detections, and black bars are the galaxies not detected in the HI search. A value of -1.0 is typical of a normal spiral galaxy.
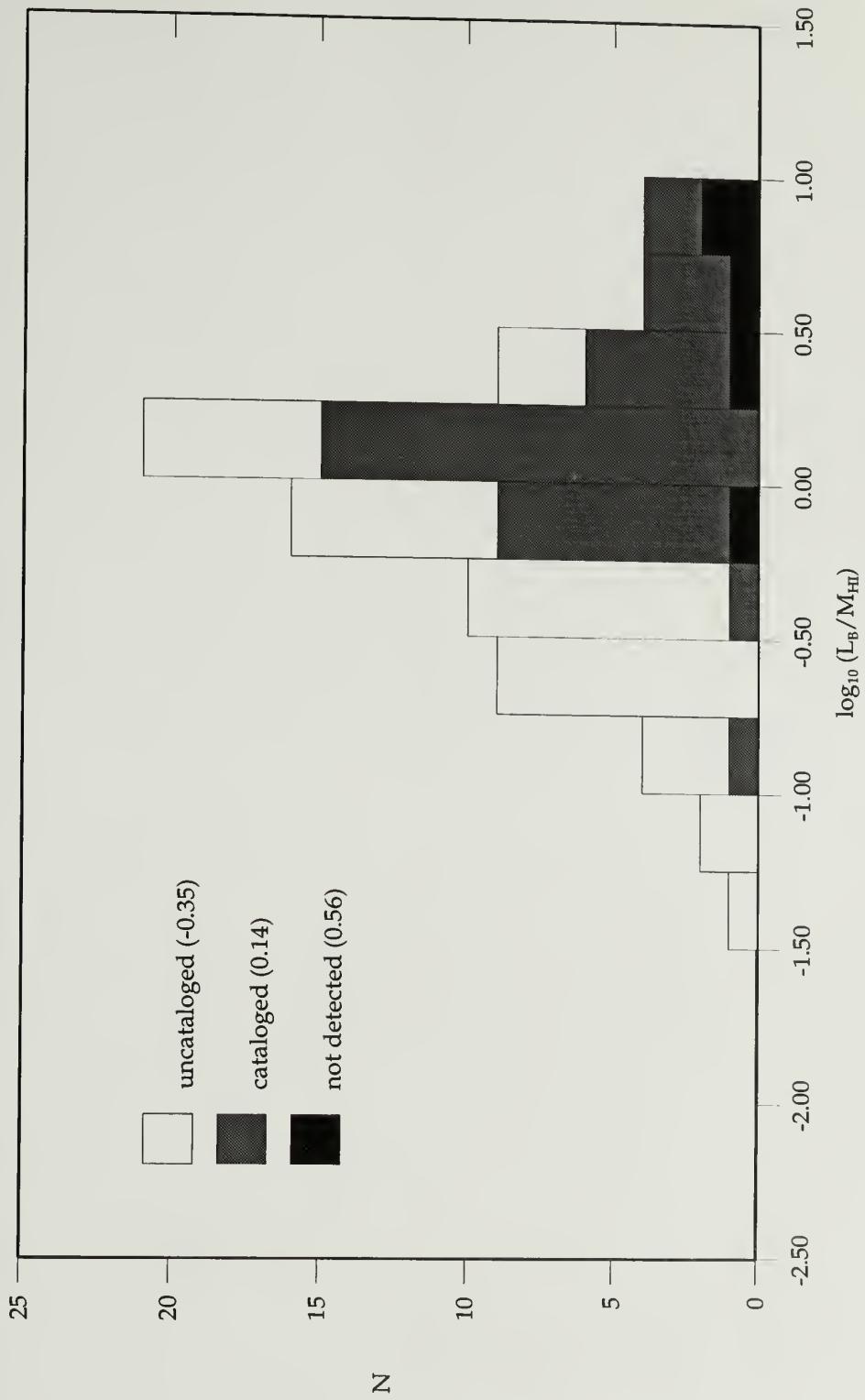
Figure 5.22. Ratios of blue luminosity to atomic hydrogen mass for all slice objects. White bars are the uncataloged HI-detected galaxies, gray bars are the cataloged galaxies with HI detections, and black bars are the galaxies not detected in the HI search. A value of 0.0 is typical of a normal spiral galaxy.
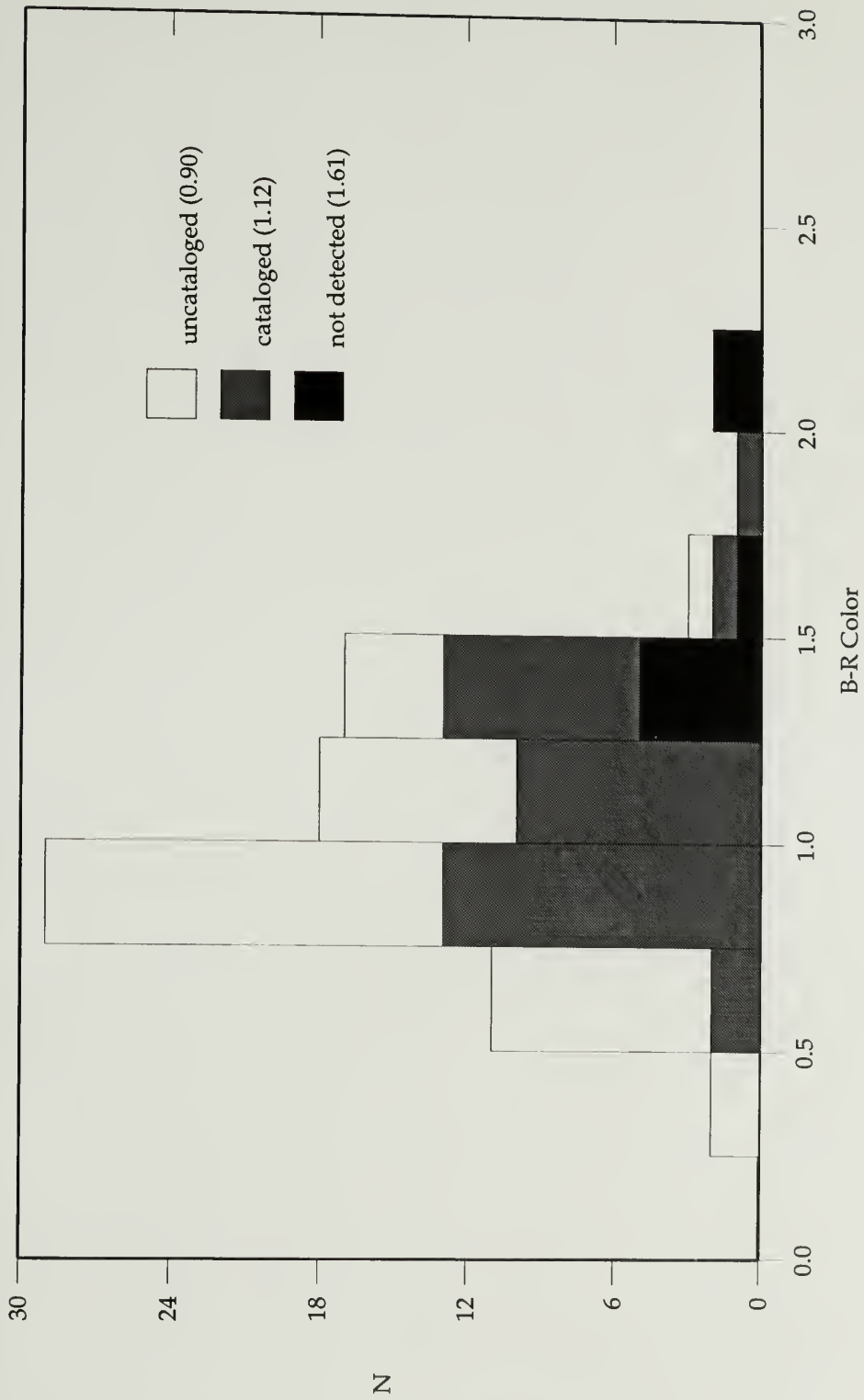
196

Figure 5.23. B-R Colors of the slice galaxies. White bars are the uncataloged HI-detected galaxies, gray bars are the cataloged galaxies with HI detections, and black bars are the galaxies not detected in the HI search.

Figure 5.24. B-R Colors of the centers of the slice galaxies. White bars are the uncataloged HI-detected galaxies, gray bars are the cataloged galaxies with HI detections, and black bars are the galaxies not detected in the HI search.
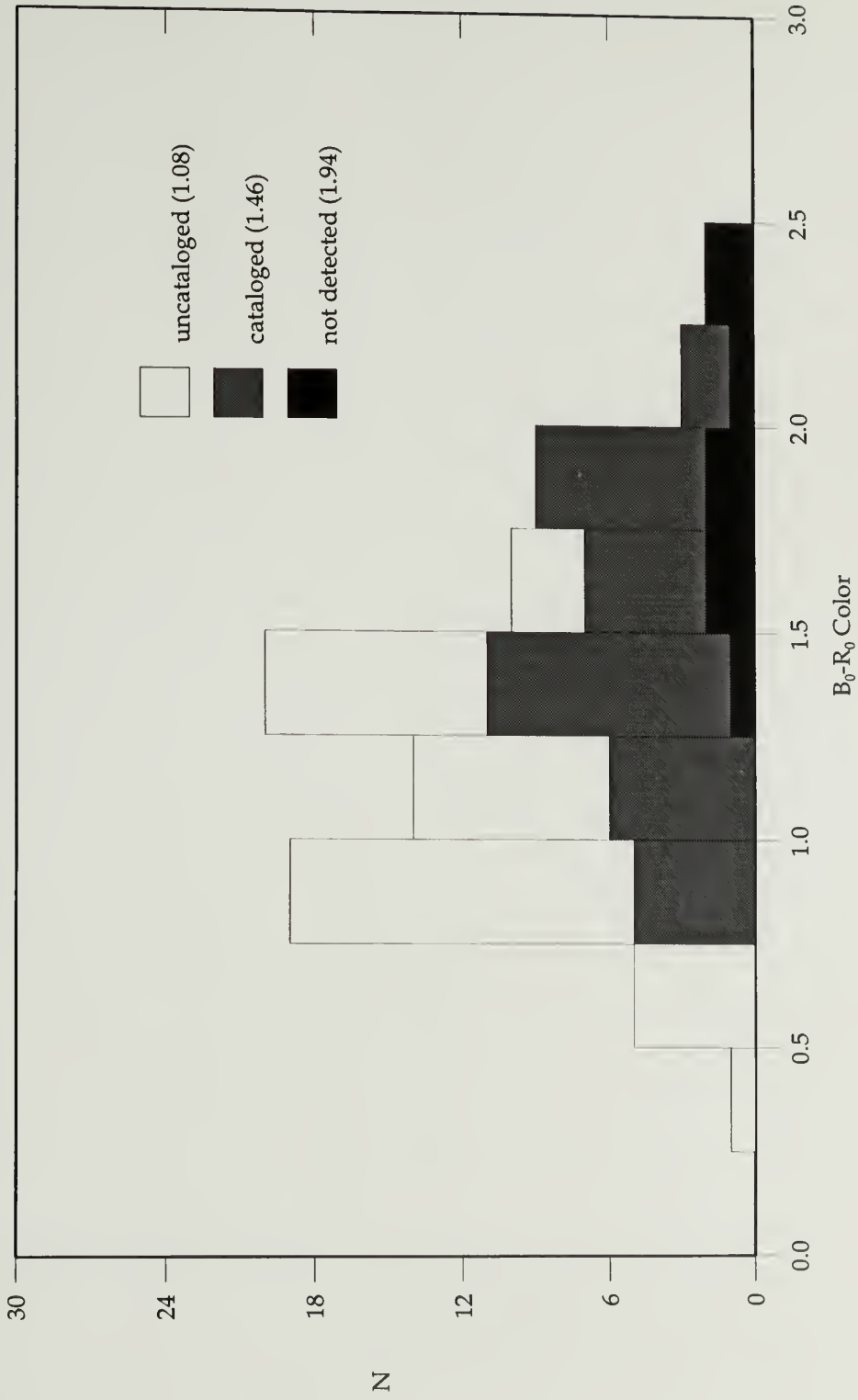
CHAPTER 6

CONCLUSIONS

The analysis in the previous chapter leads us to two conclusions about the newly discovered objects found in the slice search. First, they represent a distinctly different population of galaxies from the cataloged sample. Second, it appears that the smallest and nearest of these newly discovered objects may represent a population of objects numerous enough to significantly contribute to the integrated mass of all galaxies. In this chapter we examine what the large-scale implications of these conclusions are. We use the data obtained in the slice search to discuss the completeness of the extragalactic census in galaxy catalogs, and how it may have to be altered to accommodate our findings. We discuss how these alterations may change our overall view of galaxy types, evolution, and the large-scale structure of the Universe.

We also describe follow-up work which will build on the results of the slice search. In particular, we discuss the motivations and techniques for the recently completed Arecibo "Slice II" search, a 21cm survey on a far larger scale than our project.

Implications of the Slice Search Results

The primary mission of the slice search data analysis in the previous chapter was to discover what, if anything, distinguished the newly discovered galaxies from those which were previously cataloged. This approach had two purposes. First, we wished to understand what it was about the uncataloged objects that caused them to be missed in optical surveys. Second and more importantly we wanted to establish whether the uncataloged objects represented a population of galaxies distinctly different from the cataloged objects. Because the newly discovered galaxies were found in such large numbers, such differences could alter our fundamental understanding of the average properties of galaxies. We briefly summarize the observations from the previous two chapters:

1.	In the optical images of all of the slice objects presented in Chapter 4, the uncataloged and cataloged galaxies have different appearances. As a group, the uncataloged objects are smaller and less luminous than the cataloged galaxies, and have less distinct structure without well-defined nuclei or spiral arms.

2.	The uncataloged and cataloged galaxies appear to occupy the same regions in space. Examined independently, the two populations describe the same large-scale cluster and void structures.

3.	As a group, the cataloged galaxies are more massive than the uncataloged galaxies. The most massive galaxies are exclusively cataloged galaxies.

4.	On average, the cataloged galaxies are more intrinsically luminous than the uncataloged galaxies. Between the two groups there is very little overlap in luminosity.

5.	All groups have similar ratios of blue luminosity to dynamic mass, although we caution that the dynamic mass estimates are relatively uncertain.

6.	Atomic hydrogen mass makes up a larger fraction of the total mass of the uncataloged objects than of the cataloged objects.

7.	The uncataloged galaxies are significantly bluer in color than the cataloged galaxies.

8.	The discovery of a proportionally large number of low-mass, low-luminosity galaxies in nearby volumes of the slice search implies the presence of a very high number density of these small objects. This could be as high as a hundred times that of the cataloged galaxies, and their integrated mass could be comparable to that of the known objects.

Two notable conclusions emerge from these observation. The first is that the uncataloged galaxies do represent a population which is distinctly different from the cataloged galaxies. This can be seen in their bluer colors, smaller sizes, lower overall masses, higher atomic hydrogen mass fraction, and different morphologies. As a group, the uncataloged galaxies appear to have both different populations of stars, as indicated by their bluer colors, and a different interstellar medium, as can be seen in their ratios of atomic hydrogen mass to dynamic mass. These observations imply that the uncataloged galaxies have either evolved along a different overall path from the average cataloged galaxy or perhaps have evolved more slowly. In contrast, the cataloged galaxies exhibit properties similar to those which we would expect for

"normal" galaxies. In their masses, distributions, colors, mass-to-light ratios, luminosities, and gas contents, the cataloged galaxies consistently demonstrate fairly mundane "middle-of-the-road" qualities.

The second conclusion is that the smallest of the newly discovered galaxies appear to exist in very large numbers. The number of them detected in the slice search implies that they are comparable to the "normal" galaxies in integrated mass, and are far more numerous. The newly discovered objects are not only different, but they are numerous enough to be important.

Because of the large fraction of their mass in the form of HI, the low-mass, low luminosity galaxies may be most significant as reservoirs of unprocessed atomic hydrogen gas. As such, they may have a profound influence on the evolution of the large galaxies we see. Mergers, or more appropriately "acquisitions" of these small objects by larger galaxies are undoubtedly common. Because the low-mass galaxies are so small, these events would be fairly unspectacular, and would primarily serve to supplement the gas contents of the larger galaxies. Duprie and Schneider (1996) have proposed just such a scenario to explain the large HI components of early-type galaxies. It should be noted that because of the comparatively large Arecibo beam, the slice search does not detect smaller objects in the vicinity of larger galaxies, in contrast to studies using synthesis array instruments (Weinberg, et al., 1991).

We can further speculate about what the Universe might look like if the true numbers of dwarf galaxies are nearer the "high end" of our error bars. Instead of being dominated by the large bright galaxies we are already aware of, the bulk of the gas mass in the universe could be tied up in small, nearly invisible objects, a vast "silent majority" of low-luminosity clouds and dwarfs. Prowling the fold of these myriad HI clouds, large galaxies capture and devour them, consuming their rich gas content to supplement their own out of proportion brightness. Yet as the predator must follow the migrating flocks of its prey, the motions and positions of the largest and brightest galaxies are determined by the distribution of these tiny objects.

The slice results do not prove this picture, but they do insist that the under-luminous dwarf galaxy population has an important collective voice in the structure and evolution of the Universe.

Follow-up Work: The Next Slices

The high number of detections in the slice search has demonstrated that 21 cm surveys can be valuable tools for extragalactic exploration. It has shown that careful surveys for atomic hydrogen can be at least as successful as historical optical studies in locating optically bright galaxies within a region, and are sensitive to under-luminous galaxy types which are particularly hard to detect optically. The slice search has also highlighted some of the difficulties which will be encountered by similar work in the future.

Future work in this area should both build on the successes of the slice search and learn lessons from its difficulties:

1). Perhaps the most potentially exciting result of the slice search is the implication of great numbers of undiscovered low-mass, low-luminosity galaxies for every known, cataloged galaxy. It is unfortunate that this is in many ways the least certain of the conclusions of the slice search. It is based on the measurements of only a handful of objects, making statistical arguments subject to enormous potential errors. An obvious goal of a follow-up project would be increasing the number of detections of these small galaxies so as to generate more statistically reliable results.

2). The greatest difficulties encountered in the slice search were in discriminating weak signals from interference in the 21 cm spectra. Despite being a "protected" band, the frequency range scanned was subject to chronic intermittent interference signals. In the slice project our most successful method of locating real signals was to look at each of the 14,130 spectra by eye. This was possible, although painful, with that number of spectra. However a future search attempting to better the detection statistics will inevitably have many more spectra to search, and visual scanning of the data may not be practical. Locating signals by software is in principle not difficult, but the procedures developed for the slice search were easily fool by the interference. For a new search with many more spectra, either more efficient visual searches or better software procedures will have to be developed.

With these problems in mind, a second far larger Arecibo "slice" search was undertaken. This new survey utilized two 21cm feeds scanning different parts of the sky simultaneously. This strategy had two

advantages. First, it could cover sky more efficiently than a single-feed search, generating just short of 300,000 spectra with signal-to-noise characteristics comparable to the slice search. Second, the same interference signals were be collected by both feeds. By subtracting these two spectra from each other, much of the interference could be eliminated.

Visual examination of a small fraction of these spectra has yielded several detections, both of cataloged galaxies and of objects which appear to be similar to many of the low-mass, low-luminosity galaxies which the first slice search detected. The huge number of spectra involved in this search has required the development of innovative procedures for visual examination of the data. Software procedures based on what was learned in the first slice search will also be generated. Both of these approaches should be more successful due to the cleaner spectra generated by the two-feed observations.

The results of this second slice search are potentially very exciting. The large number of spectra involved promises to greatly improve the statistics of our count of nearby low-mass galaxies, and will hopefully establish whether, and to what extent the first slice search has altered our view of the Universe.

REFERENCES

Bahcall, J., 1975, *Ap.J.* **200**, L1.

Bosma, A., 1978, *The Distribution and Kinematics of Neutral Hydrogen in Spiral Galaxies*, Thesis, University of Groningen, Netherlands.

Bothun G. D., Impey, C. D., Malin, D. F., Mould, J. R., 1987, *A. J.* **94**, 23-29.

Briggs, F.H., 1990, *A. J.* **100**.

Burbidge, E. M., 1981, *Symposium on Recent Advances in Observational Astronomy, Ensenada, Mexico*, 45-50.

Burstein, D., Haynes, M. P., Faber, S. M., *1991, Nature* 353, 515-521.

Burstein, D. and Heiles, C., 1984, *Ap. J.* **54**, 33.

Casertano, S. and van Gorkom, J. H., 1991, *A. J.* **101**, 1231.

Chen, J., Morton, D. C., Peterson, B. A., Wright, A. E., Jauncey, D. L., 1981, *M. N. R. A. S.* **196**, 715-730.

de Vaucouleurs, G., 1959, *Handbuch der Physik* **53**, 311.

de Vaucouleurs, G., de Vaucouleurs, H., Corwin, H. G., Buta, R. J., Fouque, P., Paturel, G., 1991, *Third Reference Catalogue of Bright Galaxies*, Springer-Verlag, New York (RC3).

Devereux, N. A. and Young, J. S., 1990, *Ap. J.* **350**, L25-L28.

Disney, M. J., 1976, *Nature* **263**, 573-575.

Disney, M. J. and Phillips, S., 1983, *M. N. R. A. S.* **205**, 1253.

Disney, M. J. and Phillips, S., 1987, *Nature* **329**, 203.

Duprie, K. and Schneider, S. E., 1996, *A. J.*, submitted.

Freeman, K.C., 1970, *Ap. J.* **160**, 811.

Fish, R. A., 1964, *Ap. J.* **139**, p284.

Fisher, J. R., Tully, R. B., 1981, *Ap. J.* **243**, L23-L26.

Giovanelli, R., and Haynes, M. P. , 1989a, A. J, **97**, 633.

Giovanelli, R. and Haynes, M. P., 1989b, *Ap. J.*, **346**, L5-L7.

Haynes, M. P., Roberts, M. S., 1979, *Ap. J.* **227**, 767-775.

Helou, G. and Bicay, M.D., 1993, *Ap. J.* **415**, 93-100.

Hoffman, G. L, Lu, N. Y., Salpeter, E. E., 1992, *A. J.* **104**, 2086-2096.

Hughes, J. P., 1989, *Ap. J.* **337**, 21-33.

Huchtmeier, W. K. and Richter, O. G., 1989, General Catalog of HI Observations of Galaxies (Berlin: Springer).

Impey, C., Bothun, G., Malin, D., 1988, *Ap. J.* **330**, 634-660.

Kaiser, N., Efstathiou, G., Ellis, R., Frenk, C., Lawrence, A., Rowan-Robinson, M., 1991, *M. N. R. A. S.* **252**, 1-12.

Kent, S. M., 1987, *A. J.* **93**, 816-832.

Kerr, F.J., Henning, P.A., 1987, *Ap. J.* **320**, L99-L103.

Krumm, N., Brosch, N., 1984, *A. J.* **89**, 1461-1463.

Kuijken, K., 1991, *Ap. J.* **372**, 125-131.

Lauberts, A., 1982, *The ESO/Uppsala Survey of the ESO (B) Atlas*, European Southern Observatory, Munich (ESO).

Lo, K. Y., Sargent, W. L. W., 1979, *Ap .J.* **227**, 756-766.

Lynds, R., 1971, *A. J.* **164**, L73-78.

Materne, J., Huchtmeier, W. K., Hulsbosch, A. N. M., 1979, *M. N. R. A. S.* **186**, 563-566.

Mathewson, D. S., Cleary, M. N., 1974, *Ap. J.* **190**, 291-296.

Merritt, D., 1987, *Ap. J.* **313**, 121-135.

Nilson, P., 1973, *Uppsala General Catalog of Galaxies*, Uppsala Observatory (UGC).

Nilson, P., 1974, *Catalogue of Selected Non-UGC Galaxies*, Uppsala Observatory Report #5 (UGCA).

Pantoja, C. A., Giovanardi, C., Altschuler, D. R., Givanelli, R., 1994, *A. J.* **108**, 921.

Praton, E. A. and Schneider, S. E., 1994, *Ap. J.* **422**, 46.

Schneider, S. E., 1989, *Ap. J.* **343**, 94-106.

Schneider, S. E., Helou, G., Salpeter, E. E., Terzian, Y., 1986, *A. J.* **92**, 742-765.

Schneider, S. E., Skrutskie, M. F., Hacking, P. B., Young, J. S., Dickman, R. L., Claussen, M. J., Salpeter, E. E., Houck, J. R., Terzian, Y. Lewis, B. M., Shure, M. A., 1989, *A. J.,* **97**, 666-673.

Shostak, G. S., 1977, *A. A.* **54**, 919.

Simpson, C. E., Gottesman, S. T., 1993, *ESO/OHP Workshop on Dwarf Galaxies*, Observatoire de Haute-Provence, France.

Tyson, 1989, *Ap. J.* **335**, 552.

Tyson, N. D. and Scalo, J. M, 1988, *Ap. J.* **329**, 618-628.

Vorontsov-Velyaminov et al., 1962, *Morphological Catalog of Galaxies*, Sternberg Observatory, Moscow, (MGC).

Walker, T. P., Steigman, G., Schramm, D. N., Olive, K. E., Kang, H-S, 1991, *Ap. J.*, **376**, 51-69.

Weinberg, D. H., Szomoru, A., Guhathakurta, P., van Gorkom, J.H., 1991, *Ap. J.* **372**, L13-L16.

Wetherill, C., Sullivan III, W. T., Heckman, T., 1980, *P. A. S. P.* **92**, 551.

Wolfe, A. M., 1987, *Texas Symposium on Relativistic Astrophysics*, 309.

Young, P. J., Sargent, W. L. W., Boksenberg, A., Carswell, R. F., Whelan, J. A. J., 1979, *Ap. J.* **229**, 891-908.

Zaritsky, D., Olszewski, E. W., Schommer, R. A., Peterson, .C., Aaronson, M., 1989, *Ap. J.* **345**, 759-769.

Zwicky et al., 1961, *Catalog of Galaxies and Clusters of Galaxies*, California Institute of Technology, (CGCG).